Ollscoil na hÉireann, Corcaigh

**National University of Ireland, Cork**

University College Cork, Ireland
Coláiste na hOllscoile Corcaigh

# The ability of a naturally established forest on cutaway peatland to sequester carbon.

Thesis presented by

**Hannah Mealy, BSc**

for the degree of

**Doctor of Philosophy**

**University College Cork**

**Department of Geography**

Head of Department: Dr Denis Linehan

Supervisors: Dr Paul Leahy, Dr Fiona Cawkwell

2025

## List of Figures

## List of Tables

## Abbreviations

| | |
|---|---|
| **ANNs** | Artificial Neural Networks |
| **C** | Carbon |
| **$CH_4$** | Methane |
| **$CO_2$** | Carbon dioxide |
| **DAFM** | Department of Agriculture Food and the Marine |
| **DOC** | Dissolved organic carbon |
| **EBC** | Energy balance closure |
| **EC** | Eddy covariance |
| **EDDRS** | Enhanced Decommissioning, Rehabilitation and Restoration Scheme |
| **EF** | Emission factor |
| **EPA** | Environmental Protection Agency |
| **eq** | Carbon dioxide equivalent |
| **GAM** | Generalised Additive Model |
| **GHG** | Greenhouse gas |
| **GPP** | Gross primary productivity |
| **$GPP_{bel}$** | Below canopy gross primary productivity |
| **GWP** | Global warming potential |
| **H** | Sensible heat fluxes |
| **ICOS** | Integrated Carbon Observation System |
| **IPCC** | Intergovernmental Panel on Climate Change |
| **IPCC** | Irish Peatland Conservation Council |
| **kNN** | k-Nearest Neighbours |

| | |
|---|---|
| **LAI** | Leaf area index |
| **LE** | Latent heat fluxes |
| **LWIN** | Longwave incoming radiation |
| **LWOUT** | Longwave outgoing radiation |
| **LULUCF** | Land use land use change and forestry |
| **UNFCCC** | United Nations Framework Convention on Climate Change |
| **MAE** | Mean absolute error |
| **MDS** | Marginal distribution sampling |
| **$N_2O$** | Nitrous oxide |
| **NEE** | Net Ecosystem Exchange |
| **NFI** | National Forest Inventory |
| **NIR** | National Inventory Report |
| **NPP** | Net Primary Productivity |
| **P** | Precipitation |
| **PCAS** | Peatlands Climate Action Scheme |
| **POC** | Particulate organic carbon |
| **PAR** | Photosynthetic active radiation |
| **PPFD** | Photosynthetic Photon Flux Density |
| **$R^2$** | Coefficient of determination |
| **$R_a$** | Autotrophic respiration |
| **$R_{bel}$** | Below canopy ecosystem respiration |
| **$R_{eco}$** | Ecosystem respiration |
| **RF** | Random Forest |

| | |
|---|---|
| **RG** | Global radiation |
| **$R_h$** | Heterotrophic respiration |
| **RH** | Relative humidity |
| **RMSE** | Root mean squared error |
| **Rn** | Net radiation |
| **SE** | Standard error |
| **SHF** | Soil heat flux |
| **SOC** | Soil organic carbon |
| **SWC** | Soil water content |
| **SWIN** | Shortwave incoming radiation |
| **SWOUT** | Shortwave outgoing radiation |
| **$T_a$** | Air temperature |
| **$T_s$** | Soil temperature |
| **VPD** | Vapour pressure deficit |
| **WMO** | World Meteorological Organisation |
| **WT** | Water table |

# Declaration

This is to certify that the work I am submitting is my own and has not been submitted for another degree, either at University College Cork or elsewhere. All external references and sources are clearly acknowledged and identified within the contents. I have read and understood the regulations of University College Cork concerning plagiarism and intellectual property.

Hannah Mealy

## Acknowledgements

I would like to thank both my supervisors, Dr. Paul Leahy (Department of Engineering, University College Cork) and Dr. Fiona Cawkwell (Department of Geography, University College Cork), for their ongoing support and guidance throughout my PhD research, as well as for the expert advice they provided along the way.

Thanks to Lullymore Heritage Park, especially Johnny, Ray, Tom and Bud, for providing the power supply for the tower and for their generous assistance in transporting equipment to and from the site. Thanks to Bord na Móna and Dr. Mark McCorry (Ecology Manager, Bord na Móna) for funding this PhD project, without which this research would not have been possible. I also extend my thanks to Dr. Stephen Barry (Technical Scientific Advisor, Department of the Environment, Climate and Communications, and Lecturer at Technological University Dublin), who greatly assisted me throughout my PhD, especially during the final stages of my research, providing reassurance when I needed it most.

Additionally, I am grateful to the carbon team within Bord na Móna—Harry Kelly, Clare Doherty, Brian Mollahan, and Gráinne Heagney—as well as to my family members and friends for accompanying me to the EC tower on many occasions to ensure my safety and appreciate the views.

Finally, I want to express my deepest gratitude to my husband, Fionn, for his constant patience, support, and love throughout this PhD journey, as well as for his expertise in wiring, which was invaluable at the beginning of this project.

*"If we give space to nature and stand back, we can let these near limitless connections develop and form. And from it we may get woodlands…"*

– Susan Wright & Peter Cairns, Scotland, A rewilding journey.

.

## Abstract

This study aimed to quantify the atmospheric greenhouse gas (GHG) fluxes of $CO_2$ and $CH_4$ from a naturally regenerated mixed woodland established on a cutaway peatland. Both $CO_2$ and $CH_4$ are critical contributors to climate change. $CO_2$ is responsible for long-term warming because it remains in the atmosphere for centuries, gradually accumulating and exerting a warming effect. In contrast $CH_4$ has a shorter lifespan, but it is far more effective at trapping heat in the short term, making it a potent driver of near-term climate warming. By monitoring these emissions, this research sought to estimate the net ecosystem exchange (NEE) ($CO_2$) and $CH_4$ to assess the peatland's role as a carbon sink or source, providing crucial insights to inform climate change mitigation strategies for degraded peatland ecosystems.

Continuous measurements were collected over a 12-month period using two open-path gas analysers and a 3-D sonic anemometer mounted on an eddy covariance (EC) tower. These recorded raw atmospheric $CO_2$ and $CH_4$ concentrations and 3-D wind speeds at 10 Hz and averaged flux data over half-hour intervals. These high-frequency measurements allowed for a detailed temporal analysis of gas fluxes and contributed to calculating the ecosystem's annual carbon balance. A closed transparent chamber was designed and built and used with a portable gas analyser to examine the below canopy contribution to the overall $CO_2$ fluxes. Results revealing that the below canopy habitat made a substantial contribution to overall $CO_2$ emissions, while the whole ecosystem still maintained a net carbon sink status.

A comparison of gap-filling methods for flux data was conducted, with the random forest (RF) machine learning model outperforming other methods such as marginal distribution sampling (MDS) in terms of accuracy and reliability. This approach was crucial in addressing data gaps and modelling the fluxes.

The gap-filled dataset, simulated using the random forest method, showed that $CO_2$ was the primary contributor to the total atmospheric carbon balance, with an estimated flux of –28.9 t $CO_2$ $ha^{-1}$ $yr^{-1}$ (±0.07 SE). The model demonstrated strong predictive performance, with a correlation coefficient of 77% and a low root mean square error (RMSE) of the prediction of 3.95 µmol $m^{-2}$ $s^{-1}$ between the unseen and modeled data points. In contrast, $CH_4$ emissions were much lower, contributing only 0.01 t $CH_4$ $ha^{-1}$ $yr^{-1}$ (±0.0002 SE), with a weak

correlation between the unseen and modeled data points of 20% and a low RMSE of 0.0113 µmol $m^{-2}$ $s^{-1}$. The uncertainty in both flux estimates was low, indicating a high level of confidence in the gap-filled time series produced by the random forest model. These results provide robust assurance of the model's ability to accurately predict GHG fluxes from this peatland ecosystem.

After incorporating default GHG emissions for $N_2O$ and DOC from IPCC (2013) values to estimate the total emission factor for the Lullymore site, the study revealed that the site remained as a significant carbon sink, with a total GHG emission factor of –26.4 t $CO_2$-eq $ha^{-1}$ $yr^{-1}$. This contrasts with emission factors reported for drained forests and rewetted peatlands. Methane emissions contributed very little to the overall emissions factor, estimated at 0.28 t $CO_2$-eq $ha^{-1}$ $yr^{-1}$ (including global warming potential).

However, the study faced limitations, including data covering only one year and the absence of a below-canopy photosynthetically active radiation (PAR) sensor, which may have led to a slight overestimation of positive NEE values below the canopy. The study's findings emphasise the potential of low-maintenance, naturally regenerated mixed woodlands on degraded peatlands as an effective carbon mitigation strategy, supporting the need for this land-use category to be recognised separately from conventional forestry in GHG reporting.

Future research should focus on multi-year monitoring to account for interannual variability, and adjustments in measurement infrastructure will be necessary as the woodland matures. Overall, this research highlights the substantial carbon sequestration potential of mixed woodlands on cutaway peatlands and provides critical insights for policy makers aiming to improve carbon accounting and enhance climate mitigation efforts.

# 1 Introduction

## 1.1 Drivers of global climate change and policy

Earth's atmosphere is undergoing significant changes, which are affecting the energy balance between the atmosphere, oceans, and the land surfaces (IPCC, 2023). Greenhouse gases (GHG), such as carbon dioxide ($CO_2$), methane ($CH_4$) and nitrous oxide ($N_2O$), naturally trap heat in the atmosphere, keeping the planet habitable. However, as the concentration of GHGs in the atmosphere increase, this effect is enhanced, disrupting the natural energy balance of the Earth (Jain *et al.*, 2015; Pörtner *et al.*, 2022).

Solar radiation is partly absorbed by the Earth's surface and atmosphere, when absorbed, this radiation warms the Earth's surface, while the radiation emitted back into space helps cool it (Begon *et al.*, 1996; Kirk-Davidoff, 2018; Günther *et al.*, 2020). Figure 1.1 illustrates how incoming solar (Shortwave) radiation is absorbed and reflected, and how outgoing infrared (Longwave) radiation interacts with GHGs, some of the radiation is trapped and emitted back to earth known as the greenhouse effect.

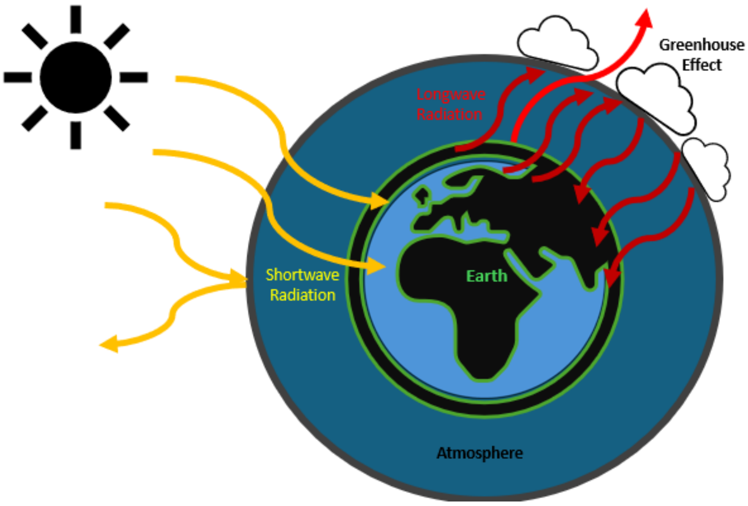


*Figure 1.1 Illustration of the greenhouse effect (photo: author)*

Increased anthropogenic GHG emissions from the burning of fossil fuels through various human activities, along with unsustainable land use and land use changes, are disrupting Earths energy balance and driving climate change (Begon *et al.*, 1996; IPCC, 2022, 2023;

Pörtner *et al.*, 2022). Since pre-industrial levels, global average emissions of $CO_2$, $CH_4$, and $N_2O$ have risen by 151%, 265%, and 125%, respectively (WMO, 2024).

The consequences of these increases are evident across the globe, temperatures are increasing the frequency and intensity of extreme weather events. In 2024, regions worldwide experienced record-breaking conditions, including droughts and wildfires in Chile, the western USA, and Canada ,while Brazil experienced severe flooding (WMO, 2024). Southeast Europe endured heat waves throughout the summer of 2024, followed by extreme flooding in central Europe between September and October 2024 (WMO, 2024). These implications pose unprecedented threats to people as well as wildlife and are increasing in frequency and severity (IPCC, 2022, 2023; Pörtner *et al.*, 2022).

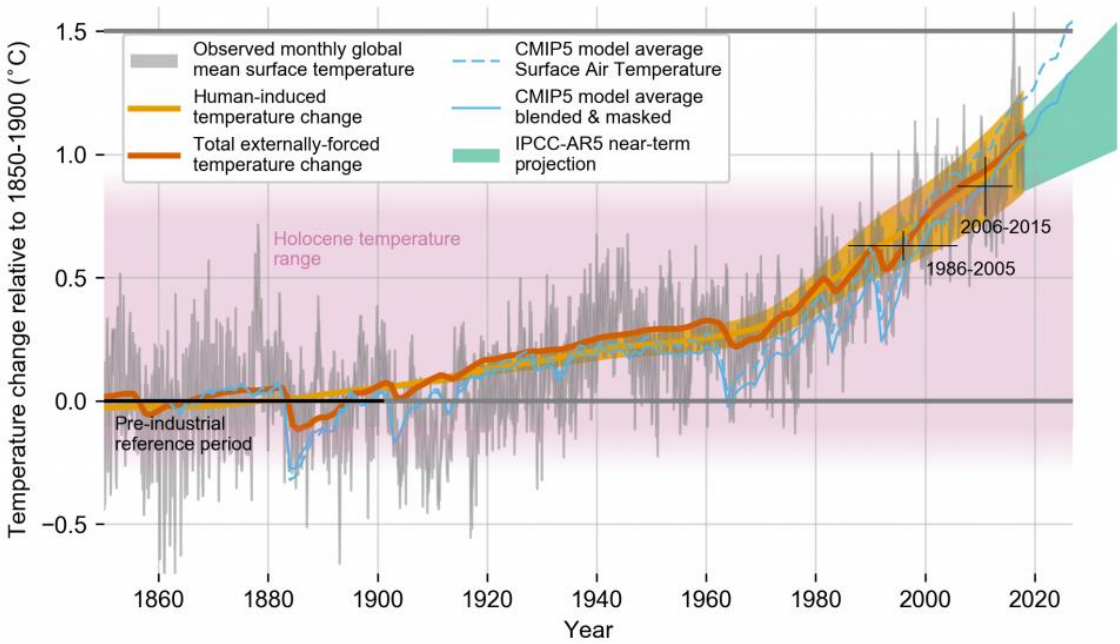


*Figure 1.2 Observed and modelled global temperature trends from 1850 to 2020. (IPCC, 2018).*

Global temperature trends indicate a clear human influence (IPCC, 2018, 2023). Figure 1.2 illustrates observed and modelled global temperature change relative to the pre-industrial period (1850-1900), highlighting a steady rise in temperature particularly from the mid-20$^{th}$ century onwards, with the decades (1986-2005, 2006-2015) seeing pronounced warming exceeding 1°C above pre-industrial levels, largely attributed to human activity (IPCC 2018).

In 2024, global temperatures exceeded an average of 1.5°C above the pre-industrial level, with January to September 2024 recording the highest global average temperatures (WMO, 2024).

The 2015 Paris Agreement, established under the United Nations Framework Convention on Climate Change (UNFCCC), set a global framework to limit the rise in average global temperatures to well below 2°C above pre-industrial levels, aiming to limit the increase to 1.5°C (UNFCCC and Change, 2017). The IPCC recommends achieving global net zero $CO_2$ emissions by 2050, with a plan to bring the net emissions of all other GHGs to zero later in the century (IPCC, 2018, 2022; Pörtner *et al.*, 2022). In response, the European Union developed 'The European Green Deal,' outlining measures to make the EU climate-neutral by 2050 through actions such as expanding renewable energy, improving energy efficiency in buildings, promoting sustainable transport and farming, advancing a circular economy, protecting biodiversity, strengthening carbon pricing, and investing in green finance and green jobs (The European Commission, 2025). As part of the deal, the Nature Restoration Law was introduced in 2024 with the aim of restoring degraded ecosystems across Europe. This law sets binding targets to rejuvenate ecosystems, particularly those with the greatest potential to capture and store carbon, while also helping to prevent and mitigate the impact of natural disasters (Directorate-General for Environment, 2024; HAAHR, 2024). These measures are critical to reducing emissions, protecting ecosystems and limiting the most severe impacts of climate change.

### 1.1.1 climate trends in Ireland

In line with the changes in global climate, Ireland has also experienced intense weather events (Laino and Iglesias, 2025). As an island in Western Europe the climate in Ireland is heavily influenced by the Atlantic Ocean, therefore as temperatures increase in the ocean driven by increased GHG emissions this is contributing to shifts in Ireland's weather patterns and temperature trends. A key indicator of these impacts is the rise in mean annual air surface temperatures recorded in Ireland, which has increased by approximately 1°C since the early 20$^{th}$ century (Noone *et al.*, 2023), with warmer days becoming more frequent and frost days declining (Cámaro García and Dwyer, 2021).

Average rainfall has increased by nearly 7% since 1961, and the wettest decade on record was 2006–2015, highlighting both increased precipitation and unpredictability (Murphy *et* *al.*, 2018; Cámaro García and Dwyer, 2021; Noone *et al.*, 2023). Extreme weather events are already causing tangible impacts. Severe rainfall leading to flash flooding in Sligo and Dublin in Ireland, mobilised contaminants such as agricultural runoff and sewage into waterways, posing public health risks (Laino and Iglesias, 2025).

Future projections from climate models for 2041-2070 predict further disruption. Summer rainfall may decrease by up to 8% under low emissions and up to 5% under very high emissions, while heavy rainfall events are expected to rise significantly, days with over 20mm of rain could increase by 8.8%-21% and days with over 30mm by 9-38% under low and high emission scenarios respectively (Nolan, 2024). These trends point to wetter autumns and winters and drier summers and more extreme weather emphasising the urgent need for adaption and climate mitigation measures.

## 1.2 Peatlands and their role in the carbon cycle

Peatlands can be described as a landscape with a deep layer of partially decomposed organic rich soil with a naturally high-water table (Page and Baird, 2016; Green and Page, 2017). Similarly, the IPCC Sixth Assessment Report describes peatlands as carbon rich wetland ecosystems (IPCC, 2022). Peat soils contain over 30% organic matter, at least 50% carbon and have low bulk density, although classifications vary with factors like location, peat formation rate, water resources and climate (IPCC, 2013; Page and Baird, 2016). Peatlands are also known as 'bogs' in Ireland, but for the purpose of this study, they will be referred to as peatlands. Fens are a type of peatland ecosystem, but unlike raised or blanket peatlands which are primarily rain fed, fens receive water from groundwater sources. As a result, fens tend to be wetter and have slightly more alkaline soils (Feehan and O'Donovan, 1996).

*Figure 1.3 A near-pristine peatland in Clara, Co. Offaly Ireland (photo: author).*

In pristine peatland ecosystems (Figure 1.3 is an example of a near pristine peatland in Ireland) the amount of carbon released by respiring plants, animals, and micro-organisms, is balanced by the carbon that is fixed by plants through photosynthesis (Begon *et al.*, 1996) and the carbon that is accumulated in the peat over time (Holden, 2005). However, this balance can be disrupted when environmental conditions change such as a drop or a rise in water table, air temperature, soil pH, vegetation, and peat depth, leading to the interference of the natural carbon cycle (Holden *et al.*, 2004; Frolking *et al.*, 2011; Renou-Wilson *et al.*, 2011; Jovani-Sancho *et al.*, 2018). This disruption can cause large losses of carbon to the atmosphere as $CO_2$ and $CH_4$ (Rigney *et al.*, 2018) and as Dissolved Organic Carbon (DOC) in waterways (Battin *et al.*, 2009; Evans *et al.*, 2017).

Pristine peatlands have high water tables (WT) and dense vegetation adapted to acidic

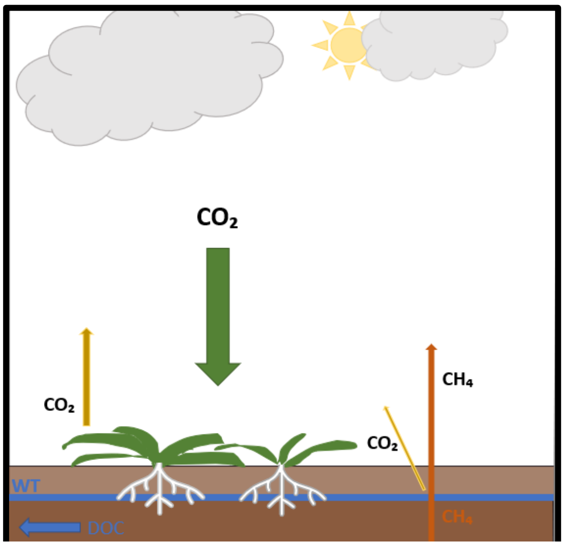


*Figure 1.4 Schematic of the carbon exchange of a pristine peatland ecosystem during daylight (photo: author).*

waterlogged conditions (Feehan and O'Donovan, 1996; Page and Baird, 2016; Green and Page, 2017). These conditions slow aerobic decomposition significantly, as micro-organisms inhibit the rate of decay which remains lower than the production rates (Feehan and O'Donovan, 1996). Vegetation varies with climate, topography, and water resources (Page and Baird, 2016). Northern peatland species such as *sphagnum mosses* decompose slowly, further reducing decay and peat accumulates from this partially decomposed material that is laid down in the wet conditions (Holden, 2005).

Peat formation captures and stores carbon, with $CO_2$ sequestration increasing as peat depth grows (Feehan and O'Donovan, 1996; Holden, 2005; Frolking *et al.*, 2011; Yu *et al.*, 2011; Page and Baird, 2016). Figure 1.4 represents the carbon exchange within a pristine peatland. As peatlands mature anaerobic decomposition intensifies, releasing $CH_4$ and balancing the overall carbon exchange (Feehan and O'Donovan, 1996; Holden, 2005; Frolking *et al.*, 2011; Renou-Wilson *et al.*, 2011; Yu *et al.*, 2011).

Peatlands play a crucial role in regulating climate by capturing and storing vast amounts of atmospheric carbon over long periods. Their function is tightly linked to weather and climate, as changes in temperature and precipitation directly affect soil respiration and GHG exchange (Begon *et al.*, 1996; Wilson, Farrell, *et al.*, 2016).

Global increases in average temperatures (WMO, 2024) threaten peatland hydrology, increasing evapotranspiration and causing a drop in the WT (Roulet *et al.*, 1992; Renou-Wilson *et al.*, 2022). A study examining long-term peatland dynamics since the Holocene highlights that WT in peatlands is primarily influenced by precipitation, with temperature playing a secondary or indirect role (Charman *et al.*, 2009). However, rising temperatures can accelerate drying, potentially increasing $CO_2$ and $CH_4$ emissions through enhanced soil respiration (Jovani-Sancho *et al.*, 2018; Wilson *et al.*, 2022).

Peatlands also release DOC and particulate organic carbon (POC), both representing carbon loss through oxidation and erosion (Schindler *et al.*, 1996; Palmer *et al.*, 2001; Evans *et al.*, 2017). Both DOC and POC contribute to off-site GHG emissions as waterlogged conditions can be leached or eroded in nearby water courses (Evans et al., 2017), where they can be retained in sediments altering nutrient ratios in the water (Dillon and Molot, 1997) potentially causing biodiversity loss.

### 1.2.1 The importance of soil organic carbon in peatlands

Peatlands cover less than 3% of the global land area (Figure 1.5), yet they store a significant one-third of the Earth's total Soil Organic Carbon (SOC) therefore they have a crucial role to play in regulating climate change (Baldocchi, 2003; Holden, 2005; Yu *et al.*, 2011; Green and Page, 2017; Xu and Goodacre, 2018).

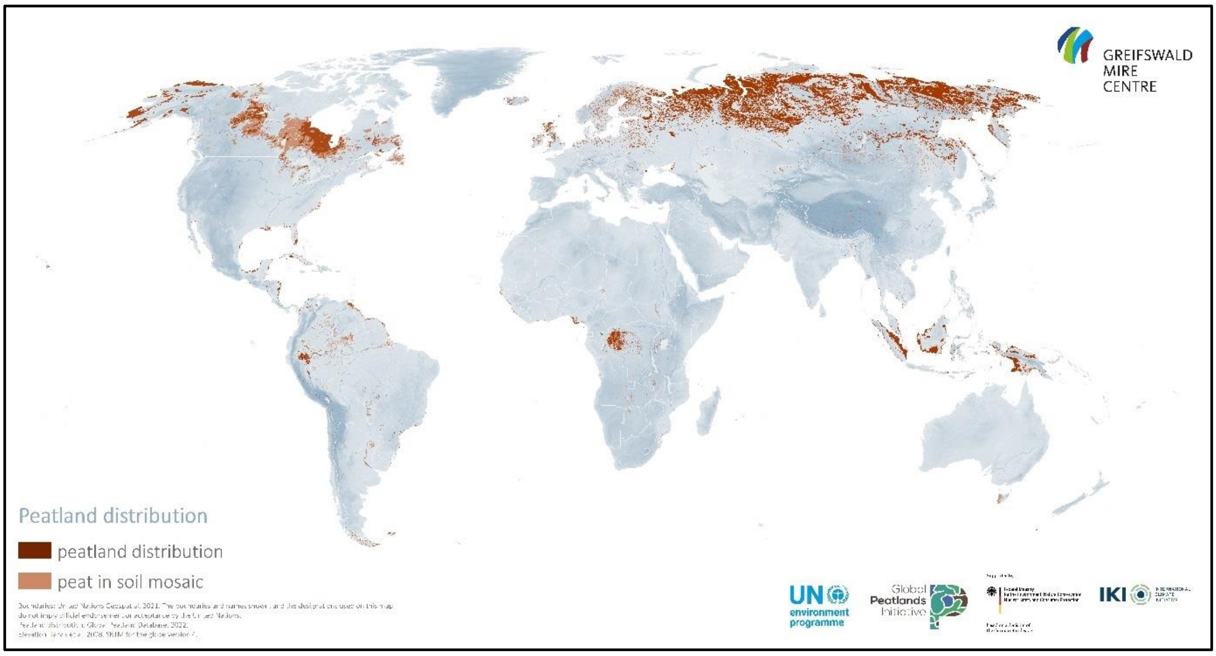


*Figure 1.5 Global land area map of peatlands* (Greifswald Mire Centre, 2022).

Land use change such as drainage of peatlands and removal of peat and vegetation disrupts natural functions and releases stored carbon. Globally in 2023 organic soils (primarily peatlands) contributed 1.2 Gt $CO_2$ to the LULUCF sector (Crippa *et al.*, 2024). Between 2000-2009 land use change on peatlands solely was estimated to release 0.9 Gt $CO_2$-eq $yr^{-1}$ , highlighting their vulnerability to land-use change (Wilson *et al.*, 2015; IPCC, 2018).

Peatland restoration through rewetting has the potential to restore their carbon sequestration function. Compared to drained conditions, rewetting typically reduces $CO_2$ emissions from organic soils and under favourable conditions can even restore the site to a net $CO_2$ sink (Wilson *et al.*, 2013, 2022). However, in the first few years following rewetting, some sites may still act as a $CO_2$ source, the time required for recovery varies (David Wilson Catherine Farrell, and Müller, 2012; Wilson *et al.*, 2015, 2022; Wilson, Farrell, *et al.*, 2016; Rigney *et al.*, 2018). Based on global data, it is estimated that rewetting could capture between 0.5 and 1.3 Gt $CO_2$-eq per year (IPCC, 2021).

Globally, $CH_4$ has risen 265% since the pre-industrial era (WMO, 2024), accounting for 18.9% of total GHG emissions in 2023 (Crippa *et al.*, 2024; WMO, 2024). Intact northern peatlands are a notable source of $CH_4$, (7.6–15.7 g C m−2 year−1 across 186 sites), with emissions influenced by water table depth, vegetation and soil pH peaking when WT is near the peat surface, or just above in fen ecosystems (Abdalla *et al.*, 2016).

Peatlands worldwide are increasingly affected by climate change and rising temperatures may reduce $CH_4$ emissions but increase $CO_2$, potentially disrupting the carbon balance (Turetsky *et al.*, 2014). A study by Swindles et al. (2019) examining long-term records show a clear drying trend. They found that 60% of sites across European peatlands including Britain, Ireland, Scandinavia, and mainland Europe, were drier in the past two centuries than over the previous 600 years, with 24% drier than they had been for the past 2,000 years. These findings emphasise the growing vulnerability of peatlands and urgent need for improved management and restoration. As drying continues, even restored or near-natural peatlands risk becoming carbon sources, releasing carbon into the atmosphere (Dieleman *et al.*, 2016; IPCC, 2021, 2022). A 12-year study in Sweden supports this concern, showing that when the water table fell below 20 cm, net $CO_2$ uptake declined to -18 g C $m^{-2}$ from the 12-year average of -58 g C $m^{-2}$, highlighting that prolonged drier conditions could significantly alter peatland carbon dynamics (Peichl *et al.*, 2014).

### 1.2.2 Irish peat soils organic carbon

Estimates of Irelands peatland area have become increasingly more precise over time. Connolly and Holden (2009) reported that 20.6% of Ireland is peatland, a significantly larger proportion than earlier estimates (Hammond, 1981; Connolly *et al.*, 2007). Recent advances in remote sensing and mapping technologies have further refined these estimates (Gilet *et al.*, 2024; Habib *et al.*, 2024; O'Leary *et al.*, 2025). Gilet et al. (2024) introduced the third version of the Adaptive Mapping Framework (AMF), originally developed by Connolly et al. (2007), incorporating detailed data on both shallow and deep peat soils critical for carbon storage. With an additional 20,000 data points, the updated framework indicates that peat soils cover approximately 1.66 million hectares, 23% of Ireland's land area, demonstrating the extent of these crucial carbon rich soils (Figure 1.6).

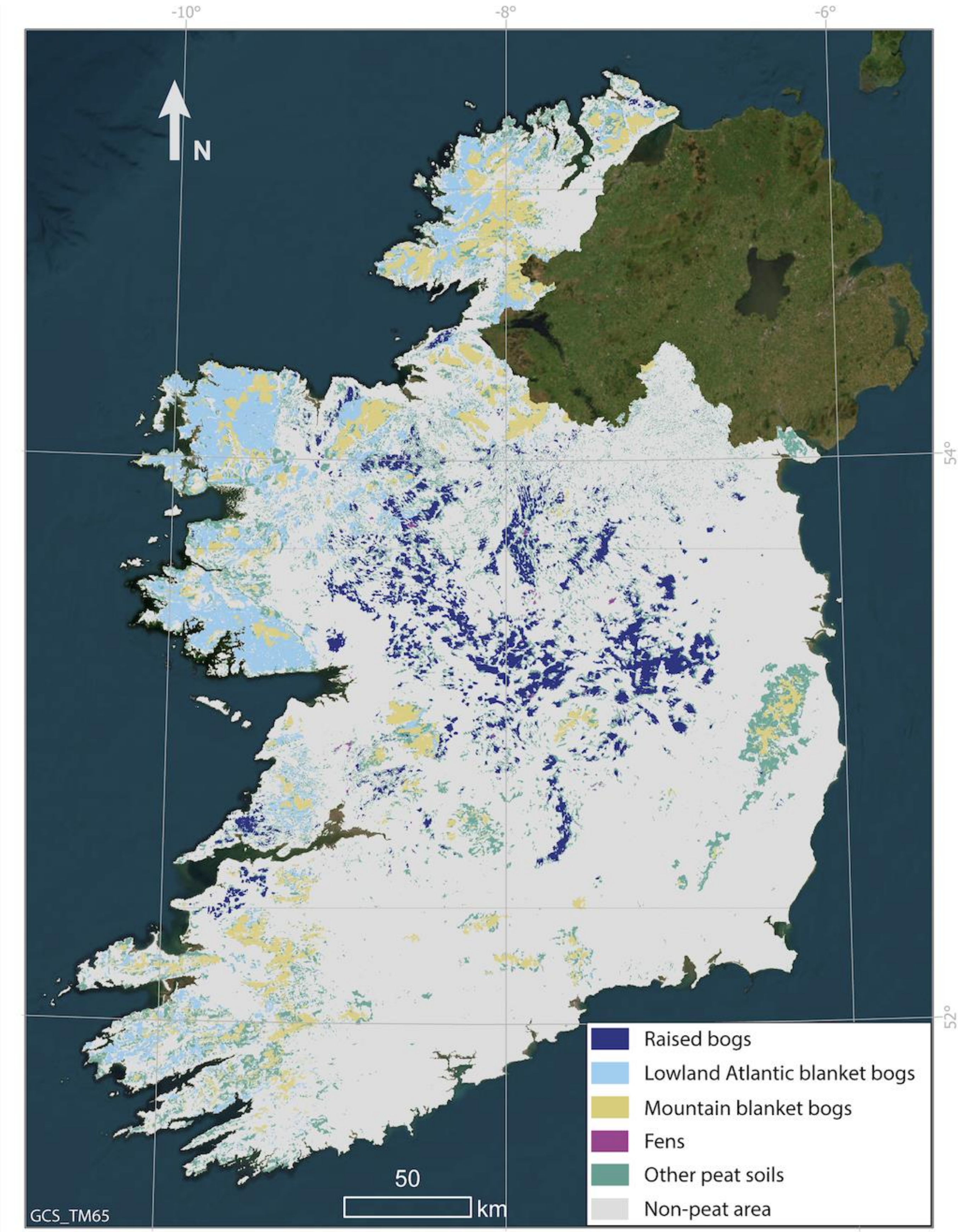


*Figure 1.6 The third version of the adaptive mapping framework (AMF), Irish peat soils map (Gilet et al, 2024).*

Renou-Wilson et al. (2022) based SOC estimates on the peatland map produced by Connolly and Holden (2007), but no updated SOC estimates have yet been made using the latest Irish peatland maps. Renou-Wilson et al.'s (2022) findings indicate that intact raised bogs in Ireland store 3,037 t C $ha^{-1}$, significantly higher than the 2,000 t C $ha^{-1}$ estimated by Feehan and O'Donovan (1996). Moreover, lowland and mountain blanket peatlands hold 1,550 t C $ha^{-1}$ and 1,248 t C $ha^{-1}$, respectively, underscoring the carbon storage potential of Irish peatlands (Renou-Wilson *et al.*, 2022).

Renou-Wilson et al. (2022) reported that cutover raised peatlands (Figure 1.7) (drained but not harvested) retain about 80% of the SOC capacity of intact peatlands, whereas cutaway peatlands (Figure 1.8) (drained and industrially harvested) hold only around 40% of the SOC of intact peatlands.  Based on their data, the report concludes that all peatlands in Ireland, whether degraded, intact, or altered through land use change, store approximately 2,216 Mt of carbon. Of this, 42% is held in raised peatlands, another 42% in lowland blanket peatlands, and 15% in mountain blanket peatlands.

This SOC estimate from Renou-Wilson et al. (2022), for Irish peatlands is significantly higher than previous estimates, such as Eaton et al. (2008), which estimated 1,469 Mt, and Tomlinson (2005), who reported 1,071 Mt. The underestimation in these earlier reports is likely due to limited knowledge of peat depth variability and how carbon density changes with depth (Wellock *et al.*, 2011; Renou-Wilson *et al.*, 2022). Given that the new map by Gilet et al. (2024) identifies nearly 3% more peatland coverage than Connolly and Holden (2009), these figures are expected to increase, highlighting the even greater importance of peatlands in Ireland. Additionally, the more advanced classification of peatlands, particularly regarding peat soil coverage and peat depths (O’Leary *et al.*, 2025), will enable more accurate estimates of SOC in Irish peat soils. Peat soils in Ireland represent a substantial proportion of the national land area and play a key role in carbon storage and climate regulation.

*Figure 1.7 A Cutover Peatland, Cloncrow, Tyrrellspass County Westmeath Ireland (photo: author).*

*Figure 1.8 A Bord na Móna cutaway bog in County Offaly Ireland (photo: author).*

## 1.3 NEE on peatland ecosystems

Net ecosystem exchange (NEE) represents the balance between $CO_2$ uptake through photosynthesis and $CO_2$ release through ecosystem respiration. In peatlands, measuring NEE provides valuable insights into whether the ecosystem acts a net carbon sink or source for $CO_2$ (IPCC, 2001; Kirschbaum *et al.*, 2001). In Ireland, approximately 85% of peatlands are degraded due to land use change, drainage and extraction, these activities alter carbon balance (Renou-Wilson *et al.*, 2019). Rewetted peatlands often display mixed NEE results, reflecting the intricate processes of recovery. For instance, a rewetted raised bog in Offaly, Ireland was a small carbon source (66 ± 168 g C $m^{-2}$ $yr^{-1}$) (Wilson *et al.*, 2015), while a similar site in Galway, Ireland, acted as a modest sink (-49 ± 68 g C $m^{-2}$ $yr^{-1}$) (Renou-Wilson *et al.*, 2019). Rewetted blanket bogs in Clare and Tipperary, Ireland, ranged from moderate to substantial sources of NEE values observed (131.6 ± 298.3 g C $m^{-2}$ $yr^{-1}$ and 585.3 ± 241.52 g C $m^{-2}$ $yr^{-1}$ , respectively)(Rigney *et al.*, 2018), highlighting the influence of prior land use and recovery time on NEE outcomes.

In contrast, near-pristine peatlands typically remain consistent carbon sinks, such as those in Sweden (NEE -58 ± 21 g C $m^{-2}$ $yr^{-1}$ )(Peichl *et al.*, 2014), and Scotland (NEE -114 g C $m^{-2}$ $yr^{-1}$ )(Hambley *et al.*, 2019), where wetter conditions enhance $CO_2$ uptake. Drained and extracted bogs, on the other hand, emit significant carbon, as seen from NEE values estimated in Mayo, Ireland (42 ± 23 g C $m^{-2}$ $yr^{-1}$ to 138 ± 11 g C $m^{-2}$ $yr^{-1}$), (Wilson, Farrell, *et al.*, 2016), Boora, Offaly (182 g C $m^{-2}$ $yr^{-1}$), and Middlemuir, Scotland (93 g C $m^{-2}$ $yr^{-1}$) (Wilson et al., 2015).

Together these findings illustrate how peatland condition whether drained or pristine fundamentally determines $CO_2$ exchange and underscores the importance of understanding NEE dynamics to guide restoration and climate mitigation efforts.

*Table 1-1 NEE measurements from temperate peatlands, ordered from negative NEE (carbon sink) to positive NEE (carbon source) (table: author).*

| Location | Peatland Type | Condition | Peat Depth (m) | Rainfall (mm) | Temp (°C) | NEE (g C $m^{-2}$ $yr^{-1}$) | References |
|---|---|---|---|---|---|---|---|
| Cross Lochs,Scotland | Near-Pristine Peatland | Near-Pristine Peatland | 2.2 | 1000 | 8 | -114 | Levy et al. 2015 |
| Sweden | Near-Pristine Peatland | Near-Pristine Peatland | 4 | 523 | 1.2 | −58 ± 21 | Peichl et al, 2014 |
| Mayo, Ireland | Rewetted (7 years) Blanket Bog (revegetated) | Rewetted | 0.5 | 1245 | 10.3 | -260 ± 179 | Wilson et al. 2016 |
| Moyarwood, Galway Ireland | Rewetted Raised Bog | Rewetted | 4.4 | 1193 | 9.9 | -103.7 ±37.2 | Wilson et al. 2022 |
| Mayo, Ireland | Rewetted (7 years) Blanket Bog (revegetated) | Rewetted | 0.5 | 1245 | 10.3 | -84 ± 103 | Wilson et al. 2016 |
| Mayo, Ireland | Rewetted (7 years) Blanket Bog (revegetated) | Rewetted | 0.5 | 1245 | 10.3 | -74 ± 67 | Wilson et al. 2016 |
| Talaheel,Scotland | Rewetted (16 years) Peatland | Rewetted | 2 | 1000 | 8 | -71 | Hambley et al. 2019 |
| Galway, Ireland | Rewetted Raised Bog | Rewetted | 4.4 | 1193 | 9.9 | -49 ± 68 | Renou-Wilson et al. 2019 |
| Mayo, Ireland | Rewetted (7 years) Blanket bog (no vegetation) | Rewetted | 0.5 | 1245 | 10.3 | 57 ± 30 | Wilson et al. 2016 |
| Offaly, Ireland | Rewetted Raised Bog | Rewetted | 1.5 | 948 | 9.6 | 66 ± 168 | Renou-Wilson et al. 2019 |
| Mayo, Ireland | Drained Blanket bog (no vegetation) | Drained | 0.5 | 1245 | 10.3 | 42 ± 23 | Wilson et al. 2016 |
| Lonielist,Scotland | Rewetted (10 years) Peatland | Rewetted | 2 | 1000 | 8 | 80 | Hambley et al. 2019 |
| Middlemuir, Scotland | Drained Raised bog | Drained | 0.7- 3.1 | 851 | 8 | 93 | Wilson et al. 2015 |
| Moyarwood, Galway Ireland | Drained Raised Bog | Rewetted | 4.4 | 1193 | 10 | 114 | Wilson et al. 2015 |
| Clare, Ireland | Rewetted (8years) Blanket Bog | Rewetted | NA | 1435 | 10 | 131.6 ± 298.3 | Rigney et al. 2018 |
| Bellacorrick, Mayo, Ireland | Drained Blanket bog | Drained | 0.5 | 1245 | 10.3 | 138 | Wilson et al. 2015 |
| Mayo, Ireland | Drained Blanket bog (revegetated) | Drained | 0.5 | 1245 | 10.3 | 138 ± 11 | Wilson et al. 2016 |
| Moyarwood, Galway Ireland | Drained Raised bog | Drained | 4.4 | 1193 | 9.9 | 141.1 ±25.5 | Wilson et al. 2022 |
| Blackwater, Offaly, Ireland | Drained Raised bog | Drained | 1.5 | 907 | 9.8 | 153 | Wilson et al. 2015 |
| Little Woolden, England | Drained Raised bog | Drained | 0.5- 1.75 | 867 | 10.2 | 170 | Wilson et al. 2015 |
| Clara, Offaly, Ireland | Drained Raised bog | Rewetted | 4 | 970 | 9.3 | 176 | Wilson et al. 2015 |
| Boora, Offaly, Ireland | Drained Raised bog | Drained | 1 | 970 | 9.3 | 182 | Wilson et al. 2015 |
| Glenlahan, Laois, Ireland | Drained Blanket Bog | Rewetted | 0.4 | 804 | 9.3 | 203 | Wilson et al. 2015 |
| Turraun, Offaly, Ireland | Drained Raised bog | Drained | 0.5-1.8 | 807 | 9.3 | 286 | Wilson et al. 2015 |
| Tipperary Ireland | Rewetted (1 year) Raised Bog | Rewetted | NA | 948.2 | 9.8 | 585.3 ± 241.52 | Rigney et al. 2018 |

Table 1.1 summarises NEE values from various studies on temperate peatlands, organised in order from negative to positive NEE values. This order highlights a trend, correlating NEE values with the condition of the peatland, ranging from near pristine or rewetted sites acting as carbon sinks (negative NEE), to some rewetted and all drained peatlands typically functioning as carbon sources (positive NEE).

## 1.4 Exploitation and land use change of peatlands in Ireland

### 1.4.1 Peatlands in Ireland

Irish peatlands are some of the oldest remaining ecosystems in the country and are home to a unique range of flora and fauna. Consisting of blanket bogs, raised bogs and fens they have shaped distinctive landscapes across the country (National Parks and Wildlife Service, 2015). Gilet et al. (2024) estimate that peat soils cover 1.66 million hectares (23%) of Ireland's 6.89 million hectares. This extensive coverage underscores their importance for the country's environmental and carbon management efforts.

Human activities are the primary cause of degraded peatlands in Ireland, due to activities such as drainage for the extraction of peat and land reclamation for agriculture, afforestation and wind farm development, and have severely altered peatland hydrology and ecology (Renou-Wilson *et al.*, 2011, 2019; Eaton *et al.*, 2008; Malone and O'Connell, 2009; Renou-Wilson *et al.*, 2019; The Climate Change Advisory Council, 2019). Peat harvesting in particular, involves the removal of upper layers of peat, until extraction is no longer economically viable, leaving behind cutaway sites (Feehan and O'Donovan, 1996; Schouten, 2002).

#### *1.4.1.1 Raised peatlands*

Raised peatlands are more commonly found in the midlands of Ireland, where annual average precipitation is 750- 1000 mm (Renou-Wilson and Byrne, 2015). Formed on higher ground approximately 10,000 years ago at the end of the last ice age, vegetation around shallow meltwater lakes partly decomposed, accumulating into thick peat layers that rose above ground water level. These became ombrotrophic peatlands, receiving water solely from precipitation (Mitchell and Ryan, 1997). When fully established, raised peatlands have a significant peat depth ranging from 3 to 12m with an average of 7.5m (Feehan and O'Donovan, 1996). Peatlands have also been influenced by climate. Around 5,200 years ago, wetter conditions, likely linked to shifts in North Atlantic weather patterns, brought increased rainfall to northwest Europe, including Ireland, promoting development and expansion of peatlands and affecting both their water balance and carbon accumulation (Roland *et al.*, 2015). Deeper peat in raised peatlands also rendered them valuable for exploitation by peat extraction (Renou-Wilson and Byrne, 2015).

#### 1.4.1.2 Blanket peatlands

Blanket peatlands, more extensive than raised peatlands in Ireland (see Figure 1.6, section 1.2.2) are divided into Atlantic and Mountain types, found in western lowlands and mountain tops, respectively (Feehan and O'Donovan, 1996). They developed 4,000 and -7,500 years ago in areas receiving over 1200 mm of annual precipitation (Mitchell and Ryan, 1997). Their formation and Holocene expansion were mainly driven by cool, wet climatic, conditions, with distribution tightly controlled by thresholds of temperature and moisture (Gallego-Sala *et al.*, 2016). Shallower than raised peatlands, averaging 2.5m depth, they are sometimes named "blanket bog" or "blanket peatland" because they form a 'blanket'-like layer of peat across the land area (Renou-Wilson and Byrne, 2015). Peat is usually more acidic in blanket peatlands than in raised peatlands (Foss *et al.*, 2001). Both peatlands types are naturally treeless (Renou-Wilson and Byrne, 2015) and develop ground cover vegetation such as *sedges, bog rushes*, *purple moor grass, bog cotton* and *sphagnum mosses* (Laine, 2006; Sottocornola, 2007).

### 1.4.2 Industrial peat extraction and Bord na Móna

Peat has been used in Ireland as a domestic fuel since at least the 7th century, initially being extracted by hand which did not require extensive drainage (Clarke, 2010). Often referred to as barren land or wasteland, gained commercial value in the 19th century, when they were drained for use as agricultural land. Later in a report produced by the 'Dáil Peat Committee' in 1921 (Clarke, 2010) the commercial value of peat was underlined, marking the beginning of industrial peat extraction for fuel in Ireland (Hammond, 1981).

In 1934 the Turf Development Board (TDB) was established (Clarke, 2010) with the intention to industrialise peat extraction for the production of electricity and fuel (Hammond, 1981; Mitchell and Ryan, 1997) . In 1946, TDB officially changed names to Bord na Móna (Andrews, 1982) and established an agreement with Electricity Supply Board (ESB) to use peat for industrial electricity and fuel, peaking at 40% of the national energy supply in the early 1960s (Feehan and O'Donovan, 1996).

By the 1970's, Bord na Móna exploited 55,000 ha of peatlands across mainland Ireland (see Figure 1.6, section 1.2.2 for map of raised peatlands), producing approximately 4 million tons of peat per annum (Mitchell and Ryan, 1997), yet harvesting equipment and weather limitations hindered targets, causing financial strain (Feehan and O'Donovan, 1996; Clarke, 2010). Although there were continuous setbacks to the industry, between 1946-1974 Bord na Móna had acquired approximately 90,000 ha of peatlands in Ireland and was the second largest peat extraction company in the world by 1995, with 13 active production sites in Ireland alone (Feehan and O'Donovan, 1996; Clarke, 2010) The scale of industrialisation underscores the significant environmental pressure and degradation inflicted on Irish peatlands.

### 1.4.3 The impact of drainage on peatlands

Peatlands have been drying out over the past 2,000 years due to climate change, with drainage from human activity greatly accelerating this trend (Swindles et al., 2019). Globally 15% of peatlands, mostly in Europe and Asia have been drained, contributing 5% of anthropogenic GHG emissions (Green and Page, 2017). Changes in WT directly impact peatlands' potential to act as a sink (to absorb) or a source (to release) GHGs (Laine, 2006; Kiely *et al.*, 2009; Yamulki *et al.*, 2013; Goffin *et al.*, 2015; Jovani-Sancho *et al.*, 2018). In pristine peatlands the WT is naturally high, slowing decomposition, limiting $CO_2$ release but producing $CH_4$ (Feehan and O'Donovan, 1996; Frolking *et al.*, 2011; Renou-Wilson *et al.*, 2011). When peatlands are drained the rate of decomposition increases, thus reducing $CH_4$ production however increasing $CO_2$ production (Laine, 2006). Drainage accelerates decomposition, reducing $CH_4$ but sharply increasing $CO_2$ emissions, with losses up to 8 t C $ha^{-1}$ $yr^{-1}$, approximately ten times more than the amount of carbon peat is estimated to accumulate in the same time period (Feehan and O'Donovan, 1996).


*Figure 1.9 Open drainage ditch on a cutaway peatland Lullymore county Kildare Ireland (Photo: author*

Draining peatlands consists of constructing furrows which are shallow and close together, and ditches (Figure 1.9) that are typically deeper and broadly dispersed (Holden *et al.*, 2004). These alter the peatlands hydrology and further influence surrounding water resources (Strack *et al.*, 2006). A study of drained, afforested peatland in Ireland, found that high winter precipitation substantially increased in the maximum rate of run-off. The increase was similar to what would be expected if the area had no vegetation, implying that afforestation offers little benefit to the hydrological balance, when compared to a pristine peatland due to the drainage carried out (Lewis *et al.*, 2013). It was also noted by Holden *et al.*, (2004) that the hydrology of peatlands is not only influenced by the initial process of drainage, but even after the forests are semi-mature or established the hydrological balance remains affected.

### 1.4.4 Sink source function of industrialised forestry on peatlands

It is estimated 11.6% of Ireland's landcover is forested (Figure 1.10), just over 1% increase since 2012 (10.5%) (DAFM, 2022). Since the late 1980's, Ireland has invested heavily in grant aided afforestation schemes to increase the percentage of forest land cover (DAFM, 2015), with Industrial forestry often targeting peatlands which make up a large proportion of forestry land (Byrne and Farrell, 2005.). The percentage of forestry planted on peat soils is estimated at 38.4%, declining since the previous report in 2020 from 39.2% (DAFM, 2020, 2022). The presence of peat soils under agricultural land has contributed to the stabilisation of the percentage of peatlands being afforested.

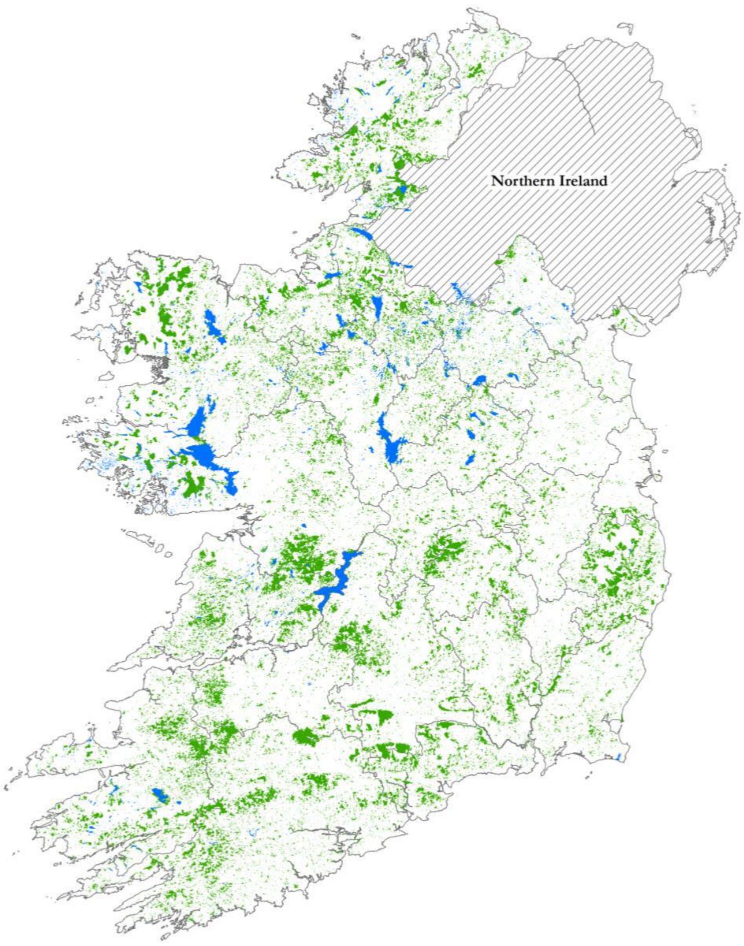


*Figure 1.9 Map of Irish forestry cover in green (DAFM 2022).*

However, there has been a decline in afforestation on blanket peatlands (DAFM, 2022). The decrease in peatlands being afforested or continuously used for forestry, may be due to the slow return on investment and the increasing awareness of the high ecological value peatlands have for biodiversity (Feehan and O'Donovan, 1996; Foss *et al.*, 2001). In addition, the role of peatlands in carbon sequestration has also gained greater attention in research (Sottocornola and Kiely, 2010; Wilson, Farrell, *et al.*, 2016).

In Ireland, industrialised forests were typically monocultures, predominantly comprising of non-native coniferous species such as *Sitka spruce* (Byrne and Farrell, 2005). Currently the land forest area consists of 69.4% conifer species (DAFM, 2022), significantly impacting both the carbon and hydrological balances of these ecosystems (Wellock *et al.*, 2011). Hargreaves et al. (2003) found that afforestation with Sitka spruce on peatlands produced relatively low $CO_2$ and $CH_4$ emissions, suggesting potential GHG benefits. The study in Scotland, tracked various stages of afforestation: as a pristine peatland, sequestered around -0.25 t C-$CO_2$ ha$^{-1}$ yr$^{-1}$, which increased to a source 2-4 t C-$CO_2$ ha$^{-1}$ yr$^{-1}$ following drainage and ploughing. During early tree growth (4-8 years), carbon uptake was approximately -3 t C-$CO_2$ ha$^{-1}$ yr$^{-1}$ rising to -2 to -5 t C-$CO_2$ ha$^{-1}$ yr$^{-1}$ as the forest matured (8-26 years). By year 26, the site had accumulated around -54.2 t C-$CO_2$, highlighting the net carbon sequestration potential of industrialised forests (Hargreaves *et al.*, 2003). Figure 1.11 displays the data from Hargreaves et al. (2003) regarding carbon sequestration in afforested peatlands at different stages. The lower emissions from the afforested peatland were estimated to last until harvest, with carbon stored in tree biomass remaining in situ until the trees are harvested or reach the end of their lifespan (Hargreaves *et al.*, 2003). It is important to note that this study focused on industrial forests intended for harvesting once mature and centred on gas exchange while the areas were vegetated.

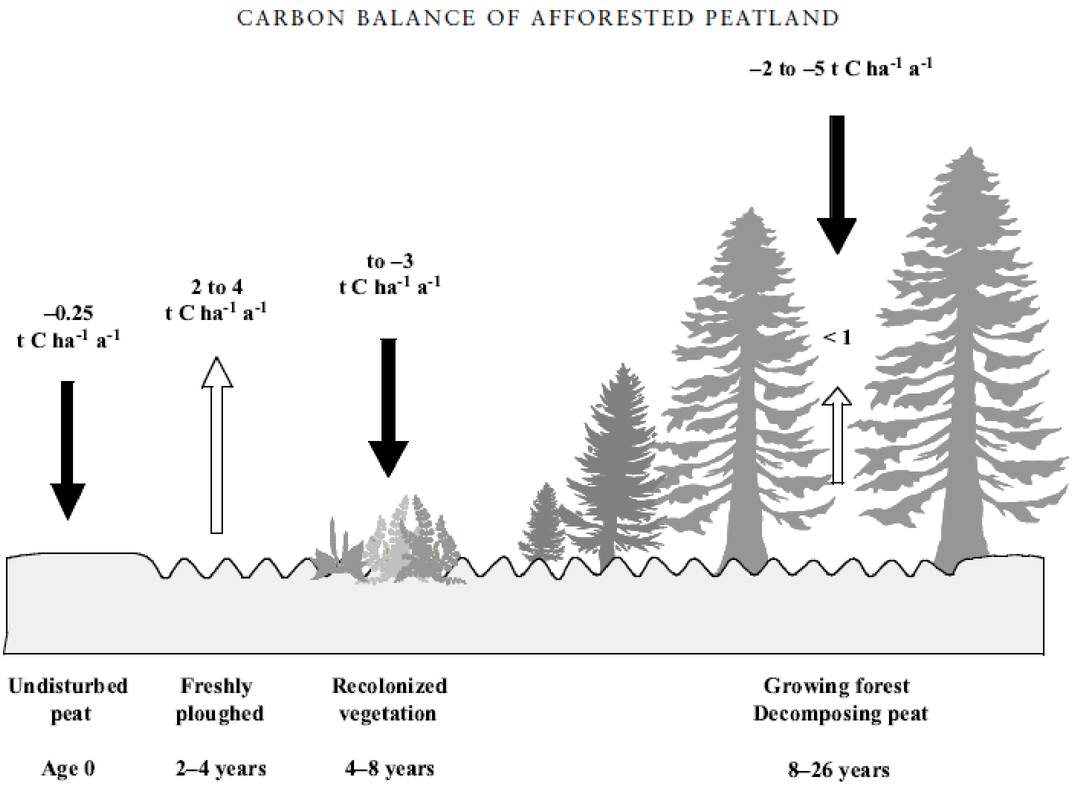


*Figure 1.10 Estimated carbon sequestration in afforested peatlands at different stages (Hargreaves et al., 2003).*

The study by Hargreaves et al. (2003) highlights the relationship between forest age and GHG exchange over time. Supporting this, Besnard et al. (2018) found that carbon sequestration varies with forest age, and that both age and management practices significantly influence the spatial and interannual variability of NEE across 126 forest eddy-covariance flux sites globally.

In addition to age, a study found that clear felled peatland forests are significant sources of GHGs, with $CO_2$ emissions accounting for the majority of the total annual GHG balance (82.5%, 23.3 t $CO_2$-eq ha$^{-1}$ yr$^{-1}$). $N_2O$ emissions also contributed significantly (17.1%, 4.8 t $CO_2$-eq ha$^{-1}$ yr$^{-1}$), while $CH_4$ emissions were minor (0.4%, 0.1 t $CO_2$-eq ha$^{-1}$ yr$^{-1}$) (Tikkasalo *et al.*, 2024). Harvesting industrial forests leaves behind waste biomass, which decomposes on-site and releases the stored carbon back into the atmosphere (Jovani-Sancho *et al.*, 2021). Beyond the impact of clear-felling, pre-planting activities also contribute to carbon emissions. A two-year study by Hommeltenberg et al. (2014), of an industrial peatland forest in Germany found it acted as a strong carbon sink (−130 ± 31 and −300 ± 66 g C m$^{-2}$ yr$^{-1}$ in the first and second years, respectively). However, when the emissions from drainage and peat extraction prior to planting were included, the site became a carbon source. The authors estimated that the forest would need to remain for over 140 years to offset the emissions, which were estimated to be 134 t C $ha^{-1}$ over the previous 44 years (Hommeltenberg *et al.*, 2014).

Wellock et al, (2011) found that SOC in established peatland forests was lower than those in intact peatlands, likely due to pre-afforestation actions such as drainage, which also affected the WT. similarly a 60-year simulation of a coniferous plantation on drained agricultural peatland in Sweden, found that when focusing on $CO_2$ and $N_2O$ emissions from tree biomass and soil, the forest acted as a source of emissions for the first 39 years and a sink thereafter (He *et al.*, 2016). When carbon losses from harvested tree biomass were included, the study concluded that an 80-year rotation could not offset the carbon lost from the peat during the same period (He *et al.*, 2016).

Not all cutaway peatlands or pristine peatlands are suitable for commercial forestry and certain measures must be implemented before afforestation. Deep peat, often associated with a high WT, inhibits most tree growth, so the area's physical and biochemical properties must first be altered. This may involve the creation of drainage channels, continued drainage, the addition of fertiliser, occasional ploughing, and weed control (Renou-Wilson *et al.*, 2008). Yamulki *et al.,* (2013) suggest that planting pine trees on peat, without intensive drainage, could produce lower net GHG emissions compared to those from near-pristine peatlands. Though, this study does not account for vegetation respiration or NEE. Renou-Wilson *et al.*, (2007), found that afforesting cutaway peatlands with native birch could help restore the woodland's carbon sequestration potential, but impact on the GHG balance depends on the management approach (Renou-Wilson *et al.*, 2008).

## 1.5 The concern for environmental sustainability

Environmental concerns over peatland degradation was highlighted as early as the 1980's (Clarke, 2010), with conservation measures introduced in the 1990s (Feehan and O'Donovan, 1996). Bord na Móna produced a report in 1988 suggesting that cutaway with deep peat should be used for forestry or natural revegetation, and low-lying areas should be converted to wetlands or lakes (Clarke, 2010). Later Renou-Wilson *et al.,* (2008) demonstrated that industrialised forestry on cutaway depends on environmental factors and is often not economically viable. As awareness of peat's unsustainability in horticulture grew, Bord na Móna began to look at alternative growing media for horticultural products, such as green waste and bark mulch to reduce the use of peat-based compost and products (Clarke, 2010). These developments marked the beginning of recognising the environmental impacts of peat exploitation and the need for restoration strategies on cutaway.

Following the introduction of the Kyoto protocol in 1997, which aimed to reduce GHG emissions introducing a tax on the use of certain energy products in the EU (The Climate Change Advisory Council, 2019), an Irish government report (1998) recommended closing peat power stations to reduce emissions (Clarke, 2010). This shift prompted Bord na Móna to explore alternative business models and invest in research on peatland carbon dynamics (Clarke, 2010). Bord na Móna who own around 80,000 ha of peatlands, ceased peat extraction in 2020. Since then, two remaining power stations have closed (Bord na Móna, 2021b) and the remaining Edenderry power station in December 2023 transitioned to a biomass based power station (Bord na móna, 2024). Research in the late 1990's, determined that restoring peatlands could re-establish their carbon sink function (Feehan and O'Donovan, 1996) afterwards international initiatives were launched to develop management strategies to restore peatlands GHG balance (Clarke, 2010).

### 1.5.1 Restoration of peatlands in Ireland

As recognition of the need to conserve peatlands grew, the EU Habitats Directive (1992), designated intact and undisturbed peatlands as special areas of conservation (SAC) (Feehan and O'Donovan, 1996; National Parks and Wildlife Service, 2015). Despite ongoing peat extraction at the time , progress since then has improved to protect the remaining intact peatlands and restore exploited peatlands (Clarke, 2010). Central to these initiatives is re-establishing peatlands function as carbon sinks, crucial for addressing climate change mitigation, while also supporting biodiversity and improving water quality. By prioritising restoration on degraded peatlands, Ireland aligns with national and global climate goals, optimising the environmental and climate benefits these ecosystems can provide (Girkin *et al.*, 2023).

National initiatives such as the National Peatlands Strategy (NPWS, 2015) and the Peatlands and Climate Change Action Plan 2030, outline management frameworks that promote sustainable ecosystems services, including improving biodiversity, water filtration, nutrient cycling, flood and erosion control and carbon sequestration (O'Connell *et al.*, 2021). The strategy, developed by the National Parks and Wildlife Services (NPWS) includes detailed management plans, policies, monitoring and reporting of progress , providing more effective and responsible management of Irish peatlands (National Parks and Wildlife Service, 2015). The peatlands and Climate Change Action Plan 2030 developed by the Irish Peatland Conservation Council (IPCC) (2021), aims to protect and support ecosystem functions, across peatlands. By enhancing their resilience to climate change, allocating funding, implementing good management plans, and educating people on the importance of peatlands (O'Connell *et al.*, 2021). This was further reinforced by the EU Nature Restoration Law (2024), which states that at least 20% of the EU's land and seas areas must be restored by 2030, including 30% of drained peatlands under agricultural use, aiming for 50% by 2050 (HAAHR, 2024).

In Ireland, The Peatlands Climate Action Scheme (PCAS), also known as the Enhanced Decommissioning, Rehabilitation, and Restoration Scheme (EDRRS), launched in 2021 represents one of the largest restoration efforts on peatlands (Bord na Móna, 2021a; O'Connell *et al.*, 2021). Funded through €108 million from the EU Climate Action Fund and €18 million from Bord na Móna, the scheme focusses on rewetting and restoring cutaway peatlands to enhance carbon storage and reduce emissions (Government of Ireland, 2020; Bord na Móna, 2021a). In addition to this, the restoration efforts will also enhance biodiversity, improve water quality, and support effective catchment management (Bord na móna, 2024).

Since 1990, approximately 37,000 hectares of peatlands have been rehabilitated, including 19,000 hectares under the EDRRS scheme, about 45% of Bord na Móna's land holdings. In addition to EDRRS, other projects are also funding restoration work on peatlands. The " Peatlands and People" project for example, involves planting *sphagnum* plugs on rehabilitated sites to promote vegetation recovery and accelerate the reestablishment of peatland species across these restored areas (Bord na móna, 2024).

As part of the EDRRS, monitoring and verification was established to assess the ecological status of rehabilitated areas and to monitor carbon emissions across 11 different peatlands at varying stages of restoration, ranging from cutaway pre-rehabilitation, recently rewetted to 30 years post-rewetting. The goal of monitoring and verification is to assess the progress of rehabilitation processes across Bord na Móna sites, track environmental improvements, and provide accountability for the restoration work undertaken (Author).

### 1.5.2 Rewetting peatlands for restoration

Rewetting peatlands is central to restoration and climate mitigation, encouraging recolonisation by natural vegetation and gradual carbon accumulation (Waddington *et al.*, 2010; Wilson, Farrell, *et al.*, 2016; Renou-Wilson *et al.*, 2019; Wilson *et al.*, 2022; Aitova *et al.*, 2023).Figure 1.13 shows a rewetted cutaway peatland of around 20 years. Rewetting also helps preserve the rare ecosystems typically found in pristine peatlands (Bonn *et al.*, 2014). However, restoration success is widely variable. Hydrological manipulation, such as adjusting WT, can promote the establishment of *sphagnum mosses* and initiate peat formation (Farrell and Doyle 2003). Rewetting has transformed some cutaway blanket peatlands from carbon sources to sinks (Wilson *et al.,* 2016), though raised peatlands may remain $CO_2$ sources (Wilson *et al.*, 2007). Recovery is influenced by previous land use, peatland type and restoration methods (Renou-Wilson *et al*., 2019, Rigney *et al*., 2018, Holden *et al.*, 2011).

*Figure 1.11 A rewetted cutaway (20 years) raised peatland located at Lullymore county Kildare Ireland (photo: author).*

Restoration can also increase $CH_4$ emissions due to anaerobic decomposition under higher WTs (Holden *et al.*, 2007, Abdalla *et al.,* 2016, Holden., 2005; Renou-Wilson *et al.*, 2011). Industrially exploited sites may emit both $CO_2$ and $CH_4$, whereas domestic degraded sites may show mixed responses (Renou-Wilson *et al.*, 2019). Nonetheless, long term $CO_2$ reductions typically outweigh short term $CH_4$ increases, supporting rewetting as an effective climate mitigation strategy (Gunther *et al.,* 2020). Other factors affecting GHG dynamics include WT, vegetation cover, soil pH and temperature (Abdalla *et al.*, 2016, Price and Ketcheson, 2009).

Overall, restoring cutaway peatlands to an active state is complex and site dependant. In Ireland, only about 0.1% of raised peatlands are considered active, encompassing a mixture of degraded, restored, and near-natural sites (Fernandez *et al.*, 2014). These findings highlight the challenges of peatland restoration and emphasise that not all management practices are suitable for every site. Different states of degradation require tailored strategies, and some peatlands may never fully regain their carbon sink function (Renou-Wilson *et al.*, 2022; Aitova *et al.*, 2023).

### 1.5.3 Natural diverse forests for non-commercial use

Ireland recognises the value of diverse native forests, for both biodiversity and carbon sequestration, with increasing efforts to establish species rich woodlands under the Native Woodland Scheme (NWS) (DAFM, 2022). Afforestation of peatlands, often involves drainage and addition of fertiliser to increase growth, these can lead to substantial losses of peatland biodiversity (Renou-Wilson *et al.*, 2008), this can also be said for native diverse woodlands planted on intact peatlands (Graham *et al.*, 2017). Biodiversity is also linked to productivity of forests: a 10% loss in species diversity can reduce forest growth by 3% (Liang *et al.*, 2016) highlighting the dual importance of conserving native woodland for ecosystem and carbon benefits (Phelps *et al.*, 2012).

While active peatlands may be vulnerable to species loss from afforestation, degraded cutaway peatlands offer opportunities for establishing industrial or native woodlands enhancing biodiversity, as the land was previously a low-value species habitat (Bremer and Farley, 2010). Species-diverse forests often demonstrate higher biomass productivity than monoculture plantations, although results vary (Forrester and Bauhus, 2016), and companion planting, to enhance growth and resilience (Forrester and Bauhus, 2016; Brockerhoff *et al.*, 2017). Native forests are better known for boosting biodiversity than non-native or monoculture plantations (O'Callaghan *et al.*, 2017).

The IPCC Wetlands Supplement (2013) provides default emission factors for forestry on organic soils in temperate climates, distinguishing between Tier 1 and Tier 2 estimates. Tier 1 estimates are based on global default values that can be applied where site specific data are lacking. For example, Tier 1 $CO_2$ emission factor is 2.6 t $CO_2$-C $ha^{-1}$ $yr^{-1}$ and $CH_4$ is 3 kg $ha^{-1}$ $yr^{-1}$. In contrast, Tier 2 relies on country or region-specific data, which reflect local soil, climate and management conditions and therefore often provides a more accurate estimate. Tier 2 suggests lower value for $CO_2$ (2 t $CO_2$-C $ha^{-1}$ $yr^{-1}$) but a slightly higher value for $CH_4$ (5 kg $CH_4$ $ha^{-1}$ $yr^{-1}$). The main limitation is neither tier differentiates forest types, such as broadleaf, evergreen, or unharvested native woodland.

Evans et al. (2017) expand on the IPCC's (2013) values and estimate drained peatland forests emit 9.91 t $CO_2$-eq $ha^{-1}$ $yr^{-1}$, including $CO_2$, $CH_4$, $N_2O$, and fluvial losses, but again without forest-type distinction. Aitova et al. (2023) using Ireland's National Inventory Report (Duffy *et al.*, 2021), show combined EFs of 0.38 t C $ha^{-1}$ $yr^{-1}$ for drained forestry and 0.93 t C $ha^{-1}$ $yr^{-1}$ for rewetted forestry, indicating that even rewetted forestry may remain net carbon sources. These values include living biomass, litter sinks, and emissions from $CO_2$ and $CH_4$, drawing on data from Duffy et al. (2021) and the IPCC (2013). Importantly, Aitova et al. (2023) assessments do not include unharvested, species-diverse native woodland on peat soils, leaving a gap in both the National Inventory Report and IPCC reporting.

Bord na Móna and Coillte Nature are planting over 600,000 trees on previously harvested peatlands, including native *Downy Birch, Scots Pine, Alder*, and other broadleaves (Bord na Móna, 2019). Native Birch trees have low commercial timber value, however they are generally better for biodiversity (Renou *et al.*, 2007). There are already small areas of semi-natural woodlands across the country which are protected and maintained by schemes (Renou-Wilson and Byrne, 2015), such as the Native Woodland conservation scheme (NWCS), which aims to establish new native forests on low-value land to improve biodiversity, water quality, and overall forest cover toward the EU average (DAFM, 2015).

Overall, planting woodland (industrial or native) on intact peatlands is generally detrimental, as it disrupts the natural ecosystem dynamics. In contrast, establishing woodland on degraded cutaway sites can enhance biodiversity and provide valuable ecosystem services. Allowing natural unharvested woodland to develop on sites that are unlikely to regain their peatland carbon sink function may offer a suitable land management strategy, potentially restoring carbon sequestration while supporting biodiversity.

## 1.6 Research motivation and objectives

Peatlands are globally significant carbon stores, containing approximately one-third of the world's soil carbon while covering only 3% of land area (Baldocchi and Vogel, 1996; Baldocchi, 2003; Holden, 2005; Green and Page, 2017; Xu *et al.*, 2018). In Ireland, peatlands cover 23% of the land (Gilet *et al.*, 2024), but drainage and peat extraction have led to carbon emissions and habitat loss (Eaton *et al.*, 2008; Malone and O'Connell, 2009; National Parks and Wildlife Service, 2015). Although restoration efforts, such as rewetting, are critical, the recovery of peatlands' carbon sequestration capacity remains uncertain, with some sites still vulnerable to drought and ongoing GHG emissions (Farrell and Doyle, 2003; Holden, 2005; Holden *et al.*, 2007; Waddington *et al.*, 2010; Holden and Connolly, 2011; Günther *et al.*, 2015; Wilson, Farrell, *et al.*, 2016; Hambley *et al.*, 2019). This underscores the need for ongoing monitoring of carbon emissions to better understand peatland vulnerabilities and inform effective management strategies for future carbon sequestration.

To help define site-specific strategies for cutaway peatlands to mitigate climate change, the present study focuses on a cutaway peatland in Lullymore county Kildare Ireland. The site ceased industrial harvesting in the 1990's, has undergone partial rewetting, and has naturally developed a native woodland. The overall aim of this study was to assess whether the Lullymore site, under a low-maintenance management strategy, acts as a strong carbon sink for $CO_2$ and $CH_4$ emissions. Based on the results, the study will evaluate whether this specific management approach could be a successful strategy for cutaway peatlands that have not been effectively restored.

The objectives of this study are as follows:

i. Assess the proportion of total NEE below tree canopy, using a closed-loop clear chamber to measure $CO_2$ exchange ($NEE_{bel}$).
ii. Estimate overall NEE with the eddy covariance method, employing continuous monitoring of atmospheric $CO_2$ concentrations above the tree canopy, while relating gas emissions to environmental parameters.
iii. Gauge the total annual $CH_4$ concentrations alongside NEE using the EC method, as these are two GHGs of primary concern. Derive an emission factor for this habitat on

peat soils, using default emission values where direct measurements are not measured.

# 2 Literature review

The EC and chamber methods are commonly used to measure carbon fluxes in ecosystems, aiding the understanding of carbon dynamics and enabling researchers to quantify the exchange of GHGs. These techniques allow for monitoring carbon fluxes across different spatial and temporal scales, thereby enhancing the understanding of key ecosystem processes such as NEE, GPP, $R_{eco}$ and decomposition.

However, each method comes with specific advantages and limitations. For example, while the EC method offers continuous, landscape-scale measurements, it can often underestimates below-canopy carbon fluxes, especially in forested ecosystems (Leuning *et al.*, 2008; Foken *et al.*, 2011; Paul-Limoges *et al.*, 2017; Poyda *et al.*, 2017; Burba, 2022). On the other hand, chamber methods provide more precise measurements at smaller spatial scales but are limited by issues related to microclimate alterations and intermittent sampling (Wilson *et al.*, 2015; Jovani-Sancho *et al.*, 2017; Pavelka *et al.*, 2018; Rigney *et al.*, 2018).

In recent years, ML models have also been applied for gap filling and upscaling flux data, offering enhanced flexibility and predictive power compared to traditional models. While ML models can capture complex, non-linear relationships in the data, they often require larger datasets and can be less interpretable compared to process-based models (Holl *et al.*, 2020; Kim *et al.*, 2020; Zhu *et al.*, 2022; Ingle, Bhatnagar, *et al.*, 2023; Habib *et al.*, 2024).

This section will review the key methods used to monitor atmospheric carbon fluxes, focusing on the EC and chamber methods. It will also explore how ML models are employed for gap filling, comparing their strengths and weaknesses to earlier models. Additionally, a review of previous studies on GHG emissions from peatlands and forests will be discussed, with a particular emphasis on the variations between peat soil and mineral soil sites, and how these differences impact emission rates and carbon dynamics.

## 2.1 Greenhouse gases and the global carbon cycle

Greenhouse gases, whether naturally occurring or human-induced, play a crucial role in regulating Earth's climate by absorbing and re-emitting infrared radiation from the plants surface (Figure 1.1 ), thereby contributing to global warming (Jain *et al.*, 2015; Günther *et al.*, 2020; Pörtner *et al.*, 2022). The primary GHGs in Earth's atmosphere, as identified by the IPCC (2022) are water vapour ($H_2O$), carbon dioxide ($CO_2$), methane ($CH_4$), nitrous oxide ($N_2O$) and ozone ($O_3$).

Global assessments show a steady rise in net anthropogenic GHG emissions over recent decades. In 2019, global net emissions were estimated at 59 ± 6.6 Gt $CO_2$-eq, representing a 54% increase from 1990 levels of approximately 32 Gt $CO_2$-eq (IPCC, 2023). Between 1990 and 2023, global anthropogenic GHG levels (excluding LULUCF) increased by about 61.8%, averaging nearly 1.5% growth per year (Crippa *et al.*, 2024). In Europe, total emissions for 2023 were reported at 3.16 Gt $CO_2$-eq, with Ireland contributing an estimated 0.05 Gt $CO_2$-eq during the same period (Crippa *et al.*, 2024).

This study focuses on the two GHGs of greatest concern, $CO_2$ and $CH_4$ which together account for the majority of global emissions. Since pre-industrial times, atmospheric $CO_2$ concentrations have increased by 151%, and $CH_4$ by 265% primarily due to increased fossil fuel combustion, agriculture and land use change (WMO, 2024). In 2023, $CO_2$ accounted for approximately 73.7% of total GHG emissions, while $CH_4$ contributed 18.9%, together representing 92.6% of total emissions (Crippa *et al.*, 2024).

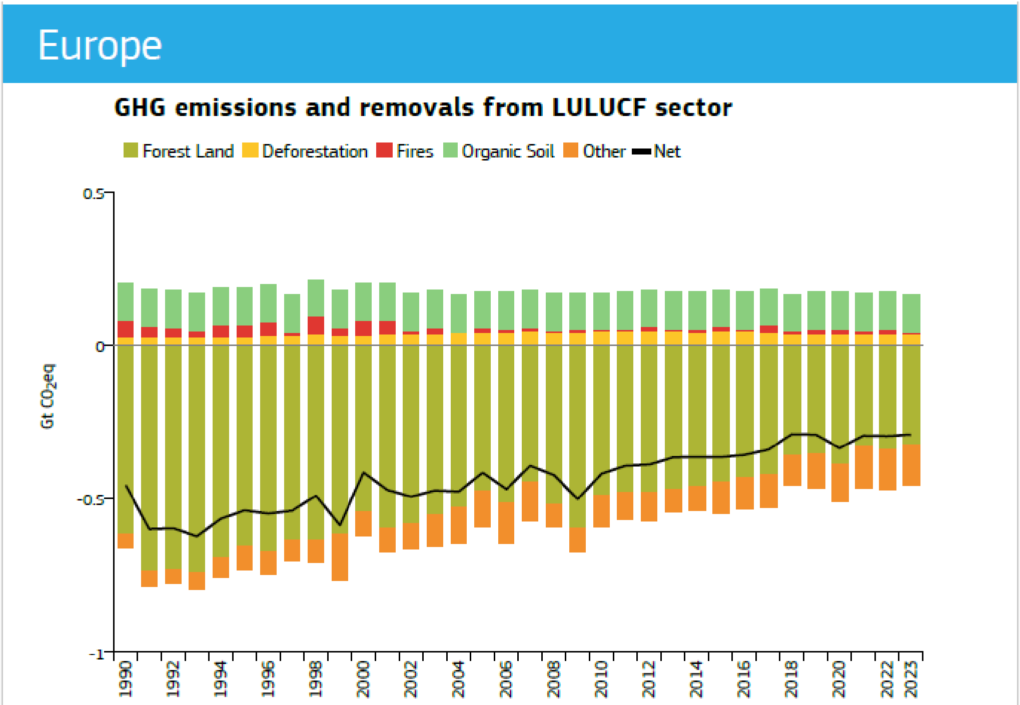


| Year | 1990 | 2000 | 2015 | 2023 |
|---|---|---|---|---|
| Net flux (Gt $CO_2$eq /yr) | -0.455 | -0.414 | -0.363 | -0.290 |

*Figure 2.1 GHG emissions and removals from LULUCF sectors estimates for Europe (Crippa et al. 2024)*

The LULUCF sector is excluded from global emissions estimates, as it represents an overall net carbon sink (Crippa *et al.*, 2024). In Europe, LULUCF also remains a net sink, though it's capacity has weakened, increasing from -0.455 Gt $CO_2$-eq in 1990 to -0.290 Gt $CO_2$-eq in 2023 (Crippa *et al.*, 2024). Figure 2.1 illustrates the contributions of different subsectors within LULUCF, highlighting that forest land acts as the largest carbon sink, removing approximately -0.4 Gt $CO_2$-eq per year. In contrast, deforestation, wildfires, and emissions from organic soils (including peat soil), contribute emissions not removals. Notably, figure 2.1 shows that organic soils play a significant role in the overall net source of emissions within this sector (Crippa *et al.*, 2024).

The IPCC Sixth Assessment Report (2006) defines global warming potential (GWP) as the standard metric for comparing the climate impact of different GHGs over a 100-year period. $CO_2$, with a GWP of 1, serves as the baseline reference gas. Other GHGs, like $CH_4$ and $N_2O$ have higher GWPs due to their greater heat-trapping capacities and longer atmospheric lifetimes. To enable direct comparison, all GHG emissions are expressed as $CO_2$-equivalents ($CO_2$-eq) by multiplying the mass of each gas by its respective GWP value (IPCC, 2023; EPA, 2024).

Emission factors (EFs) quantify the amount of a specific GHG released from an activity, process, or source, typically expressed as emissions per unit of activity. These link the quantity of GHGs to the observed data (e.g., fuel consumed, area of land managed, wastewater treated) (IPCC, 2023; EPA, 2024). EFs are a foundation of national GHG inventory reporting, compiling observed data or modelled data to estimate emissions where direct measurements are unavailable (EPA, 2024). The 2006 IPCC Guidelines introduced a tiered system for EFs to account for regional and sectoral variability (EPA, 2024).

- Tier 1 uses global default factors, suitable when local data are lacking.
- Tier 2 relies on country or region-specific factors that reflect local conditions.
- Tier 3 involves detailed modelling or site-level measurements for the highest accuracy.

Most recent global GHG emissions estimates are derived using IPCC Tier 1 EF's, or where possible Tier 2 values from other sources (Crippa *et al.*, 2024). Previous studies, such as Evans et al. (2017) and Aitova et al. (2023) emphasise the importance of developing region-specific emission factors, particularly for ecosystems like peatlands, to improve inventory accuracy and guide targeted climate mitigation efforts.

Although GWP and EFs are globally recognised metrics, they have limitations. Neither fully captures the dynamic behaviour of GHGs in the atmosphere, including their lifetime and radiative forcing effects. Günther et al. (2020) describe a radiative forcing model that estimates the radiative forcing effects of atmospheric changes in GHG fluxes. The report highlights that $CO_2$ and $N_2O$ act as long-term forcers, whereas $CH_4$ exerts stronger but is a short-term forcer. Consequently, relying solely on GWP-based metrics can oversimplify the true climate impact of emissions and could mislead conclusions drawn from emissions estimates (Günther *et al.*, 2020).

### 2.1.1 Carbon Dioxide

Atmospheric $CO_2$ is a naturally occurring gas central to ecosystem processes and contributes significantly to the Earth's energy balance (IPCC, 2023; EPA, 2024). It is also a major by-product of human activities, making it the most abundant anthropogenic GHG and the standard reference for comparing other GHGs, with a GWP of one (IPCC, 2023; EPA, 2024). In 2023, $CO_2$ accounted for 73.7% of total global GHG emissions (Crippa 2024).

The $CO_2$ molecule consists of one carbon atom (12.01 g/mol) and two oxygen atoms (16.00 g/mol each), giving a molecular mass of 44.01 g/mol (IUPAC and Chemistry, 2022). It is linear in structure (O=C=O), and its vibrational modes strongly influence its infrared absorption properties. $CO_2$ molecules absorb radiation through specific vibrational motions, including an antisymmetric stretching vibration (~4.27 µm) and a bending vibration (~15.2 µm), which underpin its role in radiative forcing and climate warming (Baranov *et al.*, 2004; Solomon *et al.*, 2010). Importantly, $CO_2$ displays exceptional atmospheric persistence: according to Solomon et al. (2010), a sizeable fraction of emitted $CO_2$ remains in the atmosphere for centuries to millennia, with some models estimating that 20-60% of a pulse of fossil-fuel $CO_2$ may persist for over 1,000 years. This long atmospheric lifetime is a critical factor when assessing GHG emissions from peatlands, as the balance between $CO_2$ uptake and release can have long-term climate impacts (Günther *et al.*, 2020; Wilson *et al.*, 2022).

### 2.1.2 Methane

Although $CH_4$ is a naturally occurring GHG, is also produced by human activities such as agriculture, fossil fuel extraction, and waste management (IPCC, 2023). Though it is less abundant than $CO_2$, $CH_4$ has a much higher radiative efficiency, trapping significantly more heat per molecule over its atmospheric lifetime (Allen *et al.*, 2018). Over a 100 year period, $CH_4$ is assigned a GWP, 28 times that of $CO_2$ (IPCC, 2024). It is also a precursor of tropospheric ozone, which poses a health risk to all life on Earth (WMO, 2022). In 2023, $CH_4$ accounted for approximately 18.9% of total global GHG emissions (Crippa *et al.*, 2024).

The $CH_4$ molecule consists of one carbon atom (12.01 g/mol) bonded to four hydrogen atoms (1.008 g/mol each), giving a molecular mass of 16.04 g/mol (IUPAC, 2022). Its molecular structure and strong C–H bonds allow $CH_4$ to absorb infrared radiation efficiently, particularly through asymmetric stretching and bending vibrations that contribute to its GHG properties (Allen *et al.*, 2018). Unlike $CO_2$, $CH_4$ has a relatively short atmospheric lifetime, averaging 12 years (IPCC 2023), yet its high radiative forcing per molecule makes it a critical contributor to near-term climate warming (Solomon *et al.*, 2010; Günther *et al.*, 2020; Crippa *et al.*, 2024).

In the context of peatlands, $CH_4$ emissions arise primarily from anaerobic decomposition under waterlogged conditions and are strongly influenced by water table depth, vegetation type, and microbial activity (Solomon *et al.*, 2010; Rigney *et al.*, 2018; IPCC, 2023). Rewetting drained peatlands can increase $CH_4$ emissions due to anaerobic decomposition under waterlogged conditions, creating a trade-off with $CO_2$ reductions from restored carbon sequestration (Allen *et al.*, 2018; Günther *et al.*, 2020; Wilson *et al.*, 2022). Because $CH_4$ has a much greater radiative efficiency than $CO_2$, even small fluxes can substantially affect overall radiative forcing (Allen et al., 2018; Wilson et al., 2022).

The balance between $CO_2$ and $CH_4$ fluxes on radiative forcing is highly site-dependent (Wilson et al., 2022). Studies have shown that afforestation on nutrient-rich peatlands can enhance $CO_2$ sequestration and reduce net radiative forcing (cooling effect), while nutrient-poor sites may continue to exhibit net warming (Lohila *et al.*, 2011). Wilson et al. (2022) found that rewetting can rapidly shift drained peatlands from carbon sources to sinks, though elevated $CH_4$ emissions may initially offset gains. These findings highlight the importance of considering both gases and local conditions when assessing climate mitigation potential.

### 2.1.3 Nitrous Oxide

Although $CO_2$ and $CH_4$ are the dominant GHGs associated with peatlands (Abdalla et al., 2016; Kiely, 2019; Wilson et al., 2016; Aitova, 2023; Rigney et al., 2018), $N_2O$ can also be associated with an emission from some peatlands (IPCC, 2013). $N_2O$ is a simple linear molecule composed of two nitrogen atoms and one oxygen atom (N–N–O) (Allen et al., 2018; IUPAC, 2022). In natural peatlands, $N_2O$ is generally a minor GHG compared to $CO_2$ and $CH_4$, because waterlogged conditions suppress the microbial processes (nitrification and denitrification) that produce it (Abdalla et al., 2016; Wilson et al., 2016; IPCC, 2013).

$N_2O$ emissions can increase if peatlands are drained, fertilised, or otherwise managed, as these conditions enhance nitrogen availability and microbial activity (EPA, 2024; IPCC, 2013). Otherwise, in intact or rewetted peatlands, $N_2O$ is typically negligible. Previous studies of carbon dynamics in forested peatlands in Ireland and Scotland also reported low emissions of $N_2O$ (Yamulki *et al.*, 2013).

### 2.1.4 Ireland's land use and land use change GHG emissions

Ireland's National Inventory Report (NIR) (EPA, 2024), provides a detailed breakdown of GHG emissions from 1990 to 2022 (Figure 2.2). In 2022, $CO_2$ accounted for 60.6% of Ireland's total 60,604.9 kt $CO_2$-eq emissions (excluding LULUCF), with $CH_4$ contributing 29.1% and $N_2O$ accounting for 9.1%. More recently, Crippa (2024) suggest that in 2023, $CO_2$ made up 56.1% and $CH_4$ approximately 30.4% of total national emissions, again excluding LULUCF emissions/removals

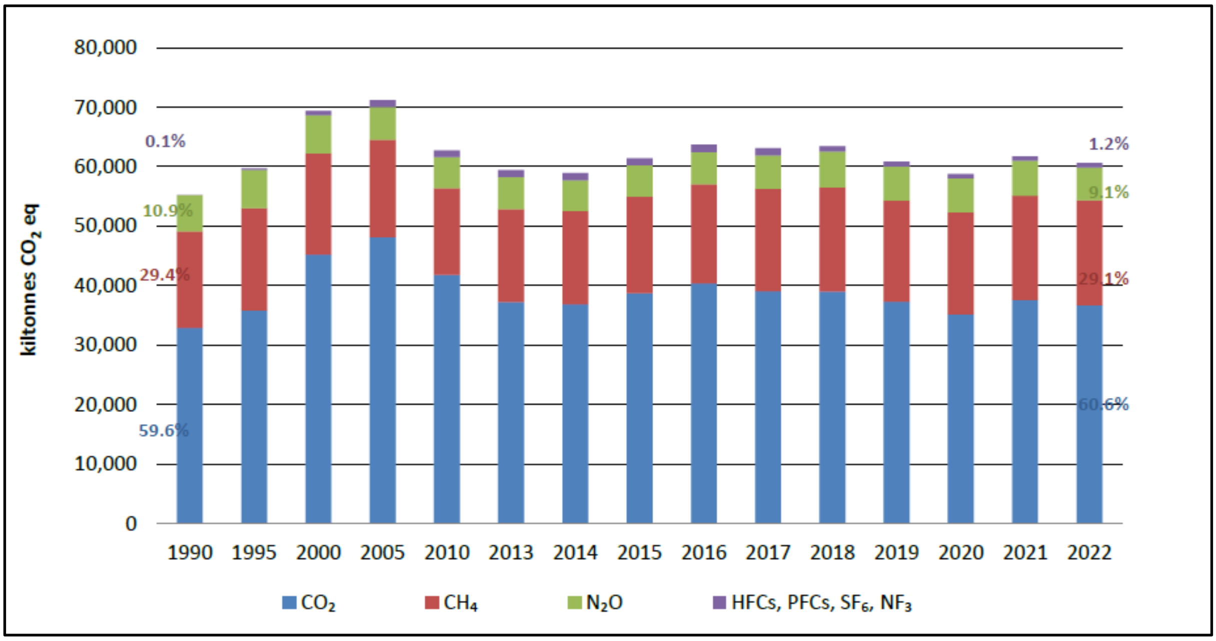


*Figure 2.2 GHG emissions breakdown estimates from 1990-2022 from NIR (EPA 2024)*

According to the NIR, $CO_2$ remains the dominant contributor to Ireland's GHG emissions. In 2022, the energy industry and transport sectors were responsible for 26.9% and 31.6% of total $CO_2$ emissions, respectively, while other sectors contributed 21.5%, manufacturing and construction 11.7%, and the remaining 8.3% came from miscellaneous sources. $CH_4$ is the second-largest GHG emitted in Ireland, primarily linked to agriculture (EPA, 2024). In 2022, $CH_4$ emissions totalled 17,658.2 kt $CO_2$ eq, an 8.8% increase from 1990. Agriculture was responsible for 94.4% of $CH_4$ emissions in 2022, up from 86.2% in 1990. in contrast $CH_4$ emissions from waste decreased from 9.1% in 1990 to 3.6% in 2022, due to improved landfill management and gas recovery for electricity generation (EPA, 2024).

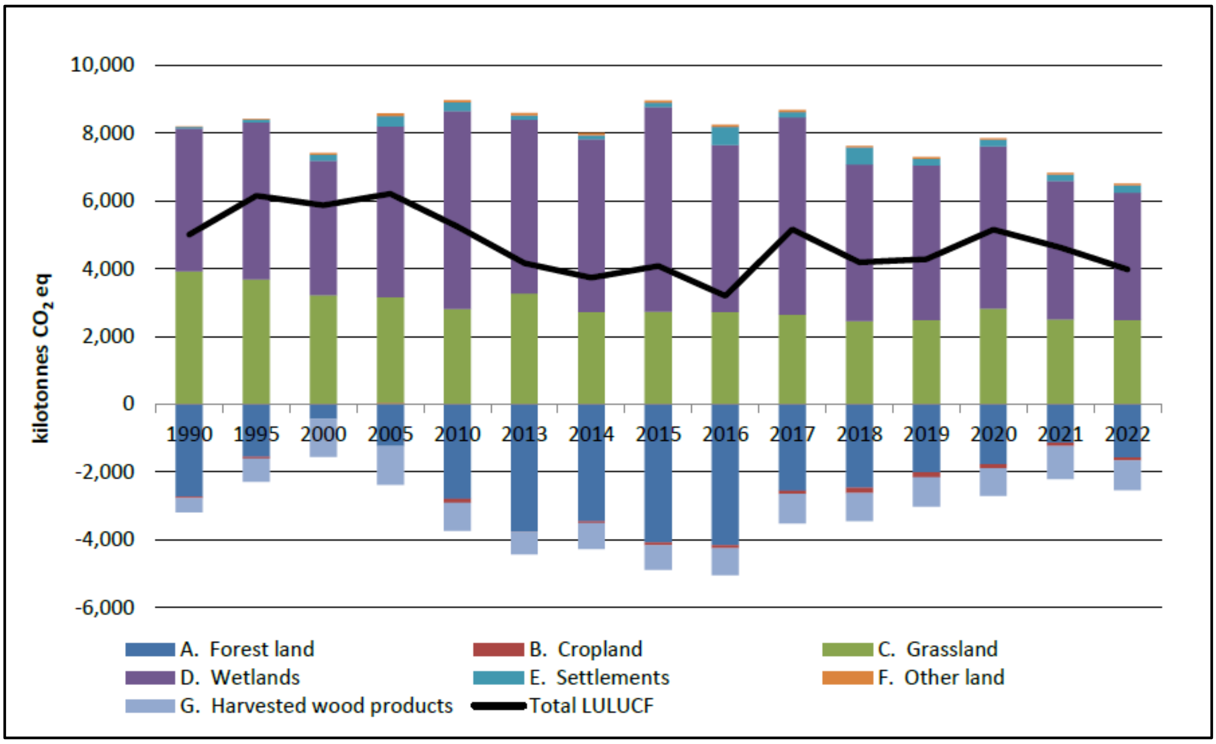


*Figure 2.3 GHG estimated for LULUCF Ireland 1990-2022 from NIR (EPA, 2024).*

While global and European estimates for LULUCF sectors as act as a net sink for GHGs (Crippa *et al.*, 2024), Ireland's LULUCF sector remains a net source (EPA, 2024). Figure 2.3 represents the breakdown of these LULUCF emissions, showing the varying contributions of different land-use categories. The net source in all years is primarily driven by emissions from grasslands and wetlands, resulting from soil drainage and fertiliser use, whereas forests serve as a carbon sink (EPA, 2024).

Given that wetlands and forests are the primary LULUCF categories relevant to this research, they are examined in greater detail in the following sections. A recent study by Habib et al. (2024) applied remote sensing and machine learning to estimate GHG emissions from Irish raised peatlands, covering four key land use types: cutover, cutaway, forestry, and grassland. Together these categories cover approximately 85% of Ireland's raised peatland area. Based on Tier 1 and Tier 2 IPCC emission factors, the estimated emissions were around 1.92 Mt $CO_2$-eq $yr^{-1}$ and 0.68 Mt $CO_2$-eq $yr^{-1}$, respectively (Habib *et al.*, 2024).

## 2.2 Key biological processes affecting ecosystem carbon exchange

### 2.2.1 Plant respiration

Respiration is the biochemical process by which carbohydrates, are oxidised to release usable energy required for essential cellular functions such as ion uptake, and repair, with $CO_2$ as a principal by-product (Ryan, 1991). Respiration rates are strongly controlled by environmental drivers such as temperature, WT, $CO_2$ and oxygen availability (Ryan, 1991). Warmer temperatures and lower WTs usually accelerate the rate of respiration by increasing metabolic rates and oxygen diffusion (Wilson *et al.*, 2015; Wilson, Farrell, *et al.*, 2016). Both plant respiration and root respiration are referred to as autotrophic respiration ($R_a$) (Waring and Running, 2007). Plant respiration is tightly coupled to the amount of energy rich chemical compounds (glucose) produced from the process of photosynthesis, hence, plant respiration and photosynthesis are closely linked (Begon *et al.*, 1996). Approximately half of the chemical compounds produced from gross primary production (GPP) are utilised by plants through respiration for the growth of living cells and the $CO_2$ released during the process can contribute to GHG emissions (Ryan, 1991; Begon *et al.*, 1996). Heterotrophic respiration ($R_h$), the microbial decomposition of organic matter, is a key pathway through which stored soil carbon is returned to the atmosphere as $CO_2$ (Luo & Zhou, 2007; Kirschbaum, 2006) and is discussed in further in section 2.2.3. It is a separate process from $R_a$ but it is included in total ecosystem respiration ($R_{eco}$). Both components of respiration are similarly influenced  by environmental changes, such as variations in the WT (Tuittila *et al.*, 2004).

### 2.2.2 Photosynthesis

Photosynthesis is the process by which chlorophyll in plant cells absorbs solar radiation and converts it into organic carbon compounds. These compounds provide energy required for the plant to produce new biomass (Luo and Zhuo, 2007). Radiation from blue and red wavelengths on the electromagnetic spectrum supplies the energy needed for photosynthesis reactions. The efficiency of this process also depends on the WT, vegetation type, soil pH, temperature, $CO_2$ levels and the levels of solar radiation (Begon *et al.*, 1996). The WT influences photosynthesis in two key ways: first by regulating $CO_2$ uptake through stomatal conductance, and secondly, by altering the vegetation structure, which in turn affects leaf area available for photosynthesis. A high WT can restrict oxygen availability to roots, limiting plant growth (Tuittila *et al.*, 2004). The total amount of organic compounds or energy produced through the process of photosynthesis is referred to as Gross Primary Production (GPP) (Begon *et al.*, 1996).

Photosynthesis is powered by radiation in the 400 to700 nm wavelength range, which is absorbed by the leaf area and is also known as photosynthetically active radiation (PAR) (Tsubo and Walker, 2005). PAR is the primary energy source for plants to drive photosynthetic reactions and convert solar energy into chemical energy stored in organic compounds (Tsubo and Walker, 2005). Photosynthetic photon flux density (PPFD) quantifies the number of photons in this wavelength range incident per unit area per unit time, expressed in units of µmol $m^{-2}s^{-1}$. PAR is used to measure PPFD in order to identify the intensity of the photosynthetic fluxes (Yamashita and Yoshimura, 2019). Throughout the carbon cycle $CO_2$ is released back into the air through $R_a$ as described in the previous section 2.2.1, but it is simultaneously captured and stored through GPP (Luo and Zhuo, 2007).

Peatlands in their natural state have low pH levels (3-5), which can limit photosynthetic activity by reducing the availability of essential nutrients for plant growth. Among peatland types, active fens generally exhibit higher photosynthesis rates compared to active raised peatlands, due to their higher pH and greater nutrient availability (Bubier *et al.*, 1998; Frolking *et al.*, 1998). Within raised peatland vegetation, deciduous species such as certain sedges and shrubs often show high photosynthetic rate during early stages of leaf development, but as the canopy matures, leaf tissue ages and photosynthesis becomes saturated and gradually declines (Wehr *et al.*, 2016). In contrast evergreen species found in peatlands, such as *sphagnum mosses*, can maintain photosynthetic activity year round, provided the environmental conditions are appropriate, such as light and temperature are suitable (Bubier *et al.*, 1998).

### 2.2.3 Soil respiration and decomposition

Soil respiration refers to the process of aerobic decomposition, whereby micro-organisms break down decaying biomass and other organisms living within the soil, converting them into $CO_2$ and other chemical components (Luo and Zhuo, 2007). Total soil respiration includes heterotrophic respiration ($R_h$) from microbes and root respiration from $R_a$ . $R_h$ represents $CO_2$ released from microbial decomposition, while $R_a$ reflects $CO_2$ produced by living roots during metabolic activity (Kirschbaum *et al.*, 2001). Rhizosphere processes can also enhance peat soil respiration by stimulating microbial decomposition in the root zone. Root exudates and rhizodeposition increase microbial activity and accelerate the mineralisation of soil organic matter, leading to higher $CO_2$ emissions where vegetation is present (Kuzyakov, 2010). In afforested peatlands, deeper root systems may further intensify these effects by expanding the volume of peat influenced by root activity, although this process is less well documented than in mineral soils. On average, root respiration accounts for about 50% of total soil respiration, though estimates can vary significantly between 10% to 90% depending on factors such as plant species, growth stage, and seasonal changes in temperature and moisture availability (Bubier *et al.*, 1998; Hanson *et al.*, 2000). Research suggests that 90% of the total soil respiration occurs within the top 30cm of the soil surface, where root and microbial activity are concentrated (Goffin *et al.*, 2015).

In Irish afforested peatlands, severing roots to a depth of just 5 cm led to underestimations of total soil respiration by 32–47%, highlighting the significance of shallow root respiration (Jovani-Sancho et al., 2017). Understanding soil respiration is critical for assessing $CO_2$ fluxes and GHG emissions from ecosystems (Luo and Zhuo, 2007; Jovani Sancho et al., 2017; Jovani-Sancho et al., 2021). Soil $CO_2$ efflux, measured at the surface, reflects the combined activity of $R_a$ and $R_h$ (Luo and Zhuo, 2007).

#### *2.2.3.1 Peat soil respiration*

Peat soils differ from mineral soils due to their high organic content and water saturation under pristine conditions (Feehan and O'Donovan, 1996; Renou-Wilson *et al.*, 2022). Unlike mineral soils, which tend to support rapid aerobic decomposition due to greater aeration and higher mineral nutrient availability, peat soils are typically waterlogged, acidic, nutrient-poor and oxygen-limited, resulting in reduced microbial activity and slower rates of organic matter decomposition (Laiho, 2006). As a consequence, baseline rates of $R_h$ and therefore $CO_2$ release are substantially lower in intact peatlands compared to drained peat soils or mineral soils.

Peat soil respiration is strongly regulated by soil temperature and WT depth, both of which influence microbial activity and substrate accessibility (Jovani-Sancho *et al.*, 2018). According to Jovani-Sancho et al. (2018) soil respiration in an afforested peatland was influenced by the change in soil temperature and the WT. In their report the impact that the

WT had on soil was reliant on the temperature, and the soil respiration rates reacted to the variation in both the WT and temperature. If conditions became too dry or too wet, there was a direct impact on the soil $CO_2$ emissions.

Multiple studies have shown that a higher WT suppresses decomposition by restricting oxygen diffusion into the peat therefore reducing soil respiration and reducing $CO_2$ emissions. When conditions were reversed with lower water levels that dried out soil conditions, $CO_2$ emissions were higher (Laine, 2006; Kiely *et al.*, 2009; Yamulki *et al.*, 2013). The lower WT was found to have a cut off point for increasing soil respiration at 30 cm (Tuittila *et al.*, 2004). Similar patterns have been observed elsewhere in Europe: for example, Peichl et al. (2014) reported that an intact Swedish peatland shifted from a strong $CO_2$ sink to a weaker sink, when the WT dropped below 20cm. This indicates the WT respiration relationship is consistent across peatland types and regions including Irish peatlands and also in other parts of Europe.

#### *2.2.3.2 Anaerobic decomposition*

Although soil respiration primarily releases $CO_2$, via aerobic microbial pathways, anaerobic conditions in saturated peatlands also supports the release of $CH_4$ emissions. The production and release of $CH_4$ emissions from rewetted or near-intact peatlands are closely tied to WT and the anaerobic decomposition processes that occur in saturated peat soils (Denman *et al.*, 2007; Turetsky *et al.*, 2014). In these saturated peatlands there is limited oxygen available and aerobic respiration is supressed favouring anaerobic microbial communities. While active peatlands sequester $CO_2$ through long term peat accumulation, , they can simultaneously act as natural sources of $CH_4$ (Feehan and O'Donovan, 1996; IPCC, 2013, 2024; Holl *et al.*, 2020).

Methane emissions are closely linked to the WT depth, remaining negligible when the WT is more than 20cm below the surface but increasing significantly as it rises (IPCC, 2013; Holl *et al.*, 2020; Wilson *et al.*, 2022). As the WT rises and anoxic conditions expand upward, methanogenic activity increases and $CH_4$ emissions rise correspondingly (IPCC, 2013; Abdalla *et al.*, 2016). A review of degraded northern peatlands found average $CH_4$ emissions of 12 ± 21 g C $m^{-2}$ $yr^{-1}$. With rewetting increasing emissions by 46%, suggesting that raising the WT can enhance $CH_4$ production, although with high uncertainty in the results (Abdalla *et al.*, 2016). A more recent study by Wilson et al. (2022) observed low $CH_4$ emissions from a drained peatland averaging 0.5 g C $m^{-2}$ $yr^{-1}$ over the five-year study period. The rewetted peatlands showed higher $CH_4$ emissions averaging 19.3 g C $m^{-2}$ $yr^{-1}$ in the same period (Wilson *et al.*, 2022).

At a microbial level, $CH_4$ cycling in peatlands is controlled by two main groups, methanogens and methanotrophs. Methanogens produce $CH_4$ in anaerobic conditions, waterlogged conditions, using compounds like $CO_2$, hydrogen or acetate. In contrast, methanotrophs consume $CH_4$ in the oxygenated layers of peat, reducing the amount that reaches the surface or atmosphere. The balance between methanogenesis and methanotrophs determines net $CH_4$ emissions and can shift rapidly with changes in WT, temperature, or vegetation composition (Oh *et al.*, 2022).

Once produced, $CH_4$ is released through several transport pathways. Diffusion allows $CH_4$ to move through soil layers, though some is oxidised to $CO_2$ in areas where oxygen is rich (Oh *et al.*, 2022). Ebullition is the release of $CH_4$ gas bubbles that accumulate in soil pores and rise to the surface. This process accounts for the majority of $CH_4$ emissions from intact peatlands (Whalen, 2005; Oh *et al.*, 2022). Additionally, vascular plants can alter $CH_4$ transport via aerenchyma tissues in vegetation, which create low-resistance pathways for $CH_4$ movement and can significantly enhance emissions (Oh *et al.*, 2022; Wilson *et al.*, 2022).

Vegetation type therefore strongly modulates $CH_4$ emissions, as plant structure and root activity influence both WT conditions and gas transport pathways (Le Mer and Roger, 2001; Whalen, 2005; IPCC, 2013; Holl *et al.*, 2020). This underscores the complex relationship between WT management and GHG emissions in peatlands, indicating that while rewetting restores hydrological functioning and peat accumulation potential, it can also lead to, higher $CH_4$ emissions depending on vegetation community, WT position, and microbial activity.

#### 2.2.4 Dissolved and Particulate Organic Carbon Losses

In addition to atmospheric emissions, peatlands also lose carbon through the export of DOC and POC, both of which represent significant pathways of carbon loss. DOC originates from the oxidation and partial decomposition of organic matter and vegetation, as well as from hydrological mobilisation and erosion processes (Dillon and Molot, 1997; Palmer *et al.*, 2001; Battin *et al.*, 2009; Dieleman *et al.*, 2016; Evans *et al.*, 2017). POC consists of larger, physically eroded peat particles transported during runoff or soil disturbance (Dillon and Molot, 1997).

These forms of carbon are important because once DOC and POC enter streams, rivers, or drainage networks, they contribute indirectly to off-site $CO_2$ and $CH_4$ emissions. DOC is readily decomposed by aquatic microbes into $CO_2$, meaning that carbon lost from peat soils ultimately re-enters the atmosphere downstream (Evans et al., 2017). Similarly, POC can be mineralised during transport or deposition. In slow-moving waters, both DOC and POC may accumulate in sediments, where they can alter nutrient ratios and negatively affect water quality (Dillon and Molot, 1997).

DOC and POC losses occur in both drained and rewetted peatlands, although the processes differ: drainage promotes oxidation and DOC formation, while high water tables favour hydrological flushing of DOC-rich porewater. Regardless of the pathway, these losses represent an important component of peatland carbon budgets, as they transport carbon away from the soil system and contribute to catchment-scale GHG emissions (Evans *et al.*, 2017).

## 2.3 Methods for quantifying ecosystem-atmosphere gas exchange

Two widely used ground-based approaches for quantifying carbon exchange in terrestrial ecosystems are the chamber method and the Eddy Covariance (EC) technique (Frolking *et al.*, 1998; Burba, 2013; Wilson, Farrell, *et al.*, 2016; Hambley *et al.*, 2019). The EC method is particularly effective for capturing continuous carbon fluxes between ecosystems and the atmosphere over long time periods, typically a full annual cycle or more (Baldocchi, 2003; Tuittila *et al.*, 2004; Burba, 2013). However, EC measurements integrate fluxes over large areas and do not readily separate soil respiration from plant respiration, with both processes generally combined as $R_{eco}$ (Griffis *et al.*, 2000; Laine, 2006). In contrast, the chamber-based measurements allows direct quantification of soil respiration by enclosing small areas of the soil surface and measuring gas exchange under controlled conditions (Waring and Running, 2007). Such plot-scale measurements are particularly valuable for disentangling below-ground carbon processes, but they lack the temporal continuity provided by EC systems (Wilson *et al.*, 2015; Wutzler *et al.*, 2018)

Because peatland carbon dynamics exhibit substantial interannual variability, driven largely by fluctuations in temperature, precipitation, and water table depth, robust monitoring requires both reliable measurement approaches and appropriate strategies for dealing with flux time-series data (Lafleur *et al.*, 2003). Accordingly, this chapter examines EC and chamber methods in detail and evaluates contemporary approaches for gap filling and modelling flux datasets, including both traditional environmental-response models and emerging machine-learning techniques.

### 2.3.1 Eddy covariance methodologies

#### *2.3.1.1 Underpinning concepts of Eddy covariance*

The EC method is based on a micrometeorological process, that effectively estimates flux measurements between a terrestrial ecosystem and the atmosphere. By simultaneously measuring changes in wind and gas concentration from the atmosphere, flux computation can be estimated for a desired ecosystem (Baldocchi, 2003, 2014; Tuittila *et al.*, 2004; Burba, 2013). By doing this the data collected can be processed and allow researchers to determine the overall uptake or loss of carbon and other gases from an ecosystem. The method has assisted scientists in distinguishing trends in GHG emissions and climate change across the globe (Baldocchi *et al.*, 2001; Baldocchi, 2003, 2014; Tuittila *et al.*, 2004; Burba, 2013). In comparison to other micrometeorological methods, EC is considered to be a useful method to implement when researching peatlands in particular and when monitoring emissions on a continuous basis (Poyda *et al.*, 2017). FLUXNET is a network that was established to examine flux data from across the globe, advances in EC techniques have allowed them to demonstrate how different ecosystems vary in levels of GHG emissions (Baldocchi *et al.*, 2001). The EC method has been in use since around the 1980's and is widely used across the globe today. This is due to improvements in instruments accuracy and the ability to take long term quasi-continuous observations with little disturbance to the surrounding area or vegetation (Baldocchi, 2014; Hambley *et al.*, 2019; Zhu *et al.*, 2023).

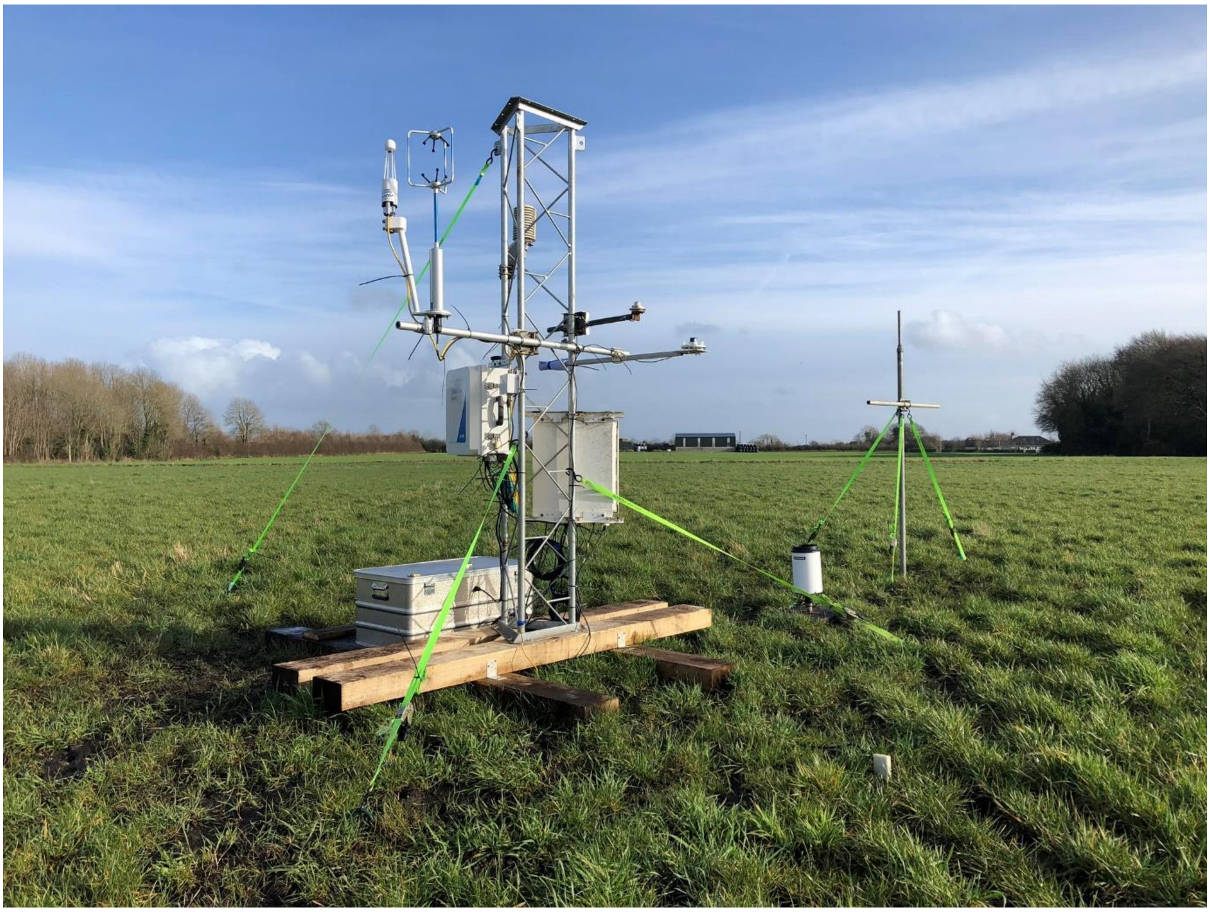

*Figure 2.4 Eddy covariance system, monitoring $CO_2$ fluxes from a grassland on peat soils, located at Lullymore Kildare Ireland (photo: author).*

Figure 2.4 illustrates a fully operational EC tower setup, designed to monitor $CO_2$ emissions from a grassland situated on peat soils. To correctly understand the concept of the EC method it is important to understand the different layers contained within the atmospheric boundary layer from where the EC instruments take measurements (Stull, 1988; Burba, 2013). The atmospheric boundary layer (ABL) consists of the lower part of the troposphere, the ABL and the earth's surface have a perpetual synergy due to frictional drag and shifting warm and cool temperatures. The depth of the ABL varies in time and space, ranging from hundreds of meters to tens of kilometres (Stull, 1988).

The land surface of the earth warms in response to absorption of solar radiation, this creates a degree of diabatic heating which results in rising columns of air. This warmer air or thermals, push the ABL upward increasing its size. This warmer air decreases in temperature as it rises leading to thermal mixing and therefore creates unstable conditions, this is more prominent throughout the daytime (Stull, 1988; Kaimal and Finnigan, 1994). At night-time land surface temperatures reduce thus cooling air temperature, leading to a reduction in the depth of the ABL, this normally creates more stable conditions (Stull, 1988; Kaimal and Finnigan, 1994). The depth of the ABL is also dependent on surface roughness for example non-homogeneous terrain, such as forests, generally have a deeper ABL as they have more frictional drag in the canopy leading to increased turbulent flow. With these fluctuating air temperatures and surface roughness, turbulent motions in the ABL continuously rise and fall generating turbulence (Kaimal and Finnigan, 1994). Turbulence consists of irregular swirls of motion, and these are referred to as eddies (Stull, 1988). The eddies are unstable entities losing energy as they make contact with surfaces and other eddies, gradually becoming smaller in size until viscosity can convert their kinetic energy into heat. Thus as a result of these instabilities eddies are mostly responsible for the transport in turbulence (Kaimal and Finnigan, 1994).

The atmospheric boundary layer (Illustrated in Figure 2.5) can be divided into sub sections, and each section or layer has different characteristics. For this research two layers are focused on, the inner layer closest to the earth's surface known as the surface layer (SL) (Kaimal and Finnigan, 1994) and the layer that lies above this which is referred to as the Boundary layer (BL) (Stull, 1988). The surface layer is not directly influenced by the earth's rotation, it is a relatively stable layer with turbulence largely influenced by frictional drag and temperature fluctuations from the earth's surface (Kaimal and Finnigan, 1994). Although vertical wind direction in this layer can vary logarithmically with height, the vertical fluxes can be considered constant over time (Dabberdt *et al.*, 1993). The boundary layer is unstable with turbulence influenced by frictional drag and fluctuating temperatures and by the Earth's rotation (Stull, 1988; Kaimal and Finnigan, 1994). The free atmosphere is the layer above both of these layers that is no longer influenced by the surface friction and is mainly affected by the earth's rotation (Kaimal and Finnigan, 1994). The SL is the layer of most significance to this study as it is the layer in which GHG emissions become trapped in (Stull, 1988) and therefore the eddy covariance measurements must be taken from within this layer. In the lower SL vertical wind speed increases but becomes constant moving further upwards from the surface, therefore wind speed fluctuation in the upper surface layer is so small it is assumed that it is constant and in EC terms this is referred to as the constant flux layer. The gas transfer in the constant flux layer within the surface layer is dominated by turbulence mixing from eddies (Aubinet *et al.*, 2012). Eddies can be detected by high-frequency measurement instruments on the EC tower (Burba, 2013). The instruments on the tower monitor the movement of the eddies and the concentration of gases simultaneously within the SL (Baldocchi *et al.*, 1988; Burba, 2013). From there a spatially representative estimation of flux density measurements between the land and the atmosphere for a specific area can be established (Baldocchi *et al.*, 1988; Schmid, 1994; Falge *et al.*, 2001; Baldocchi, 2003, 2014; Burba, 2013).

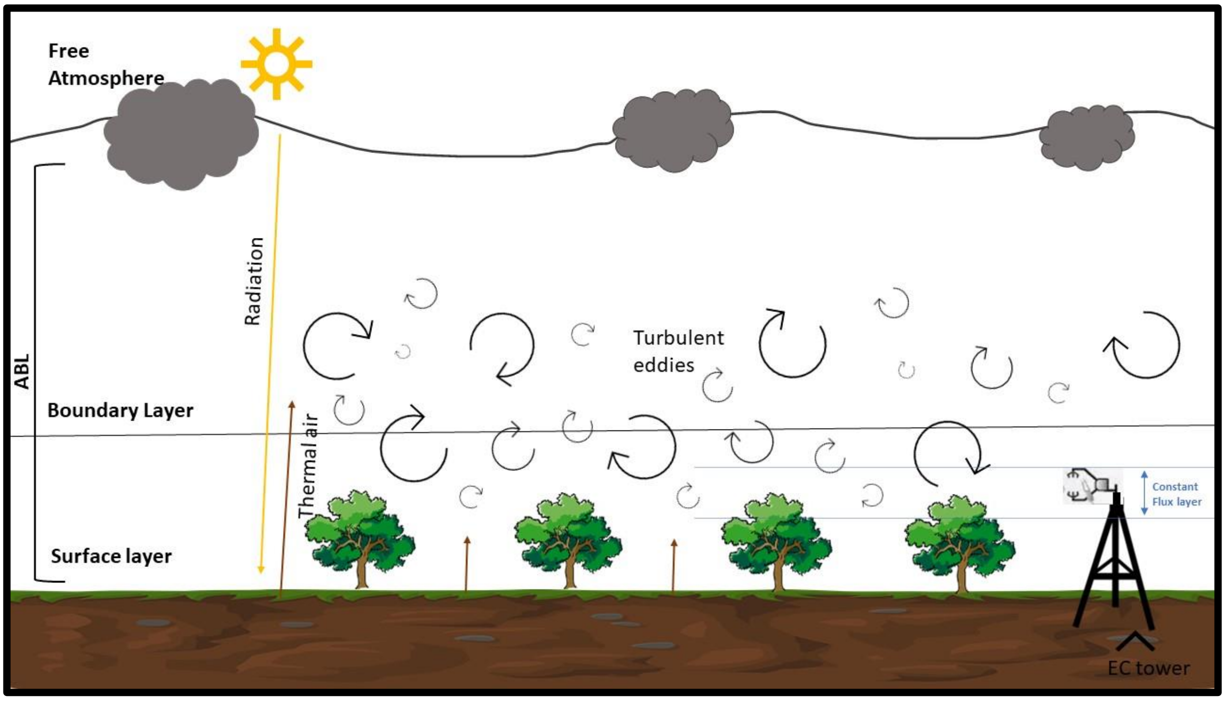


*Figure 2.5 A schematic of the atmospheric boundary Layer in daylight conditions over homogeneous woodland terrain (photo: author).*

Flux can be defined as an amount of entity passing through a unit of area per unit of time and can vary depending on the number of objects, size of the area being crossed and the time it takes for the objects to pass through the area (Burba, 2013). The eddy flux is calculated from the measure of gas concentration through a defined volume over a given time (PP Systems, 2013) (*Equation 2.1*).

*Equation 2.1*

$$Flux = < w'C' >$$

Where w' represents the fluctuation of the vertical wind speed and C' is the fluctuation of the gas of interest's concentration. Figure 2.7 visualises this concept of $CO_2$ flux. The box in

Figure 2.6 represents the known area, and the movement of eddies is measured over time. The $CO_2$ flux is represented by the amount of $CO_2$ that is transported away from the area by the eddies during the observation period.

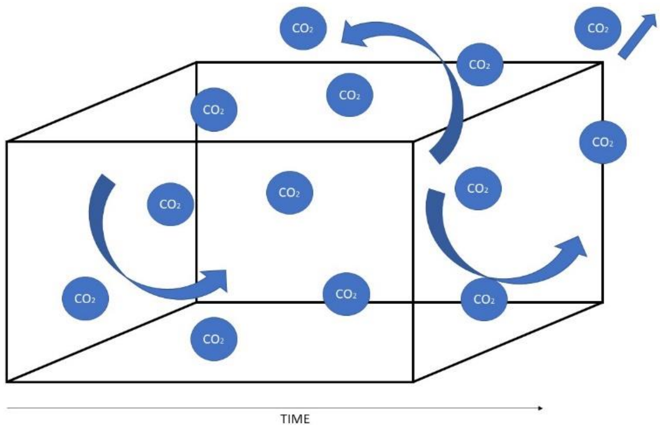


*Figure 2.6 Diagram representing the eddy flux concept for $CO_2$ (photo: author).*

Taking measurements approximately 10 times per second or more, over half hourly intervals is necessary to capture the fast-moving eddies and gas exchange. This allows the computation of the average flux density of the gas exchanged between the biosphere and atmosphere. By assimilating these quasi-continuous and half hourly averages, long term estimations of the gas of interest can be established for an ecosystem (Baldocchi *et al.*, 1988, 2001). The mean air temperature, mean humidity, mean pressure, and PAR (photosynthetically active radiation) are also necessary to compute gas flux measurements. These variables are used for unit conversions and to apply necessary corrections to the data (Burba, 2013). There is an assumption of horizontal homogeneity (Kaimal and Finnigan, 1994) which becomes problematic in heterogeneous terrain such as woodlands. Variations in vegetation structure can disrupt airflow and lead to spatial differences in the depth of the ABL (Stull, 1988).

*Figure 2.7 Eddy covariance tower on study site for this research, Lullymore Kildare Ireland (photo: author)*

To collect a continuous time series of measurements from an ecosystem using the EC method, an EC tower is erected at the location of interest (Figure 2.7 shows an EC tower structure designed for woodland habitat), known as an eddy covariance tower. The EC tower is equipped with instruments that take high-frequency measurements to estimate gas fluxes, including infrared gas analysers (IRGA) and a 3-D sonic anemometer (Fowler *et al.*, 1995; Baldocchi *et al.*, 2012; Burba, 2013).

### 2.3.1.2 Open path infrared gas analyser

There are various types of infrared gas analysers that have been installed on EC towers to monitor gas concentrations at high frequency from the atmosphere. They are differentiated by the technique that is used by the sensors sample air, whether it's through an 'open' or 'closed' path. The open path gas analysers ($CO_2$ IRGA Figure 2.8) have certain advantages compared to the closed path analyser. As the name suggests it has an open-air design, this means that there is little disturbance to air flow while the instrument is sampling, minimising spectral attenuation and therefore requiring less corrections (Polonik *et al.*, 2019) . With its open-air design, it is also easier to carry out regular maintenance on the sensor while in situ. However, a disadvantage of the open design, means precision is compromised when there is accumulation dirt and dust and when the analyser is monitoring gas concentrations during precipitation (Baldocchi, 2003).The Closed-path analysers, which draw air samples into a sealed analyser, are less sensitive to environmental conditions like precipitation (Polonik *et al.*, 2019). However, they have time delays compared to sonic anemometers, requiring more corrections, and consume more power due to the inbuilt pump. Maintenance is also challenging while in situ (Burba, 2013). Despite these differences a study carried out comparing sensor types found all sensors to be successful in measuring $CO_2$ and $H_2O$ concentrations, providing that the appropriate corrections are applied, and data is filtered from flow distorted wind directions (Polonik *et al.*, 2019).In addition to $CO_2$ flux measurements, trace gas analysers such as the Li-7700 (Figure 2.8) can also be integrated into EC systems to quantify $CH_4$ fluxes using the same principles of high-frequency concentration and turbulence measurements. These instruments enable direct, continuous monitoring of $CH_4$ exchange. Previous studies using the Li-7700 $CH_4$ analyser highlight that although data is continuously collected from sites, it is a trace gas analyser highly sensitive to weather conditions leading to gaps in timeseries (Abdalla et al., 2016; Rigney et al., 2018). Various methods and models have been applied to fill the data gaps that occur in the time series (Abdalla et al., 2016; Rigney et al., 2018; Holl et al., 2020; Kim et al., 2020). Although gaps are persistent in the timeseries using this analyser, they are generally smaller compared to the chamber method, which consists of spot samples as opposed to continuous measurements. Studies using the EC method to monitor $CH_4$ exchange from ecosystems such as wetlands and rice paddies have shown that it is a highly effective approach for capturing continuous $CH_4$ fluxes. These findings highlight that EC, when supported by appropriate gap-filling approaches including machine-learning methods, is a robust and reliable technique for quantifying $CH_4$ exchange at the ecosystem scale (Kim et al., 2020; Holl et al., 2020).

*Figure 2.8 Li-Cor 7500 $CO_2$ IRGA*

### *2.3.1.3 The eddy covariance footprint*

The footprint is a term used to describe the area upwind from the EC tower where the meteorological instruments essentially take vertical flux measurements from. The footprint estimations can vary depending on a combination of the measurement height, the vegetation cover, roughness of the surface, and the stability of the ABL. The longitudinal dimension of the estimated footprint (distance from the anemometer to the perimeter line of the footprint) is generally referred to as the fetch (Baldocchi and Vogel, 1996; Kljun *et al.*, 2004, 2015; Burba, 2013).

In earlier years accurately determining flux footprint across a rough surface such as woodland was challenging (Schuepp *et al.*, 1990), as the turbulent fluxes are spatially inhomogeneous up to a certain height in the ABL (Schmid and Lloyd, 1999). The distance between the contribution of the flux and the peak of the footprint increases as the tower's height above the vegetation canopy increases. However, when surface roughness increases, such as over a forest, the flux contribution decreases. The footprint is also influenced by the stability of the ABL, with the flux contribution expanding outward throughout the night when conditions are generally more stable and decreasing in the daytime with more turbulence present (Kljun *et al.*, 2002). The footprint size increases with the height of the tower, smoothness of the surface, and the change from unstable to stable conditions (Schmid and Lloyd, 1999; Burba, 2013). If the height of the tower is low, and surface area rough along with very unstable conditions, the area directly surrounding the tower will make a big contribution to the footprint. Therefore, it is recommended to minimise disturbance to areas surrounding the EC tower to avoid disorder to data collected in this case (Burba, 2013).

There are past models that have been implemented to estimate the flux footprint from EC towers. Based on Horst and Weil's (1992) footprint model, the spatial context of a largely non-homogeneous area was analysed by Schmid and Lloyd (1999). They found using the footprint model that estimations of bias could be made however, suggested using multiple monitoring sites in a large ecosystem allows much more accurate estimations of flux footprint where possible. Although there is potential room for errors on inhomogeneous surfaces, Baldocchi et al (2003) express that measurements from these sites are still valuable.

Before installing an EC tower, the footprint area must be determined, as it influences which ecosystems are measured (Aubinet *et al.*, 2012; Burba, 2013). Previous footprint models, based on the type of ecosystem, were computationally intensive and unsuitable for long-term use (Schuepp *et al.*, 1990; Baldocchi, 2003; Kljun *et al.*, 2004, 2015; Aubinet *et al.*, 2012; Burba, 2022).

Kljun et al. (2015) improved upon these models with a two-dimensional parameterisation for flux footprint prediction (FFP), using a scaling approach for crosswind distribution. This revised model, based on the Lagrangian footprint model by Kljun et al (2004), and can be applied to various measurement heights, boundary stabilities, and roughness lengths. It requires conditions like measurement heights greater than 1m but below the ABL, dynamic terrain, and a friction velocity above a specific threshold. The simple parameterisation accounts for surface roughness, making it quick and accurate for assessing footprint dimensions (Kljun *et al.*, 2015).

Another advantage of estimating accurate FFP is to enhance the quality control and filtering process of analysing the flux data. The ability to exclude or include areas within the footprint is highlighted in a recent study carried out by Holl et al. (2020) using just one EC tower to take measurements from two opposing ecosystem types, which included a recently rewetted site and an actively harvested drained peatland site. The study sites were parallel and divided by a railway dam, allowing researchers to filter sites by placing the EC tower in the center. They effectively measured fluxes from both sites within the EC tower's footprint. By using remotely sensed imagery they could discriminate between three types of land classification including drained, rewetted, and vegetated. Creating these classifications meant that data from undesired areas could be discarded. The authors did highlight that although it was achievable to do this, it did require a thorough amount of filtering data this evidentially led to a reduction in usable data, which in turn gave rise to substantial data gaps in the time series. They concluded that a great deal of additional work was needed to carry out the process of differentiating fluxes from both sites, but none the less it proved to be a successful method (Holl *et al.*, 2020).

#### *2.3.1.4 Eddy covariance gap filling techniques*

##### 2.3.1.4.1 Marginal distribution sampling

Marginal distribution sampling (MDS) is a statistical method commonly used to fill gaps in datasets, particularly those from EC measurements in ecological studies (Pastorello *et al.*, 2020). The model developed by Reichstein et al. (2005) models the relationship between observed and missing data based on a predefined set of drivers or variables, as well as their seasonal and temporal variations. Tolerance levels for each driver are established to ensure that only values within acceptable ranges are used, thus improving the accuracy of the gap-filling process. This method allows estimates for missing flux values to account for the variability and dependencies between the drivers. A coding package called REddyProc, developed by Wutzler et al. (2018) facilitates the integration of standard post-processing with extended analysis. It first utilises a lookup table and, if needed, applies a mean diurnal curve method.

##### 2.3.1.4.2 Multiple linear regression

Multiple linear regression (MLR) builds on linear regression analysis and is particularly useful for datasets where the relationships between the dependant and independent variables are linear. It is a statistical technique that predicts dependent variables based on the relationship between that variable and the one or more independent variables (Tranmer *et al.*, 2020). MLR is often used to gap-fill time series data by exploring explanatory variables that influence changes in the response variable. It assumes that the relationship between variables is linear and that certain conditions, such as normally distributed residuals and no multicollinearity between independent variables, are met for valid results. When these assumptions are violated, the results may be unreliable, and alternative models may be required (Tranmer *et al.*, 2020).

#### 2.3.1.5 Sampling errors

Random uncertainty in carbon flux measurements, often caused by insufficient sampling of large eddies within a 30-minute sampling period, can lead to turbulent sampling errors, particularly since large eddies contribute significantly to flux (Finkelstein and Sims, 2001; Aubinet *et al.*, 2012). Uncertainties related to this error can be calculated using two methods in EddyPro software, based on Mann and Lenschow, (1994) and Finkelstein and Sims (2001). Both methods require information such as vertical wind component, gas concentration or environmental factors, time, and time lag between instruments. Finkelstein and Sims (2001) improved on previous methods by incorporating additional error sources. Their approach, applied to $CO_2$ flux measurements from five field sites, found random uncertainty of 25-30% for $CO_2$ and emphasised the importance of correcting large sampling errors when calculating ecosystem carbon or energy balances. A study on forest ecosystems also applied various data correction techniques to reduce uncertainties, including spike detection, time lag compensation, sonic temperature correction, spectral corrections, and planar fit for coordinate rotation (Kováč *et al.*, 2022).

The EC covariance method is most reliable during daylight hours because, as night falls, advection causes the respired $CO_2$ produced by the ecosystem to stay near the land surface (Aubinet *et al.*, 2012; Baldocchi, 2014). Because of these stable conditions, the eddies of air are non-turbulent and therefore the EC tower cannot sample all the eddies (Baldocchi, 2003). This is particularly true in forested areas, where the $CO_2$ flux beneath the canopy of the trees cannot be registered by the EC tower and may lead to an underestimation of respiration and overestimation of NEE from the site. These errors can lead to substantial bias even when measurements are averaged over long periods (Leuning *et al.*, 2008). There is no correction for this using a single EC system above canopy and nighttime data requires further quality control (Burba, 2022).

Although there is no correction to implement, generally low friction velocity (u*) tests in these conditions are applied to determine a threshold for filtering underestimated nighttime data sets (Aubinet *et al.*, 2001, 2012). By looking at the behaviours of airflow from annual data sets, limits of low turbulent exchange can be established then flagged and removed from the data set before further analysis (Burba, 2022). The fluxes above the u* threshold are considered of good quality and data falling below this is often discarded in studies (Reichstein *et al.*, 2005, 2007; Burba, 2022).

In a study by Winck et al*.* (2023) the seasonal u* threshold was determined for each of the three-month seasons, with filtering done on a seasonal basis rather than using an overall annual u* threshold as in Klumpp et al. (2011). They found this approach to be more effective, as the u* varied significantly between the winter and summer months (Winck *et al.*, 2023). However, in a study by Sottocornola and Kiely (2005) on a pristine blanket peatland they found that there was no clear pattern looking at friction velocity to exclude measurements on this basis, but they did find negative $CO_2$ fluxes on infrequent night measurements and these fluxes were then rejected as they were illogical. Vegetation characteristics at this site were low lying and homogeneous which may have been a reason why the friction velocity was negligible. As suggested by Holl *et al.*, (2020) in a study carried out in Germany they highlight the problems associated when carrying out a great deal of filtering processes on data from their EC tower. Although the processes proved to be successful in acquiring the relevant and accurate data required, it led to a large amount of data loss, necessitating an arduous task of gap filling and increased predicted values.

Another approach to monitor the rate of gas exchange is the installation of additional EC instruments at a lower level, or the use of additional sensors in conjunction with the above canopy EC system to estimate fluxes below the tree canopy (Janssens *et al.*, 2000; Aubinet *et al.*, 2003, 2012; Baldocchi, 2014). A study by Paul-Limoges et al. (2017) continuously monitored fluxes both above and below the canopy in Switzerland using the EC method. The study focused on a broadleaf woodland on mineral soils and found that above-canopy EC measurements indicated the site was a $CO_2$ sink, with a flux of -27.81 ± 0.37 tonnes of $CO_2$ $ha^{-1}$ $yr^{-1}$. However, when they examined the relationship between above-canopy and below-canopy wind speeds, discrepancies were observed, particularly during periods of maximum canopy closure in the growing season.

By calculating a threshold for significant differences between the wind speeds, they were able to adjust their results. They added NEE from below the canopy to the above-canopy measurements to account for the underestimation of respiration during periods of varying wind flow. This dramatically reduced the sink function of the site, resulting in an average annual NEE value of -0.327 ± 0.004 t C-$CO_2$ $m^{-2}$ $yr^{-1}$. This method, while useful, is costly, as it requires additional instrumentation below the canopy. Moreover, the below-canopy respiration might be overestimated, leading to potential overcompensation. The authors also noted that the below-canopy NEE will largely depend on the understory vegetation cover at each specific site (Paul-Limoges *et al.*, 2017).

Utilising the chamber method in conjunction with the EC tower to take measurements from below tree canopy in order to establish the rate of respiration or just soil respiration alone has been implemented to avoid overestimating NEE (Baldocchi, 2003; Badorek *et al.*, 2011; Jovani-Sancho *et al.*, 2017). Although previous studies have shown conflicting results on the reliability of using the chamber method in situ with EC measurements, other studies have highlighted the benefits of using the chamber method to estimate below canopy carbon storage with the EC method (Badorek *et al.*, 2011; Ojanen *et al.*, 2012; Jovani-Sancho *et al.*, 2017, 2018; Jovani-Sancho *et al.*, 2021). The study by Badorek et al. (2011) used the chamber method to measure forest floor NEE in a drained peatland forest in Finland found that the method allowed for detailed analysis of ground vegetation communities' carbon flux dynamics, though the method may overestimate respiration and underestimate photosynthesis, with below-canopy contributions accounting for approximately 39% of the total NEE, representing a significant portion.

#### *2.3.1.6 Limitations using the eddy covariance method*

Implementing the EC method can be an accurate means of assessing long term flux measurements between an ecosystem and the atmosphere. Its advantages over other techniques include the ability to take direct measurements from an ecosystem with little disturbance to the surrounding area which can include large sampling areas over long time periods of a year or more (Baldocchi, 2003, 2014). However, the EC method presumes air density fluctuations are negligible and assuming horizontal homogeneity the mean vertical flow is equal to zero (Baldocchi *et al.*, 1988). Consequently, if the surrounding terrain is level with underlying homogeneous vegetation and stable atmospheric conditions, EC can take precise measurements (Schmid and Lloyd, 1999; Baldocchi, 2003; Aubinet *et al.*, 2012). However, natural conditions are complex, because of this the sonic anemometer may not be perfectly perpendicular to the mean flow of wind (Baldocchi, 2003; Burba, 2013). In order to correct this, certain algorithms developed for tilt correction can be applied. These include the double rotation method, the triple rotation method, and the planar fit method (Wilczak *et al.*, 2001).

The double rotation and the planar fit models are the most widely used methods. The double rotation method is recommended for sites that are relatively flat with homogenous lying vegetation, for example a grassland which could assume to have wind streams parallel to the surface of the land and applying the double rotation method will compensate for minor vertical misalignments in the sonic anemometer. It is also a recommended method for ecosystems where the underlying vegetation can change significantly over a relatively short period of time (i.e. the harvest of a crop) (Wilczak *et al.*, 2001). The planar fit model is deemed most suitable for sloping topography when the mean vertical wind component differs from zero. The planar fit model allows for a certain amount of horizontal wind speed to be measured and will apply an equation to correct for this. This method can only be applied to data collected over a period of time not like the double rotation method which can be applied to continuous real time data (Wilczak *et al.*, 2001).

Under the term frequency response errors there are several errors that can occur while monitoring gas exchange from EC, some of which include the following:

- Instrument time response, this can impact results if there are motions of eddies that are moving too fast to be detected by all the instruments.
- Sensor separation, which can occur if instruments are placed too far apart leading to a lack of correlation between air samples.
- Sensor response mismatch occurs when a delay in time occurs between sensors.

These errors can all effect the flux measurements taken. However, corrections for these errors can be carried out through careful installation of EC instruments and if needed the response frequency correction model can be applied during data processing stage (Burba, 2013).

#### *2.3.1.7 Estimating Net ecosystem exchange*

As discussed in Section 1.3, NEE is a key biophysical process controlling $CO_2$ fluxes between ecosystems and the atmosphere and is therefore a key indicator of whether they function as a carbon sink or source (IPCC, 2001; Kirschbaum et al., 2001). NEE represents the net balance of $CO_2$ uptake and release, calculated as the difference between net primary production (NPP), the carbon fixed in new biomass, and the amount of $CO_2$ lost through $R_h$ (IPCC, 2001; Kirschbaum *et al.*, 2001). Equation 2.1 expresses this relationship:

*Equation 2.2*

$$NEE = NPP - R_h$$

NPP is derived from the Gross Primary Production (GPP), the total carbon fixed through photosynthesis minus $R_a$, representing actual biomass accumulation by plants (Begon *et al.*, 1996), as shown in equation 2.2:

*Equation 2.3*

$$NPP = GPP - R_{\mathrm{a}}$$

NEE provides a direct indication of an ecosystems net $CO_2$ balance, showing how much carbon from $CO_2$ is stored or lost based on these biological processes. Figure 2.10 illustrates this concept showing GPP and $R_{eco}$.

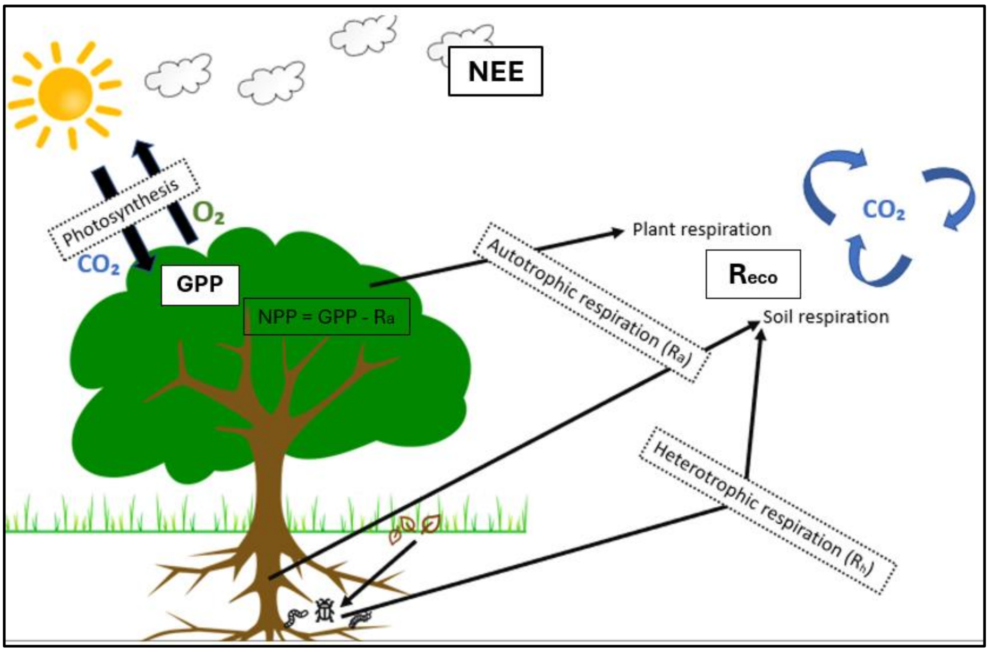


*Figure 2.9 Schematic of Net ecosystem exchange (photo: author).*

Figure 2.9 shows an example of NEE processes in a habitat. As mentioned in section 2.2.1 and 2.2.3, separating respiration processes within an ecosystem can be challenging. For this reason, equations 2.2 and 2.3 are often used interchangeable in $CO_2$ exchange studies (Wilson *et al.*, 2015; Swenson *et al.*, 2018). NEE can be measured directly from an ecosystem, therefore, estimating GPP from an ecosystem requires the use of equation 2.4, which is represented as:

*Equation 2.4*

$$-GPP = NEE - R_{eco}$$

This equation illustrates that by directly measuring NEE and $R_{eco}$ from an ecosystem, researchers can estimate GPP, the total amount of $CO_2$ fixed through photosynthesis, indirectly (Wilson *et al.*, 2015; Wilson, Farrell, *et al.*, 2016; Swenson *et al.*, 2018). Negative NEE values indictive a net sink of $CO_2$ within an ecosystem and positive NEE represents a net source.

Typically, fluxes are separated into GPP and $R_{eco}$ by using radiation data to distinguish between day and night periods. This separation is crucial for applying specific models to each process, as they are driven by different biological variables (Begon *et al.*, 1996; Burba, 2022). Additionally, it enables a clearer understanding of the variables influencing NEE, which can be better pinpointed by separating the processes (Reichstein *et al.*, 2005, 2007).

The temperature sensitivity of respiration is commonly described using the Lloyd and Taylor (1994) function, which relates $R_{eco}$ to temperature through a well-established exponential response. However, reliance on long-term temperature relationships can introduce bias, particularly in high-carbon ecosystems such as peatlands. To address this Reichstein et al. (2005) developed a short-term, time-dependent model of temperature sensitivity that incorporates both daytime and nighttime data, reducing bias associated with seasonal variation and improving gap-filled $R_{eco}$ estimates.

Earlier methods relying solely on nighttime data, (Hollinger *et al.*, 1998; Falge, Tenhunen, *et al.*, 2002; Law *et al.*, 2002; Reichstein, Tenhunen, Roupsard, J-M Ourcival, *et al.*, 2002; Reichstein, Tenhunen, Roupsard, Jean-marc Ourcival, *et al.*, 2002; Rambal *et al.*, 2003) successfully accounted for seasonal temperature sensitivity but had limitations, including heavy reliance on temperature as the sole driver, site-specific calibration, and potential systematic errors when extrapolating to daytime values. Alternatively, models estimating $R_{eco}$ from light-response curves using daytime data (Falge, Baldocchi, *et al.*, 2002; Gilmanov *et al.*, 2003; Papale and Valentini, 2003), used both day and night data, offering greater flexibility and the ability to adjust parameters over time. However, these approaches depended on the light-response model, which can introduce high standard errors, and often limited direct comparisons of GPP estimates across sites. (Reichstein *et al.*, 2005).

Analysis of EC data across boreal, temperate, and Mediterranean climates indicated potential overestimation of respiration by more than 25% in boreal and temperate ecosystems when relying solely on long-term temperature relationships, while Mediterranean ecosystems could see underestimation (Falge, Baldocchi, *et al.*, 2002; Reichstein *et al.*, 2005). The short-term, time-dependent model by Reichstein et al. (2005) addresses these issues by allowing parameters to vary over time and by incorporating both day and night measurements. Implementation occurs at seasonal and short-term (≈15-day) scales.

Air temperature was chosen as the primary predictor due to stronger correlations with $R_{eco}$ compared to soil temperature. Short-term temperature sensitivity tended to be overestimated during the growing season due to increased biological activity, while long-term sensitivity captured seasonal patterns more accurately in temperate and boreal forests. Careful selection of meteorological data and analysis over shorter time frames can further improve gap-filling (Reichstein *et al.*, 2005). The standard equation derived from the study is presented in Equation 2.5.

*Equation 2.5*

$$\frac{dR_{eco}}{R_{eco}} = \frac{dR_{ref}}{R_{ref}} + dE_0\left(\frac{1}{T_{ref} - T_0} - \frac{1}{T - T_0}\right)$$

This equation describes how changes in the baseline respiration rate ($R_{ref}$) and the temperature sensitivity parameter ($E_0$) affect the relative change in ecosystem respiration ($R_{eco}$), considering the differences in temperature (T) between the reference temperature and the base temperature (Reichstein *et al.*, 2005).

### 2.3.1.8 Energy balance closure

Biological processes in ecosystems rely on the exchange of energy fluxes, which are influenced by environmental factors like water availability, air, and soil temperatures. These factors closely correlate with carbon cycle balance (Begon *et al.*, 1996). The energy balance closure (EBC) helps quantify the accuracy of carbon flux values and ensures EC instruments are functioning properly (Cai and Kim, 2005; Burba, 2022).

EBC represents the energy taken in by an ecosystem through solar radiation, ideally equalling the energy released back via radiation, heat, or evapotranspiration:

*Equation 2.6*

$$LE + H + G = Rn$$

Where LE is latent heat, H is sensible heat, G is ground heat flux, and Rn is net radiation. The reliability of EBC is assessed through linear regression, with values closer to one being most accurate (Barr *et al.*, 2006). Ground heat flux also referred to as soil heat flux (SHF) is especially relevant for studies involving low vegetation and agricultural lands (Sauer and Horton, 2015). However, in woodland sites it is deemed less prevalent for the energy budget and can be frequently ignored from *Equation 2.6*, as it is deemed the smallest contributor to the energy balance (Sauer and Horton, 2015).

A study carried out by Wilson et al (2002) on the role of energy storage below the canopy and energy heat storage was carried out. The study focused on sites with grass vegetation and forested sites. When looking at the components of the EBC from *Equation 2.6,* the study found that SHF was more relevant to include for sites with small canopies of approximately less than 8m high. Sites with taller canopies did not depend as heavily on SHF for the accuracy of the EBC. It was concluded that because of the dense canopy in a woodland or a site with tall vegetation over 8m, the SHF component had much less of an impact when calculating the average slope of the line. This is because the canopy is dense, and the direct sun is not reaching the ground level (Wilson *et al.*, 2002). This is in agreement with the statement from Sauer and Horton, (2015). Wilson *et al.*, (2002) also found no significant difference between open and closed path gas analysers regarding EBC.

A study by Barr et al. (2006) found that boreal forests exhibit consistent energy imbalance patterns across different sites, with similar relationships between $CO_2$ and energy imbalances. Zhou et al. (2023) compared methods for calculating EBC, concluding that sensible and latent heat fluxes are the dominant components. The Bowen ratio method was the most accurate for closing energy balances, although it was ineffective for fluxes from horizontal advection. Errors in heterogeneous surfaces can be difficult to detect due to sensor variation. Accurate EBC methods are more relevant for modelling future changes in ecosystem carbon cycles (Sottocornola, 2007), although in forest ecosystems it is common to have non-EBC (Aubinet *et al.*, 2001).

### 2.3.2 Chamber Methodologies

Similar to the EC method, the chamber method is commonly used to estimate the gas exchange between the biosphere and atmosphere (Tuittila *et al.*, 2004; Waddington *et al.*, 2010). This method is commonly used to monitor the rate of soil respiration, photosynthesis, $N_2O$ and $CH_4$ emissions. The chamber method has assisted in establishing trends in GHG emissions from ecosystems all over the globe (Matson *et al.*, 1995; Griffis *et al.*, 2000; Tuittila *et al.*, 2004; Waddington *et al.*, 2010). The chambers are relatively inexpensive compared to the costly EC tower and are easily transportable allowing them to be used on multiple sites (Matson *et al.*, 1995). However, unlike the quasi-continuous measurements taken from the EC method, generally measurements from the chamber

*Figure 2.10 Static chamber made from translucent material intended to measure NEE & Respiration (photo: author).*

method are carried out fortnightly or monthly (Wilson, Farrell, *et al.*, 2016).

Chamber types can be classified as steady state and non-steady state chambers (Livingston and Hutchinson, 1995) or otherwise known as dynamic and static chambers (Figure 2.10) (Griffis *et al.*, 2000). Commonly a collar is inserted into the ground where samples are required and the chamber is then placed onto the collar, creating a vacuum seal between the collar and the chamber (Heinemeyer *et al.*, 2011).

Steady state or dynamic chambers (Figure 2.10) allow a constant controlled airflow through the chamber measuring the gas fluxes before and after entering the chamber, whereas the non-steady state chambers or static chambers are closed off and the air within the chamber is circulated and sampled (Livingston and Hutchinson, 1995).

Dynamic chambers consist of a more expensive automated system taking continuous direct samples and analysing them in real time. Static chamber heads are less costly but can be more labour-intensive, depending on the experimental design. A cost effect approach includes manual air samples collected by syringe from the static chamber head, that are then analysed off site. However, this approach is very labour intensive and time consuming. The static chambers also have the potential to become semi-automated by connecting them to portable gas analysers. This is less labour intensive while remaining relatively cost effective and is a widely used method for GHG monitoring (Laine, 2006; Heinemeyer *et al.*, 2011; Wilson, Farrell, *et al.*, 2016; Jovani-Sancho *et al.*, 2017). It is suggested that the dynamic chambers are an appropriate method for taking soil $CO_2$ flux measurements (Janssens *et al.*, 2000) on the other hand, the static chamber is a more accurate means of measuring trace gases such as $CH_4$ (Livingston and Hutchinson, 1995). Chambers can be constructed from a translucent material or a non-translucent solid material, this permits the measurement of NEE or soil respiration respectively (Griffis *et al.*, 2000; Waddington *et al.*, 2010). This is beneficial as both measurements can be easily differentiated, unlike the EC method it can be difficult to separate soil respiration from plant respiration (Griffis *et al.*, 2000; Janssens *et al.*, 2000; Waring and Running, 2007).

#### 2.3.2.1 Chamber structure and collar insertion

Environmental variables such as topography, vegetation type and height, and the entity of interest to be measured will determine the dynamics and dimensions of the chamber structure. Therefore, there is no consistency of chamber composition across the board. However, there are general guidelines set out by Pavelka *et al.*, (2018) and Fiedler *et al.*,(2022) that highlight some points to consider when designing a chamber experiment. They recommend having a chamber which suits the needs of that of the vegetation being measured. For example, taller vegetation will require a higher chamber head, but all the while keeping the volume to base area of the chamber small enough that the gas of interest is still quantifiable within the deployment period of the measurements.

Implementing the chamber method generally involves the use of collars that are inserted into the ground at desired areas, with the intention of avoiding horizontal gas leakage when estimating total soil respiration (Heinemeyer *et al.*, 2011). The depth at which collars are inserted into the ground varies across different ecosystem types. Past research methods carried out use various collar depths depending on chamber size or site type and in some cases, there is no mention of collar insertion depth (Janssens *et al.*, 2001; Wang *et al.*, 2010; Heinemeyer and McNamara, 2011; Heinemeyer *et al.*, 2011; Wilson, Farrell, *et al.*, 2016; Jovani-Sancho *et al.*, 2017; Jovani-Sancho *et al.*, 2021).

#### 2.3.2.2 Chamber modelling

The chamber method collects spot samples at the time of emission. To estimate an annual emissions budget using this method, the data must be modeled annually based on the collected spot samples and in situ meteorological data. A correlation between the flux measurements and the meteorological data is essential for successful modeling of the dataset (Wilson *et al.*, 2015; Wilson, Farrell, *et al.*, 2016). Prior studies have applied various models to peat soils, yielding diverse explanatory effectiveness.

NEE is measured during daylight hours, while respiration is measured in darkness. To effectively model the time series from chamber measurements, it is necessary to obtain GPP and $R_{eco}$. Thus, GPP can be calculated using the *Equation 2.4* in section 2.3.1.7. These components are modeled separately, as respiration is influenced by biotic factors such as temperature, as discussed in section 2.2.3. Similarly, GPP is related to PPFD or PAR, as noted in section 2.2.2; therefore, these processes must also be modeled independently.

In a previous report by Wilson et al., (2015), a model was developed to estimate GPP by using PPFD and soil temperature as independent variables (*Equation 2.7*). This model is based on a Michaelis–Menten-type relationship (Tuittila *et al.*, 1999, 2004; Wilson, Farrell, *et al.*, 2016) that describes the saturating response of photosynthesis to light and soil temperature, and incorporates Levenberg–Marquardt multiple nonlinear regression technique (Wilson *et al.*, 2015; Wilson, Farrell, *et al.*, 2016).

*Equation 2.7*

$$GPP = Pmax\left(\frac{PPFD}{PPFD\ +\ kPPFD}\right).LAI.T_5$$

Where $GPP$ refers to gross primary productivity, $Pmax$ indicates the maximum rate of photosynthesis, $PPFD$ stands for photosynthetic photon flux density, and $kPPFD$ represents the $PPFD$ level at which $GPP$ attains half of its maximum value. Additionally, $LAI$ denotes leaf area index, and $T_5$ refers to soil temperature measured at a depth of 5 cm.

In the study by Wilson et al. (2015) applied their modelling approach across nine peat extraction sites in Ireland and the UK and found that GPP was strongly driven by PPFD, which alone explained around 70% of the variation in model residuals. Incorporating additional variables such as LAI and temperature further improved model performance, demonstrating that the algorithm was effective and responsive to key environmental controls across both industrial and domestic peat extraction sites

The respiration model applied in the study was loosely based on equation by Lloyd and Taylor (1994), and identified soil temperature at a depth of 5cm as the strongest factor influencing flux change in respiration measurements. When WT data was included in the model, it slightly enhanced the model's ability to explain variability across sites by 55% to 85%. However, at one site, there was no observed relationship between WT and the fluxes, leading to the exclusion of WT from the model for that specific location. The model used to estimate $R_{eco}$ in the paper is as follows:

*Equation 2.8*

$$Reco \; = \; a.exp.\left[b\left(\frac{1}{T_{\mathrm{r}} - T_{\mathrm{o}}}\right) - \left(\frac{1}{T - T_{\mathrm{o}}}\right)\right].WT$$

Where $Reco$ represents ecosystem respiration, $T_{\mathrm{r}}$ is the reference temperature set at 283.15 K, $T_{\mathrm{o}}$ is the minimum temperature at which respiration is zero, set at 227.13 K, $T$is the soil temperature at a depth of 5cm, WT is the water table depth, and $a$ and $b$ are the fitted model parameters.

Other research utilised similar modeling techniques derived from the original reference sources, such as the Michaelis–Menten-type relationship and the respiration model proposed by Lloyd and Taylor (1994). However, each study introduced slight variations to tailor the models to specific sites, linking independent variables based on the relationships observed in meteorological data and the trends in fluxes over time (Laine, 2006; Badorek *et al.*, 2011; Jovani-Sancho *et al.*, 2018).

Previous studies that employed the chamber technique to measure $CH_4$ emissions at peatland sites in Ireland, taking fortnightly and monthly measurements, used simple linear interpolation to gap-fill the $CH_4$ data. The authors noted that this method may not have fully captured the day-to-day variation in $CH_4$ emissions at the site. They also acknowledged that using more sophisticated models could have provided different results and that their approach may have led to an underestimation of $CH_4$ emissions (Rigney *et al.*, 2018).

#### *2.3.2.3 Evaluating the chamber method: advantages and challenges*

This section reviews previous research that applied the chamber method in different ecosystems, focusing on the characteristics of each study. It also discusses the limitations of the method, particularly within forest ecosystems. Several studies have explored the use of the chamber method to estimate carbon fluxes in peatland ecosystems, highlighting both its advantages and limitations, especially in comparison to other techniques such as the EC method.

The chamber method is more successfully carried out in areas with low growing vegetation or no vegetation, for example it cannot calculate an accurate rate of NEE from a forest canopy, because it is unable to measure photosynthesis from the entire canopy (Baldocchi, 2014). However, the chamber method can be a useful resource when estimating the soil carbon balance of a forest ecosystem and below canopy NEE.

One major disadvantage of the chamber method is that it is disruptive and invasive to the area being monitored. The chamber head is sealed off between the vegetation and soil, which can alter the microclimate. This may result in an increase in temperature inside the chamber, potentially affecting the gas concentrations being measured (Livingston and Hutchinson, 1995; Hutchinson *et al.*, 2000). This effect can be particularly problematic when using static chambers (Heinemeyer and McNamara, 2011). To reduce these risks, strategies such as avoiding collar insertion (Jovani-Sancho et al., 2017), careful placement of chamber heads (Wilson, Farrell et al., 2016) and using fans to circulate air within the chamber (Renou-Wilson *et al.*, 2019; Fiedler *et al.*, 2022) can help maintain more reliable measurements. Dynamic chambers with automatic cooling systems are also available, but they are generally more expensive (Heinemeyer & McNamara, 2011).

Despite these challenges, the chamber method offers a more reliable and accurate estimation of GHG concentrations than older methods, such as the 'soda-lime' approach (Byrne and Farrell, 2005). However, a limitation of the chamber method is its inability to provide continuous measurements, which can result in significant changes in environmental parameters between measurements (Heinemeyer et al., 2011). This makes it difficult to capture short-term variations in carbon flux in real time, especially during periods of rapid environmental change.

When comparing chamber and EC methods, both are used to monitor GHG fluxes, but the spatial scales they represent differ. The chamber method, which typically measures smaller, more localised areas, can be more accurate for capturing fluxes that may be missed by EC towers, particularly during seasonal transitions or in ecosystems undergoing regrowth after disturbance (Poyda *et al.*, 2017). However, the EC method provides a broader spatial coverage and is often better suited to capturing large-scale ecosystem fluxes.

A study by Poyda et al. (2017) comparing $CO_2$ fluxes from both chamber and EC methods from grassland on peat soils, found that during peak changes in vegetation, the chamber measurements showed a net release of $CO_2$, while the EC measurements showed a net $CO_2$ uptake. This discrepancy highlights the challenge of making direct comparisons between the two methods, especially in ecosystems undergoing seasonal changes or disturbance-induced regrowth. In contrast, a study comparing the chamber and EC methods in larger ecosystems, such as those in temperate forests, have found that the chamber method may overestimate respiration compared to EC data (Wang *et al.*, 2010). In a later study comparing global data sets the authors came to a similar conclusion, finding that EC data estimated approximately 10% less ecosystem respiration compared to chamber methods (Wang *et al.*, 2017).

These studies highlight the importance of cross-validation between the chamber and EC methods to improve the accuracy of $CO_2$ flux estimates. Because chamber data are often sparse, modeling is necessary to estimate annual carbon budgets. Chamber measurements rely on environmental predictors such as photosynthetic photon flux density (PPFD), soil temperature, and leaf area index (LAI) to model GPP and Reco at finer scales (Wilson et al., 2015). These models build on earlier approaches, including Michaelis–Menten formulations (Tuittila et al., 1999) and the Lloyd & Taylor (1994) respiration function. Variants of these models have been adapted to specific site conditions, for example substituting LAI with water table depth (Laine, 2006; Badorek et al., 2011; Jovani-Sancho et al., 2018).

EC datasets also require gap-filling to address missing data from instrument issues or quality filtering, with MDS being the standard approach used across FLUXNET (Wutzler et al., 2018; Pastorello et al., 2020). While effective for continuous EC time series, MDS cannot be directly applied to chamber datasets due to their lower temporal resolution. Instead, chamber modelling typically separates GPP and $R_{eco}$ and estimates each independently using site-specific environmental relationships, providing useful process-level insights despite more limited temporal and spatial coverage (Wilson et al., 2015; Wilson, Farrell, et al., 2016).

By integrating modeling with careful chamber deployment, researchers can maximise the reliability of soil and below-canopy flux estimates while complementing EC data for a more comprehensive understanding of ecosystem carbon dynamics. especially when assessing complex forest ecosystems (Wang et al., 2017).

### 2.3.3 Machine learning models for estimating data gaps and upscaling fluxes

Machine learning (ML) algorithms have become increasingly prevalent in environmental research, particularly for analysing complex ecosystems with highly variable datasets. The application of ML methods to study atmospheric GHGs has gained significant traction, offering valuable insights in recent studies (Xu and Goodacre, 2018; Hamrani et al., 2020; Holl et al., 2020; Kim et al., 2020; Zhu et al., 2022; Winck et al., 2023).

Both traditional gap-filling approaches, such as MDS for EC datasets and the empirical models developed by Wilson et al. (2015) for chamber-based measurements, have proven effective for their respective data types; however, they are designed for different measurement systems and are not interchangeable. Recent advancements in ML represent a major step forward in improving the accuracy and reliability of gap-filling in environmental datasets across multiple methods (Winck et al., 2023; Zhu et al.,2022). Studies increasingly show that ML algorithms offer strong alternatives to traditional approaches such as MDS, often achieving higher accuracy and reduced bias in flux modelling and gap-filling application (Xu and Goodacre, 2018; Hamrani et al., 2020; Holl et al., 2020; Kim et al., 2020; Zhu et al., 2022; Winck et al., 2023). ML methods can model more complex relationships between environmental parameters and carbon fluxes and have been shown to be especially effective for estimating gaps in trace gases such as $CH_4$ (Kim et al., 2020). While MDS remains a widely used and effective method, particularly for smaller gaps in EC data, ML techniques are rapidly emerging as a more flexible and precise option for both EC and chamber-based datasets.

Studies (Breiman, 2001; Xu and Goodacre, 2018; Hamrani et al., 2020; Holl et al., 2020; Kim et al., 2020) have highlighted the importance of properly separating data for training and testing when applying ML methods for gap filling. This is particularly relevant for chamber-based datasets, which are often smaller and collected as spot samples. The effectiveness of ML models depends on the way the data is split, as it ensures that the model is trained on one portion of the data and tested on another, unseen portion. This separation helps prevent overfitting, where the model may perform well on the training data but fail to generalise to new data. For larger datasets (e.g., 1000 samples), the data-splitting method has minimal impact on the results, while smaller datasets (e.g., 30 samples) exhibit more variability depending on the chosen method (Breiman, 2001; Xu and Goodacre, 2018; Hamrani et al., 2020; Holl et al., 2020; Kim et al., 2020).

Xu and Goodacre (2018) conducted a study comparing various data-splitting methods and found that no single approach consistently outperformed the others. However, they found that random sampling, bootstrapping with multiple repetitions, and balanced splits between training and validation sets tended to yield better results. Although the ideal number of splits was not definitively established, this underscores the flexibility of ML methods in optimising data splitting, ultimately enhancing the reliability of model outputs compared to more traditional techniques.

Multiple studies demonstrate that ML algorithms consistently outperform traditional linear approaches for modelling and gap-filling GHG fluxes. On agricultural soils in Canada, deep learning models showed markedly higher $R^2$ and lower RMSE than simple linear regression, indicating more accurate predictions of GHG emissions (Hamrani et al., 2020). Similarly, at an industrial peatland site in Germany, ML methods achieved higher model coefficients and lower RMSE compared to multilinear regression when gap-filling $CH_4$ fluxes, particularly under conditions where microbial activity was strongly influenced by variables such as VPD and soil temperature (Holl et al., 2020).

In a broader evaluation of $CH_4$ flux gap-filling across wetlands and rice paddies, Kim et al. (2020) compared MDS, RF, and ANNs using different environmental inputs. RF produced the most accurate and least biased predictions across all sites, followed closely by ANNs, while MDS performed better when driven by soil temperature, NEE, and water table rather than standard meteorological variables(Kim *et al.*, 2020).

In Ireland, ML techniques have been employed to monitor and assess peatland cover, improving the accuracy and efficiency of land-use classification and upscaling of carbon flux estimations (Ingle, Bhatnagar, *et al.*, 2023; Habib *et al.*, 2024). As ML techniques continue to advance, their integration into environmental research holds great potential for improving the accuracy of carbon flux estimates and enhancing our understanding of carbon dynamics across diverse ecosystems. This section will explore the general concepts of ML methods.

#### 2.3.3.1 Random forest

Random forest (RF) is a supervised learning algorithm that essentially builds an ensemble of decision trees, creating a "forest." It typically uses training data with a technique called bootstrapping, where multiple subsets of the training data are created by randomly sampling with replacement. This enhances the model's overall performance by incorporating a combination of learning patterns. Since each tree is independent of the others, this approach allows for greater diversity in learning. The algorithm builds multiple decision trees and merges their predictions to achieve a more accurate and stable outcome. Random forest requires only two parameters, making it relatively simple to implement: the number of trees to build and the number of variables to randomly sample at each point of independence (Breiman, 2001).

RF has emerged as an effective ML algorithm for gap-filling large datasets, particularly for long gaps in time series data. For example Winck et al. (2023) applied RF to an 18-year dataset of GHG fluxes from a managed upland grassland in France, using RF for long gaps and MDS for short ones. They found that RF demonstrated robust performance in managing noise, identifying complex relationships, and accounting for temporal dependencies within the data. Similarly, Zhu et al. (2022) showed that RF outperformed MDS for gap-filling $CO_2$, latent heat, and sensible heat fluxes, especially for longer gaps. RF's superior performance in handling long gaps and its ability to model intricate environmental relationships make it a promising alternative to traditional methods. Kim et al. (2020) further validated the superiority of RF over MDS and ANNs in gap-filling $CH_4$ flux timeseries, reinforcing its applicability in environmental flux modeling.

#### 2.3.3.2 Gradient boosting

Gradient boosting machines (GBMs) are a machine learning technique used for regression and classification by combining weak decision trees to create a more accurate model (Friedman, 2001). Unlike random forests, which build independent trees and average their predictions, GBMs build models sequentially, with each new model correcting the errors of the previous one. The process involves iteratively adding models, calculating negative gradients, fitting a base learner to the errors, and adjusting the learning rate to control the model's error correction. GBMs require independent variables and a dependent variable, with enough data to train the model for either regression or classification tasks (Natekin and Knoll, 2013).

#### 2.3.3.3 XGBoost model

The XGBoost model, developed by Chen and Guestrin. (2016), is an advanced implementation of the gradient boosting framework, often referred to as "Extreme Gradient Boosting." It employs decision trees as base learners and applies the gradient boosting algorithm to iteratively combine these trees, progressively refining the model by minimising residual errors. However, XGBoost introduces several key enhancements to improve both the efficiency and performance of gradient boosting. These include regularisation techniques to reduce overfitting, sparsity awareness for handling sparse datasets more effectively, parallelisation to speed up training through distributed processing, and tree pruning to produce more efficient decision trees. As a result, XGBoost offers a scalable, high-performance solution that is particularly well-suited for large and complex datasets, distinguishing it from traditional gradient boosting methods (Chen and Guestrin, 2016).

#### 2.3.3.4 Artificial neural networks

Artificial neural networks (ANNs) are a type of machine learning algorithm inspired by the structure and functioning of the human brain. They consist of interconnected nodes, organised in layers. The input layer contains independent variables, such as meteorological data from various sites in environmental research. Hidden layers process these inputs through complex mathematical equations, while the output layer provides the predicted values (Holl *et al.*, 2020).

#### 2.3.3.5 Generalised additive models

Generalised additive models (GAMs), developed by Hastie and Tibshirani (1986), extend linear models by incorporating nonlinear relationships through smooth functions, like splines, to capture complex patterns in data. GAMs are flexible, allowing for continuous or binary data, and use additive effects of predictor variables with likelihood-based estimation. Key steps in implementing GAMs include selecting appropriate smoothers, specifying the model structure, and using algorithms like local scoring or backfitting for estimation. While GAMs offer flexibility and clear visualisation of predictor effects, they can be computationally intensive, and careful selection of tuning parameters is crucial for performance (Hastie and Tibshirani, 1986; Hastie, 2017).

#### 2.3.3.6 k-Nearest Neighbours

Originally developed by E. Fix and J.L. Hodges in (1951), the k-nearest neighbours (kNN) method is used for both classification and regression tasks, employing a simple instance-based learning approach. The method relies on the principle that similar data points are likely to have similar outcomes, making it a non-parametric method, meaning there is no assumption made about the underlying data distributions. However, there is a key assumption and that is that similar data points are located close to each other in the feature space, which allows predictions for a new point based on its nearest neighbours. Key steps in kNN include selecting the number of neighbours (k), calculating distances using metrics like Euclidean or Manhattan, and aggregating the neighbours' responses through majority voting (for classification) or averaging (for regression). KNN is valued for its simplicity and versatility, requiring only a labelled dataset and a distance metric. However, it faces challenges, such as selecting the optimal number of neighbours (k), computational inefficiency with larger datasets, and its sensitivity to noise and high-dimensional data. These challenges can be addressed through techniques like cross-validation and efficient data structures (Halder *et al.*, 2024). Therefore, kNN may be useful for filling gaps in datasets with smaller gaps, but for larger datasets with significant gaps, more complex machine learning models may be more effective.

## 2.4 Previous research on emissions and reductions from peatlands and forests

Previous literature on the evaluation of GHG emissions from different peatland types, including peat soils under various land uses and the effectiveness of peatland rewetting, varies considerably across studies, particularly regarding their carbon sink and source functions. Additionally, vulnerability to drying and other environmental factors differ across sites. This section reviews and highlights these variations, examines emissions from various peatlands and woodland ecosystems, and identifies key areas where further research is needed to better understand and quantify emissions from peatlands.

### 2.4.1 Studies on degraded and rewetted peatlands

A significant body of research has been conducted on degraded and rewetted peatlands in Ireland, the UK, and beyond, providing valuable insights into their restoration potential and the challenges they face in regaining carbon sequestration. Farrell and Doyle (2003) demonstrated that hydrological manipulation on cutaway peatlands can encourage *sphagnum moss* growth, a key factor in peat formation, enhancing the return of the sink function. Similarly, Wilson et al. (2016) observed that rewetting a cutaway blanket peatland successfully converted it from a carbon source into a carbon sink, adding to the growing evidence of rewetting's benefits. However, Wilson et al. (2007) highlighted that not all rewetted peatlands show the same positive results. In their study of a vegetated cutaway raised peatland, rewetting did not achieve the same success, with the site remaining a $CO_2$ source after restoration. The difference in outcomes between blanket and raised bogs suggests that peatland type is a critical factor influencing restoration success.

Holden et al. (2011) further emphasised the difficulties in restoring hydrological conditions on drained peatlands, even years after rewetting, making it harder to achieve pre-drainage water table levels and full carbon sink functionality. This is echoed by Wilson, Farrell, et al. (2016), who found that although rewetting reduced $CO_2$ emissions compared to drained peatlands, net GHG emissions were still higher than those from undrained sites. Additionally, Renou-Wilson et al. (2019) provided evidence of a rewetted peatland in Galway acting as a carbon sink, but Rigney et al. (2018) observed that a rewetted blanket peatland in Clare and raised peatland in Tipperary exhibited different outcomes. While the Clare site remained a carbon source, the Tipperary site showed a larger carbon source, demonstrating the variability in peatland recovery outcomes.

Moreover, studies outside Ireland reveal additional insights in rewetted peatland functionality. Levy et al. (2015) reported that a near-pristine peatland in Cross Lochs, Scotland, acted as a carbon sink, while Peichl et al. (2014) found similar results in near-pristine peatlands in Sweden, both showing the importance of maintaining near-pristine hydrological conditions. Hambley et al. (2019) showed that a rewetted peatland in Talaheel, Scotland, sequestered carbon, supporting the view that long-term rewetting (16 years in this case) can lead to positive carbon outcomes in cooler climates.

However, drained peatlands present more complex challenges. For example, Wilson et al. (2015) observed that drained blanket bogs and raised bogs, such as those in Galway, Mayo, and Offaly, continued to act as carbon sources despite varied hydrological conditions. This aligns with Holden et al. (2011), who emphasised the difficulty of fully restoring WT in rewetted peatlands. These studies reinforce the idea that rewetting alone may not be enough to restore carbon sink functionality, especially if the site remains vulnerable to drying out.

One of the key challenges is that rewetted peatland sites, though improved in that carbon emissions reduced compared to drained peatlands, remain sensitive to environmental changes (Wilson, Farrell, et al.,2016; Holden et al.,2011). These variations highlight the importance of factors such as land-use history, peat depth and local environmental conditions in determining whether rewetted peatlands can return to a functioning carbon sink. This underscores the need to refine restoration strategies and tailer them to specific characteristics of each peatland to enhance long-term success.

The variability in outcomes, points to the need for continued research, especially on the effects of climate and site-specific factors such as peat depth, vegetation cover, and hydrological management. O'Leary et al. (2025) used advanced airborne radiometric techniques to map peat soils in Ireland, identifying areas under current other land uses on peat soils, such as agricultural and woodland. This advancement in land-use mapping is important for accurately estimating GHG emissions from peat soils, as hectares of peatland can be multiplied by the reported land use emission factors to determine overall contributions to national inventories, such as the NIR (EPA, 2024).

Previous Irish research on degraded, rewetted, and near-natural peatlands such as those by Wilson et al. (2015) and the review by Aitova et al. (2023) have contributed to a more refined understanding of emissions from rewetted and degraded peatlands. These studies have informed the NIR (EPA, 2024) and highlight the importance of Irish peatland research in global climate change mitigation frameworks. However, while these contributions are significant, Tier 1 emission factors, which are less sensitive to country-specific conditions, are still used in the NIR. Tier 2 and Tier 3 methods offer more detailed and accurate emissions calculations but are not yet fully implemented for all land use on peat soil.

### 2.4.2 Mixed woodland emission and reductions

Previous literature on atmospheric GHG emissions from various forest habitats and soil types shows considerable variation in findings. Research on atmospheric carbon dynamics in European woodland ecosystems, particularly broadleaf woodlands, is relatively limited. However, two key studies on broadleaf woodlands are discussed below. In contrast, there is a greater body of research on industrial forests, likely due to their economic significance. A comparison is made between these two forest types, broadleaf and industrial, followed by a review of relevant Irish research on woodland carbon dynamics. The studies discussed provide insight into these different forest ecosystems.

A study conducted in Belgium using EC techniques examined a patchy forest consisting of mixed coniferous (*Douglas fir*) and deciduous (*beech*) plots. The forest sits on mineral soil with a soil depth of approximately 100–150 cm. The total NEE was estimated at -6 t $CO_2$ $ha^{-1}$ $yr^{-1}$. However, this result was considered preliminary, as it does not account for the night-time flux error, which was estimated to be between 10–20% (Aubinet *et al.*, 2001).

In contrast to this, a naturally diverse woodland in Switzerland was examined by Paul-Limoges et al. (2017), using eddy covariance techniques both above and below the canopy over a two-year period. While Aubinet's study presented preliminary NEE values, Paul-Limoges et al. observed a strong division between photosynthesis and respiration processes, with photosynthesis dominating the above-canopy measurements and respiration dominating below the canopy. This difference in fluxes above and below the canopy led them to analyse the vertical wind profile, where they identified significant air mass differences during the growing season when the canopy was fully closed.

To address these discrepancies, they developed a correction method to adjust for the influence of the below-canopy fluxes on the above-canopy NEE measurements. The above canopy values indicated the site was a significant $CO_2$ sink, with NEE estimated to be -27.81 ± 0.37 t $CO_2$ $ha^{-1}$ $yr^{-1}$, a much stronger sink compared to the -6 t $CO_2$ $ha^{-1}$ $yr^{-1}$ estimated in the Belgian study (Paul-Limoges *et al.*, 2017). However, by incorporating the below-canopy data, they refined their total NEE estimates, resulting in a much lower average range of -0.327 ± 0.004 t C-$CO_2$ $m^{-2}$ $yr^{-1}$. However, the study may have overestimated respiration from below canopy.

### 2.4.3 Industrial forests emissions

In contrast to the naturally diverse forests discussed above, two studies focusing on industrial forests on peat soil reveal quite different carbon dynamics due to the unique properties of peatlands and their history of drainage and extraction.

The first study by Hommeltenberg et al. (2014) looked at an industrial peatland forest in Germany over two years. Initially, the forest acted as a strong carbon sink, sequestering -130 and -300 g C $m^{-2}$ $yr^{-1}$ (-1.3 and -3.0 t C $ha^{-1}$ $yr^{-1}$) in the first and second years, respectively. However, when factoring in emissions from drainage and peat extraction prior to planting, the forest shifted from a carbon sink to a net source of emissions. According to the study, the forest would need to remain in place for over 140 years to fully offset the emissions generated over the prior 44 years, which were estimated at 134 t C $ha^{-1}$.

Similarly, the study by He et al. (2016) examined a coniferous plantation on drained agricultural peatland in Sweden. The forest acted as a source of emissions for the first 39 years of a 60-year simulation, only becoming a carbon sink thereafter. The simulated average carbon uptake was -413 g C $m^{-2}$ $yr^{-1}$ (-4.13 t C $ha^{-1}$ $yr^{-1}$) over the 60-year period. NEE varied, with the system acting as both a carbon sink and source during the first 19 years. After 1981, the forest generally functioned as a continuous carbon sink, with an average NEE of -217 g C $m^{-2}$ $yr^{-1}$ (-2.17 t C $ha^{-1}$ $yr^{-1}$) after this period. Despite the forest beginning to sequester carbon after the 39th year, the total carbon lost from the peat could not be offset by the forest's sequestration during the 80-year rotation, resulting in a negative overall GHG balance.

Studies on atmospheric GHGs from both industrially monocultured forests and diverse mixed forests are limited within Ireland. Research by Black et al. (2007) estimated the NEE of a closed canopy Dooary Forest, a Sitka spruce plantation in Co. Laois, Ireland over two years using EC techniques. The study found that the estimated NEE from EC ranged from -7.69 to -9.44 t C $ha^{-1}$ $yr^{-1}$. In addition to this, Saunders et al. (2012) later found similar results for NEE from the same site. Their study assessed NEE using EC before and after thinning of the woodland. The results from all years are comparable to those of the Black et al. (2007) study. Pre-thinning (2002–2006) NEE ranged from -8.44 to -8.87 t C $ha^{-1}$, and post-thinning (2007–2009) ranged from -6.75 to -10.33 t C $ha^{-1}$. This site investigated in these studies was on mineral soil and was monoculture industrial spruce forest plantation. In contrast to these results from mineral soils, studies on peat soil forests, particularly in Europe, show that industrial plantations on drained peatland have a generally lower uptake of NEE (He et al., 2016). Possibly due to the dry peat soil having considerable emissions through respiration.

Although conducted in a different climatic region, an interesting study on a *black spruce-sphagnum* wetland biome in Canada's boreal climate found that, over a decade, annual net NEE estimates fluctuated between -0.058 and 0.084 t C-$CO_2$ $m^{-2}$ $yr^{-1}$, with an average of 0.024 t C-$CO_2$ $ha^{-1}$ $yr^{-1}$ for the entire period. This is a much lower NEE value than the studies mentioned above, likely due to the differences in climate region (Dunn *et al.*, 2007).

The differences in emissions between mixed woodlands and industrial forests in previous research are challenging to interpret due to variations in soil type and regional factors. In Aubinet et al. (2001), carbon flux contributions from conifer and beech sub-plots were analysed using a flux footprint model. The researchers successfully separated the two sub-plots during most daytime conditions, but this was not possible at night due to the larger footprint size. A difference in energy balance closure was observed between the conifer and beech stands, likely caused by differences in stand albedo. Although no difference in respiration rate at 10°C was found between the two sub-plots, a clear distinction in dark respiration was noted, likely due to the larger flux footprint at night. This highlights some differences in the potential GHG sink/source function of deciduous versus coniferous trees.

Similar results from the Irish studies (Black *et al.*, 2007; Saunders *et al.*, 2012) on industrial forests on mineral soils align with the findings from Aubinet et al. (2001) and Paul-Limoges et al (2017). This could be attributed to the similarities in soil type between the study sites or similar forest age. However, the lack of data on mixed woodlands on peat soils makes it difficult to draw direct comparisons between industrial sites on peat soils and mixed woodlands on peat soils. This gap in research is a key limitation in understanding the potential differences in carbon emissions between these forest types.

#### 2.4.4 Below canopy studies

There is limited research on NEE above peatland forest canopies, whereas studies below canopy are more prevalent. The chamber method has proven effective in estimating below-canopy photosynthesis and respiration, which can be underestimated by EC towers due to reduced turbulence beneath the tree canopy (Baldocchi, 2003; Jovani-Sancho et al., 2017). Forest floor vegetation biomass is closely linked to tree stand biomass, as canopy shading controls the sunlight reaching the ground (Reinikainen et al., 1984). Although research has primarily focused on SOC, this section places more emphasis on below-canopy NEE, an area that remains less explored despite its significance.

A study in a pine-dominated forest on peat soil in Finland explored $CO_2$ exchange within ground vegetation and the impact of environmental factors on gas exchange (Badorek et al., 2011). This research, unlike many chamber studies that focus on soil $CO_2$ fluxes alone, utilised a transparent, closed chamber to measure the total $CO_2$ exchange of the forest floor. Measurements were taken fortnightly using a 30 cm-high polycarbonate chamber. First, the NEE of the forest floor was recorded, followed by the measurement of respiration by covering the chamber with dark fabric. GPP was calculated by subtracting total respiration from NEE. The study showed significant variation in $CO_2$ exchange between different plant communities, with *sphagnum moss*-dominated areas acting as stronger carbon sinks. This highlights the variability of forest floor ecosystems across different peatland sites.

Badorek et al. (2011) found that $CO_2$ absorbed by the forest floor accounted for 20–30% of the total NEE of the forest, as measured by Lohila et al. (2011) using EC above the canopy. This contribution was equivalent to one-third of the $CO_2$ exchanged by the trees, which was estimated at -2700 g $CO_2$ $m^{-2}$ $yr^{-1}$ (-27 t $CO_2$ $ha^{-1}$ $yr^{-1}$). The high proportion of $CO_2$ uptake was attributed to the dense ground cover and significant light penetration through the canopy (Badorek *et al.*, 2011). However, the forest floor acted as a net $CO_2$ source due to the inclusion of tree root respiration. Comparisons with earlier studies showed similar findings. Mälkönen (1974) observed that forest floor vegetation in a Scots pine forest on mineral soil contributed 21–29% of total biomass production, while O'Connell et al. (2003) reported that feather moss in a Canadian black spruce peatland contributed 14% to total net primary production. Badorek et al. (2011) recommended year-round, high-frequency measurements with automatic chambers and comprehensive carbon balance calculations for greater accuracy.

In contrast, Paul-Limoges et al. (2017) conducted a study on both above and below-canopy NEE, finding that below-canopy respiration contributed an impressive 79% to the overall ecosystem respiration. The study, conducted in a temperate mixed forest on mineral soil in Switzerland, used EC techniques both above and below the canopy, as well as vertical $CO_2$ and wind profiles within the understory. Average below-canopy respiration values were 769 g C $m^{-2}$ $yr^{-1}$ (7.7 t C $ha^{-1}$ $yr^{-1}$), with GPP accounting for only 9% of the total ecosystem GPP was estimated to be -122 g C $m^{-2}$ $yr^{-1}$ (-1.2 t C $ha^{-1}$ $yr^{-1}$). Total below-canopy NEE was estimated at 647 g C $m^{-2}$ $yr^{-1}$ (6.5 t C t C $ha^{-1}$ $yr^{-1}$). Although this study used more advanced EC techniques compared to chamber methods, it emphasised the significant role of the understory in the carbon balance of complex forest ecosystems.

Both studies underscore the importance of below-canopy processes in forest carbon cycling. While chamber studies like Badorek et al. (2011) provide detailed insights into forest floor dynamics, studies like Paul-Limoges et al. (2017) highlight the need for comprehensive approaches that capture the contributions of both the canopy and understory. Each approach offers valuable perspectives, but the combination of advanced methods, like EC, with detailed chamber studies may provide the most accurate assessments of forest carbon balance across various soil types and forest compositions.

A study by Jovani-Sancho et al. (2018) on soil carbon balance in afforested peatlands in Ireland found that soil $CO_2$ efflux was influenced by soil temperature and water WT. Total soil respiration, including heterotrophic, root, and litter respiration, ranged from 26.7 to 40.6 t $CO_2$ $ha^{-1}$ $yr^{-1}$ (7.2 to 11 t C $ha^{-1}$ $yr^{-1}$ ). While these values are similar to other results from below-canopy NEE studies, Jovani-Sancho et al. (2018) focused solely on respiration rather than NEE. Additionally, their research examined monoculture forestry plantations (Sitka spruce and lodgepole pine) across eight sites, in contrast to other studies which focus on diverse mixed woodlands.

Other studies, such as Tikkasalo et al. (2024), examine emissions post-clear felling, finding peatland forests to be significant sources of GHGs, with $CO_2$ emissions accounting for 82.5% (23.3 t $CO_2$ ha$^{-1}$ yr$^{-1}$) (6.3 t C ha$^{-1}$ yr$^{-1}$), and minimal $CH_4$ emissions at 0.4% (0.1 t $CO_2$-eq ha$^{-1}$ yr$^{-1}$)(0.0075 t C ha$^{-1}$ yr$^{-1}$). Similarly, Jovani-Sancho et al. (2021) found that decomposing waste biomass from industrial forest harvesting contributes significantly to GHG emissions.

#### 2.4.5 Inconsistency with chamber collars and structures

The inconsistencies in chamber methodologies vary across research papers, with differences in the details of how the methods are implemented. Past research has used various collar depths depending on the chamber size or site type, and in some cases, the collar insertion depth is not specified (Janssens *et al.*, 2001; Wang *et al.*, 2010; Heinemeyer and McNamara, 2011; Heinemeyer *et al.*, 2011; Wilson, Farrell, *et al.*, 2016; Jovani-Sancho *et al.*, 2017; Jovani-Sancho *et al.*, 2021). For example, Janssens et al. (2001) describe the chamber collar size and depth in detail, however in Wilson et al., (2016) study there is no description included of the placement depth of the collars used.

Another study of a temperate forest in China that compared Chamber and EC based methods, describes the dimensions and material of the chamber and collars, yet there is no mention of the depth that the collars were inserted into the soil at (Wang *et al.*, 2010). Standardisation of the implementation of collars across studies is unclear however, there are general guidelines outlined in a report by Fiedler et al. (2022) that state chamber insertion depth should depend on the soil type, vegetation root system and the intended chamber deployment period. Although a guide to depth depending on deployment period is outlined there is no direction within the report as to what depth in cm to position the collars at regarding the environmental variables of vegetation type and root systems (Fiedler *et al.*, 2022).

There is emphasis in the literature conveying the significance of using collars, which is to diminish the risk of lateral gas leakage between the surface of the soil and the chamber itself (Heinemeyer and McNamara, 2011; Heinemeyer *et al.*, 2011; Pavelka *et al.*, 2018;

Fiedler *et al.*, 2022). However, in order to place collars into the soil, first roots of the above vegetation must be severed and the soil disturbed to allow space for the collar placement.

Considering this, Heinemeyer et al. (2011) conducted an experiment comparing chamber collars inserted into the soil versus surface chambers across three ecosystem types in England (forestry, blanket peatland, and grassland). The results showed that $CO_2$ efflux estimates from inserted collars were around 15% lower than those from surface collars, with the underestimation increasing to 30-50% during peak respiration times. The study also found that root length was predominantly concentrated in the top 5 cm of soil, particularly in the peatland site, which reinforced the hypothesis that collar insertion can significantly affect soil flux measurements. The study supports the idea of using non-invasive collars to improve measurement accuracy and confirms that tree roots contribute about 50% of soil respiration in forest ecosystems (Heinemeyer *et al.*, 2011).

Later research by Jovani-Sancho (2017) supports the findings of Heinemeyer et al. (2011) regarding the drawbacks of using collars. In their study, they investigated afforested peatland in Ireland, focusing on spruce and pine plantations growing on peat soils. The study compared the results from chamber collars inserted at various depths to those from a surface collar that sits on the soil without penetrating it. The results revealed that the shallowest collar, inserted just 5 cm into the soil, resulted in the most significant underestimation of soil respiration, with a 47% and 32% underestimation in the spruce and pine plantations, respectively. This underestimation was attributed to the damage caused to fine roots and fungal hyphae near the soil surface, which are crucial for soil respiration. Given that forest ecosystems on peat soils typically have shallow root systems, this research further reinforced that collar insertion can distort soil flux measurements. Jovani-Sancho et al. (2017) concluded that the potential gas leakage from surface collars, which are less invasive, is far less problematic than the significant underestimation of soil respiration caused by collar insertion, whether shallow or deep. This highlights the need for more non-intrusive methods to obtain more accurate measurements of soil respiration in forest ecosystems.

In conclusion, while the chamber method provides valuable insights into carbon fluxes for many ecosystems at smaller scales, particularly for localised measurements like below-canopy, respiration and NEE in forests, its limitations in capturing larger-scale and continuous fluxes highlight the need for careful consideration. Additionally, the use of collars inserted into the soil should be reconsidered in forest ecosystems where tree roots are prominent, as they can affect respiration rates. By incorporating the chamber method with the EC technique, can improve accuracy and reliability of measurements, especially when studying complex ecosystems like forests.

### 2.4.6 National inventory report emission factors

Ireland calculates emission EFs for forest peat soils based on country-specific research by Jovani Sancho et al. (2021), adhering to international guidelines. For on-site emissions, the emission factor is 1.68 t C $ha^{-1}$ $yr^{-1}$, representing the mean carbon loss across all forest age classes during the first rotation. This Tier 2 EF aligns with the IPCC's Tier 1 emission factors for organic soils in cold, wet temperate climates. Additionally, an off-site emission factor of 0.31 t C $ha^{-1}$ $yr^{-1}$ is applied to account for DOC runoff from drained organic and organo-mineral soils, in line with the IPCC Wetlands Supplement (2013). These emission factors are used to estimate carbon emissions from forest soils in Ireland's national inventory submission to the UNFCCC.

The calculation of atmospheric GHG emissions for Irish forests, as detailed in NIR (EPA, 2024) follows the methodologies established in the 2006 IPCC Guidelines the IPCC Wetlands Supplement (2013). The Tier 3 carbon budget model (CBM-CFS3) (Black *et al.*, 2007; IPCC, 2013), informed by data from the Irish National Forest Inventory (NFI) (DAFM, 2022), is applied to estimate emissions. The NFI provides essential inputs, such as forest area, species composition, age structure, and soil types, which are used to derive emission factors for all forest lands, irrespective of soil type.

The CBM-CFS3 model was validated using forest NEE data from EC measurements, as referenced by Black et al. (2007). Uncertainty analysis for forest land, including land converted to forest, shows a reduction in uncertainty over time, from 30.2% in 1990 to 14% in 2022 (EPA, 2024). However, the NIR does not differentiate between forest types on peat soils; emissions from all forest types are grouped together under a single category. As a result, emissions from mixed woodland and industrial forests are not treated separately and estimates of emissions from biomass removal are included.

Black et al. (2007) compared NEE of a closed canopy Sitka spruce forest over two years using both EC and modelling techniques. The study found that the estimated NEE from EC ranged from -7.69 to -9.44 t C $ha^{-1}$ $yr^{-1}$, while the model gave values between -7.30 and -11.44 t C $ha^{-1}$ $yr^{-1}$. These differences were not statistically significant, largely due to uncertainties in estimating biomass increment (15-21%) and heterotrophic respiration (12-19%). The study concluded that despite the higher values found in model-based assessments, there was no systematic difference between Model and EC methods when applied across various forest types and geographical locations.

Furthermore, the emission factors for certain land-use categories on peat soils, such as forests, group together different forest types, including monoculture industrial forests and more diverse, species-rich broadleaf forests. This approach may oversimplify the carbon dynamics within these ecosystems.

### 2.4.7 The challenges identified in the research

The most sustainable approach to managing cutaway peatlands remains uncertain, and thus further research is essential to determine the best land use management practices for maximising the value of these degraded sites. Long-term observations on restored peatland sites are necessary to understand how they respond to climate changes, and to account for the associated GHG emissions, whether lost or gained, in compliance with EU standards (Wilson et al., 2016; Rigney et al., 2018; Renou-Wilson et al. 2019)..

Aitova et al. (2023) highlight the significant gap in data for Irish peatlands, noting that the lack of region-specific information is a major limitation for the default emission factors provided in the IPCC Wetlands Supplement (IPCC, 2013). This data gap impedes the accurate application of the outlined values in the report. Evans et al. (2017) also criticise the IPCC supplement for its failure to distinguish between peatland types and for relying on data derived from European studies, which may not accurately reflect the climatic differences in regions like England and Ireland. These gaps further underscore the inadequacy of the default reporting values for woodlands, necessitating considerable improvements.

A critical research gap exists in understanding the carbon dynamics of mixed woodlands on peat soils. While studies on industrial forestry on peatlands are more abundant, research focusing on mixed woodland forests in peatland ecosystems is limited. This lack of data makes it difficult to assess whether the carbon emissions from mixed woodlands on peat soils differ significantly from those of industrial forests on similar soils. Addressing this gap is essential for developing a more comprehensive understanding of the carbon sequestration potential of these forest types, and for creating effective management strategies for peatland restoration and conservation.

# 3 Study Site and Instrumentation

## 3.1 The Irish climate

This study was conducted in Ireland, an island located in the north-western region of Europe. Ireland experiences a temperate oceanic climate, strongly influenced by the Atlantic Ocean. Due to the North Atlantic current, which brings warmer air via prevailing winds, Ireland has milder temperatures than other locations at similar latitudes (Nolan, 2024). Ireland's climate history has closely mirrored global trends, with a notable rise in mean annual air surface temperatures of approximately 1°C since the early 20th century (Noone *et al.*, 2023). Over the 60 years leading up to 2019, it was observed that Ireland experienced more frequent days where temperatures exceeded 20°C, while the number of days with sub-zero temperatures became less common (Cámaro García and Dwyer, 2021).

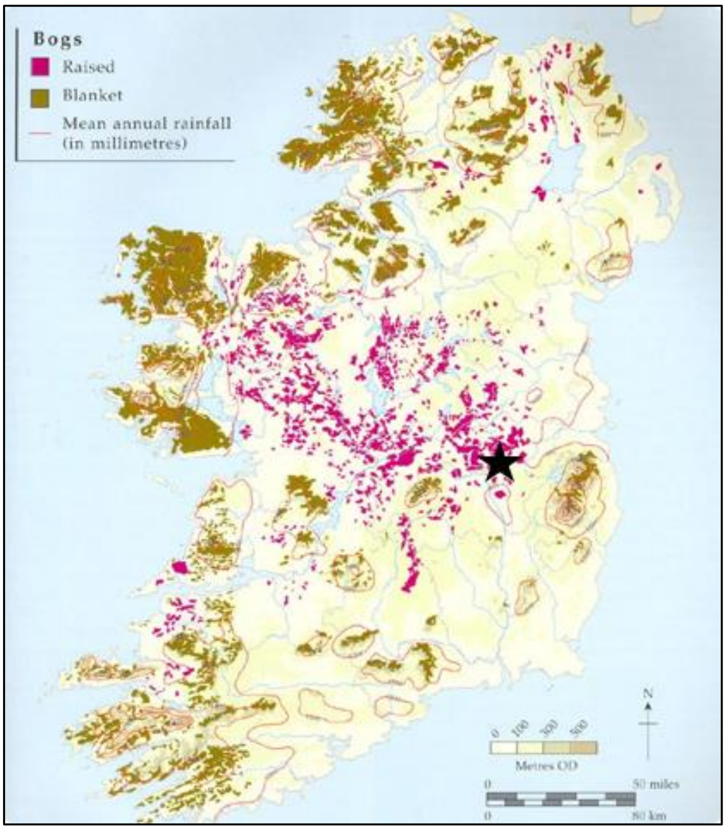


*Figure 3.1 Map of Ireland, highlighting the study area (The Atlas of the Irish Rural Landscape (1997).*

Coastal areas, influenced by the sea, tend to be the warmest, while higher elevations are cooler (Curley *et al.*, 2024). Recent climate data shows an increase in warm and wet days. Between 1991-2020, the national average annual rainfall was 1,288 mm, with the wettest areas in the west, especially at higher altitudes, ranging from 878 mm in the east to 2,045 mm in the southwest (Curley *et al.*, 2024) .

## 3.2 The study site

The study site was located on a former raised peatland situated at Lullymore heritage park, Co. Kildare in the midlands of Ireland with an approximate altitude of 81m (Latitude 53.274°N, Longitude -6.961°W) (Study site location shown in Figure 3.1). Long term historical averages were derived from Lullymore nature centre weather station (Met Éireann, 2022). The weather station is situated in close proximity to the study site at just 1.4 Km away, with an altitude of approximately 87m (Latitude: 53.279 and longitude: -6.942). The average data presented here is from 2010 up until 2022. Derived from this data the mean annual rainfall for the area was 894 mm. The daily maximum and minimum temperatures were recorded from 2012 to 2022 at the weather station, showing a mean annual temperature range from 14.3°C to -6.1°C. The average temperatures are consistent, with the maximum and minimum temperatures only fluctuating by approximately 1°C within the averages for the period.

Although annual averages for temperatures are futile, monthly averages identify distinct seasonal change throughout the year, Figure 3.2 illustrates this trend. Temperatures are higher throughout Summer and early Autumn months, averaging just under 20 °C, with the lowest temperatures occurring in January and February, but still relatively mild not dropping below 2 °C. The average rainfall is generally lowest in April, with March and May also lower than mid-summer and Autumn/Winter months with Rainfall highest in December.

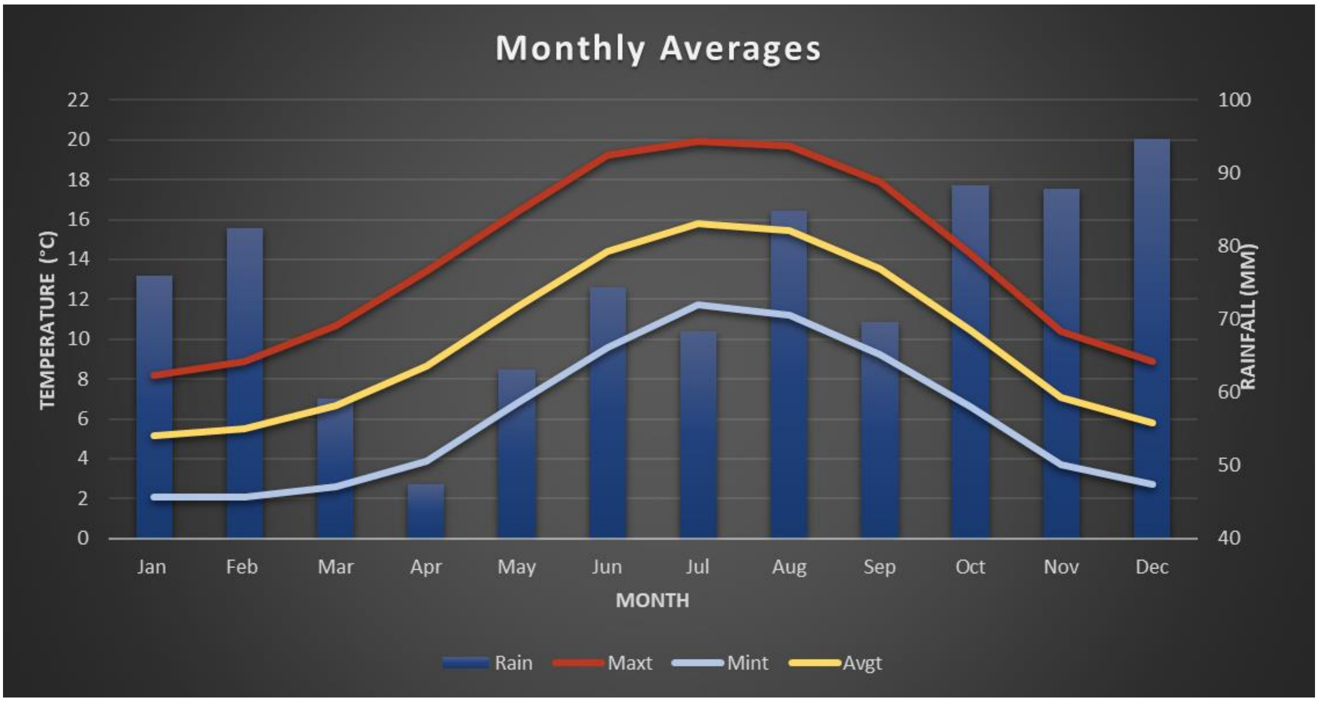


*Figure 3.2 Monthly average air temperature and total monthly rainfall (2010-2022) from Lullymore nature centre (photo: author).*

The study area was once part of a vast raised peatland with substantial peat depth, resulting in predominantly peat-dominated soils. Situated on a former raised bog, the peat soils in this region can be classified within the 'Turbary Complex' soil series, a category of degraded raised bog soils (Feehan and O'Donovan, 1996). Over time, the area has experienced extensive drainage, industrial-scale peat harvesting, and significant land-use changes. The large-scale peat extraction, primarily for electricity production, ceased over three decades ago. Today, the broader landscape, spanning approximately 100 km (Figure 3.3), consists of a patchwork of degraded peatlands, including bare cutaway areas, woodlands, and agricultural land. A review of available orthophotography by the Bord na Móna ecology team (McNicholas and Ellison, 2023), describe the establishment of this woodland began following the cessation of peat extraction in the early 1990s. A significant portion of the woodland (Figure 3.4) in the study area appears to be located on a ridge beneath the bog, where much of the peat was removed, leaving only a shallow layer of residual peat.

*Figure 3.3 100km² Lullymore catchment area, red dot marks study site (Landviewer: author).*

The Lullymore site underwent drain blocking in 2006/2007 to encourage waterlogged conditions, raise the water table, and foster the growth of peatland vegetation, with the goal of reducing $CO_2$ emissions. In 2011, additional rehabilitation efforts were made to block drains in a nearby area with the same goal of re-wetting the site. Aside from these interventions, the site remained largely unmanaged until 2015, when fertiliser was applied to the southern side to promote the growth of birch scrub. In 2016, further drain blocks were implemented, and existing drain blocks were maintained. Beyond these efforts, no further human interventions have taken place in the woodland surrounding the EC tower as of 2025, to the best of the author's knowledge.

Although certain areas have supported the growth of patches of vegetation and woodland, a large portion of the site remains severely degraded, consisting of bare peat with limited vegetation. However, the specific area studied (Figures 3.4 and 3.5) has seen minimal management since peat extraction ended decades ago, enabling the natural regeneration of native tree species. This provides a unique opportunity to investigate the carbon balance of a naturally established mixed woodland on cutaway peatland.

The EC tower is situated at a slightly higher elevated position of 82 meters, compared to the surrounding terrain, which ranges between 72 and 74 meters in altitude. A piezometer installed on site showed that the site is very dry in comparison to a 'near natural' peatland. For example Clara peatland located in County Offaly Ireland, considered to be a near-intact peatland, had a water table depth of -15 ± 5.4cm in 2022 (Ingle, Bhatnagar, et al., 2023). Whereas the water table depth for Lullymore woodland site ranged from -69.2 ± -36.54cm for one year, from August 2022 to Aug 2023. The dry soil type may be because of the vegetation cover consisting of dense woodland or it may be due to the slightly higher elevation or possibly a combination of both. None-the-less, this dense woodland site is considered a dry site. An existing drain is still in existence to the East side of the woodland site, which is another possible factor of the dryness of the site.

Soil moisture sensors installed on the site also correlate with the water table of the site on average the soil moisture content of the soil was never more than 35%. However, the water content reflectometer may not work effectively in peat soils due to the need for a unique calibration, as the standard calibration can be affected by soil properties like high electrical conductivity from free ions, or high bulk density, particularly in organic soils, potentially leading to incorrect readings from the sensor (Campbell Scientific, 2012).

The area of woodland surrounding the EC tower spans roughly 0.15 $km^2$ (blue line Figure 3.4). Following an ecological survey carried out by the ecology team within Bord na Móna (McNicholas and Ellison, 2023), the area consists of a diverse range of tree species and ground cover vegetation discussed in more detail below.

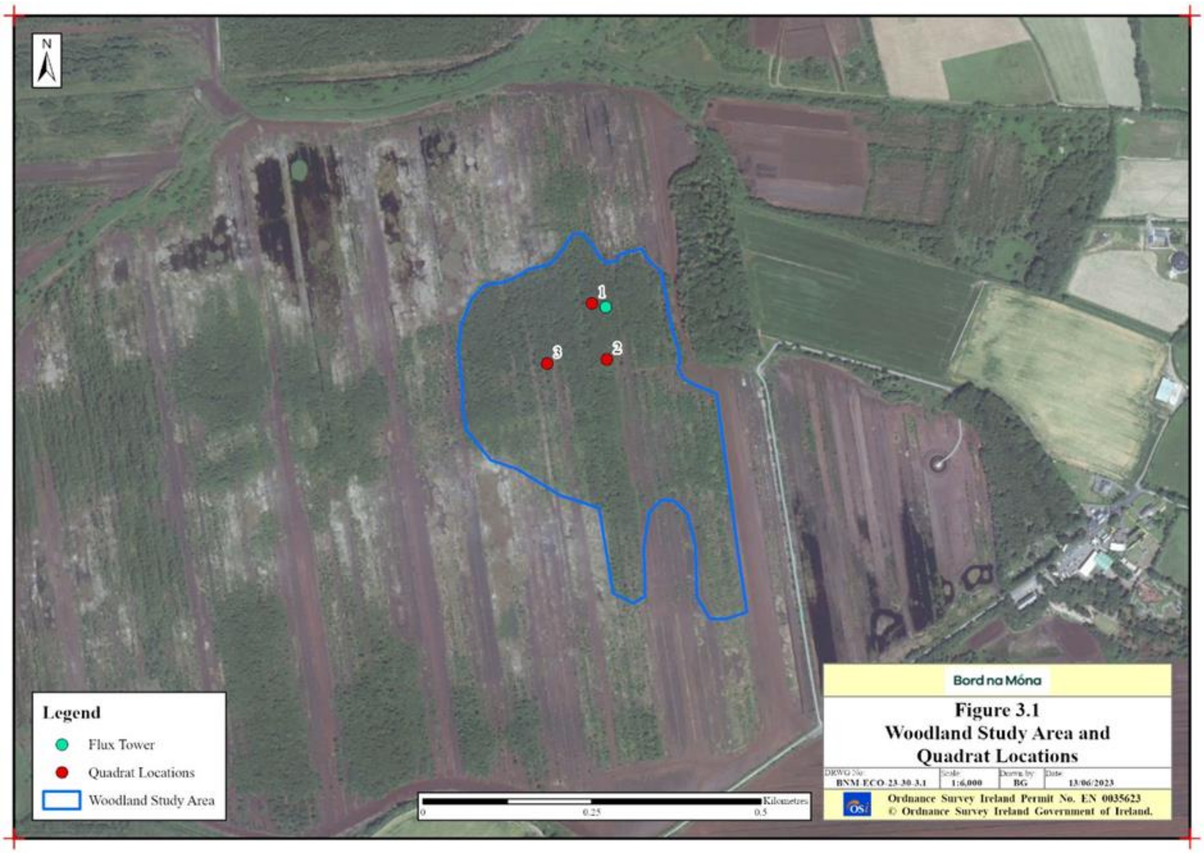


*Figure 3.4 Quadrat locations from ecology survey* (McNicholas and Ellison, 2023).

Within the footprint of the tower the ecologists reviewed three locations via quadrat surveys (red dots in Figure 3.4). For the purpose of their recordings the percentage cover of plant species within each plot, within the woodland was divided into four layers: the canopy (>4.5 metres) consisting of mature trees; the shrub layer (2-4.5 metres) made up of immature trees and woody shrubs; the field layer (0.2 metres) comprising of ferns, grasses, sedges, and herbs; and the ground layer (0-0.2 metres), which included ivy, mosses, fungi, and lichens.

The results of their findings showed the canopy was predominantly composed of Downy Birch (*Betula pubescens*) with 90% cover, along with some Grey Willow (*Salix cinerea*) and Scots Pine (*Pinus sylvestris*), each contributing 5%. The shrub layer featured species such as Oak (*Quercus robur*), Hawthorn (*Crataegus monogyna*), Beech (*Fagus sylvatica*), and Rowan (*Sorbus aucuparia*). In the field layer, saplings of Sycamore (*Acer pseudoplatanus*) and Holly (*Ilex aquifolium*) were beginning to establish, suggesting that, over time, the initial pioneer species, Downy Birch, Grey Willow, and Scots Pine, would be complemented by greater tree species diversity as the woodland matures.

Dewberry (*Rubus caesius*) dominated the field layer with 30% cover, while the ground layer was primarily composed of mosses such as *Kindbergia praelonga* and *Eurhynchium striatum* (60%), Ivy (*Hedera hibernica*) (10%), Wild Strawberry (*Fragaria vesca*) (5%), and a dense carpet of leaf litter (70%). Other species recorded included Field Horsetail (*Equisetum arvense*) and Hairy Brome (*Bromopsis ramosa*). They noted the ground was dry, with no *Sphagnum* moss species observed. Standing deadwood was also present, with five dead stems and numerous fallen stems recorded within the plots.

Their findings concluded that the woodland within the Lullymore study area does not correspond to the Annex I habitat "Bog Woodland" as defined by (NPWS, 2019). However, due to the increasing diversity of tree species establishing in the area, it is possible that, over time, this woodland may develop characteristics similar to the WN1 Oak-Birch-Holly Woodland, as described by (Perrin, 2015). Figure 3.5 shows the tree canopy from above the EC tower.

In the broader area, the forest is separated from a neighbouring mature *Scots pine* forest to the east by an open drainage ditch. To the northwest and west, the woodland is bordered by patches of bare peat and sparse vegetation, featuring species such as *bog rush, bog cotton,* and *sphagnum mosses*, interspersed with waterlogged areas. The ecology report noted that the mature woodland to the east could be classified as such and may have influenced species establishment at the site (McNicholas and Ellison, 2023).

By Bord na Móna's standards, the site as a whole is now classified as a shallow peatland, with an average peat depth of less than 1.5 meters across the area (M.McCorry, pers. Comm., 2023). Within the footprint area of the EC flux tower, 24 peat depth measurements were taken using a peat probe, revealing an average depth of just 20 cm, indicating a very shallow peat layer. Soil samples taken within the footprint of the tower revealed an average soil bulk density of 0.26 g/cm$^3$.

The classification map in Figure 3.6, provided by Bord na Móna, illustrates the various vegetation classifications according to guidelines from Fossitt (2000). It clearly indicates that a significant portion of the peatland is classified as birch willow woodland, with birch willow scrub also identified as a predominant vegetation type across the site.

*Figure 3.5 Above canopy vegetation and top of the EC tower at Lullymore (photo: author).*

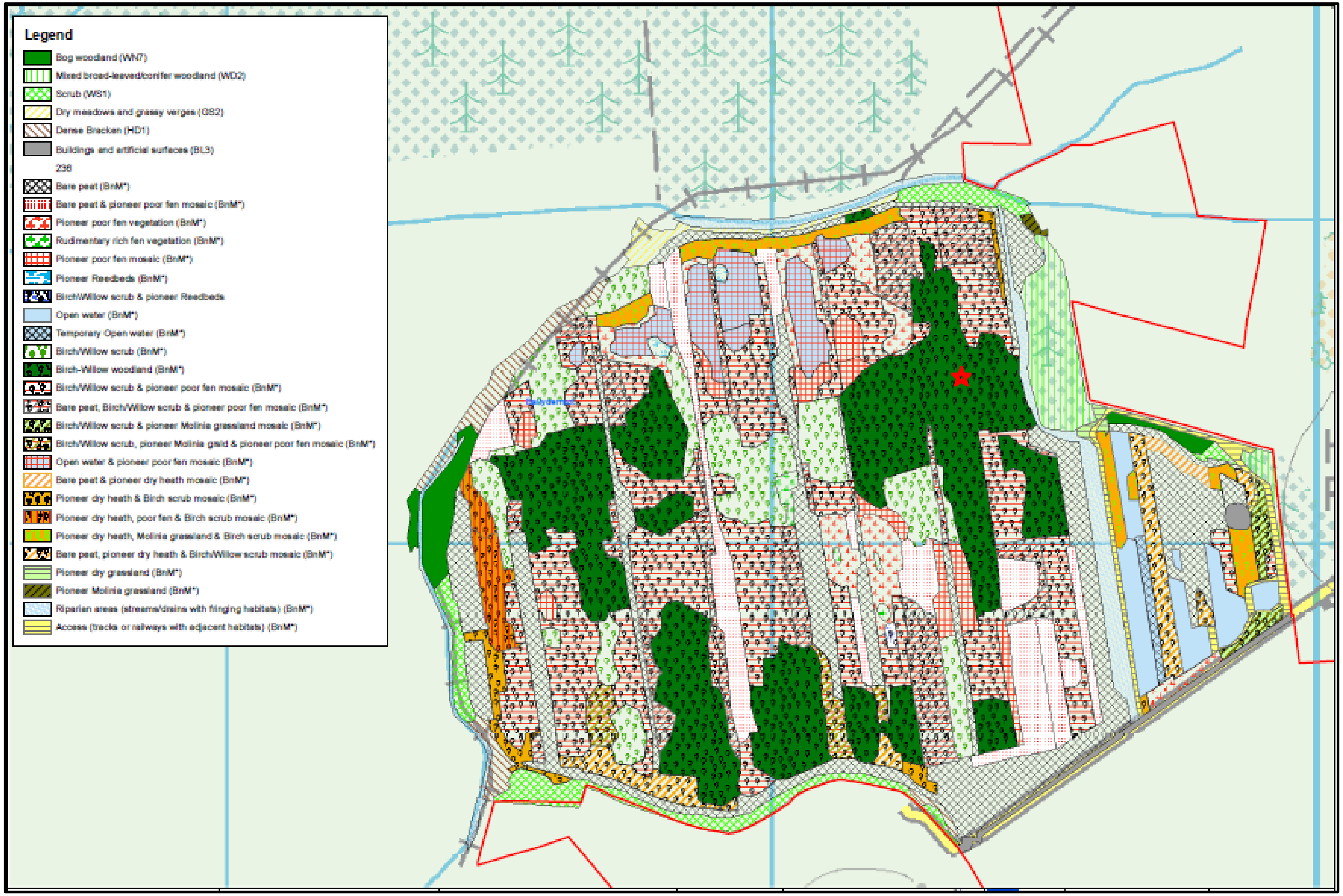


*Figure 3.6 Lullymore area classification map (2015, Bord na Móna), EC tower location shown by star*

The understory vegetation can be seen in Figure 3.7. After the detailed ecological review (McNicholas and Ellison, 2023), the below-canopy vegetation consisted of a field layer dominated by Dewberry (*Rubus caesius*) with 30% cover, while the ground layer was primarily *mosses*, including *Kindbergia praelonga* and *Eurhynchium striatum* (60%), along with *Ivy* (*Hedera hibernica*), *Wild Strawberry* (*Fragaria vesca*). Other species present were *Field Horsetail* (*Equisetum arvense*) and *Hairy Brome* (*Bromopsis ramosa*). In addition to the living vegetation, a layer of leaf litter, decaying branches, and pine needles contributes to the undergrowth. The distinct characteristics of this site present an excellent opportunity to study the carbon sequestration potential of the woodland, along with its meteorological patterns, and to compare the findings with other degraded peatland sites.

*Figure 3.7 Below canopy vegetation Lullymore site (photo: author).*

## 3.3 Instrumentation

The aim of this study was to investigate the atmospheric carbon dynamics of a natural woodland established on the cutaway peatland site, focusing on both overall canopy fluxes and below-canopy fluxes. To achieve this, two primary field methods were employed: the eddy covariance method to measure overall NEE ($CO_2$) and $CH_4$ fluxes and the chamber method to estimate NEE below the canopy ($NEE_{bel}$).

### 3.3.1 The chamber head and instrumentation

The chamber method exhibits substantial variation across published studies (Matson *et al.*, 1995; Griffis *et al.*, 2000; Tuittila *et al.*, 2004; Laine, 2006; Waddington *et al.*, 2010; Wang *et al.*, 2010; Heinemeyer *et al.*, 2011; Wilson, Blain, *et al.*, 2016; Jovani Sancho *et al.*, 2017; Jovani-Sancho *et al.*, 2021; Fiedler *et al.*, 2022) and, many studies lack sufficient detail regarding the design of the chambers and the techniques for collar insertion (Wellock *et al.*, 2011; Jovani-Sancho *et al.*, 2017; Fiedler *et al.*, 2022). Therefore, to maximise reproducibility, detailed procedures were recorded in this research.

The chamber used in this study was constructed from clear plexiglass (Figure 3.8) (40 cm diameter, 70 cm height and 5mm thickness) designed to accommodate typical understorey vegetation beneath the tree canopy. The chamber head included a hinged lid was from clear plexiglass of 5mm in thickness (40.5cm diameter) (Figure 3.8 & 3.9).

Three holes were drilled into the lid, and they were fitted with 20mm diameter glands to allow the addition of tubing while maintaining a seal. A rubber seal was fitted to the top of the cylinder to create a seal when the lid was closed. Rubber clasps were fitted on to the top of the lid and steel brackets were mounted on to the cylinder for the rubber clasps to sit into. This pulled the lid tight against the body of the chamber ensuring a seal around the bottom of the lid and the top of the chamber body. Clear rubber tubing with a diameter of 10mm and length of 150 cm were fitted into the two glands on the lid and directly connected to the $CO_2$ analyser.


*Figure 3.8 Clear static chamber connected to the EGM-4 analyser (photo: author).*

As the measurements were taken from a woodland ecosystem with the intention of estimating $R_{bel}$, keeping the roots of vegetation intact was important to gain a more accurate evaluation (Jovani-Sancho *et al.*, 2017). On consideration of previous research for this project, no chamber collars were installed in conjunction with the chamber to ensure as little soil disturbance as possible (Badorek *et al.*, 2011; Ojanen *et al.*, 2012; Jovani-Sancho *et al.*, 2017). To assess the potential for lateral $CO_2$ leakage following chamber construction, a comparative test was conducted to evaluate the difference between using a chamber collar and no collar. This experiment was carried out at a peatland restoration site in Tyrrellspass, County Offaly, Ireland. Chamber collars with the same diameter as the chamber were already installed at the site. Using the EGM-4 gas analyser, $CO_2$ measurements were taken with the chamber placed on the collar for an incubation period of three minutes. The same procedure was then repeated by placing the chamber directly onto the ground vegetation, without a collar. Upon reviewing the results, no significant difference was observed between the two measurements, indicating minimal detectable $CO_2$ leakage occurred when the chamber was placed directly to ground vegetation without a collar. Therefore, chamber collars were not used in this research (Figure 3.10).

The $CO_2$ analyser used was the EGM-4 portable $CO_2$ analyser from PP systems, USA (Figure 3.8 & 3.9). This was operated by a 12 Volt external battery connected by a customised power cable made by the manufacturers. A steel bracket inside the lid of the chamber was installed in the centre, to add internal components. On this bracket a 5 Volt fan (RS components, UK) was fitted with adequate space for the small battery USB pack to be mounted, which was the power supply for the fan. Extending out at a right angle from this bracket another small bracket was attached to hold a PAR sensor. The PAR sensor used was an AccuPAR PAR/LAI Ceptometer (Model LP-80) from Decagon Devices, Inc., USA. It was manually installed for each use, with the cable routed through the third gland on the chamber lid, and powered by four standard 1.5 V AAA alkaline batteries. Temperature inside the chamber head was monitored with a portable HI 93510 thermometer from Hanna instruments, powered by a 9 Volt battery.

*Figure 3.9  Below canopy chamber measurements at Lullymore taking an NEEbel measurement (photo: author).*

Three chamber plots were randomly selected to capture the general diversity of plant species present beneath the tree canopy. Figures 3.10, 3.11 and 3.12 show the chamber locations chosen to include the most prevalent vegetation species below canopy including *Dewberry (Rubus caesius), Ivy (Hedera hibernica)* and leaf litter. These plots were located approximately 10m west of the EC tower to minimise any potential overshadowing from the tower structure. While any shadows cast by the tower would have been comparable to those created by the surrounding trees, this was not considered a significant issue. At each designated location, the chamber was positioned for measurement. Since collars were not used in this experiment, wooden bamboo markers were placed at each chamber plot to ensure consistent positioning. The markers were placed on either side of the chamber before its removal, ensuring that the chamber was returned to the exact same position for each subsequent measurement.

For the initial placement of the chamber, minor ground disturbance was necessary to ensure an airtight seal around its base. Secateurs were used to trim surrounding ivy vines and remove large debris, creating a clear space for the chamber to sit directly on the peat soil. Before taking the first measurements at each of the three designated plots, a smoke test was conducted to check for lateral $CO_2$ leakage around the chamber base, using the same incubation time as for the measurements. The test confirmed successful sealing, though one plot required additional adjustments to improve the seal, resulting in slightly more disturbance to the soil and vegetation. However, this disturbance remained minimal compared to the insertion of permanent collars. The chamber was equipped with a hinged lid, facilitating the return of ambient air levels between measurements without disturbing the chamber head.

*Figure 3.10 Chamber Location 1 (photo: Author)*

*Figure 3.12 Chamber Location 2 (photo: Author)*

*Figure 3.11 Chamber Location 3 (photo: Author)*

### 3.3.2 The eddy covariance tower and instrumentation

To facilitate continuous gas flux measurements in order to estimate total NEE an EC tower (Figure 3.13) was established on the site in 2016 with mains power reaching the area for continued power supply. The study site is relatively flat and there is little to interrupt the wind flow from surrounding areas, these are conditions that assist in gaining accurate flux measurements when carrying out the EC method (Burba, 2013, 2022). The structure consists of lightweight scaffolding sections that intersect with one another, and crossbars attached between sections for support and stability. Unfortunately, the EC tower has been non-operational since 2016. Due to tree growth, an additional 2 meters of scaffolding was added to raise the tower, ensuring enough clearance between the tower and the vegetation canopy. The height difference before and after raising is shown in Figure 3.14.

The EC flux instruments work best when facing prevailing winds. Therefore, with wind direction in Ireland coming from a mainly South Westerly direction, flux instruments (Figure 3.14) were mounted at the highest point of the tower (15 m) and oriented South Westerly to align with prevailing winds, placed in close proximity while ensuring no interference with wind flow between sensors to maintain accurate sampling (Burba, 2013, 2022). The flux instruments used in this study included a Campbell scientific 3-D sonic anemometer (Campbell Scientific, Logan, UT, USA), to measure wind speed, a Li-Cor 7550 open path infrared gas analyser (IRGA) used to sample $CO_2$ and $H_2O$ gas concentration. Both open path gas analysers used in this experiment are less disruptive to the air flow and are easier to maintain due to the open-air design (Baldocchi, 2003). A Li-Cor 7700 $CH_4$ gas analyser (Li-Cor Environmental UK Ltd, Cambridge, UK),(Figure 3.15) was also installed to monitor $CH_4$ concentrations.

*Figure 3.13 The eddy covariance tower at the Lullymore site (photo: author).*

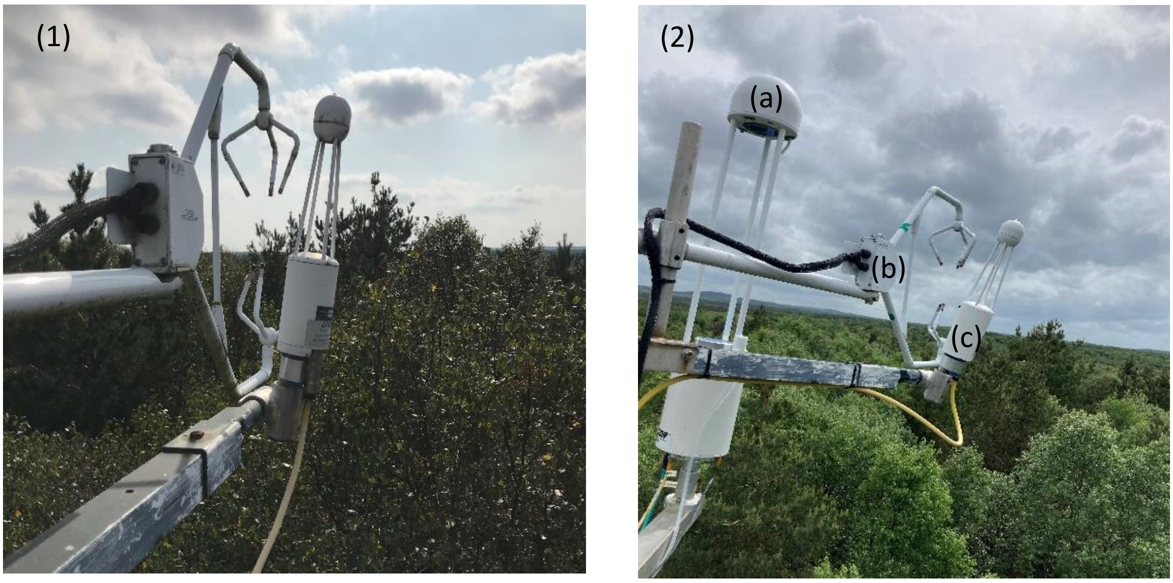


*Figure 3.14Flux instruments on the EC tower at 13m (1) and 15m (2) heights (photo: author).*

Figure 3.14 (2) shows (a) Li-Cor 7700 $CH_4$ gas analyser, (b) Campbell scientific 3-D sonic anemometer, (c) Li-Cor 7550 open path infrared gas analyser (IRGA) for $CO_2$.


*Figure 3.15 Li-Cor Li7700 open path $CH_4$ analyser (photo:author).*

Although the Li7700 $CH_4$ analyser (Figure 3.15) continuously recorded measurements, substantial data gaps arose due to the sensitivity of the analyser to the Irish climate, particularly precipitation, dust, and pollen. The $CH_4$ sensor is prone to contamination, requiring routine manual cleaning of the analyser plates with a microfibre cloth, as insects and dust frequently accumulated on the instrument.The analyser is also equipped with a self cleaning mechanism involving a pump and water reservoir. Initially the default cleaning settings were left in place at installation, but a review after the first month showed they were unsuitable for local conditions. The default settings were therefore disabled and the cleaning protocol manually reconfigured to trigger automatic cleaning when signal strength fell below 60 per cent, with water pumped onto the disc for ten seconds and the disc spun for fifteen seconds. These adjustments improved data quality and proved more appropriate for the Irish climate and habitat.

Prior to installation, all EC and meteorological instruments underwent quality checks in the laboratory to avoid hardware issues on site. The CR3000 Campbell Scientific datalogger used for meteorological data was not directly compatible with the Li-Cor Smartflux system, therefore a customised program was written in the required Li-Cor language to ensure correct interpretation of units and values. This step also synchronised EC and meteorological measurement timing, which later supported data gap-filling procedures. The programmes implemented for the CR3000 and CR200 are provided in the Appendix. During pre-installation calibration, careful consideration was given to the positioning of the 3-D sonic anemometer, $CO_2$ analyser and $CH_4$ analyser to ensure they sampled the same air parcel without disrupting airflow, and to ensure alignment with prevailing winds (Burba, 2013, 2022). Following successful lab testing and configuration, the instruments were disassembled, transported to the field site, and reassembled on the EC tower.

### 3.3.3 Meteorological instruments

As well as flux instruments, several meteorological measurements were monitored simultaneously with gas fluxes, with the aim of linking fluxes to variations in environmental parameters and to aid with gap filling flux data. The global radiation was measured using a Campbell scientific CS320 sensor (Campbell Scientific, Logan, UT, USA) in Figure 3.16 (a). Photosynthetically active radiation (PAR) was measured with Skye PAR sensor (Skye , Llandrindod Wells, Powdys, UK) in Figure 3.16 (b) and a Kipp & Zonen CNR1 sensor (Kipp &

Zonen , Kempten, Germany) (Figure 3.16 (c)) was used to monitor the short-wave incoming (SWIN) and outgoing (SWOUT) radiation and longwave incoming (LWIN) and outgoing radiation (LWOUT). These radiation sensors were all mounted on one scaffold section at the top of the EC tower parallel to the flux instruments. Air temperature, humidity (Rotronic RH/T, West Sussex, UK) and precipitation (TE525-L Rain Gauge Campbell Scientific, Logan, UT, USA) were also measured from the top of the tower (Figure's 3.18 & 3.19). These were mounted individually at two opposite corners of the tower to the flux and radiation sensors. These meteorological instruments were directly connected to a Campbell scientific CR3000 datalogger (Campbell Scientific, Logan, UT, USA), (Figure 3.17) that interpreted and stored data.


*Figure 3.16 Radiation sensors mounted at the top of the EC tower (photo: author).*


*Figure 3.17 CR3000 Campbell scientific datalogger (photo: author)*

*Figure 3.19 Rain gauge positioned on top of EC tower*

*Figure 3.18 Humidity and temperature sensor positioned on top of EC tower (photos: author).*

*Figure 3.20 below canopy meteorological station containing the CR200 datalogger (photo: author).*

Additionally, below the canopy, a meteorological station (Figure 3.20) was installed on the north side of the chamber plots to avoid artificial shading from the tower. This housed a Campbell Scientific CR200 datalogger (USA) (Figure 3.21) powered by a 12-volt battery connected to a solar panel. The CR200 recorded measurements every minute and stored 30-minute averages in its internal memory.

The station was equipped with several sensors to capture environmental conditions below the canopy. Soil temperature was measured using a Campbell Scientific 109-temperature probe (CSL), Campbell Scientific (USA), inserted at a depth of 5 cm. Soil moisture was monitored using both a CS615 Water Content Reflectometer (Campbell Scientific, USA) and a Stevens HydraProbe SDI-12 sensor (USA). WT was recorded using a Campbell Scientific CS451 pressure sensor (USA) placed inside a PVC well inserted 80 cm into the peat. Precipitation below the canopy was measured with a TE525WS-L tipping bucket rain gauge (Campbell Scientific), mounted 50 cm above the ground. All sensors were sampled every minute, with half-hourly averages stored on the datalogger and manually retrieved during site visits.

Using the radiation sensors mounted at the top of the EC tower located at the site. A Skye PAR sensor (Skye, Llandrindod Wells, Powys, UK) was used to measure photosynthetically active radiation (PAR), and a global radiation sensor (CS320, Campbell Scientific, Logan, UT, USA) and the percentage difference between above canopy and below canopy Overlapping above and below-canopy PAR measurements were used to calculate the percentage difference between the two. Above-canopy PAR values were then adjusted accordingly to estimate below-canopy PAR.

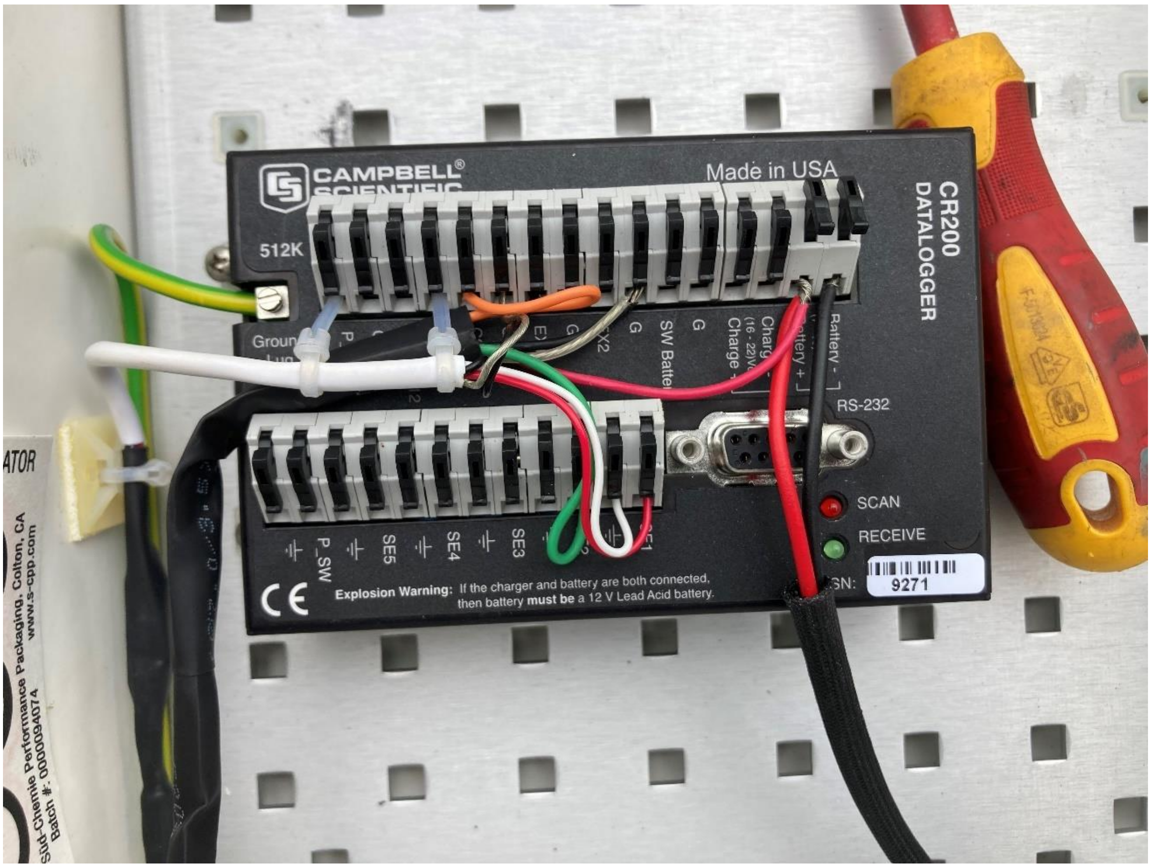


*Figure 3.21Campbell Scientific CR200 datalogger (photo: author).*

# 4 Overall Methodology

## 4.1 General data collection and processing

### 4.1.1 Data collection procedures and data storage

The EC tower used in this study monitored total NEE ($CO_2$), $CH_4$ and $H_2O$ concentrations. The eddy covariance method provides accurate quasi continuous measurements at a large scale and is well suited to a wide range of ecosystems (Baldocchi et al., 2001; Baldocchi, 2014; Poyda et al., 2017). It enables reliable estimates of fluxes between an ecosystem and the atmosphere (Baldocchi, 2003, 2014; Tuittila, Vasander and Laine, 2004). Given the vegetation canopy height at the site the EC method offered the most practical and robust approach for data collection. The Li-7500 ($CO_2$), the Li-7700 ($CH_4$) and the 3-D Sonic anemometer measure gas concentrations and wind speed simultaneously at a rate of 10 Hertz, respectively, amounting to 18,000 samples over a half-hour period.

All measurements began once the tower upgrade was completed in May 2022. However, an unexpected firmware discrepancy occurred when attempting to synchronise the $CH_4$ analyser with the Smartflux system to monitor gas concentrations. The automated PTP satellite time settings for both the $CH_4$ analyser and the Smartflux system were overridden, and local time was manually set and synchronised. As a result, $CH_4$ measurements did not commence until August 2022, and were continuously recorded throughout the study.

The Li Cor Smartflux box was connected directly to the EC instrumentation and recorded high frequency data, which were stored in compressed .ghg files to reduce file size. Although the CR3000 has limited internal memory it was networked to the Smartflux system via ethernet which supported efficient processing and storage. Data from both the CR3000 and the EC system were manually extracted using an external USB device housed within the Smartflux system on a fortnightly basis.

Due to the modest internal storage of the CR200 datalogger the data were manually retrieved on site every fortnight using an RS 232 to USB cable connected to a laptop. After each site visit all data were duplicated onto an external hard drive and backed up to a OneDrive account in their raw format. This careful approach was adopted to minimise the risk of data loss and to ensure reproducibility.

All meteorological data collected through the Campbell Scientific CR3000 datalogger above the canopy and the Campbell Scientific CR200 datalogger below the canopy were programmed to sample every minute and were averaged every half hour, apart from both rain gauges which recorded total rainfall every half hour.

$NEE_{bel}$ was measured using the transparent chamber under typical daylight conditions between 9 am and 4 pm. To measure the rate of $R_{bel}$, the chamber was covered with a blackout fabric cover to simulate night-time conditions. At the beginning of each measurement, the chamber lid was slowly closed, and after a 30 second mixing period, $CO_2$ concentrations were recorded over an incubation period of approximately 180 seconds. Between $NEE_{bel}$ and $R_{bel}$ measurements, the chamber lid was opened to allow ambient $CO_2$ levels to stabilise, which typically ranging from 400-418 ppm. Both light and dark measurements were conducted at weekly, fortnightly, and monthly intervals throughout the year.

The EGM-4 portable IRGA unit features an internal memory capable of storing only single records, which limits its ability to log continuous $CO_2$ values. To overcome this limitation, an SDI-12 to USB adapter was connected to the EGM-4, enabling continuous data logging for all measurements at approximately 4.8-second intervals (PP Systems, 2013), while connected to a laptop. This setup resulted in continuous data files for each measurement location, including both light and dark measurements as well as the non-incubation periods in between. During the incubation periods, manual records of $CO_2$ values and corresponding times were noted. Since not all continuous data collected were usable and only the measurements recorded during the chamber incubation periods were relevant, the raw data were filtered to isolate these values using the manual notes as a reference. The relevant data for each measurement were then organised into new spreadsheets to facilitate flux calculations in Excel.

Occasionally the EGM 4 performed a zero check to calibrate itself during measurements. Notes were taken during these events and any low $CO_2$ values recorded during this calibration process were discarded as they were non representative. All raw data files were saved onto USB and backed up to a hard drive and to OneDrive.

### 4.1.2 Flux calculation below canopy

For each chamber measurement the $CO_2$ flux was calculated from the linear rate of change in gas concentration as a function of time. The gas concentration for $CO_2$ was measured by the analyser in ppm, to calculate the flux and convert the units into µmol $m^{-2}$ $s^{-1}$ the following calculations below were carried out.

To determine the slope of the line for the collected data, it was essential to assess the correlation between the variables. This was accomplished using the LINEST function in Excel. The LINEST function employs the least squares method to calculate the best-fit line for two sets of data, returning an array that interprets the relationship between the chosen variables. In this study, modifications were made to the standard LINEST function due to the specific sampling characteristics of the EGM-4 device, which samples approximately every 4.8 seconds (PP Systems, 2013). This sampling interval resulted in a variable number of $CO_2$ measurements for each incubation period. When only the $CO_2$ concentration values (ppm) are selected within the LINEST function, Excel automatically assigns the cumulative sum of these ppm values to the x-axis as the second variable. To address this issue, the following equation was utilised to compute ΔC:

*Equation 4.1*

$$\Delta\mathrm{C} = LINEST((y1{:}y2) * (y3\ /180)$$

In this equation *y* represents $CO_2$ values in ppm, where $y_1$ denotes the first value and $y_2$ the last value from the incubation period for the individual measurement. The variable $y_3$ refers to the total count of $CO_2$ values, which is divided by 180 seconds, the total time of incubation. This approach returns the y-value for the slope of the line, along with the $R^2$ value, which indicates the goodness of fit for the data. The ΔC values obtained from this equation represent the change in $CO_2$ concentration over time, in ppm/s. A measurement was considered valid if the $R^2$ value was at least 0.80. However, exceptions were made based on visual assessments of the values, as light levels below the canopy were low, resulting in correspondingly low emissions, which often led to low $R^2$ values. Upon review, if the data did not exhibit a clear linear trend, the measurement was excluded due to the possibility of fan malfunction, chamber displacement, or inadequate air sealing (Alm *et al.*, 2007; Wilson *et al.*, 2015). Valid measurements were then incorporated into a subsequent equation, along with relevant environmental data, to calculate the flux. Utilising the ΔC values and the ideal gas law, the $CO_2$ flux was calculated for each measurement taken, expressed in grams of $CO_2$ per meter squared per hour (g $CO_2$ $m^{-2}$ $h^{-1}$) using Equation 4.2.

*Equation 4.2*

$$Flux\ g\ CO_2\ m^{-2}\ h^{-1} = (= \frac{\Delta C\ .44.01}{R\left(\frac{T_0 + 273.15}{P_0 . 100}\right)}\ .\ V_0\ .\ t$$

This equation is derived from the EGM-4 manual (PP Systems, 2013) and adjusted to account for the specific volume and incubation time relevant to this experiment. Delta ΔC determined from previous calculations, is multiplied by the molecular weight of $CO_2$ (44.01 g/mol) to convert the concentration change into mass. $R$ represents the ideal gas constant (8.314 J/(mol·K)), which relates pressure volume and temperature. The average temperature ($T_0$) inside the chamber throughout incubation time is converted to kelvin for use with the ideal gas law. $P_0$ denotes the average atmospheric pressure (ATMP) within the chamber during the incubation time, converted to pascals (Pa). $V_0$ is the total volume of the chamber ratio. And $t$ is the conversion of seconds to hour. The equation calculates the $CO_2$ flux by integrating the change in $CO_2$ concentration, the conditions within the chamber (temperature and pressure) and the total volume and duration of the measurement (PP Systems, 2013; Wilson *et al.*, 2015).

### 4.1.3 Flux calculation above canopy for $CO_2$ and $CH_4$

Similar to the chamber flux calculation, the eddy flux is represented by the covariance between the vertical wind velocity and the concentration of the entity of interest Accordingly, the eddy flux is calculated as the product of the mean air density ($\rho^{\mathrm{d}}$), multiplied by the mean fluctuation of vertical wind speed (w’) and the dry mole fraction (s’) of $CO_2$ or $CH_4$ (Baldocchi *et al.*, 1988; Baldocchi, 2014). The $CO_2$ flux is represented in Equation 4.3:

*Equation. 4.3*

$$F \approx \overline{\rho^{\mathrm{d}}}\ \overline{w' s'}$$

The flux over a half hour period was derived from calculating the average of the 18,000 observations taken for wind speed and gas concentration. Following Reynolds averaging (Stull, 1988), the fluctuating components of both were subtracted from the average values. So, the flux is equal to the mean fluctuation of wind velocity multiplied by the mean fluctuating gas concentration. The half hour averaged flux is defined in Equation 4.4:

*Equation 4.4*

$$F \approx \overline{w's'}$$

For this study, the micrometeorological convention considers fluxes emitted from the ecosystem to the atmosphere as positive values and the reverse fluxes are negative values. Therefore, if net flux detected from an area is positive it is referred to as a source, emitting gas from the surface. If this is reversed and net flux is negative, the area is considered a sink, absorbing the gas (Burba, 2013, 2022).

Prior to and including the calculating flux for continuous EC data accurate flux computation the double rotation model was implemented. The double rotation method was chosen for this native forest site as it is recommended for sites with relatively flat, homogenous vegetation and for ecosystems where the underlying vegetation can change significantly over a relatively short period of time (Wilczak *et al.*, 2001). Although the vegetation cover at the site is considered complex the terrain is relatively flat therefore, the double rotation model was an appropriate model to implement (Gockede *et al.*, 2008). Flux measurements began on 18 May 2022 and continued until August 2023. For the purposes of this research, however, only data collected between June 2022 and June 2023 were analysed in order to estimate a full annual carbon budget. The half hourly flux data are expressed in units of μmol $m^2$ $s^1$ for both $CO_2$ and $CH_4$ prior to modeling and annual flux totals calculated.

Initial analysis of the EC flux data required intensified processing (Figure 4.1). For this research, the following steps were taken when processing the raw flux data which were appropriately selected to suit the ecosystem being studied.

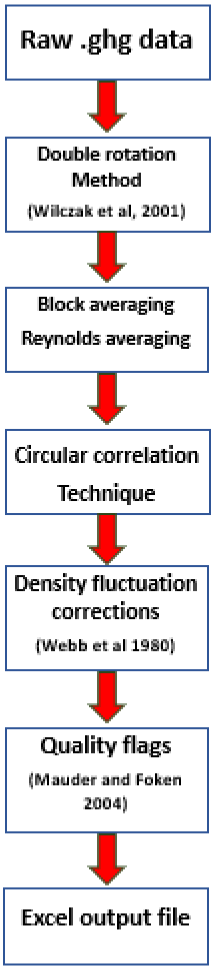


*Figure 4.1 Flux calculations and corrections workflow (photo: author)*

For raw $CO_2$ and $CH_4$ data processing the following steps were taken:

1. The double rotation method was applied to compensate for the 3-D anemometer tilt correction. Raw wind components were rotated to zero the average mean wind direction and mean vertical velocity. This method is suitable for ecosystems that undergo significant changes throughout seasons and are situated on relatively flat topography (Wilczak *et al.*, 2001).
2. Block averaging obeys the Reynolds averaging method and was applied to the raw data to calculate the mean value of the entity of interest and the turbulent

fluctuations from the mean (Burba, 2013, 2022). This averaged the data over a half hour period.

3. To allow for time lag between instruments a covariance maximum was selected for this research as an open path gas analyser was used and it was situated approximately 10cm distance from the 3-D sonic anemometer. This used the circular correlation technique to detect the time lag within a window defined by the maximum and minimum time lags selected for the variable. If the maximum is not reached, then the default value of 1 second was implemented instead (Burba, 2013, 2022).
4. Compensation of density fluctuations for the open path sensor was used in this research following Webb *et al.*, (1980).
5. Quality flags were calculated for all flux data. The quality flags were calculated based on the scheme of Mauder & Foken, (2004) (0-1-2 system). (0 meaning good quality flux, 1 meaning intermediate quality and 2 meaning poor quality).

All the methods and tests above were implemented using the EddyPro software version 7.0.8 and were processed on a seasonal basis. Once raw data was processed through EddyPro the output file consisted of half hour average fluxes for the gases of interest. Following the processing of raw data, additional filtering and modeling techniques were applied (Figure 4.2). This was necessary to facilitate further quality control of the flux data and to model missing data seasonally. These steps ensured that seasonal variations were considered when establishing thresholds for the filtering processes and data modeling.

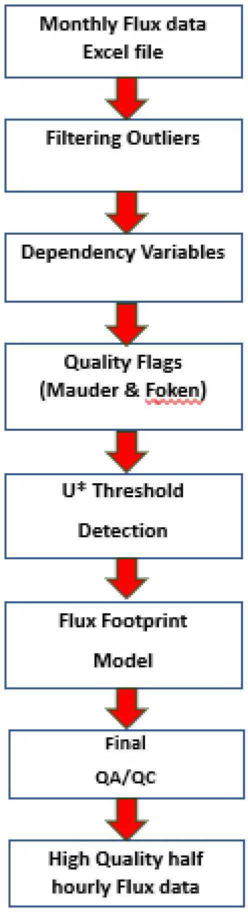


*Figure 4.2 Flux data QA/QC workflow (photo: author).*

For quality control of $CO_2$ and $CH_4$ flux data the following processing steps were taken:

1. Filtering outliers: Considering biotic factors, data was filtered for realistic values using statistical analysis to remove outliers. This was carried out by calculating the binomial distribution of the data and identifying the 25th and 75th percentiles, retaining only the data within these quartiles. Performing this on a seasonal basis was important to capture seasonal changes within the ecosystem.

2. Dependency Variables: Fluxes were also filtered based on dependency variables. Half hourly fluxes were removed if the signal strength fell below 60%, if rainfall was high or if there were outliers in the 3-D sonic anemometer data.
3. Quality flags: Using the Mauder and Folken (2004) method any unsatisfactory quality fluxes flagged with the number two were removed.

4. U*threshold: Carried out a moving point test to determine the value of U*threshold established for annual data set. Data points for friction velocity that fell below the U* threshold were removed from the flux data.

5. Flux footprint filtering: The average FFP was estimated from June 2022 to June 2023. The footprint extended beyond woodland area into a drain. Fluxes originating from that area were removed. The FFP model of Kljun et al. (2015) was applied.

6. Flux Quality Control: Conducted a thorough final visual inspection of the flux data to ensure accuracy and reliability. Filtering methods applied were centred on biotic factors, discarding eddy flux measurements that were non representative of these (Aubinet et al., 2012). For example, fluxes for $CO_2$ falling below zero under PPFD values less than 10 µmol $m^{-2}$ $s^{-1}$ were rejected as this is beyond biological limits.

Looking at previous woodland flux research studies, realistic values for native broadleaved woodland sites were reviewed, and on consideration of these values real time fluxes were compared against them to ensure measured values were realistic. Due to instrumentation failure in July 2022, two weeks flux data were discarded due to unrealistically high and low values from the tower. Again, in October there were issues with instrumentation leading to a data gap of two weeks for all flux data and metrological data sets. Including gaps in the data due to system failure and gaps due to quality control a total of 45% of the $CO_2$ and 40% of the $CH_4$ flux data were good enough quality to use for further analysis.

### 4.1.3.1 The EC Flux footprint

The flux footprint is the area upwind from the tower that flux contributions are taken from. The footprint can be modeled from data taken from the EC tower and is used to enhance flux measurements, estimate the size and position of the surface source area. Estimating the footprint accurately is important for upscaling site flux measurements and for filtering undesired source fluxes from areas outside the region of interest being measured (Aubinet *et al.*, 2012; Kljun *et al.*, 2015; Burba, 2022).

On consideration of previous literature, for this research the footprint parameterisation model from Kljun et al. (2015) was applied using an online tool. This model is valid for a wide range of boundary layer conditions and measurements across the varied ecosystems and topography making it suitable for many research sites. It requires inputs from the flux tower measurements and can be used for long term time series, and quick field estimates for filtering data or designing new sites. All conditions required to implement this model were valid at the study site.

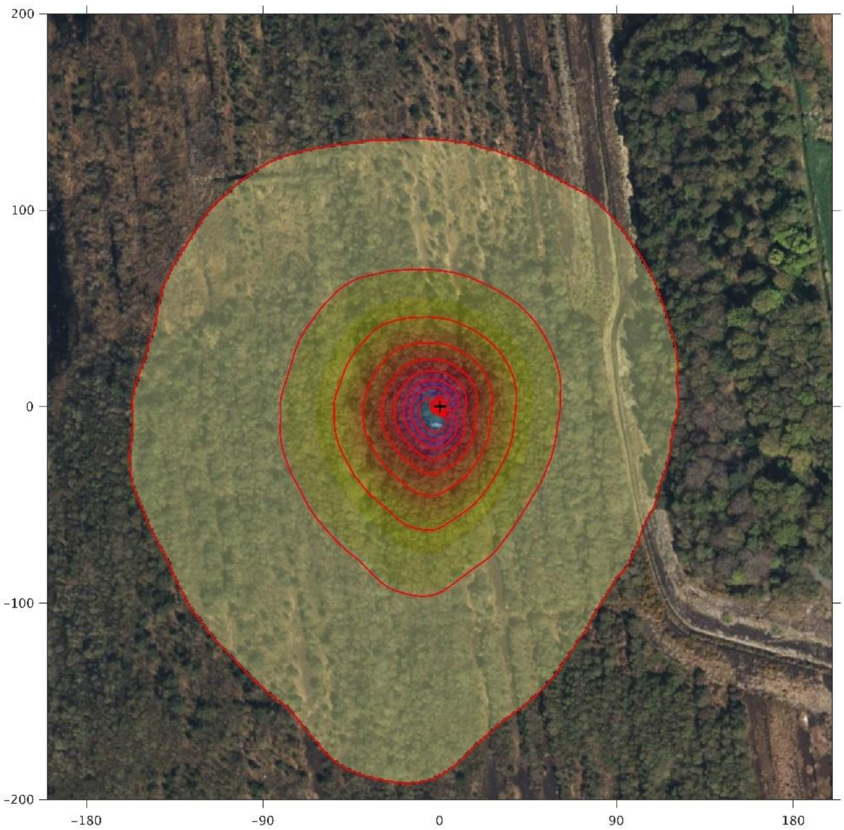


*Figure 4.3 Kljun et al. (2015) flux footprint parameterisation model for Lullymore site.*

Before estimating the footprint, several preprocessing steps were applied to ensure the accuracy of the data. Input variables were filtered to remove any outliers or erroneous values. Additionally, friction velocity (U*) values below 0.1 were excluded, as low U* measurements are often unreliable for footprint calculations. Finally, half-hourly timestamps with missing data were removed to prevent gaps from affecting the estimation process. These steps were critical in ensuring the reliability and robustness of the FFP calculation.

The flux footprint (in metres) shown in Figure 4.3 shows red contour lines for the maximum flux area. Darker yellow-red colours indicate regions contributing most to the flux, with the red dot marking the EC tower location. The study site is surrounded by a diverse patchwork of ecosystems, including dense vegetation, bare peat, woodland, and rewetted areas. Given that the objective of the study was to examine the net $CO_2$ flux from a naturally established forest on a cutaway peatland, the goal was to filter out flux measurements originating from undesirable locations. For example, emissions from a drainage area located to the east of the tower, were identified and excluded from the flux time series to ensure the accuracy of the data.

## 4.2 $CO_2$ flux measurements and modelling

### 4.2.1 Methods for estimating $CO_2$ below canopy

Measurements taken using the chamber under light and dark conditions were modeled separately using distinct environmental parameters, such as soil temperature, moisture, and PPFD values. To isolate $GPP_{bel}$ from $NEE_{bel}$ the following equation was used.

*Equation 4.5*

$$GPP_{bel} = NEE_{bel} - R_{bel}$$

Therefore, $GPP_{bel}$ was modelled independently of $R_{bel}$ and vice versa. Since photosynthetic reactions in plants respond to radiation, $GPP_{bel}$ has a relationship with PPFD and $T_s$, as discussed in section 2.3.1.7 (Ryan, 1991; Begon *et al.*, 1996; Tuittila *et al.*, 1999, 2004; Wilson *et al.*, 2015; Wilson, Farrell, *et al.*, 2016; Jovani-Sancho *et al.*, 2018). Coefficients were calculated to describe the relationship between fluxes and environmental variables, and these were obtained using the Python SciPy optimisation module with the Levenberg–Marquardt multiple nonlinear regression technique, which is also described in section 2.3. All meteorological variables were sampled every minute and averaged every half-hour on a

Campbell Scientific data logger. Therefore, the flux data was also modeled as half-hour estimates. The resampled PPFD values were used to estimate below-canopy PPFD values from sensors located at the top of the EC tower.

The machine learning algorithms evaluated prior to model development include k-Nearest Neighbours (kNN), Random Forest (RF), Gradient Boosting, XGBoost and Generalised additive model (GAM) all of which are discussed in greater detail in Section 2.3.3. These models were tested against observed data points. To facilitate this comparison, a Python script developed By Dr Stephen Barry of Bord na móna, was used to automate the execution of the models for $GPP_{bel}$ and $R_{bel}$. The script incorporates the input data for fluxes and dependent variables, applies them to train the models on the observed dataset, and evaluates the response curves based on variance ($R^2$), root mean square error (RMSE), standard error, and statistical significance (p-value) After evaluating the performance of all the tested methods, the model exhibiting the highest $R^2$ and lowest RMSE was selected to model the complete annual dataset (Hamrani *et al.*, 2020).

In some cases, data removal is used to optimise datasets in machine learning. However, in the context of this research, such an approach was not feasible due to the limited number of data points available, as only spot samples were collected. As a result, this method was not implemented. However, a 20:80 data split was applied, with 20% of the data withheld for testing, while the remaining 80% were used for training the model. The dataset was divided into two subsets: the training data, which were used to train the machine learning model, and the testing data, which had not been used during training and were reserved for model evaluation.

Among the models tested, the RF model demonstrated the best performance (see results in Appendix). Consequently, the RF model was implemented to model the annual timeseries of flux data. The results showed strong agreement between the observed and modelled flux values, as discussed below. The model successfully estimated $CO_2$ emissions below the canopy at the Lullymore research site.

To assess the performance of the model, uncertainty estimation was conducted by calculating the standard error. A narrower standard error range suggests lower variance in the predictions and greater confidence in the model's reliability. Conversely, a wider range indicates increased uncertainty and reduced confidence in the model's accuracy. The level of uncertainty directly impacts the degree of caution required when interpreting the model's results. The standard error was computed using the following equation.

*Equation 4.6*

$$\text{Standard Error of the Mean} = \frac{s}{\sqrt{n}} \times 1.96$$

Where $s$ is sample standard deviation, $n$ is the number of observations (sample size) and 1.96 accounts for the 95% confidence interval (Altman *et al.*, 2013). This was calculated for modelled $GPP_{bel}$, $R_{bel}$ and $NEE_{bel}$.

### 4.2.2 Methods for estimating $CO_2$ above canopy

Gaps in the half-hourly fluxes were identified through the QC procedures. Additionally, gaps resulted from instrumentation malfunctions and environmental conditions, such as heavy precipitation, especially when using the open path gas analyser (Baldocchi, 2003; Polonik *et al.*, 2019; Burba, 2022). In order to complete an annual NEE budget for the ecosystem, a full time series of flux data was modeled using environmental parameters and a flux-partitioning algorithm.

To determine the interactions between fluxes and environmental parameters, data was first separated into seasonal fluxes. Correlation analysis was conducted by creating scatter plots to assess the relationships between fluxes and various environmental variables. Pearson correlation coefficients were calculated to identify the most suitable dependency variables for modeling. This preliminary analysis was carried out in Rstudio version 2024.04.1+748 "Chocolate Cosmos".

#### *4.2.2.1 Marginal distribution sampling method*

Once primary, secondary and tertiary drivers for the $CO_2$ fluxes were established, the data was analysed using Tovi software version 2.9.1 Li-Cor, USA. These drivers were used in order of preference to estimate the missing values. Based on the transition periods of the half-hourly fluxes over an annual time series, separate periods were established for specific modeling parameters. This approach was chosen to account for fluctuations in the seasonal characteristics of the woodland ecosystem and to implement different dependent variables for filling in missing data.

The missing fluxes were modeled using configurable marginal distribution sampling (MDS) method developed by Reichstein et al. (2005), equation 4.7. This is a derived equation from review of previous methods (Lloyd and Taylor, 1994; Hollinger *et al.*, 1998; Falge, Baldocchi, *et al.*, 2002; Law *et al.*, 2002; Reichstein, Tenhunen, Roupsard, J-M Ourcival, *et al.*, 2002; Gilmanov *et al.*, 2003; Papale and Valentini, 2003; Rambal *et al.*, 2003) and explains how variations in the baseline respiration rate ($R_{ref}$) and the temperature sensitivity parameter (E0) influence the relative change in ecosystem respiration ($R_{eco}$). It takes into account the temperature differences (T) between the reference temperature and the base temperature (Reichstein *et al.*, 2005).

*Equation 4.7*

$$\frac{dR_{eco}}{R_{eco}} = \frac{dR_{ref}}{R_{ref}} + dE_0\left(\frac{1}{T_{ref} - T_0} - \frac{1}{T - T_0}\right)$$

Where $dR_{eco}$ is the relative change in ecosystem respiration $R_{eco}$, $dR_{ref}$ is the relative change to the baseline reference temperature ($R_{ref}$), and $dE_0$ represents the change in $E_0$. $T_{ref}$ is the reference air temperature, and $T_0$ is the baseline air temperature (Reichstein *et al.*, 2005). Depending on the primary driver (see below) the equation changed.

The data was analysed by dividing it into distinct seasonal periods, based on average monthly temperatures. The summer season spanned from 1st June 2022 to 31st July 2022, with an average air temperature ($T_a$) of 16°C. This was followed by autumn, from 1st August 2022 to 31st October 2022, with an average $T_a$ of 11°C. Winter, marked by the lowest consecutive monthly temperatures, was defined as the period from 1st November 2022 to 31st January 2023, with an average $T_a$ of 6°C. Spring, with an average $T_a$ of 10°C, was set from 1st February 2023 to 30th April 2023, and the early summer period extended from 1st May 2023 to 1st June 2023.

For each of the defined seasonal periods, primary, secondary, and tertiary drivers were established, with specific tolerance levels set for each driver to define acceptable ranges for estimates. During the growing seasons (Summer, Autumn, early Summer, and Spring), PPFD was chosen as the primary variable, with a tolerance range of 50–200 µmol $m^{-2}$ $s^{-1}$. The secondary driver was $T_a$, with a tolerance of ±2.5°C, while vapour pressure deficit (VPA) served as the tertiary driver, with a tolerance of ±5 hPa. In the dormant season (Winter), soil temperature ($T_S$) became the primary driver, with a tolerance of ±2.5°C, followed by $T_a$ and VPA, both with the same tolerances as in the growing seasons. These tolerance levels ensured that only values falling within the specified ranges were used for estimating missing data, thus enhancing the accuracy and reliability of the gap-filling process (Reichstein *et al.*, 2005).

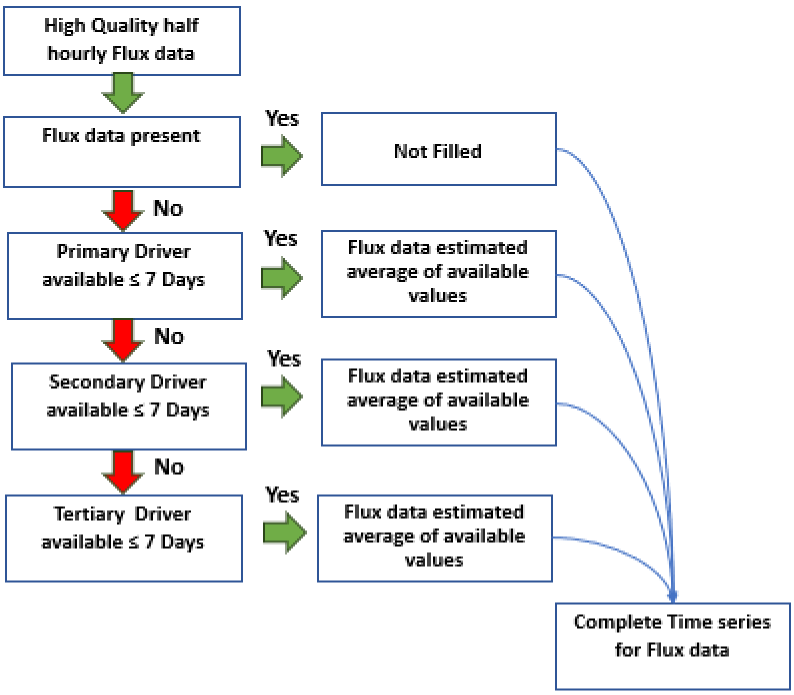


*Figure 4.4 Workflow for marginal distribution sampling (photo: author).*

The mathematical model estimated missing values based on the relationship with the primary driver, this was reiterating for the secondary and tertiary drivers in order of preference if there were missing values from primary driver. The workflow depicted in Figure 4.4 illustrates the functioning of the model.

### *4.2.2.2 Random Forest Model implemented through Rstudio*

Although MDS is a standard method for gap filling NEE (Kim *et al.*, 2020; Winck *et al.*, 2023), the machine learning algorithm RF was also implemented to estimate NEE. RF is a supervised machine learning algorithm that constructs an ensemble of decision trees through bootstrapping, where subsets of the training data are sampled with replacement. Each tree is built independently, promoting diversity among them, and the final prediction is derived by aggregating the outputs from all the trees (Breiman, 2001). The model requires a minimum of two primary parameters: the number of trees to generate and the number of variables to consider at each decision point (Breiman, 2001). RF has been widely used in studies to model fluxes for trace gases such as $CH_4$ (Kim *et al.*, 2020), however there are also studies where it has been implemented to estimate NEE and has been compared with other gap-filling techniques (Winck *et al.*, 2023).

For this study, a similar approach to Winck et al. (2023) was adopted, incorporating all available meteorological variables. The quality-controlled, filtered NEE flux data used for the MDS method were also used in the RF model. The model was implemented in RStudio, with a custom script written to include all fully gap-filled meteorological time series as predictor variables. As in Winck et al. (2023) the number of trees generated was set to 500. No specific prioritisation of predictor variables was applied, and variables employed such as $T_a$, $T_s$, RH, PPFD, RG, SWC, VPD, RN, LE, and air pressure, were treated equally. The model was executed using the "randomForest" R package (Liaw & Wiener, 2002) in RStudio 2024.09.1+394 "Cranberry Hibiscus" Release ( 2024-11-03).

Since RF aggregates predictions from multiple decision trees, it cannot be expressed with a single explicit equation. Each tree produces a prediction, and the final result is obtained by averaging these individual predictions. This characteristic distinguishes RF from more traditional methods, such as linear regression or MDS, which can be easily represented by a single equation (Breiman, 2001).

#### *4.2.2.3 Validation of methods and units' conversion*

Summary statistics were computed for both the observed and predicted data values. to evaluate the performance of both methods, several statistical tests were conducted in RStudio using 20% of the data set aside for out-of-sample testing for RF and 10% removed for the MDS approach. Holdout validation was performed by comparing the predicted values, generated through the MDS and RF models, with the actual observed values from the withheld data points (testing data). This allowed for an assessment of the models' ability to predict unseen data. The model residuals were analysed by plotting the differences between the observed and predicted values against the estimated values. The percentage difference was then calculated using the equation derived from these summary statistics.

*Equation 4.8*

$$PercentDiff = \frac{X_1 - X_2}{\frac{X_1 + X_2}{2}} * 100$$

Where $X_1$ represents the first value or statistic and $X_2$ represents the second value.

Prediction accuracy was assessed through the calculation of the Root Mean Squared Error (RMSE) and Mean Absolute Error (MAE), where lower values represent better model performance.

To analyse cumulative $CO_2$ emissions over the course of one year, it was necessary to convert $CO_2$ flux values from micromoles per second to grams per half hour, and then to tonnes per hectare. The following equation was derived:

*Equation 4.9*

$$\mathrm{t}\, CO_2\, \mathrm{ha}^{-1} = \frac{1800 * \mu\mathrm{mol\ m}^{-2}\ \mathrm{s}^{-1}}{1{,}000{,}000} * \frac{44}{1{,}000{,}000} * 10{,}000$$

The conversion factor calculates $\mathrm{t}\, CO_2\, \mathrm{ha}^{-1}$, by converting per second to per half-hour, by multiplying 1800 (second in half hour) by the $CO_2$ in µmol m-$^{2}$ s-$^{1,}$ to convert this to a half hourly measurement. Then divides by 1,000,000 to convert to moles from micromoles (1 mole = 1,000,000 micromoles). It then considers the molecular weight of $CO_2$ (44g grams per mole) and converts from grams to tonne by dividing by 1,000,000 (since 1 tonne = 1,000,000 grams). Finally, it is then multiplied by 10,000 to convert from square meters to hectares (since 1 hectare = 10,000 square meters). This conversion facilitates straightforward comparison with other research findings and enhances practical explanations and upscaling of results. The conversion process involved aggregating seasonal sums of flux data, which were then totalled to determine the annual atmospheric $CO_2$ emissions for the site in $\mathrm{t\ ha}^{-1}$. To further calculate Carbon from $CO_2$ the amount in tonnes per hectare was multiplied by $CO_2 = \frac{12}{44}$.

## 4.3 $CH_4$ flux measurements and modelling

To estimate a complete annual $CH_4$ budget at the woodland study site, the gaps in the timeseries needed to be addressed. Two methods were employed to fill the gaps in the data, and their performances were compared. MDS was applied to the annual timeseries to fill the gaps using Tovi software by Licor. Random Forest machine learning was implemented using RStudio to train the model and estimate the missing data.

#### *4.3.1.1 Marginal distribution sampling*

A random filter was applied in RStudio to remove 10% of the high-quality data in order to evaluate the performance of the MDS method in predicting and estimating the missing data gaps at the end of gap filling. Upon reviewing the timeseries, no diurnal patterns in $CH_4$ flux were identified, which meant that partitioning the data based on time of day was not necessary.

A pearson correlation matrix was calculated in RStudio for all on-site variables in relation to the $CH_4$ flux dataset, with the matrix plot available in the appendix. Based on this matrix, driver variables were selected for further analysis. The relationships between $CH_4$ fluxes and several environmental variables were assessed, revealing VPD as the primary driver, average $T_S$ as the secondary driver, and PPFD as the tertiary driver. These variables, ranked by relevance, were then used in the MDS to estimate the missing $CH_4$ flux data.

To model the missing $CH_4$ fluxes, the configurable MDS method developed by Reichstein et al. (2005) was employed through Tovi software. This method builds upon previous models (Lloyd & Taylor, 1994; Hollinger et al., 1998; Falge et al., 2002; Law et al., 2002; Reichstein et al., 2002; Gilmanov et al., 2003; Papale & Valentini, 2003; Rambal et al., 2003).The model also accounts for temperature differences (T) between the reference and baseline temperatures, as outlined by Reichstein et al. (2005) and is discussed in the previous section 4.2.2.

Although the MDS method was originally developed for gap filling $CO_2$ fluxes, which are closely linked to biological processes like respiration, it can be adapted to fill gaps in $CH_4$ fluxes with careful consideration of relevant environmental drivers. As mentioned, the variables were selected based on Pearson correlation, VPD, TS and PPFD, with tolerances set at 5 hPa, 2°C, and low and high tolerances of 50 and 200 µmol $m^{-2}$ $s^{-1}$, respectively. These were applied in the method of gap filling the missing $CH_4$ fluxes, acknowledging that while $CH_4$ fluxes are influences by biological and physical processes, their relationship with environmental variables may differ from $CO_2$ fluxes. Since $CH_4$ fluxes are influenced by microbial processes (such as methanogenesis) and environmental variables like $T_S$ (Le Mer and Roger, 2001; IPCC, 2013; Holl *et al.*, 2020), the general structure of the MDS equation is similar to that for $CO_2$, however there are differences in the inputs.

The equation for the MDS for $CH_4$ is as follows:

*Equation 4.10*

$$\frac{dFCH_4}{FCH_4} = \frac{dF_{ref}}{F_{ref}} + dE_0\left(\frac{1}{VPD_{ref} - VPD} - \frac{1}{VPD - VPD_0}\right)$$

In this equation, $dFCH_4$ represents the relative change in $CH_4$ flux ($FCH_4$), $dFref$ is the relative change in baseline reference $CH_4$ flux ($Fref$), and $dE_0$ denotes the change in the temperature sensitivity parameter ($E_0$). $VPDref$ and $VPD_0$ are the reference and baseline VPD respectively. The equation estimates missing $CH_4$ flux values based on their relationship with the primary variable, in this case VPD. If there are missing values prevalent in VPD, the model iterates through the second and then the third variable drivers (Reichstein *et al.*, 2005).

### 4.3.1.2 Machine learning random forest

RF is a supervised learning algorithm and is described in section 4.2.2. The model primarily requires two parameters: the number of trees and the number of variables sampled at each decision point (Breiman, 2001). RF has been successfully applied in previous studies to model $CH_4$ fluxes across various ecosystems and has been compared to other gap-filling methods (Xu and Goodacre, 2018; Kim et al., 2020). For example, Kim et al. (2020) used RF to estimate gaps in $CH_4$ time series data by generating 400 regression trees per case using the "randomForest" R package by Liaw & Wiener (2002) in RStudio. In their study, the biophysical variables such as NEE, LE, H, Rg, LWOUT, AirT, SoilT, RH, VPD, u*, air pressure, and WTH were incorporated (Kim *et al.*, 2020).

In this study, a similar approach was adopted, incorporating all available meteorological variables. The quality-controlled, filtered $CH_4$ fluxes used for the MDS method were also employed in the RF model. The model was implemented using RStudio, where code was written to include all fully gap-filled meteorological time series as driver variables. As in Kim et al. (2020), the number of trees generated was set to 400.  No specific order of preference was assigned to predictor variables, which included average TS, WT, TA, RH, PPFD, RG, average SWC, VPD, air pressure, RN, LE, and H. The model was executed using the "randomForest" R package (Liaw and Wiener, 2002) in Rstudio version 2024.09.1+394 "Cranberry Hibiscus" Release ( 2024-11-03).

##### *4.3.1.3 Performance validation*

To validate the performance of both methods, several statistical tests were conducted in RStudio using the 20% of data removed for out-of-sample testing for RF and the 10% removed from dataset for MDS. Holdout validation was performed by comparing the predicted (estimated) values, obtained through the MDS and RF methods, with the actual observed values from the random removed data points. This allowed for an assessment of how well the models predicted unseen data. Model residuals were analysed by plotting the residuals (the differences between observed and estimated values) against the predicted values, checking for randomness around zero, which would indicate a good fit if no discernible patterns were present. Additionally, the normality of residuals was tested using histograms, where normal distribution would suggest a well-specified model.

The $R^2$ value was calculated to quantify the proportion of variance in the observed data explained by the model, with higher values indicating better model fit. The Root Mean Squared Error (RMSE) and Mean Absolute Error (MAE) were calculated to measure prediction accuracy, where lower values indicate better performance. Finally, the correlation coefficient between the predicted and actual values from the holdout data was computed to assess the strength of the relationship, with higher correlation values suggesting a stronger model fit. As discussed in section 4.2.2

## 4.4 Meteorological data processing

Meteorological data from both onsite stations were amalgamated and processed in RStudio (Version RStudio 2023.12.1+402 "Ocean Storm" Release (2024-01-28) for Windows). The raw dataset contained half hourly averages for air temperature ($T_a$), relative humidity (RH), soil temperature ($T_s$), Soil water content (SWC), shortwave in (SWIN) and out (SWOUT) radiation, longwave in (LWIN) and out (LWOUT) radiation, global radiation (RG), photosynthetic photon flux density (PPFD) and precipitation (p). Data were initially plotted against timestamps annually to assess consistency with expected seasonal patterns. Unrealistic values beyond physical limits were flagged and removed. Due to a communication error between instruments, two short periods of data were removed from the raw dataset. The first occurred from 20$^{th}$ July 2022 to 28$^{th}$ July 2022, and the second from 2$^{nd}$ September 2022 to 6$^{th}$ September 2022. In addition to these interruptions, the above canopy meteorological station on the EC tower experienced further issues that resulted in substantial gaps in the half-hourly data, necessitating extensive gap-filling procedures. After accounting for these gaps and applying the required filters, approximately 60% of the above canopy dataset remained suitable for analysis. In comparison, data loss in the below canopy measurements was limited to about 20%, leaving roughly 80% of that dataset available for analysis.

To estimate the missing values in the Lullymore meteorological time series, data from three nearby weather stations was collected. The first station was located in Ballaghurt, County Offaly (Latitude/Longitude: 53°19'19"N 7°51'50"W, altitude of 43m) (Mealy, 2022), approximately 60 km away in a straight line from Lullymore. This was followed by Clara in County Offaly (Ingle, Habib, *et al.*, 2023) (Latitude/Longitude: 53°19'15"N 7°37'04"W, altitude of 55m), approximately 44 km away in a straight line, and the Mullingar (Met Éireann, no date) weather station in County Westmeath (Latitude/Longitude: 53°32'15"N 7°21'42"W, altitude of 102m), approximately 39 km away in a straight line. Pearson correlation coefficients assessed correspondence between these external datasets and the Lullymore measurements. Due to insufficient temporal coverage, Ballaghurt and Clara data were unsuitable for most analyses, and Mullingar data provided the primary external dataset. All meteorological variables, except precipitation, were fitted with linear regression models using corresponding Mullingar variables.

Precipitation data from Lullymore Nature Centre (53.279°, -6.942°, altitude 87m) (Met Éireann, no date) was used to replace the incomplete above-canopy precipitation record caused by a data logger malfunction. Below-canopy precipitation provided a reliable time series; however, a short period lacked overlap with the flux tower due to the later installation of the rain gauge. Mullingar (Met Éireann, no date) data included a global radiation dataset which was used to model both RG and PPFD for Lullymore. Both linear regression and GAMs (Generalized Additive Models) were employed to estimate the gaps for both radiation variables.

The function created in RStudio to fit the linear regression model performed the following calculations:

*Equation 4.11*

$$y = \beta_0 + \beta_1 * x + \epsilon$$

Where: $y$ is the independent variable, the observed data from Lullymore, $\beta_0$ is the intercept, $\beta_1$ is the coefficient for $x$, the dependent variable, $\epsilon$ is the error term. The regression coefficients $\beta_0$ and $\beta_1$ are estimated using the least squares method to minimise the sum of squared residuals:

*Equation 4.12*

$$minimize \sum i = 1n(yi - (\beta_0 + \beta_1 \times xi))2$$

Once the model was fitted, missing values in $y$ were filled using the estimated regression equation:

*Equation 4.13*

$$y\hat{} = \beta\hat{}_0 + \beta\hat{}_1 \times x$$

Where $\beta\hat{}_0$ and $\beta\hat{}_1$ are the estimated regression coefficients obtained from the model fitting process. Finally, the function evaluates the goodness of fit of the regression model by calculating the coefficient of determination ($R^2$):

*Equation 4.14*

$$R^2 = 1 - \frac{\sum i = 1n(yi - y\bar{})^2}{\sum i = 1n(yi - y\hat{}i)^2}$$

Where $\bar{y}$ is the mean of $y$ values. The $R^2$ values indicates the proportion of the variance in the $y$ that is predicted by $x$.

The net radiation (RN) was calculated from SWIN, SWOUT, LWIN and LWOUT, as shown in the equation below.

*Equation 4.15*

$$RN = (SWIN - SWOUT) + (LWIN - LWOUT)$$

Because RN showed weak correlation with Mullingar global radiation, RN gaps were filled using a combined RN record from Ballaghurt and Clara, producing a weighted average $R^2$ of 0.66. Remaining gaps were linearly interpolated. Seasonal analyses were performed by defining winter as the three months with the lowest mean temperatures (November–January). Linear regression was then applied seasonally to estimate missing values, with any remaining gaps interpolated.

Modeling PPFD and RG presented challenges due to the seasonal and diurnal nature of the data. After applying linear regression to the data seasonally, the modeled data did not align well with the yearly time series and tended to overestimate nighttime winter radiation for both variables. Subsequently, month-specific diurnal filters were applied to gap-fill the data on both seasonal and diurnal scales using linear interpolation, linear regression, and GAMs. The dataset was then divided into monthly time series to apply individual diurnal filters, using thresholds of <10 $W/m^2$ RG and <10 $\mu mol/m^2/s$ PPFD to identify nighttime conditions.

Nighttime values for both parameters were treated separately. A running mean of the nighttime data was subtracted from the full dataset, and any resulting negative values were set to zero. Remaining nighttime gaps were then interpolated, taking advantage of their low variability, using midnight (12 a.m.) and 3 a.m. as thresholds to ensure complete darkness.

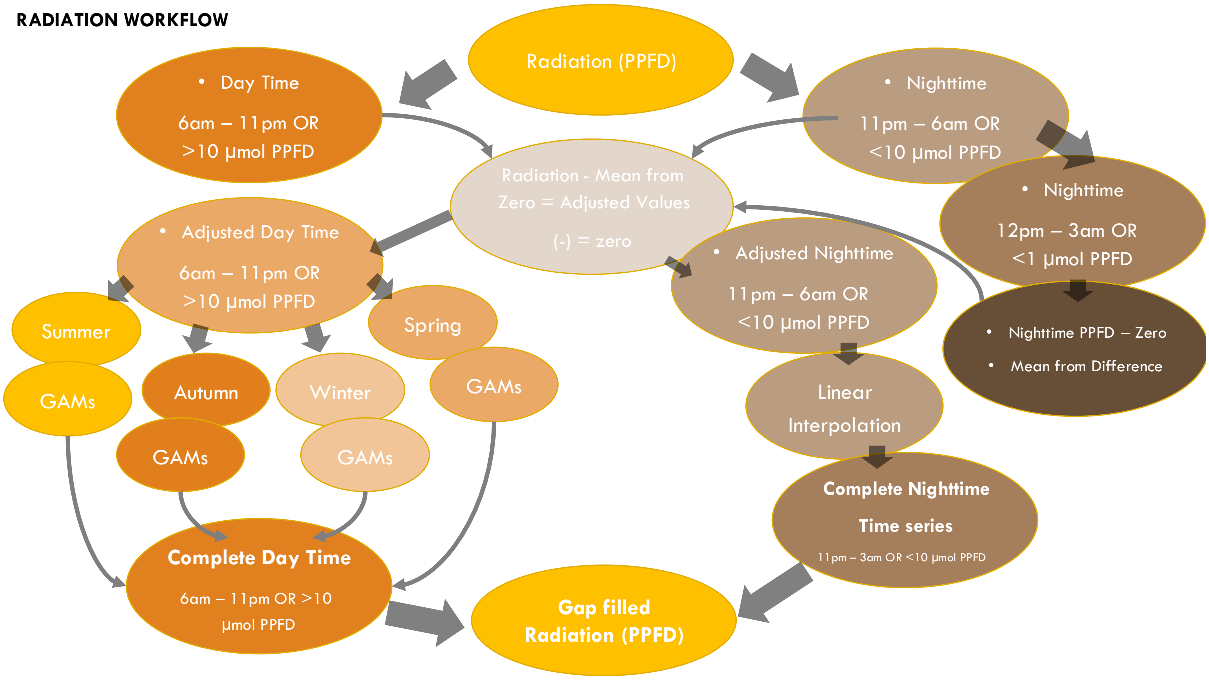


*Figure 4.5 Workflow diagram of radiation gap filling steps (photo: author)*

Daytime values were modelled using linear regression with Mullingar radiation data (Met Éireann, no date), and the performance of these predictions was evaluated using $R^2$ and RMSE. GAMs model was also applied to the same datasets and yielded very similar outcomes. The general process and workflow of gap filling radiation values can be viewed in Figure 4.5.

Air pressure was gap-filled using linear regression analysis, with $T_a$ and RH used as predictors. VPD was calculated for the annual time series using the following equation, which incorporates $T_a$ and RH along with fixed variables of saturation vapour pressure and actual vapour pressure:

*Equation 4.16*

$$VPD = e_{\mathrm{s}}(T_{\mathrm{a}}) - e_{\mathrm{a}}$$

Where $e_{\mathrm{s}}(T_{\mathrm{a}})$ is the saturation vapour pressure (calculated using $T_a$) and $e_{\mathrm{a}}$ is the actual vapour pressure (calculated using RH). Net radiation was calculated using following equation:

*Equation 4.17*

$$RN = (SWIN - SWOUT) + (LWIN - LWOUT)$$

Finally, latent heat flux (LE) and sensible heat flux (H) were gap filled using "missForest" function in RStudio with variables $T_a$, RH and VPD to estimate the gaps in the time series.

# 5 Results – Carbon Dioxide ($CO_2$) Fluxes

## 5.1 Environmental parameters

Seasonal analysis and quality control was conducted on the meteorological data collected from both stations and is discussed in section 4.4. Table 5.1 below presents the results of the linear regression analysis for $T_a$, $T_s$ and RH. Overall, the coefficient of determination was relatively high, with all values exceeding 80%, except for soil temperature probe 1. This was due to a significant period during which there was no overlap of data, resulting from a delayed sensor placement. Remaining gaps were filled using linear interpolation until a complete time series with no missing values was achieved.

*Table 5-1 Statistics for meteorological variables modelled with Mullingar data*

| **Variable** | **$R^2$** | **RMSE** |
|---|---|---|
| Air Temperature (probe 1) | 0.95 | 1.1 °C |
| Air Temperature (probe 2) | 0.95 | 1.3 °C |
| Soil Temperature (probe 1) | 0.68 | 2.7 °C |
| Soil Temperature (probe 2) | 0.85 | 1.0 °C |
| Relative Humidity | 0.83 | 5.0 % |

Similar methods were employed to analyse missing data from radiation values. However, due to their diurnal variation, radiation values required more intensive filtering processes discussed in section 4.4. Results from the analysis showed a correlation coefficient was 0.80 for RG, indicating a moderately strong relationship, and with $R^2$ value of 0.64 for the annually predicted data. The RMSE was calculated to be 110.6 W/m$^2$, and the MAE was 65 W/m$^2$. When plotted on a line graph alongside the observed data, the predicted values showed a good fit. However, a scatter plot displayed a widely dispersed linear trend. Similarly, PPFD exhibited a correlation coefficient of 0.79, suggesting a strong relationship, with an $R^2$ value of 0.62. However, the RMSE was relatively high at 228 μmol m$^{-2}$ s$^{-1}$, with an MAE of 128 μmol m$^{-2}$ s$^{-1}$.

To validate these findings, the GAMs model was also employed on the same datasets to improve the accuracy of predicted values for the time series. The results from the GAMs model were highly consistent with the previous analysis. For RG, the $R^2$ value was 0.65, with an RMSE of 109.5 µmol $m^{-2}$ $s^{-1}$ and an MAE of 64 µmol $m^{-2}$ $s^{-1}$. Regarding PPFD, the $R^2$ value was slightly higher at 0.63, with a lower RMSE of 226 µmol $m^{-2}$ $s^{-1}$ and an MAE of 125.5 µmol $m^{-2}$ $s^{-1}$. The gap filled times series for global radiation and for PPFD can be viewed in the appendix. Although the differences between the two models' predicted values were minimal, the time series predicted by GAMs was ultimately selected due to its slightly better performance metrics compared to linear regression. Table 5.2 highlights these slight differences in performance metrics between methods applied.

*Table 5-2 Comparison of performance metrics for RG and PPFD between LR and GAMs.*

| Variable | Linear Regression | GAMs |
|---|---|---|
| **RG** | | |
| $R^2$ | 0.64 | 0.65 |
| RMSE ($W/m^2$) | 110.6 | 109.5 |
| MAE ($W/m^2$) | 65 | 64 |
| **PPFD** | | |
| $R^2$ | 0.62 | 0.63 |
| RMSE (µmol $m^{-2}$ $s^{-1}$) | 228 | 226 |
| MAE (µmol $m^{-2}$ $s^{-1}$) | 128 | 125 |

Upon review of the gap filled meteorological variables, clear seasonal patterns were evident, with pronounced differences between winter and summer. Daily average air temperatures below the canopy ranged from –3.2°C in December to 20.7°C in August, with an annual average of 10.3°C. These values are consistent with Ireland's temperate climate, where long-term national averages range from 9–10°C (Walsh, 2012; Met Éireann, 2020). Average soil (10.6°C) temperature shows a similar seasonal trend, reaching a minimum of 2.8°C in December and a maximum of 16.7°C in August.

Soil moisture sensors recorded low volumetric water content throughout the year, with annual averages of 18% and 35%. These values were likely underestimated because the sensors were not calibrated for peat soils. Laboratory analysis of peat samples collected within the EC tower footprint indicated true soil moisture contents of 77% on 27 October 2023 and 75% on 30 November 2023. Comparisons with daily averages from the onsite sensors revealed underestimations of 70% and 74% respectively. Despite the inaccuracies in absolute values, the seasonal patterns were examined to check for relationships with fluxes, but none were detected. Monthly soil moisture trends from both sensors are shown in Figure 5.1.

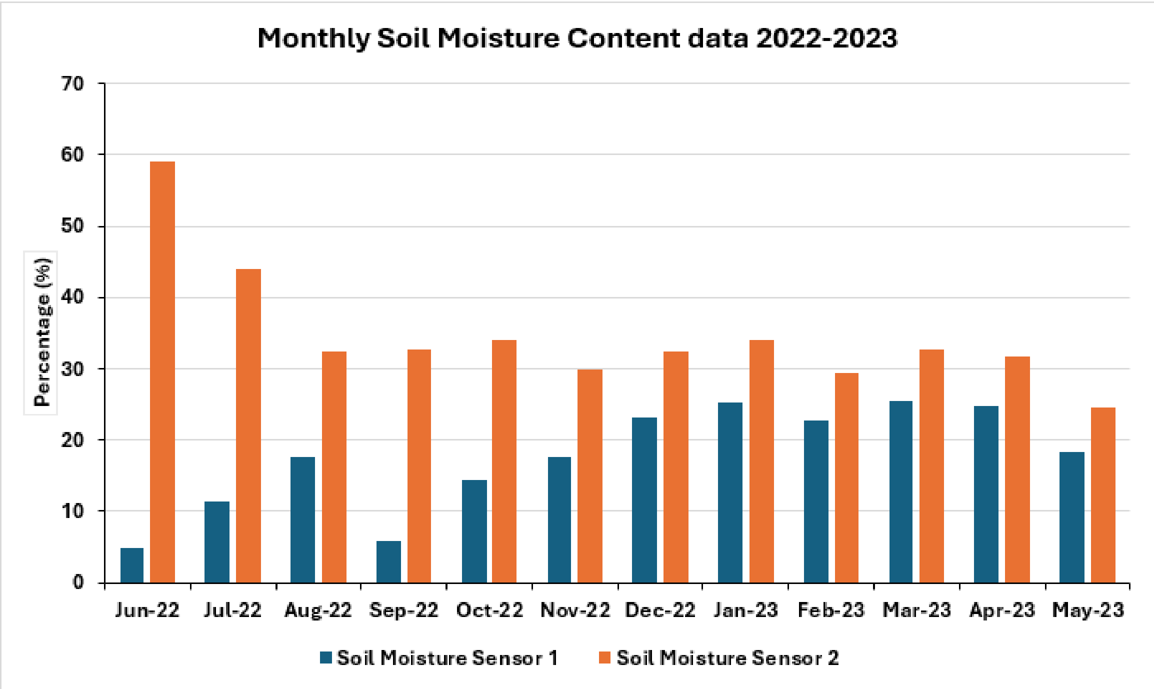


*Figure 5.1 Monthly average of soil moisture sensors for both sensors at study site*

Figure 5.2 illustrates the annual timeseries of gap filled meteorological data for (a) soil temperature at 5cm (°C), (b) below-canopy air temperature (°C), (c) above-canopy PAR (μmol/m²/s⁻¹), (d) estimated below-canopy PAR (μmol/m²/s⁻¹), and (e) average soil water content (%), for the period June 2022 to June 2023.

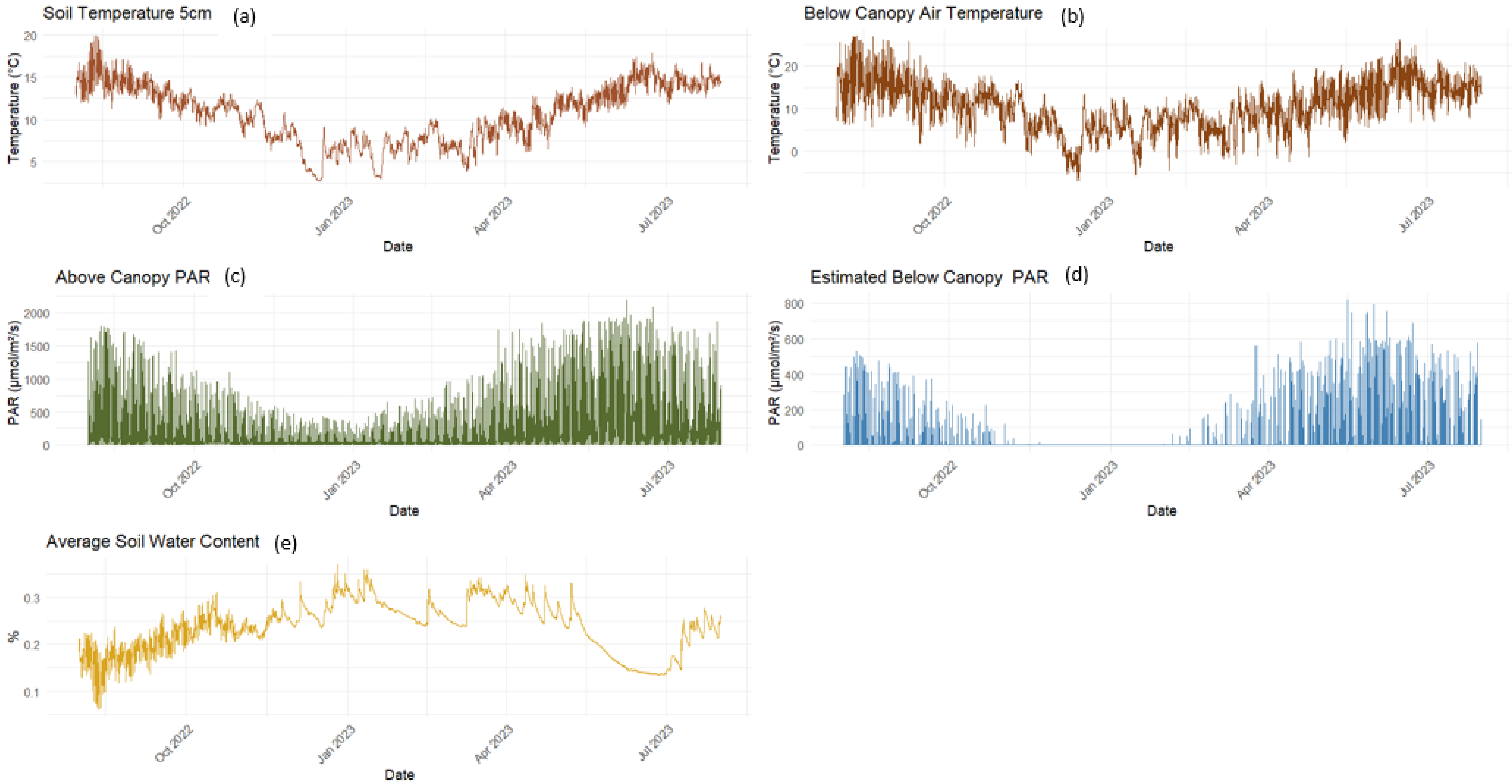


*Figure 5.2 Timeseries for meteorological data June 2022 to June 2023.*

PPFD and RG from 2022–2023 displayed expected temperate climate seasonality (Curley et al., 2024), with the highest monthly averages in June 2022 (PPFD: 402 µmol m$^{-2}$ s$^{-1}$; RG: 194 W m$^{-2}$) and the lowest in December (PPFD: 50 µmol m$^{-2}$ s$^{-1}$; RG: 32 W m$^{-2}$). Net radiation (RN) followed a similar pattern, with the lowest monthly averages in October and November (11 W m$^{-2}$). Monthly averages for all radiation variables appear in Figure 5.3. PAR below the canopy was estimated to support the modelling of GPP fluxes from chamber measurements using above-canopy PAR data. The highest daily average below-canopy PAR occurred in May, reaching 176 µmol m$^{-2}$ s$^{-1}$, while winter PAR was typically estimated to be zero. In contrast, the highest daily average PAR above the canopy was 728 µmol m$^{-2}$ s$^{-1}$, also recorded in May, with the lowest winter average value being 41 µmol m$^{-2}$ s$^{-1}$. As expected, lower PAR levels were substantially lower below the canopy, as the closing canopy effectively blocks light from reaching the forest floor.

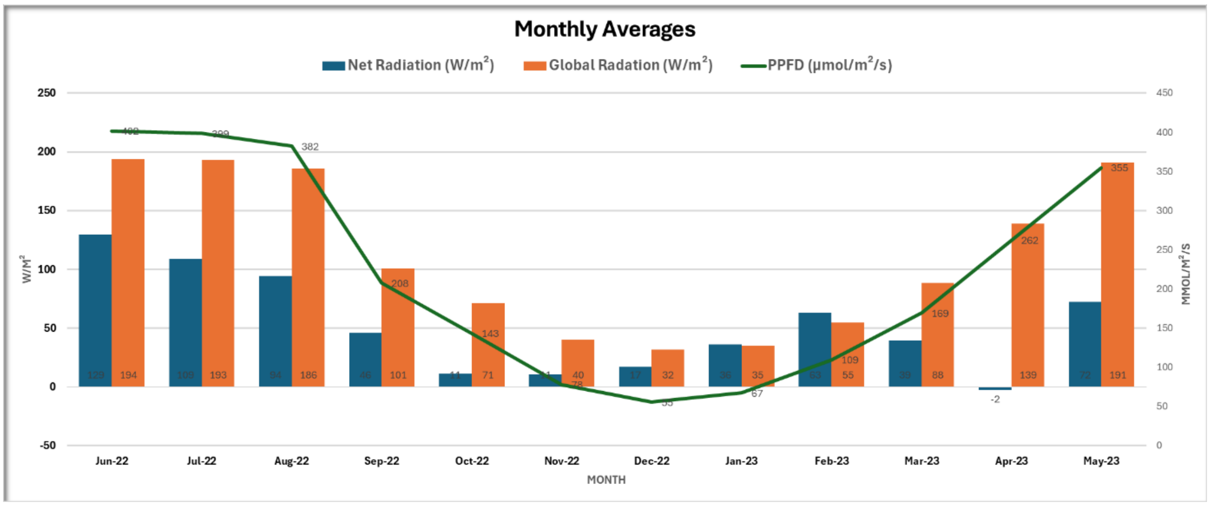


*Figure 5.3 Monthly averages for radiation at the study site from June 2022 to June 2023.*

Across the full monitoring period (June 2022–June 2023), the annual above-canopy air temperature ($T_a$) was 11°C, consistent with Ireland's climatic norms (Walsh, 2012; Met Éireann, 2020; Curley *et al.*, 2024). Long-term climate data from the nearby Lullymore Nature Centre (1.4 km away, 85 m altitude) indicate historic monthly temperatures from 2–20°C between 2010 and 2022 (Met Éireann, 2022). At the study site, the lowest temperatures occurred in December 2022 (3°C above canopy, 4°C below canopy), while the highest above-canopy temperature was recorded in July 2022 at 18°C. During the June–August 2022 growing season, below-canopy temperatures were slightly lower than above-canopy values, whereas from October 2022 to February 2023, the below-canopy sensor recorded marginally higher temperatures.

Seasonal averages of $T_a$ were 16°C in Summer 2022, 11°C in Autumn 2022, 6°C in Winter 2022/2023, and 10°C in Spring 2023. Soil temperature ($T_s$) followed the same seasonal progression, with measurements available from September 2022 onwards following sensor installation. Monthly averages of both air and soil temperature are shown in Figure 5.4.

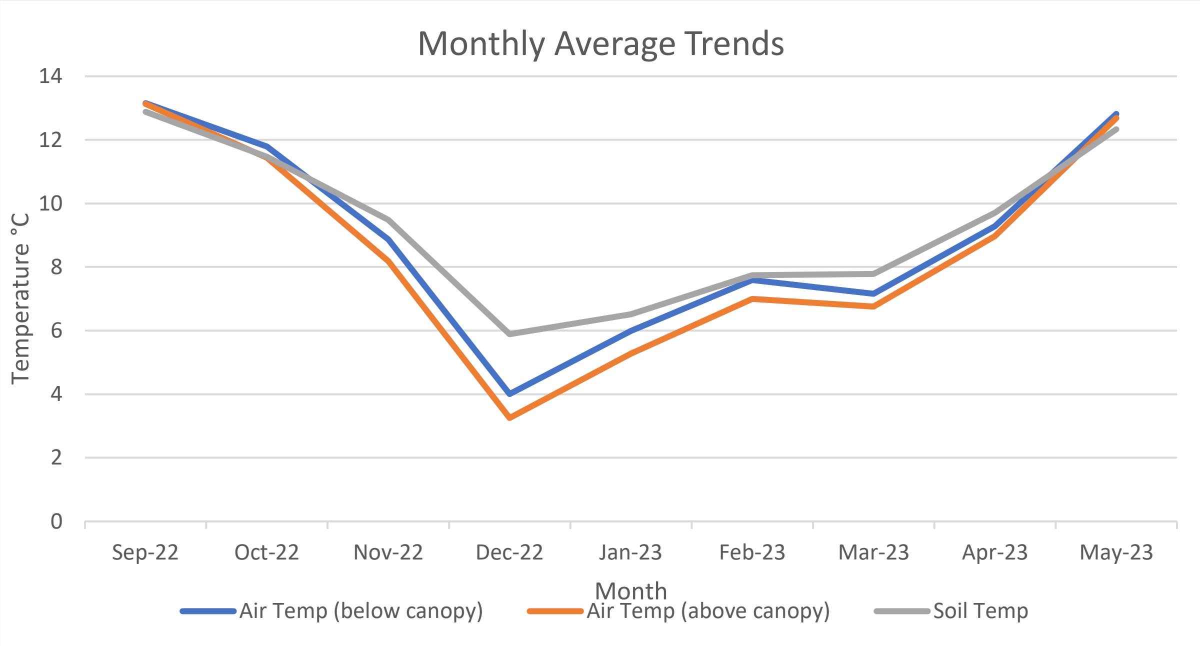


*Figure 5.4 Air temperature trends and soil temperature trends based on monthly averages.*

Relative humidity ranged from 77–90%, with higher values occurring between September and March. Water table depth remained consistently low during the entire monitoring period (–69.2 cm to –36.54 cm), reflecting the dryness of the site. As no clear relationship emerged between water table depth and carbon fluxes, WT was not included in subsequent correlation analyses. Total below canopy precipitation from September 2022 to June 2023 was 883 mm, closely matching precipitation measured at Lullymore Nature Centre (899.9 mm). Long-term mean annual precipitation at the Nature Centre is 894 mm (Met Éireann, 2022). Precipitation below the canopy was frequent throughout the year, with no clear trend or pattern observed in the annual dataset. Figure 5.5 shows total monthly precipitation below the canopy at the study site (orange) and Lullymore Nature Centre (green). Monthly totals are similar where data overlap, except for September, October, and

March, where slightly larger differences occur, likely due to canopy interception, seasonal leaf changes, and rainfall redistribution.

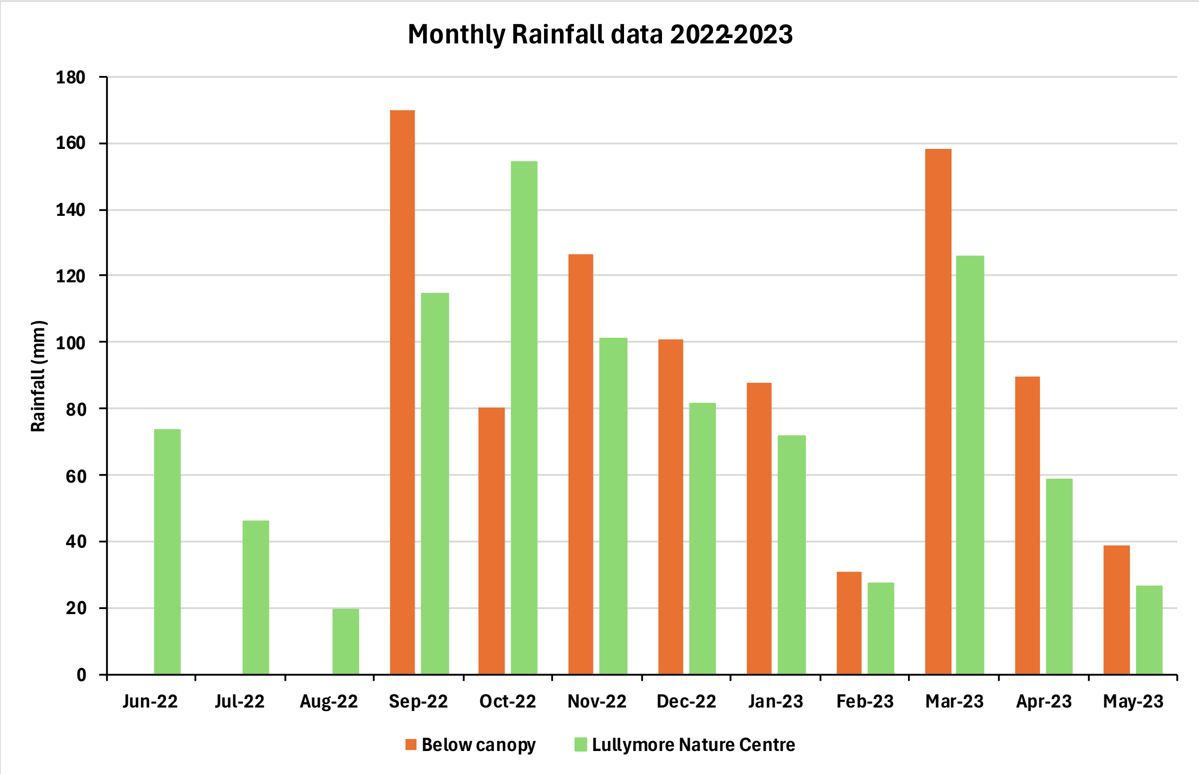


*Figure 5.5 Total monthly precipitation below canopy and Lullymore nature centre.*

## 5.2 Below-Canopy $CO_2$ Fluxes

### 5.2.1 Model performances

This section presents the modelling approaches (discussed in Section 4.2) and performance evaluation for below-canopy $CO_2$ fluxes derived from chamber measurements at the study site. Data for $GPP_{bel}$ and $R_{bel}$ were modelled separately, and several machine learning algorithms were evaluated, including kNN, RF, Gradient Boosting, XGBoost, and GAM. Performance metrics used to assess these models included $R^2$, RMSE and MAE. After comparing all the methods, the model with the highest $R^2$ and lowest RMSE was selected for modelling the complete annual dataset. Tables 5.3 and 5.4 provide the evaluation metrics for each model on both $GPP_{bel}$ and $R_{bel}$. Plots of the training and testing data against the observed data are included in the appendix.

*Table 5-3 Performance metrics for gross primary production below canopy.*

| $GPP_{bel}$ | | | | | |
|---|---|---|---|---|---|
| Model | Training Metrics $\mu mol\ m^{-2}\ s^{-1}$ | | | Testing Set Metrics $\mu mol\ m^{-2}\ s^{-1}$ | |
| | R2 | RMSE | MAE | RMSE | MAE |
| Random Forest | 0.79 | 0.091 | 0.072 | 0.406 | 0.224 |
| Gradient Boosting | 0.96 | 0.034 | 0.026 | 0.427 | 0.233 |
| XGBoost | 0.93 | 0.048 | 0.038 | 0.419 | 0.228 |
| k-Nearest Neighbors (kNN) | 0.23 | 0.132 | 0.103 | 0.384 | 0.204 |
| Generalized Additive Model (GAM) | 0.09 | 0.143 | 0.113 | 0.39 | 0.199 |

The analysis of $GPP_{bel}$ predictions (Table 5.3) using various machine learning models shows that Gradient Boosting and XGBoost performed the best during training, with high $R^2$ values (0.96 and 0.93) and low errors. However, both models experienced higher errors on the testing set, indicating some overfitting. RF also demonstrated good performance but showed a noticeable drop in accuracy when tested. In contrast, the kNN and GAM struggled, achieving very low $R^2$ during training and comparatively higher errors, making both the least effective models in this comparison. Overall, while Gradient Boosting and XGBoost lead in performance, RF demonstrated more consistent and balanced results across both training and testing, achieving a relatively high $R^2$ value of 0.79 on the training data and low RMSE (0.406) in the testing dataset.

*Table 5-4 Performance metrics for respiration below canopy.*

| $R_{bel}$ | | | | | |
|---|---|---|---|---|---|
| Model | Training Metrics | μmol $m^{-2}$ $s^{-1}$ | | Testing Set Metrics μmol $m^{-2}$ $s^{-1}$ | |
| | R2 | RMSE | MAE | RMSE | MAE |
| Random Forest | 0.81 | 0.122 | 0.098 | 0.385 | 0.175 |
| Gradient Boosting | 0.87 | 0.097 | 0.070 | 0.404 | 0.189 |
| XGBoost | 0.86 | 0.099 | 0.076 | 0.448 | 0.231 |
| k-Nearest Neighbors (kNN) | 0.52 | 0.186 | 0.139 | 0.399 | 0.206 |
| Generalized Additive Model (GAM) | 0.40 | 0.204 | 0.147 | 0.404 | 0.205 |

For the $R_{bel}$ prediction models, Gradient Boosting performed the best during training, with an $R^2$ of 0.87 and relatively low error values (Table 5.4). However, it showed increased errors on the testing set, reflecting some overfitting. XGBoost followed closely with an $R^2$ of 0.86, though it had a higher error in testing, with an RMSE of 0.448 μmol $m^{-2}$ $s^{-1}$. The RF model also delivered strong training results ($R^2$ of 0.81), but its testing performance was more stable compared to Gradient Boosting and XGBoost, with an RMSE of 0.385 μmol $m^{-2}$ $s^{-1}$. The kNN model had moderate performance, with an $R^2$ of 0.52 in training and errors that were on par with other models in testing, though slightly worse than RF. GAM had the weakest performance overall, with a low $R^2$ of 0.40 in training and testing errors similar to those of kNN, making it the least effective in predicting respiration compared to the other models.

Despite not having the highest training accuracy, RF demonstrated more stable and balanced performance on the testing sets compared to other models, showing fewer signs of overfitting. Therefore, RF was chosen to model the annual time series for both $GPP_{bel}$ and $R_{bel}$ the results of the model are discussed below.

### 5.2.2 Below canopy $CO_2$ fluxes

The annual timeseries of daily summed modeled fluxes (Figure 5.6) below the canopy shows clear seasonal trends. The $R_{bel}$ shown in dark red on the plot shows a clear seasonal trend with reduced fluxes during the winter months and increased respiration during the summer. This is consistent with soil and air temperature timeseries (Figure 5.4) for the same period, as warmer temperatures in summer stimulate microbial activity and root respiration. With cooler temperatures in winter the rate of root respiration and microbial activity reduce.

The modelled $GPP_{bel}$ shown in green, drops to zero during the winter months due to extremely low adjusted PAR values, which were near zero during this period. The near-zero values in winter correlate with the estimated below canopy PAR (Figure 5.2 (d)), which to some extend represents the dormancy of vegetation during this period, but also indicates a possible underestimation of below canopy PAR. There is considerable variation in $GPP_{bel}$ during the growing season (spring and late summer) showing substantial fluctuation. These fluctuations indicate responses to short-term environmental factors, such as soil water content (SWC). SWC reduces significantly when $GPP_{bel}$ values seem to plateau throughout summer months and then reduce again in Autumn when SWC rises somewhat.

The modeled $NEE_{bel}$, derived from $GPP_{bel}$ and $R_{bel}$, exhibits a strong correlation with $R_{bel}$, which is expected given the consistently low $GPP_{bel}$ values, particularly during the winter months, which subsequently lowers the overall average. $NEE_{bel}$.represents the net carbon balance of the below-canopy ecosystem. Based on the time series, it is evident that the below-canopy system functions as a net source of $CO_2$ throughout the year. This is more clearly highlighted in the cumulative plot in Figure 5.7. Positive $NEE_{bel}$ values indicate a net $CO_2$ source, while negative values would indicate a $CO_2$ sink, though none are observed in the $NEE_{bel}$ timeseries.

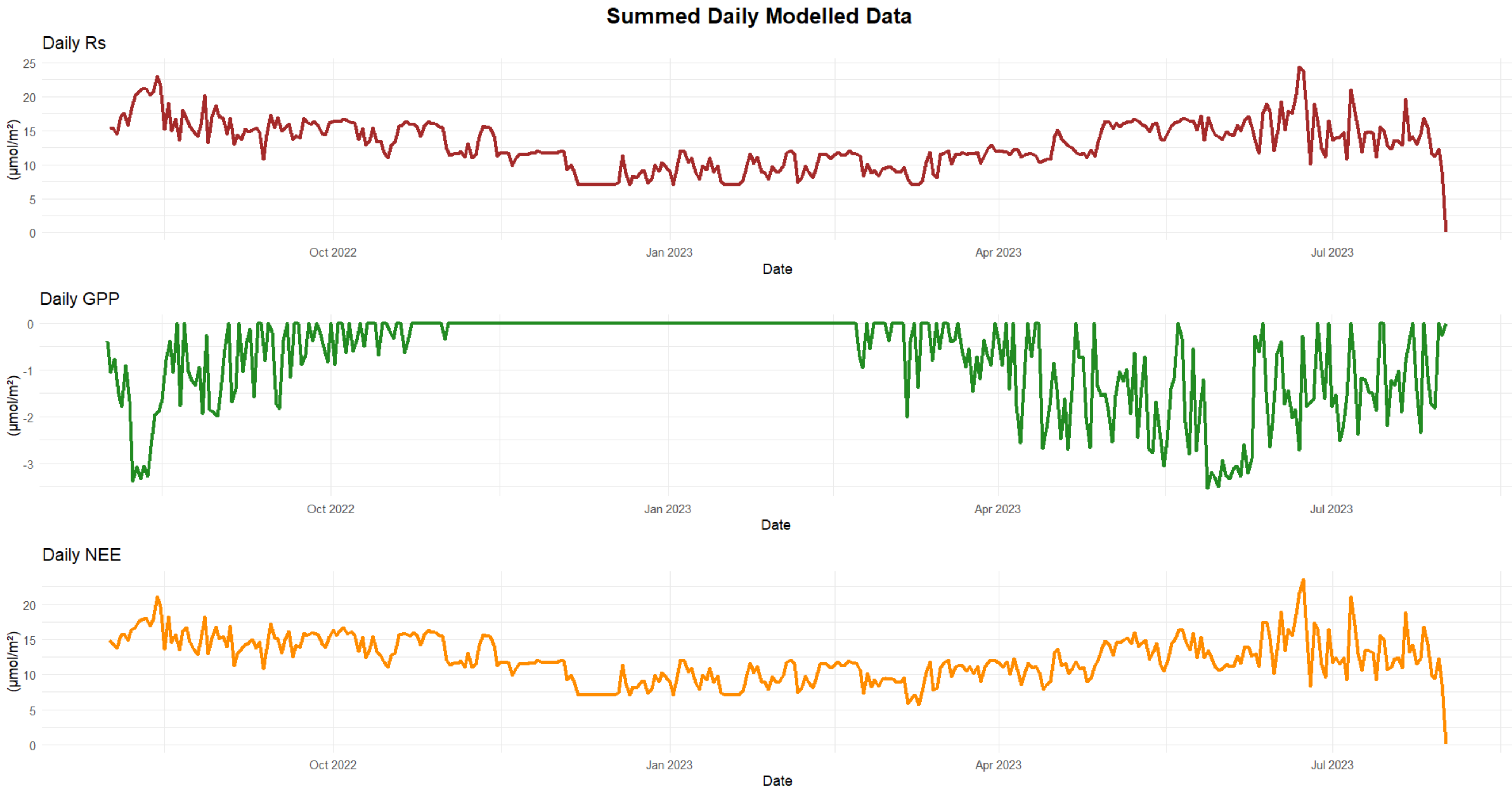


*Figure 5.6 Annual timeseries of modelled daily summed fluxes below the canopy.*

The measured $R_{bel}$ at the Lullymore research site yielded values of 47.8 (±0.3 SE) t $CO_2$ $ha^{-1}$ $yr^{-1}$ for respiration, -2.8 (±0.1 SE) t $CO_2$ $ha^{-1}$ $yr^{-1}$ for $GPP_{bel}$, and 45.0 (±0.4 SE) t $CO_2$ $ha^{-1}$ $yr^{-1}$ for $NEE_{bel}$.These values provide an essential baseline for understanding $CO_2$ flux dynamics below the canopy within temperate woodland ecosystems on organic peat soils.


*Figure 5.7 Cumulative plots for estimated annual fluxes below the canopy*

## 5.3 Total Net Ecosystem Exchange

### 5.3.1 Estimates of $CO_2$ fluxes from both methods applied

#### *5.3.1.1 Driver variables MDS*

This subsection examines the relationships between $CO_2$ fluxes and key environmental driver variables used for estimating gaps in the time series. The $CO_2$ flux data revealed correlations with several environmental variables, including PPFD, $T_a$, VPD and $T_s$. The Pearson correlation matrix is detailed in the appendix. A strong negative correlation was found between PPFD and $CO_2$ flux, with a Pearson correlation coefficient of -0.70, suggesting that as PPFD increases, $CO_2$ flux tends to decrease. The regression analysis showed a slope of -0.0175, indicating a small reduction in $CO_2$ flux for each unit increase in

PPFD. Overall, higher light levels, as represented by PPFD, are associated with decreased $CO_2$ flux.

The relationship $T_a$ above the canopy and $CO_2$ flux also showed a moderate negative correlation, with a Pearson coefficient of -0.50. As air temperature increases, $CO_2$ flux tends to decrease. The regression model revealed a slope of -0.6894, suggesting that for each unit increase in air temperature, $CO_2$ flux decreases by approximately 0.6894 units. A moderate negative correlation was observed between $CO_2$ flux and VPD, with a coefficient of -0.50. This suggests that as VPD increases, $CO_2$ flux tends to decrease. However, the slope of -0.0111 indicates only a small reduction in $CO_2$ flux for each unit increase in VPD.

All three meteorological variables have significant negative relationships with $CO_2$ fluxes, indicating that increases in these variables are associated with decreases in $CO_2$ flux. The strongest predictor among the three was PPFD. Therefore, for the following seasons Spring, Summer and Autumn, PPFD was chosen as the main driver variable, followed by $T_a$ and VPD. As in winter period there are less daylight hours, the Pearson correlation for nighttime values only for $CO_2$ and variables was calculated. Given that the nighttime variable with the most correlation to nighttime fluxes was the average $T_S$ ($R^2$ = 0.3), this was then used as the main driver variable predicting missing fluxes over the winter months, followed by $T_a$ and VPD. The annual time series of flux data was separated into seasonal segments for analysis, with the winter months including November, December, and January, and so forth.

Therefore, for each period, primary, secondary, and tertiary drivers were defined with specified tolerance levels. During the growing seasons, PPFD (50-200 µmol $m^{-2}$ $s^{-1}$), $T_a$ (±2.5°C), and VPA (±5 hPa) were used. In the dormant winter season, $T_s$ (±2.5°C) was the primary driver, followed by $T_a$ and VPA with the same tolerances. These tolerances ensured that only values within the specified ranges were used to estimate missing data, improving the accuracy of the gap-filling process (Reichstein et al., 2005).

#### *5.3.1.2 Estimated time series by MDS gap filling method*

After the filtering process and the removal of 10% of the data (for testing purposes), 41% of the $CO_2$ flux data remained. The observed fluxes refer to the actual measured $CO_2$ flux values recorded across different seasons, while the predicted fluxes were generated through gap-filling techniques using MDS, applied via the Tovi software (version 2.9.1). The fingerprint plot below presents the annual time series of $CO_2$ fluxes, both before and after gap filling.

Upon visual inspection, the gap-filling process appears to have effectively addressed the smaller data gaps. However, a prominent gap in October exhibits reduced variability compared to the overall dataset, as shown in Figure 5.8. The plot shows variations in $CO_2$ fluxes over time, with distinct patterns visible for both the original data and the MDS gap-filled data. This highlights a key limitation of the MDS approach, which struggles to accurately capture the full variability of the data when dealing with larger gaps.

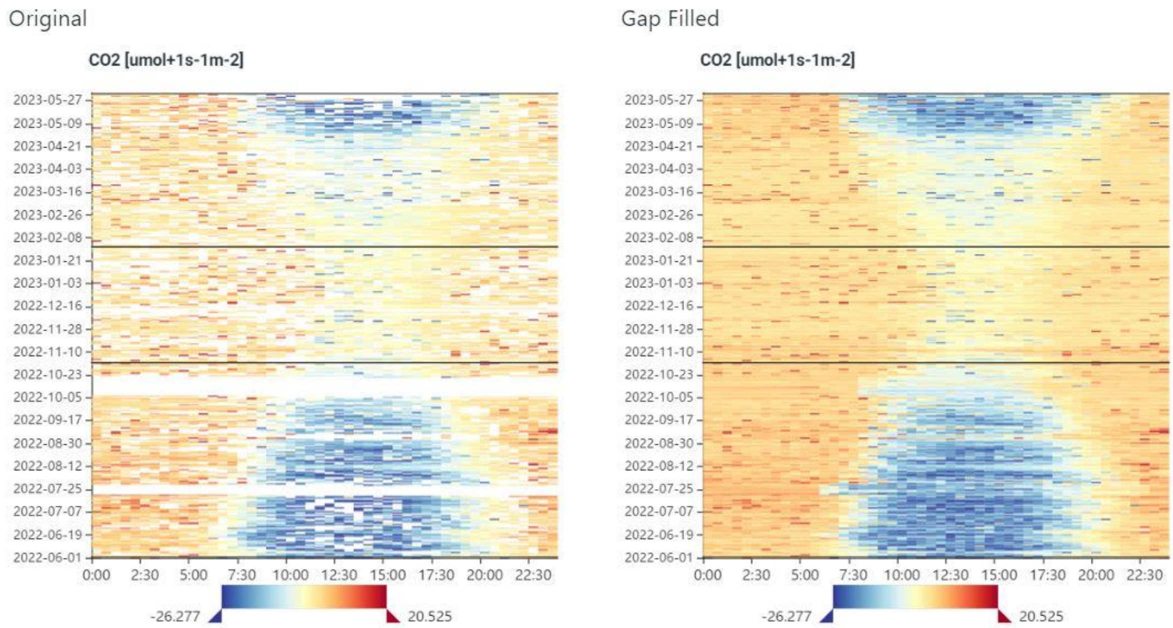


*Figure 5.8 Fingerprint plot illustrates $CO_2$ fluxes before and after gap filling using the MDS method.*

This observation becomes even more evident when the data is plotted as a time series over the year (Figure 5.9). The plot highlights the performance of the gap-filling approach across the year, showcasing deviations between estimated and observed values, particularly during periods with larger data gaps. The performance of the gap-filled data points is less robust when estimating larger gaps in the time series, particularly during specific periods. This is most evident in July and October, where the estimated data deviate more noticeably from the observed values. These discrepancies suggest that the model struggles to accurately capture variations during periods with larger gaps in the data, highlighting its limitations in predictive capability.

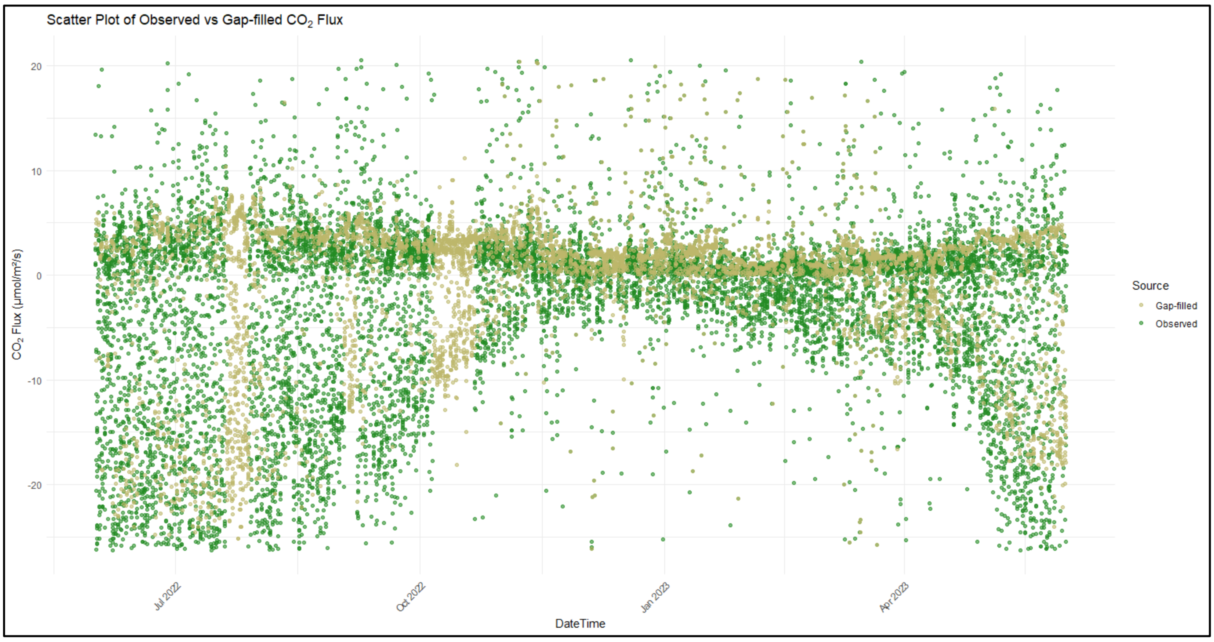


*Figure 5.9 Time series plot compares the gap-filled data using the MDS method against the observed data.*

The scatter plot of Figure 5.10 illustrates the relationship between observed and predicted $CO_2$ flux values, where the predicted values were generated using the MDS model after randomly removing 10% data points. The points in the plot indicate a strong correlation between the observed and estimated values, as evidenced by the relatively tight clustering of the data around the red dashed line. The $R^2$ value of 0.44 for the residuals suggests a moderate explanatory power of the model in capturing the variability in $CO_2$ flux. This demonstrates that while the model captures some of the underlying patterns, there remains unexplained variance.

Error metrics such as the RMSE and MAE were calculated to be 4.31 µmol $m^{-2}$ $s^{-1}$ and 2.46 µmol $m^{-2}$ $s^{-1}$, respectively, indicating that the model's predictions are reasonably accurate, with a relatively low level of overall error. However, the standard error of 4.31 µmol $m^{-2}$ $s^{-1}$ indicates that, while the model performs well overall, there is some variability in the predictions, as shown by the dispersion of points around the line.

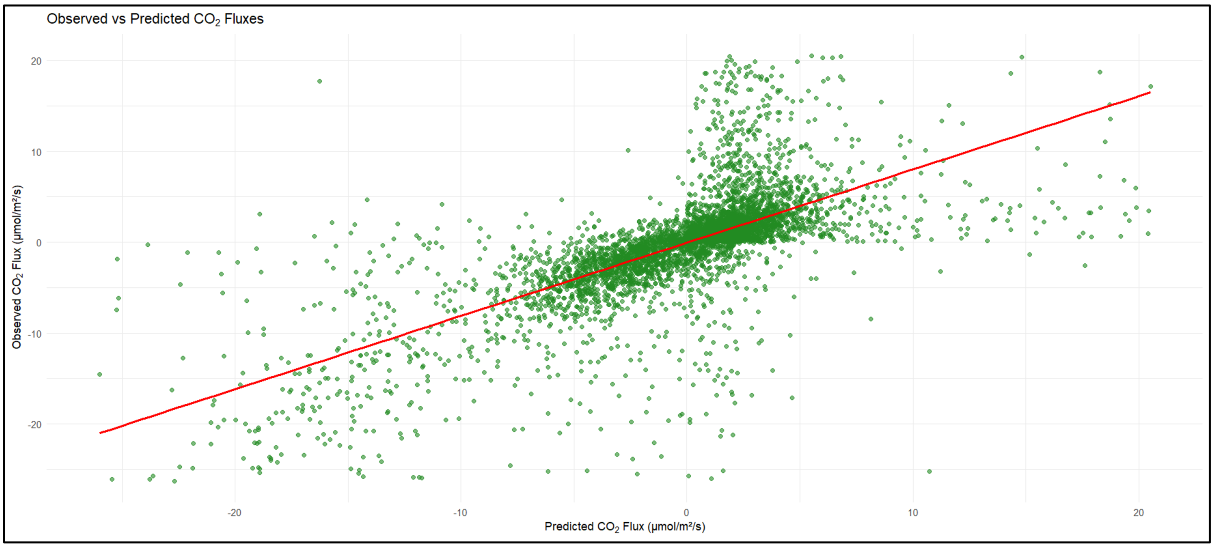


*Figure 5.10 Scatter plot shows overlapping data points for observed versus MDS gap-filled data.*

#### *5.3.1.3 Estimating the time series using RF gap filling method*

The time series plot Figure 5.11 illustrates both the observed and gap-filled $CO_2$ flux values over the course of a year, with green points representing the observed values and yellow points representing the gap-filled estimates produced by RF model. The RF model appears to have performed well in estimating missing data, as indicated by the close alignment of the gap-filled points with the observed values, particularly in periods with smaller or intermittent gaps.

Compared to the MDS method, the RF approach demonstrates improved performance, particularly in maintaining the overall variability of the data across time. The model effectively fills gaps across most of the time series, with only minor discrepancies during periods with more substantial data gaps, such as in October.

Overall, the RF method provides a more accurate and robust estimate of $CO_2$ fluxes, especially when compared to MDS on visual comparison.

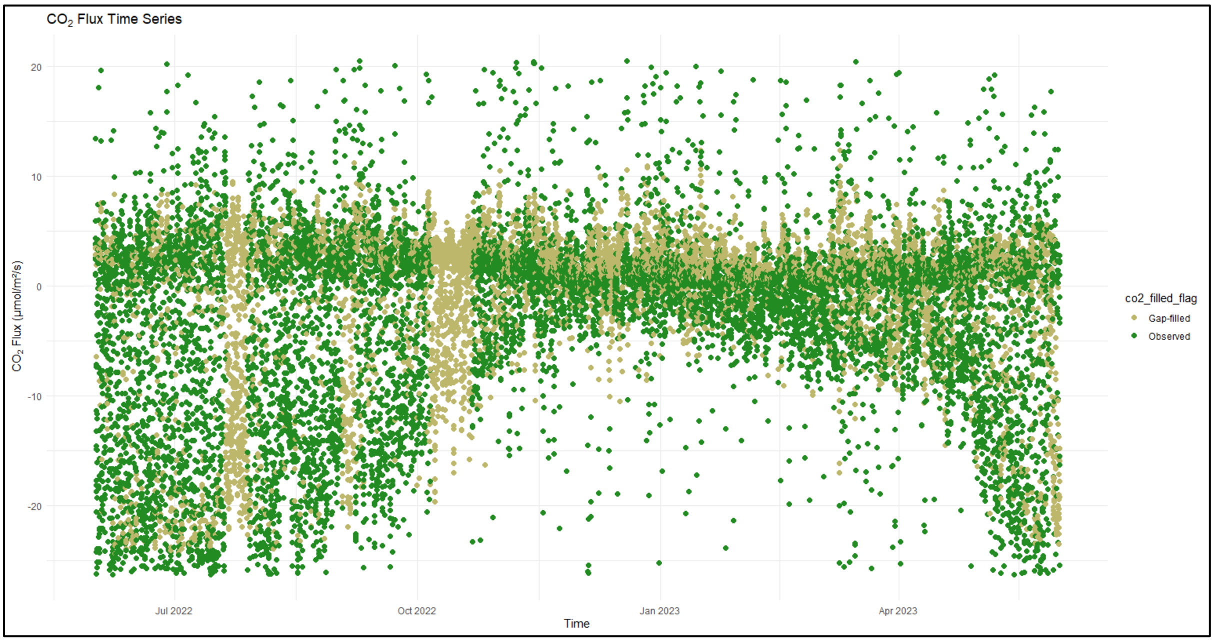


*Figure 5.11 Time series plot compares the gap-filled data using the RF method against the observed data.*

The scatter plot (Figure 5.12) illustrates the relationship between observed and predicted $CO_2$ flux values, where the predicted values were generated using the RF model after randomly removing 20% of the data points. The points in the plot indicate a strong correlation between the observed and predicted values, as evidenced by the relatively tight clustering of the data around the red line, which represents good agreement between observed and predicted fluxes.

The $R^2$ value of 0.77 for the residuals suggests good explanatory power of the RF model in capturing the variability in $CO_2$ fluxes. This demonstrates that while the model effectively captures some of the underlying patterns in the data, a small portion of the variance remains unexplained. Error metrics such as the RMSE and MAE were calculated to be 3.95 $\mu mol\ m^{-2}\ s^{-1}$ and 2.39 $\mu mol\ m^{-2}\ s^{-1}$, respectively, indicating reasonably accurate predictions with a relatively low overall error. However, the standard error of 0.07 $\mu mol\ m^{-2}\ s^{-1}$ suggests that the model performs well overall, there is small variability in the predictions, as reflected by the dispersion of points around the line.

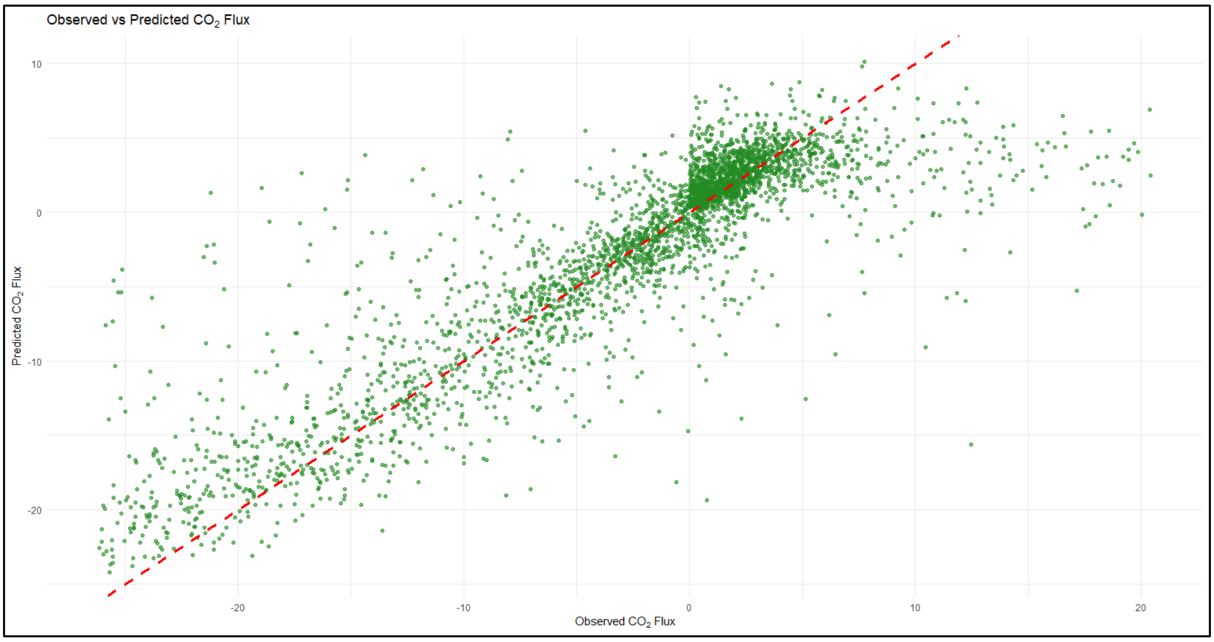


*Figure 5.12 Scatter plot of overlapping data points for observed versus RF gap-filled data.*

The boxplot (Figure 5.13) compares the RF gap-filled data with the observed data, showing that the central tendencies (medians and means) of both datasets are closely aligned, indicating that the gap-filling model has effectively captured the overall data distribution. However, the whiskers, which represent the spread of the data (extreme values or outliers), show some variation between the two datasets. This suggests that while the model performs well in predicting typical values, there may be slight differences in how it captures the more extreme data points.

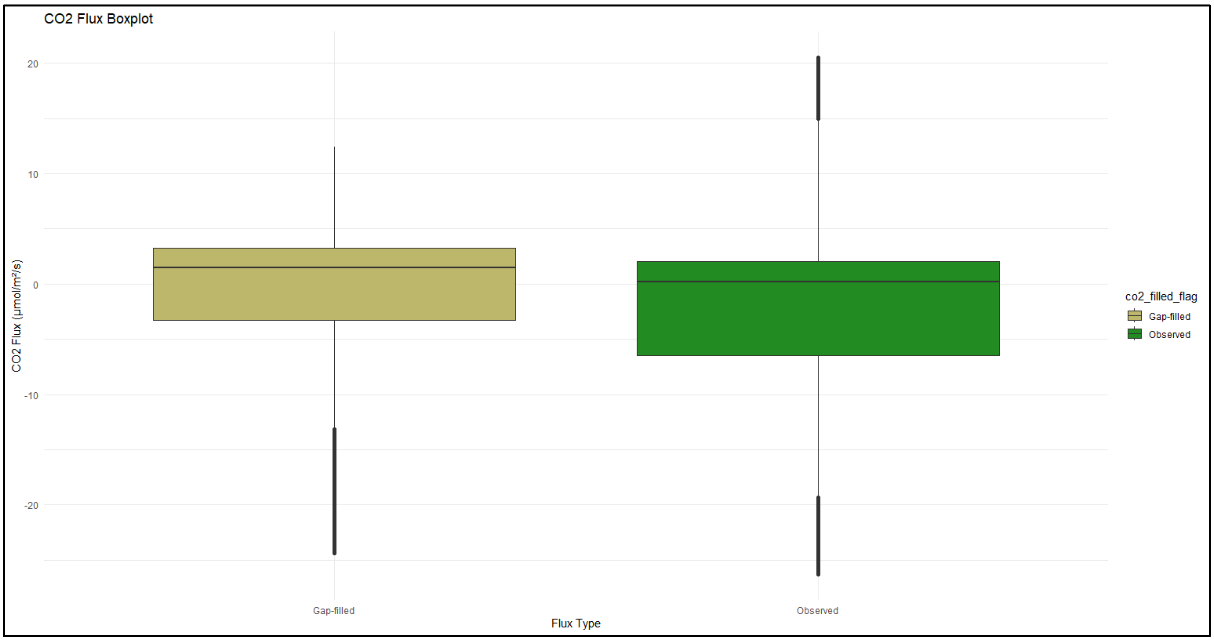


*Figure 5.13 Box plot of the gap-filled data alongside the overlapping observed data.*

#### *5.3.1.4 Performance metrics from both methods*

Table 5.5 below shows performance metrics form both methods and highlights the superiority of the RF model across most metrics. The table is rounded to four decimal places to highlight the subtle differences observed in results. The RF model achieves a higher $R^2$ value (0.77) compared to MDS (0.44), indicating that RF explains a greater proportion of the variance in the data. Additionally, RF has lower error values, with a RMSE of 3.95 and MAE of 2.39, as opposed to the higher RMSE of 4.31 μmol $m^{-2}$ $s^{-1}$ and MAE of 2.46 μmol $m^{-2}$ $s^{-1}$ for MDS. The standard error is also much lower for RF (0.07 μmol $m^{-2}$ $s^{-1}$) compared to MDS (4.31 μmol $m^{-2}$ $s^{-1}$), reinforcing the RF model's greater precision and reliability in predicting the data. Overall, RF outperforms MDS, particularly in terms of accuracy and error reduction.

*Table 5-5 Performance metrics for RF and MDS.*

| Metric | RF | MDS |
|---|---|---|
| $R^2$ | 0.7705 | 0.4428 |
| **RMSE** (μmol $m^{-2}$ $s^{-1}$) | 3.9536 | 4.3139 |
| **MAE** (μmol $m^{-2}$ $s^{-1}$) | 2.3944 | 2.4645 |
| **SE** (μmol $m^{-2}$ $s^{-1}$) | 0.0678 | 4.3147 |

Overall, the annual timeseries of $CO_2$ fluxes exhibited clear seasonal patterns and variability, which is expected from a broadleaf woodland that changes throughout the year. There was also a diurnal pattern, with low fluxes during daylight hours and higher $CO_2$ fluxes at night, driven by respiration processes. A cumulative plot (Figure 5.14) summing daily fluxes was created to compare the cumulative fluxes from both methods. Both datasets followed a very similar trend at the beginning of the measurements, where fluxes rapidly declined before levelling off as consistency occurred during autumn and winter. However, the MDS method estimated higher fluxes throughout the winter period, indicating less sequestration compared to the RF model. Despite this, both datasets followed a very similar trend over the entire timeseries. The total estimated net $CO_2$ flux derived from the MDS method was -28.1 t $CO_2$ $ha^{-1}$ $yr^{-1}$, and for the RF model, the total summed $CO_2$ for the year was -30.2 t $CO_2$ $ha^{-1}$ $yr^{-1}$. Both annual sums represent significant sinks of atmospheric $CO_2$, indicating that the site acted as a strong sink, sequestering $CO_2$ according to both models. The percentage difference between the two annual sums of predicted $CO_2$ was calculated to be 7.5%, a relatively minor difference between the total annual sum.

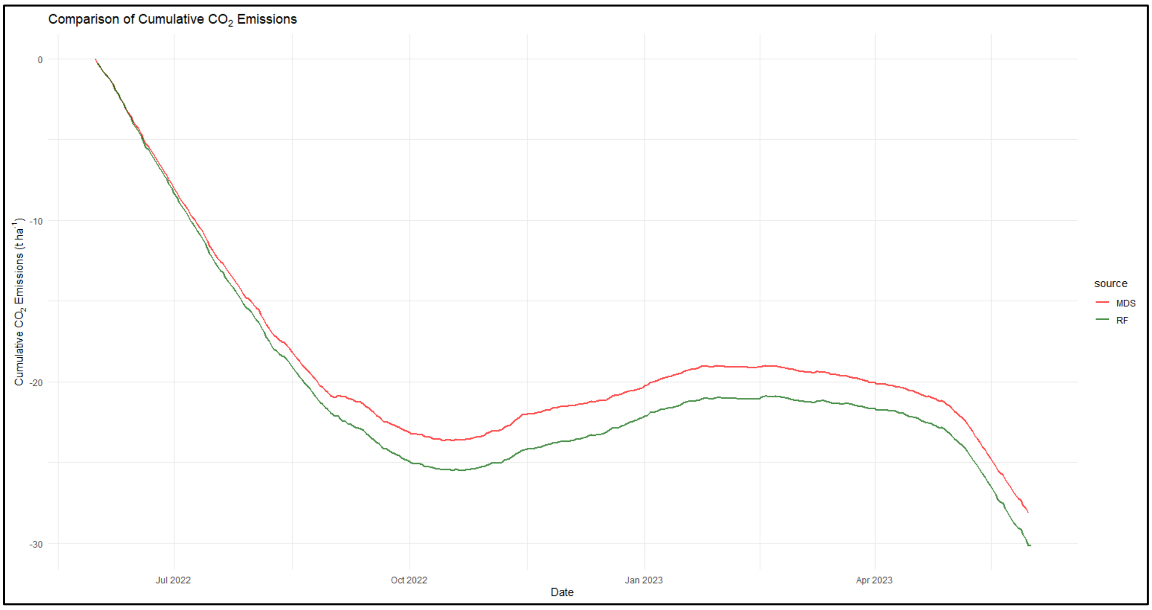


*Figure 5.14 Cumulative plot for both gap-filled time series of annual $CO_2$ fluxes.*

## 5.4 Contribution of Below-Canopy Fluxes to Total NEE

In the section 5.2, $NEE_{bel}$ was estimated for the same year as the total NEE measured above the canopy. This below-canopy estimate was incorporated into the overall NEE to account for possible underestimation during periods of low wind velocity and reduced turbulence below the canopy. The $u^*$ threshold values for each season were determined based on wind velocity, as shown in Table 5.6. These u* thresholds were then applied to the NEE time series.

*Table 5-6 Seasonal U star thresholds.*

| **Season** | **U* threshold** |
|---|---|
| Summer | 0.151 |
| Autumn | 0.318 |
| Winter | 0.150 |
| Spring | 0.122 |

For timestamps where flux values fell below the season-specific *u** threshold, the below-canopy $NEE_{bel}$ values were used to replace the corresponding above-canopy NEE values. This adjustment aimed to improve the accuracy of NEE estimates by ensuring that below-canopy respiration, particularly during periods of low wind and turbulence (common during nighttime), were not underestimated. The overall contribution of $NEE_{bel}$ canopy to the total NEE annual estimate was also evaluated (Figure 5.15).

Incorporation of $NEE_{bel}$ into the annual NEE estimates resulted in a modest adjustment of the total $CO_2$ balance. For the random forest model, the total NEE changed from -30.2 to -28.9 t $CO_2$ $ha^{-1}$ $yr^{-1}$, representing an increase of 1.3 t $CO_2$ $ha^{-1}$ $yr^{-1}$. similarly, for the MDS based estimate, inclusion of $NEE_{bel}$ altered total NEE from -28.1 to -26.8 t $CO_2$ $ha^{-1}$ $yr^{-1}$, with the same increase as RF. This adjustment slightly reduced the system's overall carbon sequestration potential, highlighting the influence of below-canopy emissions on total carbon exchange.

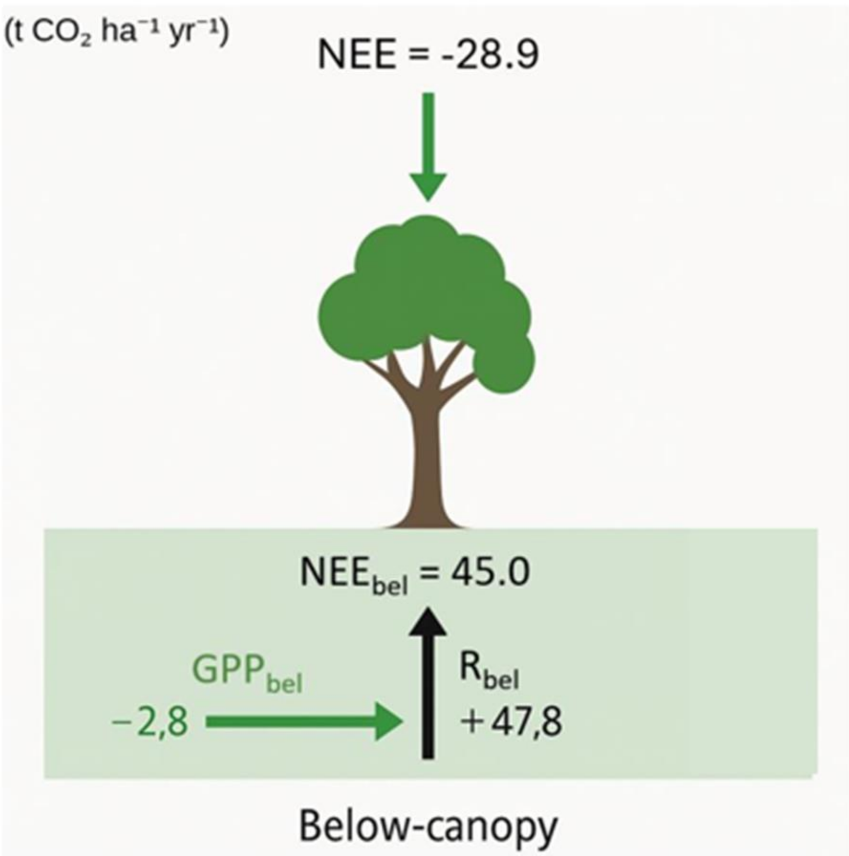


*Figure 5.15 Schematic representation of the results from $NEE_{bel}$ (including $GPP_{bel}$ and $R_{bel}$) and total adjusted NEE (RF)*

# 6 Results – Methane ($CH_4$) Fluxes

## 6.1 Environmental parameters

Upon reviewing the observed $CH_4$ flux data, the Pearson correlation matrix (see Appendix for full matrix plot) shows that methane flux exhibits very weak correlations with all measured environmental variables.

For the MDS gap-filling method, VPD was selected as the primary driver, with TS and PPFD included as secondary drivers. Figure 6.1 illustrates clear seasonal cycles, with PPFD and TS peaking during the summer months and declining through winter. VPD follows a similar pattern, with elevated values during warmer, drier periods and consistently low values throughout winter. Notably, soil temperature increases sharply in July and August, coinciding with peaks in PPFD and VPD conditions that reflect the warm and dry period at the site. These variables were chosen for gap-filling because they exhibited the most distinct and interpretable seasonal gradients, providing a stable representation of site conditions despite their weak correlations with $CH_4$ fluxes.

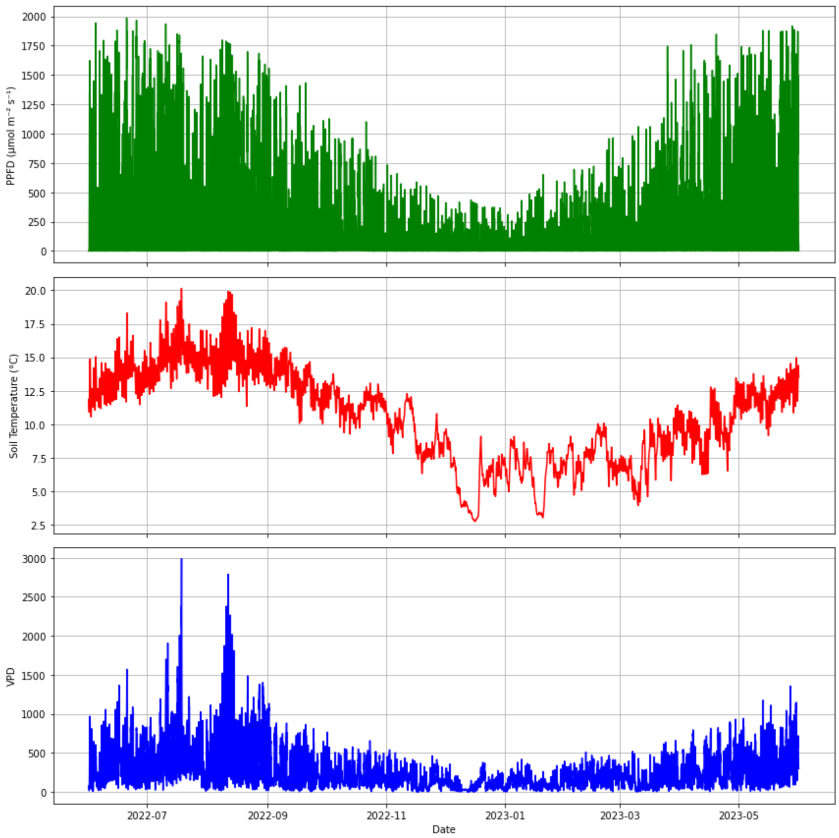


*Figure 6.1 Daily PPFD, soil temperature, and VPD (Pa) from June 2022 to June 2023*

Although all environmental variables displayed similarly low correlations with methane flux, the selected drivers had been previously applied in $CH_4$ gap-filling studies (Kim *et al.*, 2020) and therefore remained the most appropriate candidates. Nevertheless, the overall weak relationships may indicate limitations in applying the MDS method to this dataset, a point explored further in the following sections.

While previous research has reported strong links between WT position and methane emissions (Begon *et al.*, 1996; Feehan and O'Donovan, 1996; Le Mer and Roger, 2001; IPCC, 2013; Holl *et al.*, 2020; Wilson *et al.*, 2022), no such relationship emerged in this study. $CH_4$ emissions remained highly variable and did not correlate with WT or any other measured environmental parameter. This variability likely reflects the influence of multiple interacting site-specific factors including vegetation composition, microtopography, and short-term hydrological dynamics which can vary substantially across spatial and temporal scales and reduce the detectability of simple linear relationships.

## 6.2 Methane Fluxes

Drawing on both the observed and modelled $CH_4$ flux data, this section presents the annual time series and assesses model performances. No obvious diurnal patterns were detected in the $CH_4$ flux. Nevertheless, a slight seasonal variation was observed, as depicted in Figure 6.2, with a modest increase in $CH_4$ emissions from late April to June 2023. Overall, emissions remained consistently low throughout the year, with no pronounced seasonal trends.

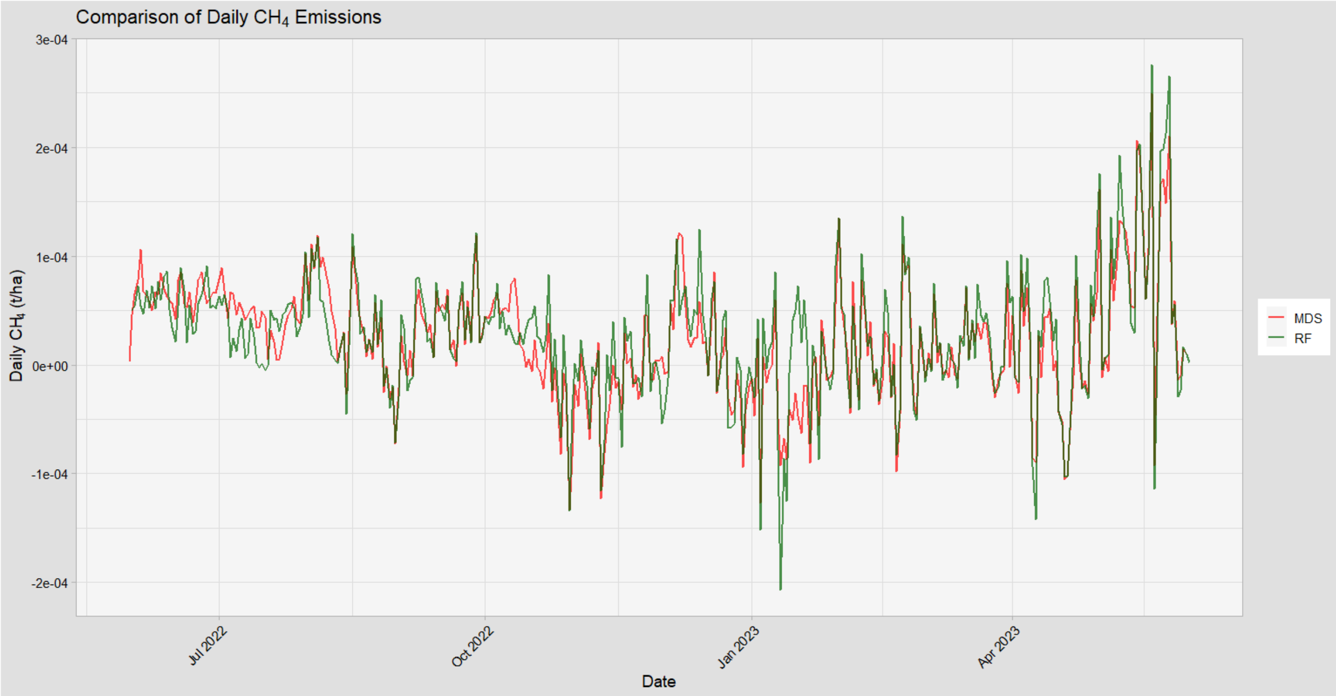


*Figure 6.2 Annual time series of summed daily $CH_4$ flux estimates, from MDS and RF.*

The time series plot Figure 6.2 illustrates the daily summed $CH_4$ fluxes derived from a gap filled time series using both methods, MDS (in red) and RF (in green). When half hourly fluxes are aggregated to daily sums, significant differences between the two methods become evident. Notably, the RF model estimated lower $CH_4$ fluxes during June and July 2022. However, at other times, the RF model overestimated $CH_4$ fluxes compared to MDS, such as in February 2023, where a spike in $CH_4$ fluxes derived from RF is apparent.

### 6.2.1 Model performances

This section evaluates the performance of the $CH_4$ flux gap-filling models, comparing observed data with estimates from the MDS method. Upon visual inspection of the time series, both models appear to effectively fill the gaps in the $CH_4$ flux data. Figure 6.3 illustrates the observed and gap-filled $CH_4$ flux time series using the MDS method. A significant gap is noticeable at the start of the series, corresponding to a period of instrumentation failure, which marks the beginning of data collection from the analyser. It is evident that the MDS method slightly underestimates the $CH_4$ fluxes when compared to the observed data, though the overall trend is maintained. This is further validated with performance metrics below.

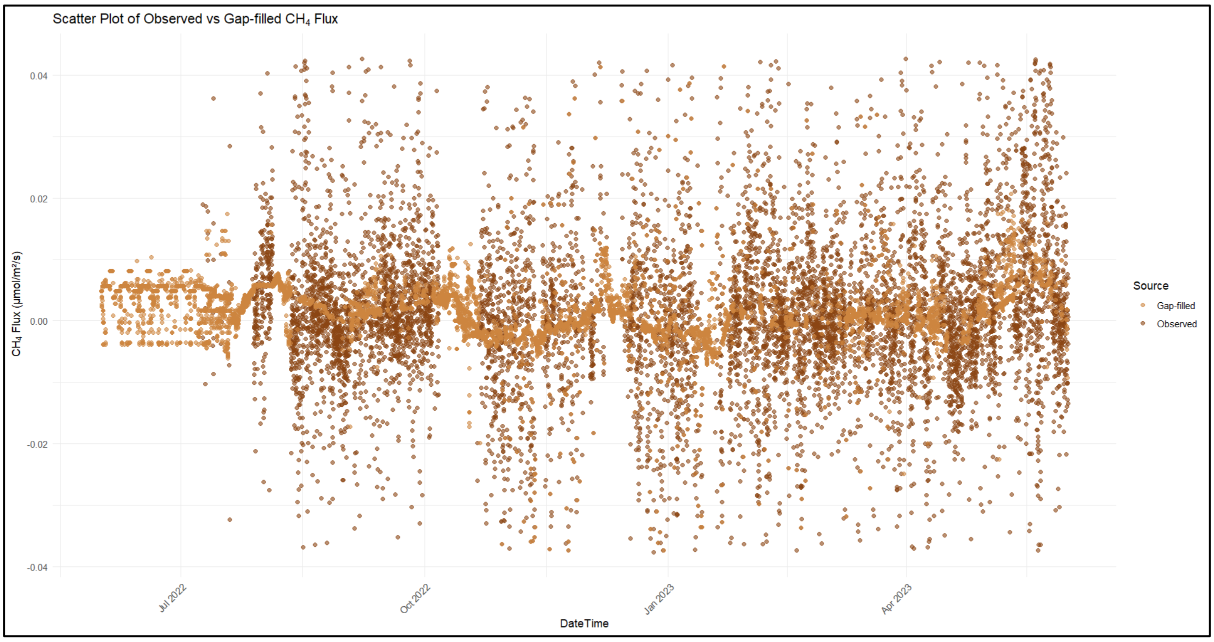


*Figure 6.3 Time series of observed and predicted $CH_4$ fluxes using the MDS method.*

The evaluation of the correlation between the observed and gap-filled $CH_4$ flux data using the MDS method is illustrated in the scatter plot (Figure 6.4). The scatter plot reveals a weak correlation between the overlapping datasets, with an $R^2$ value of -0.38. This negative $R^2$ suggests that the MDS model accounts for no variance in the observed $CH_4$ flux, and, in fact, performs worse than simply predicting the mean value. The lack of significant correlation emphasises the limitations of the MDS method in accurately estimating data gaps in this specific dataset using the selected driver variables.

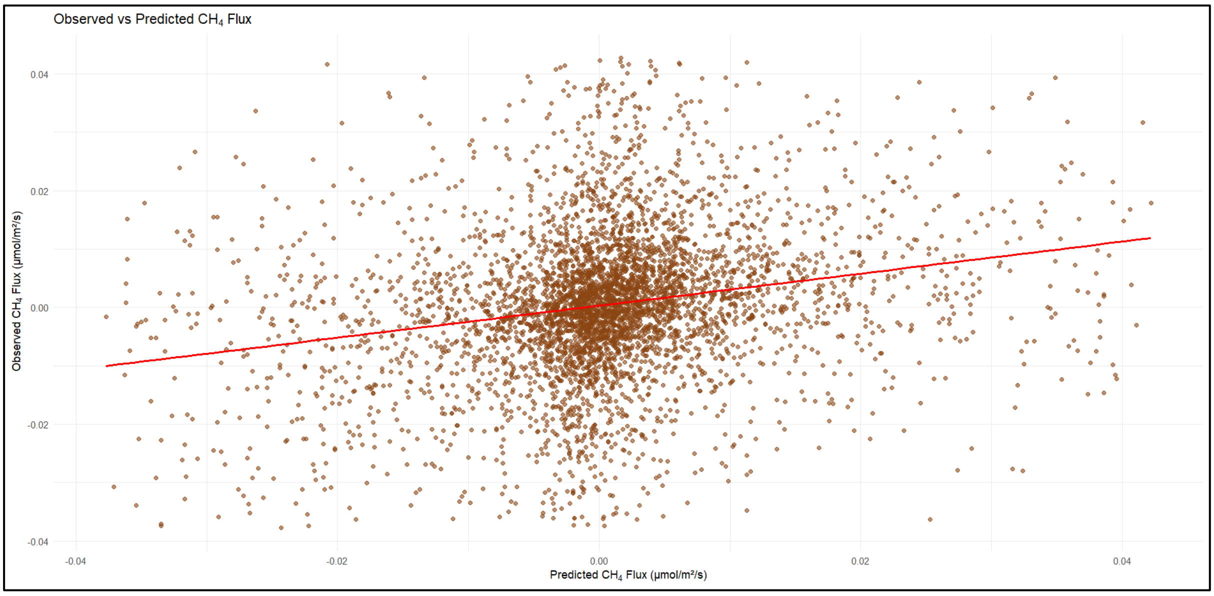


*Figure 6.4 Scatter plot of observed versus predicted $CH_4$ fluxes using the MDS method.*

Figure 6.5 displays the time series of observed data and the RF modelled data filling the gaps in the time series. This model appears to capture more fluctuations in the $CH_4$ fluxes, presenting a smoother and visually more consistent time series. However, a slight underestimation of $CH_4$ fluxes remains when compared to the observed data, which could potentially be attributed to seasonal variations or other unaccounted factors. This is verified in more detail in the performance metrics discussed below.

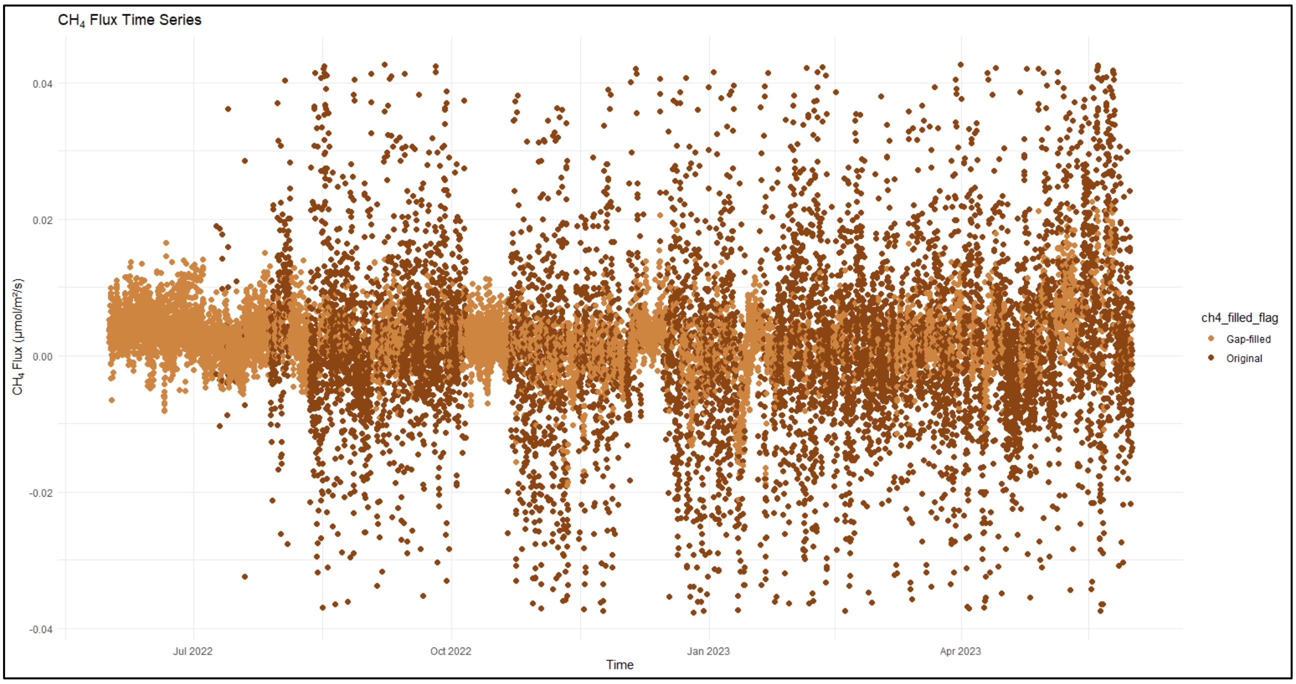


*Figure 6.5 Time series of observed and predicted $CH_4$ fluxes using the RF model.*

The scatter plot in Figure 6.6 shows the overlap between observed values (test data) and predicted values from the RF model. Although there is still a poor correlation between the data points, it is better compared to the scatter plot in Figure 6.4 for the MDS model, as the points are slightly less dispersed. The $R^2$ value for the RF model is 0.2, indicating that 20% of the variance is explained.

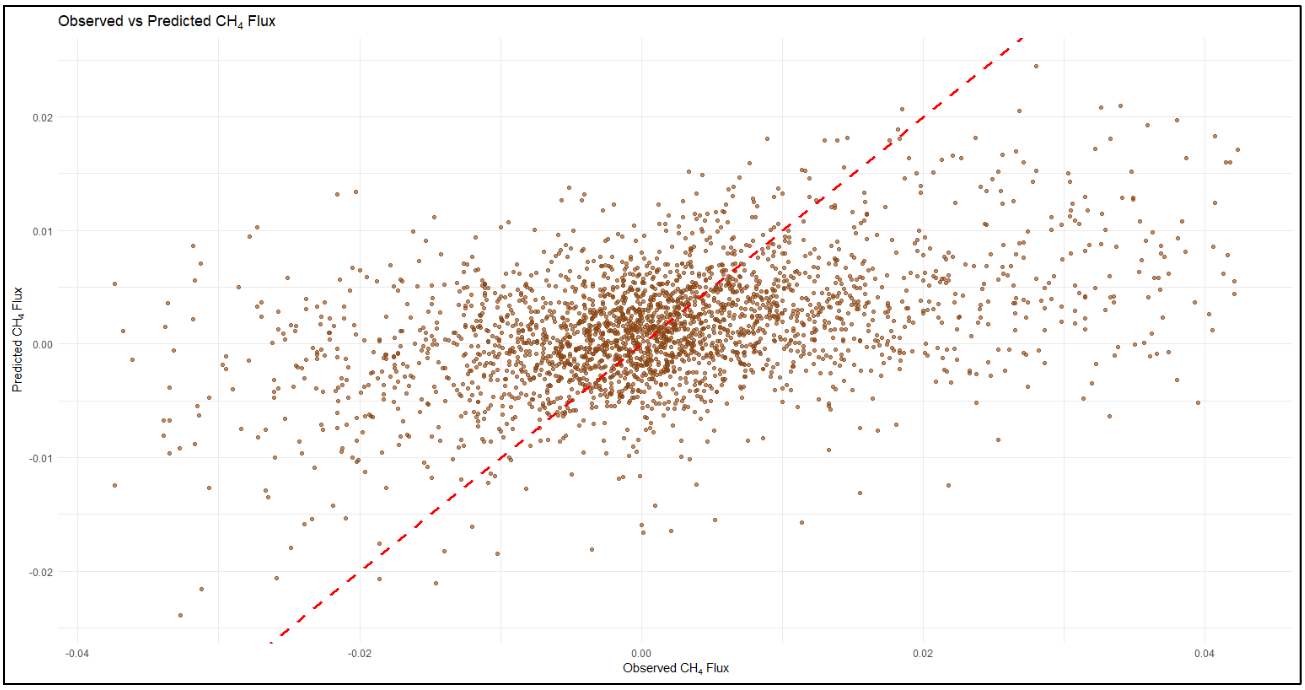


*Figure 6.6 Scatter plot of observed and predicted values using the RF model.*

In Figure 6.7 the box plots for the RF model display the comparison between the overlapping original and gap-filled $CH_4$ data. While the means of both datasets are closely aligned, the whiskers of the filled data exhibit significantly less dispersion compared to the original data. This suggests that the RF model has effectively reduced extreme values or outliers in the gap-filled dataset, resulting in a more consistent distribution of $CH_4$ flux estimates, though it may also indicate an underestimation of $CH_4$ flux values.

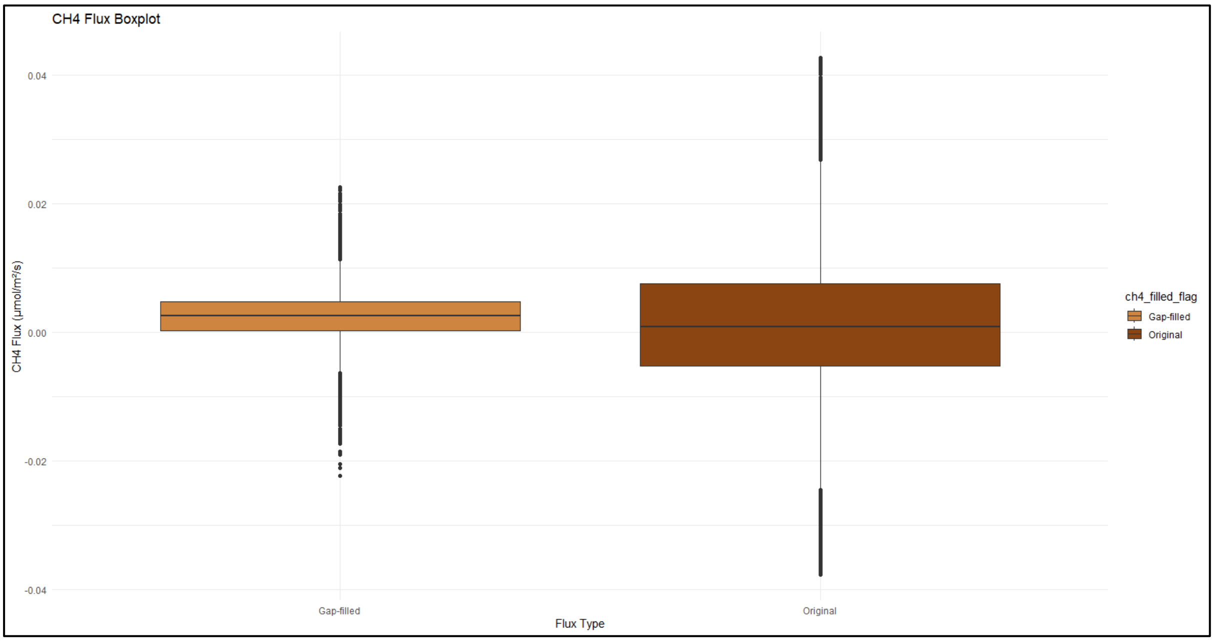


*Figure 6.7 Boxplots comparing gap-filled and original $CH_4$ flux data using the RF model.*

The bar chart (Figure 6.8) and Table 6.1 display the performance metrics for both the MDS and RF methods estimating $CH_4$ fluxes, with key metrics including the MAE, $R^2$, RMSE, and SE. From the chart, it can be observed that the RF model outperforms MDS in several areas. Table 6.1 displays values rounded to four decimal places to highlight small differences between metrics. The $R^2$ values for RF are significantly higher (0.2) compared to the negative $R^2$ value for MDS (-0.3), suggesting that RF explains more variance in the data while MDS performs poorly, even worse than a mean-based prediction.

*Table 6-1 Performance metrics for MDS and RF methods.*

| Metric | RF | MDS |
|---|---|---|
| $R^2$ | 0.1879 | -0.3104 |
| RMSE (µmol $m^{-2}$ $s^{-1}$) | 0.0113 | 0.0147 |
| MAE (µmol $m^{-2}$ $s^{-1}$) | 0.0083 | 0.0107 |
| SE (µmol $m^{-2}$ $s^{-1}$) | 0.0002 | 0.0147 |

In terms of the estimated errors, both models have very small values for MAE, RMSE and SE, indicating relatively low prediction error. However, RF performs slightly better than MDS across all these metrics, with lower MAE (0.0083 µmol $m^{-2}$ $s^{-1}$ for RF vs. 0.0107 µmol $m^{-2}$ $s^{-1}$ for MDS), lower RMSE (0.0113 µmol $m^{-2}$ $s^{-1}$ for RF vs. 0.0147 µmol $m^{-2}$ $s^{-1}$ for MDS), and marginally lower SE (0.0004 µmol $m^{-2}$ $s^{-1}$ for RF vs. 0.0147 µmol $m^{-2}$ $s^{-1}$ for MDS).

In summary, the RF model demonstrates better predictive performance than MDS, with a higher $R^2$ value and smaller estimated errors, making it the more effective method for estimating $CH_4$ fluxes in this time series for this site.

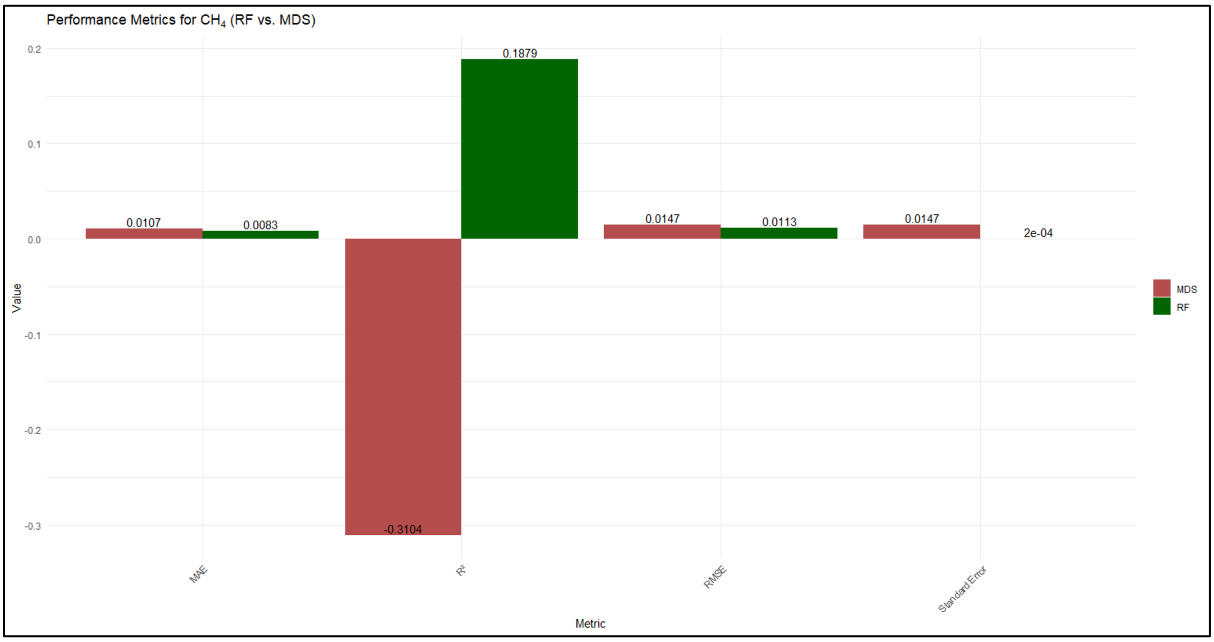


*Figure 6.8 Bar chart of performance metrics for gap-filled fluxes for both methods.*

The annual cumulative plot (Figure 6.9) for $CH_4$ emissions compares the performance of the MDS (red line) and RF (green line) models over the study period from June 2022 to June 2023. There are notable differences in the cumulative $CH_4$ emissions estimated by both models. Although the two lines follow a broadly similar trend, they diverge at several points throughout the year, indicating differences in the $CH_4$ estimates.

The MDS model estimates higher cumulative $CH_4$ emissions during certain periods, particularly in the early part of the study from June to October 2022, where it is consistently higher than the estimates from RF. However, in the latter half of the study (January to April 2023), the RF model increases, with its cumulative estimates for $CH_4$ surpassing those of the MDS estimates.

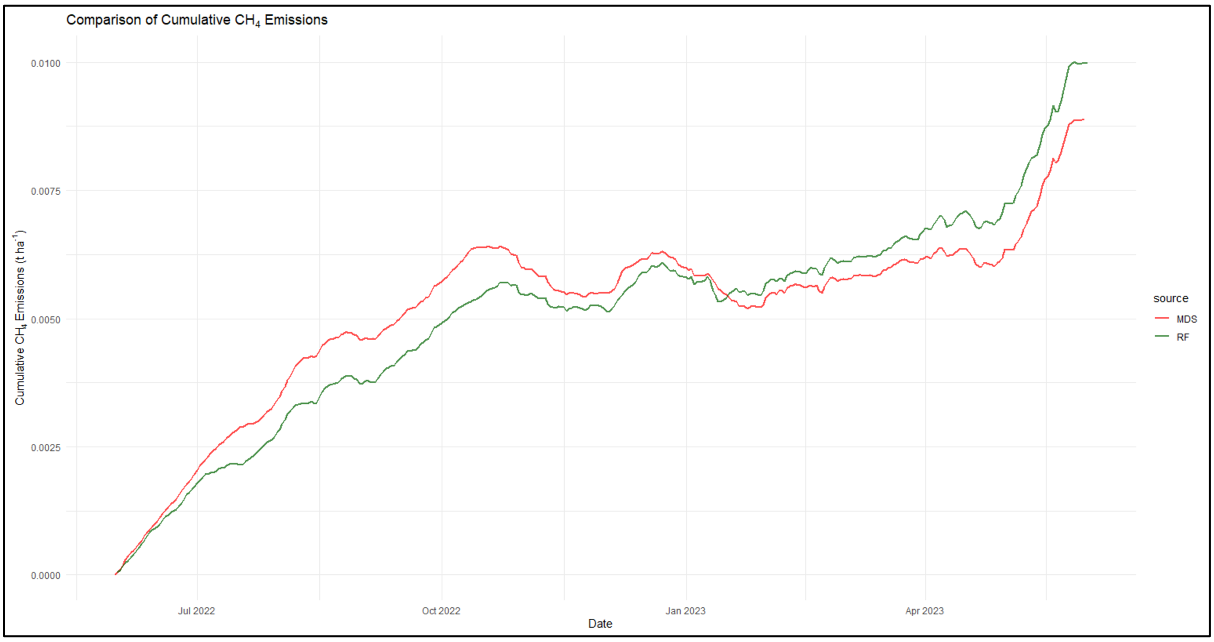


*Figure 6.9 Cumulative plots for estimated $CH_4$ emissions for both MDS and RF.*

The total accumulated atmospheric $CH_4$ emissions for the entire study period are estimated as 0.00888 t $CH_4$ $ha^{-1}$ $yr^{-1}$ (8.88 kg $CH_4$ $ha^{-1}$ $yr^{-1}$) for the MDS method and 0.00999 t $CH_4$ $ha^{-1}$ $yr^{-1}$ (9.99 kg $CH_4$ $ha^{-1}$ $yr^{-1}$) for the RF model, resulting in a 12% difference between the two. These differences are likely due to variations in how each method handles gaps in the data, driver variables, and estimates $CH_4$ fluxes. Additionally, there are distinct periods of contrasting $CH_4$ emission observed in the cumulative plot, occurring at different stages for both datasets. This indicates that the models respond differently to certain environmental factors, influencing the timing and magnitude of $CH_4$ emissions.

# 7 Integrated discussion

The study provides a comprehensive assessment of GHG dynamics in a natural woodland ecosystem established on a cutaway peatland in Ireland. Its primary objective was to quantify the atmospheric exchange of $CO_2$ from a cutaway peatland that has undergone natural regeneration into a woodland dominated by native tree species. To achieve this, the research pursued several interconnected objectives. First, it assessed the contribution of below-canopy $CO_2$ fluxes to the overall NEE by measuring $NEE_{bel}$ at the forest floor using a closed-loop clear chamber. Second, it estimated total NEE through continuous $CO_2$ measurements using the EC method. Third, it monitored $CH_4$ emissions above the canopy employing the EC technique. By linking these fluxes to environmental parameters, the study evaluated how ecosystem carbon dynamics respond to fluctuations in temperature and other meteorological variables. The study calculated a complete annual carbon budget for the ecosystem using measured $CO_2$ and $CH_4$ fluxes and provided an estimate of an emission factor for the habitat by combining these measurements with literature values for fluvial losses and $N_2O$ emissions.

The results from Lullymore woodland show the modelled $R_{bel}$ contributed 47.8 (±0.3 SE) t $CO_2$ $ha^{-1}$ $yr^{-1}$, $GPP_{bel}$ was -2.8 (±0.1 SE) t $CO_2$ $ha^{-1}$ $yr^{-1}$, yielding $NEE_{bel}$ of 45.0 (±0.4 SE) t $CO_2$ $ha^{-1}$ $yr^{-1}$ . Above canopy $CO_2$ flux (NEE) estimates from the EC tower indicated significant atmospheric uptake, with an annual total of -30.2 t $CO_2$ $ha^{-1}$ $yr^{-1}$ based on the RF-derived dataset and -28.1 t $CO_2$ $ha^{-1}$ $yr^{-1}$ from the MDS-filled dataset. When the $NEE_{bel}$ adjusted annual NEE value is included, the annual flux becomes -28.9 t $CO_2$ $ha^{-1}$ $yr^{-1}$ (using the RF dataset). Total accumulated atmospheric $CH_4$ emissions for the study period were comparatively low, estimated at 0.00888 t $CH_4$ $ha^{-1}$ $yr^{-1}$ (8.88 kg $CH_4$ $ha^{-1}$ $yr^{-1}$) using the MDS method and 0.00999 t $CH_4$ $ha^{-1}$ $yr^{-1}$ (9.99 kg $CH_4$ $ha^{-1}$ $yr^{-1}$) from the RF model.

To accurately estimate an EF that can be applied or upscaled to assess the sink/source function of this habitat on peat, other elements such as fluvial losses and $N_2O$ emissions needed to be considered. Since measurements of these additional essential GHGs were beyond the scope of this research, default values from IPCC (2013) and Evans et al. (2018) were used to estimate the EF for this habitat type. The GWP of 28 was multiplied to the annual $CH_4$ estimate, to calculate the emission factor in $CO_2$-eq. The total $CH_4$ emission (Using RF) including GWP was 0.28 t $CO_2$-eq $ha^{-1}$ $yr^{-1}$. Table 7.1 summarises the findings from this study and the default values from Evans et al. (2018) presenting the total annual EF derived for this habitat.

*Table 7-1 Estimated emission factor for Lullymore mixed woodland.*

| This study $CO_2$-eq | This Study $CH_4$-eq | Evans et al. (2018) DOC & POC | Evans et al. (2018) $N_2O$ | Total EF |
|---|---|---|---|---|
| t $CO_2$-eq $ha^{-1}$ $yr^{-1}$ | | | | |
| -28.9 | 0.28 | 1.44 | 0.79 | -26.4 |

Even when default literature values are used to account for other GHGs not directly measured in this study (e.g., DOC, POC, and $N_2O$), the estimated emission factor for the site indicates that Lullymore woodland remains a substantial GHG sink, at -26.4 t $CO_2$-eq $ha^{-1}$ $yr^{-1}$. These results demonstrate that the naturally regenerated Lullymore woodland effectively sequesters atmospheric carbon, providing a comprehensive picture of carbon dynamics at the site. The ecosystem removes a significant amount of $CO_2$ from the atmosphere, contributing meaningfully to climate mitigation, while comparatively low $CH_4$ emissions are counteracted by the uptake of $CO_2$ further reinforce the net climate benefit.

Collectively, these findings highlight the potential of establishing low-maintenance woodlands on cutaway peatlands as a viable land-use management strategy to reduce GHG emissions from degraded peatlands. This approach contributes to climate mitigation through enhanced carbon sequestration, while also supporting ecosystem resilience.

Below-canopy $CO_2$ flux estimates from the Lullymore woodland were compared with values reported in other studies to contextualise the site's carbon dynamics within similar ecosystems. $NEE_{bel}$ estimated at 45.0 t $CO_2$ $ha^{-1}$ $yr^{-1}$, indicates that the woodland ecosystem at Lullymore is contributing substantially higher $CO_2$ emissions compared to similar ecosystems than those reported in the NIR (2024) and other studies (Badorek et al., 2011; Paul-Limoges et al., 2017). While the IPCC (2013) reports emission factors for drained organic soils under forest land ranging from 0.5 to 25 t $CO_2$-C $ha^{-1}$ $yr^{-1}$, depending on climate zone, vegetation type, and rotation length, the emissions from the Lullymore site are higher than expected. It is important to acknowledge the methodological and environmental differences that may influence these findings, particularly since the reported values are not exclusive to below-canopy $CO_2$ emissions. In mineral soils, forest studies have shown that photosynthesis from forest floor vegetation can offset respiration from forest floor vegetation in spring, while during other seasons, the net ecosystem flux from the forest floor (NEFF) consistently remained negative (Kolari et al., 2009).

A study by Jovani-Sancho et al. (2018) on soil carbon balance in afforested peatlands in Ireland found soil respiration, including heterotrophic, root, and litter respiration, varied between 26.7 and 40.6 t $CO_2$ $ha^{-1}$ $yr^{-1}$, which is more aligned to the values found in this research. However, their study focused solely on respiration, not NEE, and examined eight sites dominated by monoculture forestry plantations (Sitka spruce and lodgepole pine).

The emission factors reported by IPCC and NIR are based on data from various sites across Europe, including total soil emissions for sites, not specifically below-canopy NEE. The NIR for Ireland (1990–2019) reports a much lower EF of 0.59 t $CO_2$-C $ha^{-1}$ $yr^{-1}$ for afforested peatlands, equivalent to approximately 2.17 t $CO_2$ $ha^{-1}$ $yr^{-1}$. This EF is significantly lower than both the IPCC default range and the $NEE_{bel}$ observed in this study. Duffy et al. (2021) proposed that this lower EF might result from the interpretation of soda-lime-derived soil respiration rates, originally reported by Byrne and Farrell (2005). Previous studies examining below-canopy habitats in woodlands have primarily focused on soil respiration (Janssens et al., 2001; Heinemeyer et al., 2011; Jovani-Sancho et al., 2018). There are limited studies in Ireland that investigate NEE below the canopy.

Direct comparisons for total NEE using the EC method with other research sites are also challenging, as no similar Irish sites have been measured on mixed woodland with peat soils. The IPCC Wetlands Supplement (IPCC, 2013) offers default values for forestry on organic soils in temperate climates, with Tier 1 estimated to be 2.6 t $CO_2$-C $ha^{-1}$ $yr^{-1}$ and Tier 2 at 2 t $CO_2$-C $ha^{-1}$ $yr^{-1}$, both considerably higher than Lullymore's results. When converted from $CO_2$ to C, the Lullymore values are -8.2 t $CO_2$-C $ha^{-1}$ $yr^{-1}$ (RF), -7.66 t $CO_2$-C $ha^{-1}$ $yr^{-1}$ (MDS), and -7.87 t $CO_2$-C $ha^{-1}$ $yr^{-1}$ (adjusted NEE). These figures are lower than the IPCC default values, indicating a stronger carbon sink in this study.

A comparable EC-based study in Belgium on a mixed conifer deciduous woodland growing on mineral soil (100–150 cm depth) reported a total carbon uptake of approximately -6 t $CO_2$-C ha$^{-1}$ yr$^{-1}$ (Aubinet *et al.*, 2001). This is slightly less that the estimate from this research. However, the differences could be attributed to the soil type difference and the 20-year gap in study periods and outdated gap filling methods used such as linear interpolation for nighttime values (Aubinet *et al.*, 2001).

A long-term study using the EC technique on a *black spruce-sphagnum* wetland in boreal Canada reported annual NEE values ranging from 0.41 (1995) to -0.21 (2004) t C-$CO_2$ ha$^{-1}$ yr$^{-1}$ (Dunn et al., 2007). This boreal wetland biome was a small source of $CO_2$ emissions becoming a very small sink, contrasting with this research site's substantial sequestration. The habitat and climate of this region differ significantly from that of the research area, making a direct comparison challenging, though it highlights the variability in $CO_2$ dynamics across different climatic regions.

An additional study conducted over two years at two peatland sites in Germany, using the EC technique, examined a natural pine bog forest and an industrially planted forest. The natural pine bog forest had a peat depth of 5 meters, while the industrially planted forest, dominated by Sitka spruce trees, had a peat depth of 3.4 meters. In the first year the estimates for the natural bog pine forest were approximately -0.53±0.28 t C- $CO_2$ ha$^{-1}$ yr$^{-1}$, while the industrially planted forest had estimates of -1.3±0.31 t C- $CO_2$ ha$^{-1}$ yr$^{-1}$. In the second year, the estimates were -0.73±0.38 t C- $CO_2$ ha$^{-1}$ yr$^{-1}$ for the natural bog pine forest and -3.0±0.66 t C- $CO_2$ ha$^{-1}$ yr$^{-1}$ for the industrially planted forest (Hommeltenberg *et al.*, 2014). The NEE values from these German sites are lower than those from the current research site and the interannual variability showed a decrease between years. The significantly deeper peat at these sites could contribute to this variation.

In a more recent study in Switzerland, Paul-Limoges et al. (2017) monitored a broadleaf woodland on mineral soils and found that the site acted as a $CO_2$ sink, with a reported uptake of −7.57 ± 0.10 t C ha$^{-1}$yr$^{-1}$. This number is very similar to findings from this study and provides a better comparison as it focuses on atmospheric $CO_2$ exchange. Although it differs from this study in that it involves mineral soils rather than organic soils.

An Irish study on industrial forestry on wet mineral soils, specifically a first-rotation Sitka spruce plantation in Co. Laois, measured NEE. The results from this study showed that the forest acted as a net carbon sink throughout the study period (2002–2009). Pre-thinning (2002–2006), the annual NEE ranged from -8.44 (±1.34) to -8.87 (±1.48) t C $ha^{-1}$ $yr^{-1}$, with a mean NEE of -8.66 (±1.43) t C $ha^{-1}$ $yr^{-1}$. Post-thinning (2007–2009), the annual NEE ranged from -6.75 (±1.19) to -10.33 (±1.41) t C $ha^{-1}$ $yr^{-1}$, with a mean of -8.41 (±1.42) t C $ha^{-1}$ $yr^{-1}$. The annual average NEE from this study are comparable to the findings from Lullymore study site, although the study was on mineral soils.

Table 7.2 presents a comparison of previous research on forest carbon dynamics, with the results displayed in order from the highest levels of carbon sequestration to emissions. For simplicity, the term 'Forestry' refers to monoculture industrial forestry, typically including Sitka spruce, while 'mixed woodland' refers to woodlands with a diverse mix of tree species, which may include both broadleaf and conifer trees. The table highlights the trend that as forests age, their carbon sequestration decreases, with younger forests showing the highest rates of carbon uptake. The data suggest that the greatest reductions in carbon sequestration occur in forests that are 14-21 years old, which show negative NEE values. In contrast, the older forests, often aged 150-160 years or more, are very small sinks and in some cases a small source of NEE. This pattern aligns with the findings of Hargreaves et al. (2003) and Besnard et al. (2018) who also noted that younger forests are strong carbon sinks, while older forests show diminished sequestration capabilities, eventually reaching a carbon-neutral or emission state due to complex interactions between soil, plant, and microbial activity. Figure 7.1 shows a visualisation of the comparison between this site and the research sites discussed above, the brown dots represent organic soils based on table 7.2.

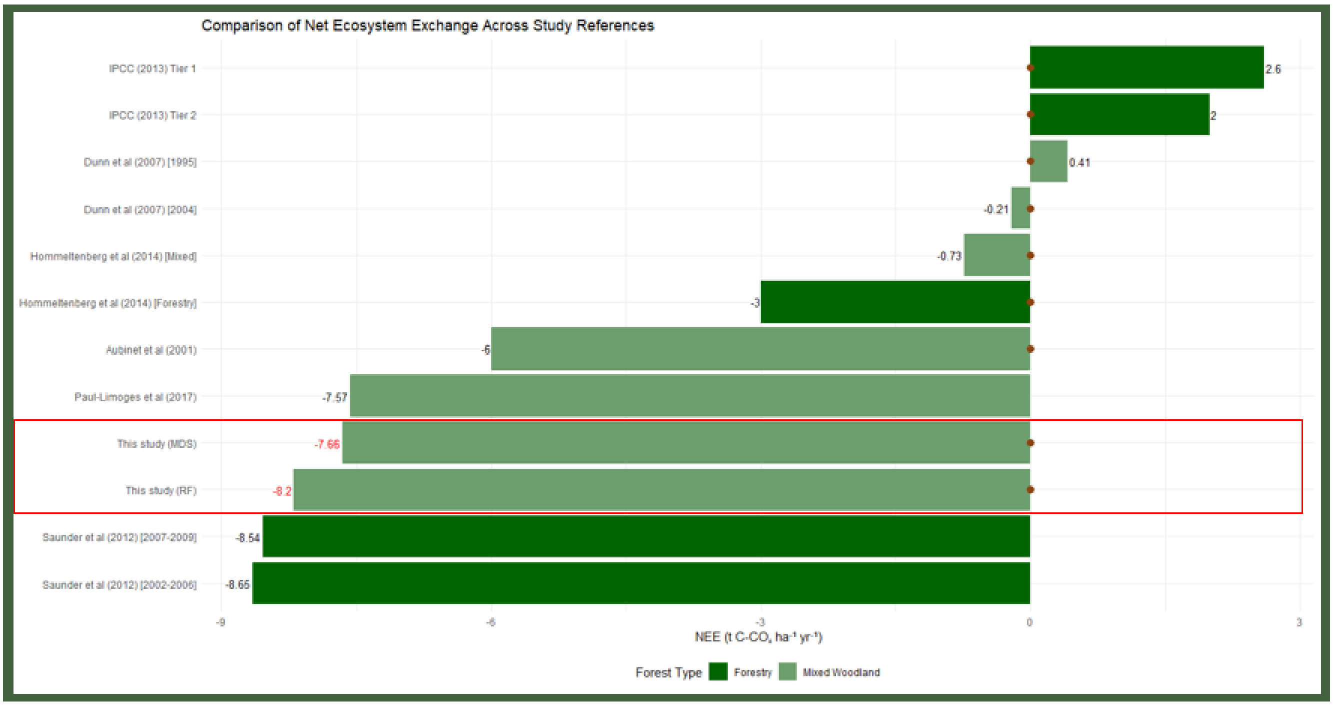


*Figure 7.1 Comparison of NEE studies on woodland sites (Photo: author).*

*Table 7-2 Comparison of NEE studies on woodland sites (table: author).*

| Location | Forest Type | Forest Age at time of study | Soil Type | Peat Depth | climate | NEE ($t\ C\text{-}CO_2\ ha^{-1}\ yr^{-1}$) | Study Year | Reference |
|---|---|---|---|---|---|---|---|---|
| Laois, Ireland | Forestry | 14-21 years | Mineral Soil | NA | Temperate | -6.75 to -10.33 | 2007-2009 | Saunder et al (2012) |
| Laois, Ireland | Forestry | 14-21 years | Mineral Soil | NA | Temperate | -8.44 to -8.87 | 2002-2006 | Saunder et al (2012) |
| Kildare, Ireland | Mixed Woodland | 20 years | Organic soil | 0.2m | Temperate | -8.2 | 2022-2023 | This study (RF) |
| Kildare, Ireland | Mixed Woodland | 20 years | Organic soil | 0.2m | Temperate | -7.66 | 2022-2023 | This study (MDS) |
| Switzerland | Mixed Woodland | NA | Mineral Soil | NA | Temperate | -7.57 | 2014-2015 | Paul-Limoges et al. (2017) |
| Belgium | Mixed Woodland | 59-89 years | Mineral soil | 1.0-1.5m | Temperate | -6 | 1996-1997 | Aubinet et at (2001) |
| Germany | Forestry | 44years | Organic soil | 5m | Temperate | -3 | 2011-2012 | Hommeltenberg et al (2014) |
| Germany | Mixed Woodland | 1-150years | Organic soil | 3.4m | Temperate | -0.73 | 2010-2011 | Hommeltenberg et al (2014) |
| Canada | Mixed Woodland | 160 years | Organic soil | NA | Boreal | -0.21 | 2004 | Dunn et al. (2007) |
| Canada | Mixed Woodland | 159 years | Organic soil | NA | Boreal | 0.41 | 1995 | Dunn et al. (2007) |
| Global | Forestry | NA | Organic soil | NA | Temperate | 2 | Tier 2 | IPCC (2013) |
| Global | Forestry | NA | Organic soil | NA | Temperate | 2.6 | Tier 1 | IPCC (2013) |

Due to the limited availability of previous work on $CH_4$ emissions on mixed woodland peat soils in Ireland, the discussion draws primarily on studies from forestry sites and rewetted peatland environments to contextualise the findings. Methane emissions from this study are notably low, with estimates of 0.00999 t CH4 $ha^{-1}$ $yr^{-1}$ (RF) and 0.00888 t CH4 $ha^{-1}$ $yr^{-1}$ (MDS). These values are slightly higher than, the IPCC (2013), Tier 1 emission factor for drained organic soils under temperate forest, which is 0.003 t $CH_4$ $ha^{-1}$ $yr^{-1}$. They are also marginally above the Tier 2 woodland estimate of 0.005 t $CH_4$ $ha^{-1}$ $yr^{-1}$ reported for the United Kingdom (IPCC, 2013; Evans et al., 2017). Evans et al. developed these Tier 2 factors through a comprehensive meta-analysis, and their value of 0.005 t $CH_4$ $ha^{-1}$ $yr^{-1}$ aligns closely with, but remains slightly lower than, the $CH_4$ emissions observed in this study. Similarly, Tikkasalo et al. (2025) reported a $CH_4$ flux of approximately 0.004 t $CH_4$ $ha^{-1}$ $yr^{-1}$ from a drained boreal peatland forest in the year following clear felling, again indicating very low emissions from forested peat soils.

When compared with rewetted peatland systems, the contrast becomes more pronounced. Holl et al. (2020) examined a degraded cutover bog in north western Germany and reported substantially elevated methane fluxes from the rewetted area. Emissions increased from 0.133 (± 0.019) to 0.183 (± 0.015) t $CH_4$ $ha^{-1}$ $yr^{-1}$ over two consecutive years, while the adjacent drained area emitted 0.072 (± 0.018) and 0.121 (± 0.014) t $CH_4$ $ha^{-1}$ $yr^{-1}$.

The low methane emissions observed at the Lullymore woodland site are also considerably below those reported for rewetted industrial extraction peatlands. Aitova et al. (2023) reports fluxes of 0.160 t $CH_4$ $ha^{-1}$ $yr^{-1}$ in nutrient rich rewetted sites and 0.110 t $CH_4$ $ha^{-1}$ $yr^{-1}$ in nutrient poor rewetted sites in Ireland, values that are an order of magnitude greater than those recorded in the present study.

Figure 7.2 shows the relative position of methane emissions from this study within the wider range of values discussed in this section for forested and rewetted peatland systems. Emissions from the Lullymore woodland fall clearly within the lower end of the spectrum, clustering with other forest and mixed-wood sites. The underlying values for all studies are provided in Table 7.3, which accompanies the plot. In contrast, rewetted peatlands consistently occupy the highest part of the distribution, illustrating a strong separation between the two land-use types.

The pattern shown in the comparison plot highlights the clear distinction in $CH_4$ dynamics between woodland peat soils and rewetted peatlands. Woodland sites consistently exhibit much lower emissions, whereas rewetted peatlands occupy the higher emissions. Although the emissions measured in this study sit slightly above some values reported for drained temperate forest soils, they remain far below those typical of rewetted peatlands. These findings point to woodland establishment on degraded cutaway peat as a promising low-$CH_4$ land-use option in Ireland. They also demonstrate the need for further targeted research on woodland peat soils in Ireland, as existing studies have focused mainly on forestry or rewetting scenarios and have rarely addressed naturally regenerated or planted woodland systems on peat.

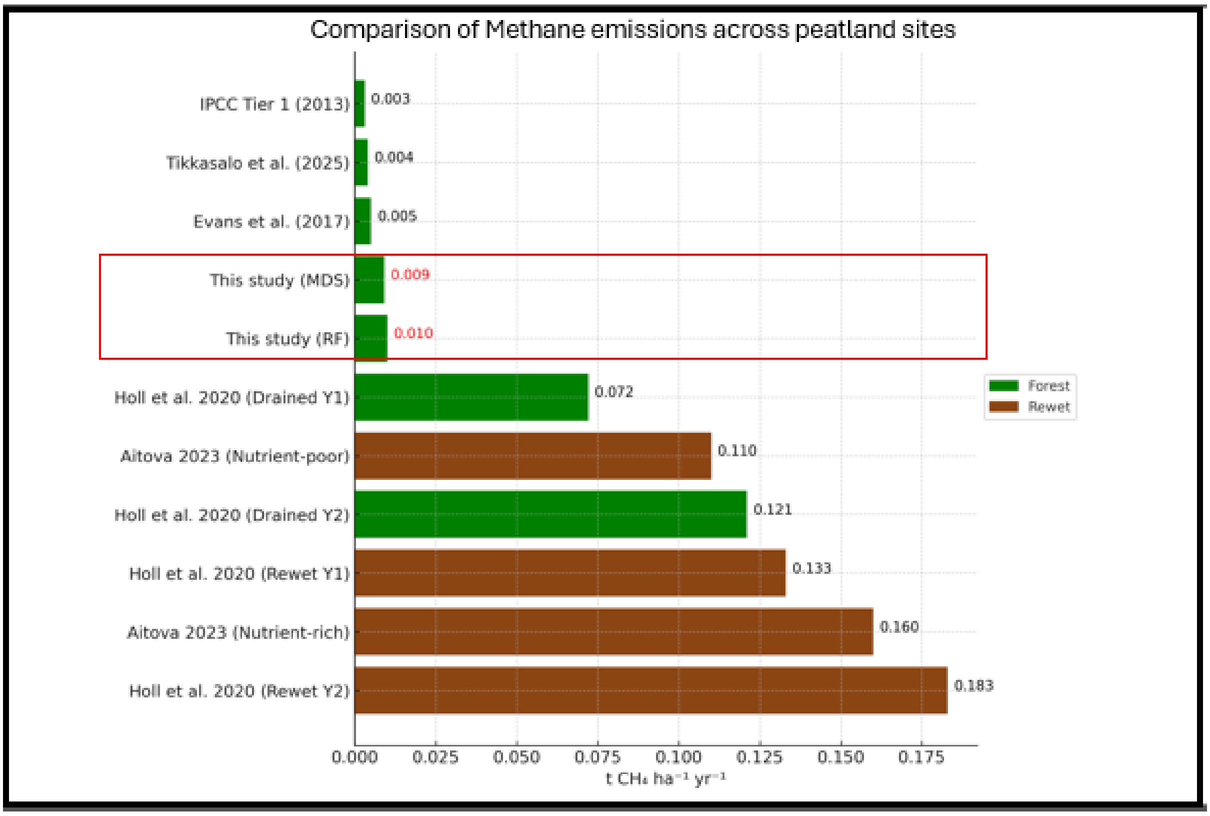


*Figure 7.2 Comparison of $CH_4$ studies on peatland sites, figures rounded to three decimal places (Photo: author).*

*Table 7-3 Comparison of $CH_4$ studies on peatland sites (table: author).*

| Location | Habitat | Soil Type | Climate | t $CH_4$ $ha^{-1}$ $yr^{-1}$ | Reference |
|---|---|---|---|---|---|
| Germany | Rewet | Peat | Temperate | 0.183 | Holl et al. 2020 (Rewet Y2) |
| Ireland | Rewet | Peat | Temperate | 0.160 | Aitova 2023 (Nutrient-rich) |
| Germany | Rewet | Peat | Temperate | 0.133 | Holl et al. 2020 (Rewet Y1) |
| Germany | Forest | Peat | Temperate | 0.121 | Holl et al. 2020 (Drained Y2) |
| Ireland | Rewet | Peat | Temperate | 0.110 | Aitova 2023 (Nutrient-poor) |
| Germany | Forest | Peat | Temperate | 0.072 | Holl et al. 2020 (Drained Y1) |
| Kildare, Ireland | Forest | Peat | Temperate | 0.010 | This study (RF) |
| Kildare, Ireland | Forest | Peat | Temperate | 0.009 | This study (MDS) |
| UK | Forest | Peat | Temperate | 0.005 | Evans et al. (2017) |
| Finland | Forest | Peat | Boreal | 0.004 | Tikkasalo et al. (2025) |
| Global | Forest | Peat | Temperate | 0.003 | IPCC Tier 1 (2013) |

The results also reveal that $NEE_{bel}$ makes a substantial contribution to total $CO_2$ exchange. Although the overall NEE remained a $CO_2$ sink, the below-canopy fluxes accounted for approximately 61**%** of the total NEE underscoring the importance of ground-layer processes in mixed woodland on peat soils.

One notable study conducted in Finland on diverse below-canopy vegetation beneath a forest canopy on peat soils assessed both photosynthesis and respiration (Badorek *et al.*, 2011). The findings indicated that the total contribution of fluxes from the below-canopy area represented 20-30% of the total ecosystem $CO_2$ exchange, as determined by an EC study conducted at the same site (Ojanen *et al.*, 2012). This constituted almost a third of the total $CO_2$ emissions estimated at 2700 g $CO_2$ $m^{-2}$ $yr^{-1}$ (Badorek *et al.*, 2011). When considered alongside these studies, the substantially higher below-canopy contribution observed in this research reinforces the need to explicitly quantify ground-layer fluxes in emerging woodland ecosystems on peat soils. Such measurements are essential for accurately characterising whole-site $CO_2$ exchange and for understanding how vegetation development, soil conditions, and management choices influence carbon outcomes during the early stages of woodland establishment on degraded peatlands.

## 7.1 Model evaluations

On evaluation of model performances for estimating $CO_2$ fluxes using the chamber method the results showed that Gradient Boosting and XGBoost achieved the highest accuracy during training but tended to overfit, resulting in reduced performance on testing data. Random Forest, while not the top performer in training, demonstrated more consistent and reliable results across both training and testing sets, indicating better generalisability. In contrast, k-Nearest Neighbours and Generalised Additive Models performed less effectively, with lower accuracy and higher errors. Overall, Random Forest was considered the most balanced and robust model for predicting both $GPP_{bel}$ and $R_{bel}$.

The EC flux time series for both $CO_2$ and $CH_4$ required substantial gap filling and two approaches, Marginal Distribution Sampling (commonly used by Reichstein *et al.*, 2005; Wutzler *et al.*, 2018; Pastorello *et al.*, 2020) and Random Forest, were evaluated to determine the most suitable method for this woodland peatland site. Prior to gap-filling, relationships between $CO_2$ fluxes and key environmental drivers (PPFD, $T_a$, VPD, and $T_s$ in winter) were examined. $CO_2$ fluxes showed strong negative correlations with several drivers, particularly PPFD, reflecting expected biological behaviour and supporting findings from previous work in similar ecosystems (Reichstein et al., 2005; Wutzler et al., 2018; Pastorello et al., 2020). Methane fluxes showed no strong correlations with the environmental drivers examined. Nonetheless, VPD, $T_s$, and PPFD were selected as the primary driver variables for the MDS approach, as these have been widely applied in previous studies (Kim et al., 2020) and are known to capture seasonal variation effectively.

Across the full time series, the RF model consistently outperformed the MDS approach for $CO_2$ flux estimation. RF achieved higher explanatory power, lower error metrics, and substantially lower standard error, providing more realistic temporal dynamics and avoiding the winter overestimation of $CO_2$ emissions observed in MDS. While both models followed a similar trend throughout the year, the RF estimates of $CO_2$ sequestration were more consistent with observed flux patterns. The MDS method, however, tended to estimate higher fluxes during the winter period, suggesting a potential underestimation of sequestration in the MDS model when compared to the RF model. Regardless of model accuracy and performance in both instances the site was an overall sink for atmospheric $CO_2$ fluxes.

A similar pattern emerged for $CH_4$. The weak relationships between environmental drivers and $CH_4$ fluxes meant that MDS performed poorly, with negative $R^2$ values and large residual errors. RF again demonstrated clearly superior performance, producing lower RMSE and MAE values and more stable predictions, although the $R^2$ remained modest compared with studies where $CH_4$ fluxes show stronger driver response relationships (Kim et al., 2020). The findings indicate an approximate 12% difference between the overall annual estimates of $CH_4$ emissions for both methods, with the RF model yielding a slightly higher value. This percentage difference suggests a level of discrepancy between the two methods.

Overall, the findings show that RF was the more accurate reliable method for gap filling both $CO_2$ and $CH_4$ fluxes at this site. Its performance advantages for both gases underscore the value of machine learning approached in complex peatland ecosystems, where nonlinear responses and weak driver correlations can limit the effectiveness of traditional empirical model such as MDS.

## 7.2 Implications of findings

This study set out to contribute to the broader body of research focused on developing more effective management strategies for peatland restoration to mitigate GHG emissions.

Ireland has extensive raised peatlands, many of which have been heavily degraded, leaving large areas of cutaway peatlands that require rehabilitation to meet national climate action objectives (Hammond, 1981; Feehan and O'Donovan, 1996; Clarke, 2010; Malone and O'Connell, 2009; David Wilson et al., 2013). These areas of cutaway peatland in Ireland remain significant sources of $CO_2$, with recent estimates indicating annual emissions of 65,705 t $CO_2$ -C $yr^{-1}$ using Tier 2 emission factors and 152,046 t $CO_2$–C $yr^{-1}$ using Tier 1 for the 54,302 ha of cutaway peatlands nationwide (Habib *et al.*, 2024). These landscapes are among the most degraded peatlands in the country and typically support very little vegetation following decades of industrial extraction(Renou-Wilson *et al.*, 2011). Rewetting has been promoted as a primary restoration pathway, yet outcomes on cutaway peatlands have been highly variable. Studies across Ireland and elsewhere show that rewetted cutaway sites can remain substantial carbon sources for many years and are often sensitive to drought (Wilson *et al.*, 2015; Wilson, Farrell, *et al.*, 2016; Renou-Wilson *et al.*, 2019) (Farrell and Doyle, 2003; Holden, 2005; Holden *et al.*, 2007; Waddington *et al.*, 2010; Holden and Connolly, 2011; Günther *et al.*, 2015; Wilson, Farrell, *et al.*, 2016; Hambley *et al.*, 2019). This vulnerability highlights the risk of certain peatlands continuing to function as carbon sources even after restoration (Wilson, Farrell, *et al.*, 2016).

This variability makes it difficult to predict when or whether restored sites will return to net carbon sequestration (Wilson et al., 2016; Peichl *et al.*, 2014). Alongside the uncertainty surrounding the recovery of $CO_2$ sink function, there is considerable concern regarding elevated $CH_4$ emissions across many rewetted and near intact peatlands, where emissions typically increase as the WT is closer to the surface (Abdalla et al.,2016; Ingle, Habib, et al., 2023). Vegetation also plays a key role because vascular plants can efficiently transport $CH_4$ to the atmosphere through their hollow stems (IPCC, 2013; Wilson, Blain, *et al.*, 2016; Holl *et al.*, 2020; Wilson *et al.*, 2022).

In contrast, $CH_4$ emissions from this woodland on cutaway peat were extremely low, and the water table did not play a major role in controlling fluxes. This difference highlights the potential for woodland establishment to avoid the high $CH_4$ emissions commonly associated with rewetting and suggests that such systems may offer a more stable short to medium term pathway for reducing GHG emissions from degraded peat soils.

Given these uncertainties, there is a clear need to expand carbon flux monitoring across a wider range of peatland restoration trajectories. This study contributes to that effort by evaluating an alternative management option for degraded cutaway peatlands: the natural establishment of woodland systems on shallow peat. The findings demonstrate that this approach can maintain low $CH_4$ emissions and promote substantial uptake of $CO_2$ while providing a contrasting pathway to restoration in comparison to conventional rewetting, which can often produce elevated $CH_4$ emissions and variable $CO_2$ outcomes.

The IPCC (2013) does not differentiate between forestry types (such as evergreen, broadleaf, or monoculture) on peat soils, Evans et al. (2017) reports an emission factor of 9.91 t $CO_2$-eq $ha^{-1}$ $yr^{-1}$ for drained forests on peat soils, accounting for direct $CO_2$ emissions, fluvial losses, $CH_4$, and $N_2O$, indicating that forests are a net source of GHGs. Aitova et al. (2023) derived an emission factor for forestry on peat soils by combining data from Ireland's NFI (DAFM, 2017), which includes both emissions and removals. The combined emission factor for forestry on drained peat soils was 0.38 t C $ha^{-1}$ $yr^{-1}$, and for rewetted forestry, it was 0.93 t C $ha^{-1}$ $yr^{-1}$, both indicating a slight net source. These values include living biomass and litter sinks, alongside $CO_2$ and $CH_4$ default emissions from the IPCC (2013). The default values for forestry on organic soils in temperate climates, as outlined in the IPCC Wetlands Supplement (IPCC, 2013), are 2.6 t $CO_2$-C $ha^{-1}$ $yr^{-1}$ for Tier 1 and 2 t $CO_2$-C $ha^{-1}$ $yr^{-1}$ for Tier 2 for carbon dioxide ($CO_2$), and 3 kg $CH_4$ $ha^{-1}$ $yr^{-1}$ for Tier 1 and 5 kg $CH_4$ $ha^{-1}$ $yr^{-1}$ for Tier 2 for methane ($CH_4$).

However, these values contrast significantly with the findings of this study, where the emission factor for mixed woodland on cutaway peatlands was calculated to be a substantial net carbon sink of -26.4 t $CO_2$-eq $ha^{-1}$ $yr^{-1}$. The emission factors derived from the IPCC (2013) apply to forests on peat soils, including emissions associated with harvesting. In contrast, Lullymore is not a site for harvesting, which could explain the significant difference in emission factors between the two.

This difference highlights the importance of establishing a separate emission factor category for mixed woodlands on shallow cutaway peatlands, as they function differently from other forest types. Recognising these unique carbon dynamics could significantly alter the management outlook for degraded peatland sites in Ireland, where mixed woodlands may offer a more effective strategy for carbon sequestration. This further reinforces the fact that removing naturally established mixed woodlands on degraded peatland sites would be highly impractical and counterproductive, given their significant potential as carbon sinks.

The strong $CO_2$ uptake observed at Lullymore shows that this habitat and soil type has considerable capacity to contribute to national climate mitigation, particularly when compared with heavily degraded cutaway sites that continue to act as substantial sources of carbon (Wilson et al., 2015; Habib et al., 2024).The study highlights that woodland establishment on cutaway peatlands may provide an overlooked yet highly effective management option in Ireland, distinct from conventional forestry and deserving recognition as a separate land use category. Such systems offer near term climate benefits by supporting sustained $CO_2$ sequestration while avoiding the elevated $CH_4$ emissions often associated with rewetting. As Ireland works toward ambitious climate targets, acknowledging current woodland areas on cutaway and developing strategies that deliver rapid and reliable GHG reductions is essential. The evidence from this research indicates that low maintenance woodland establishment has significant potential to meet this need.

While the results from Lullymore clearly demonstrate the strong carbon-sink potential of naturally established woodland on cutaway peat, the analysis is based on a single year of flux data. This may not be sufficient to capture the full range of environmental variability, particularly in terms of long-term trends or extreme weather events. As a result, the magnitude of the sink observed here, although substantial may fluctuate in wetter or drier years, and as the stand continues to develop. Extended monitoring over a longer period would provide a more comprehensive understanding of interannual variability, offering deeper insights into how these ecosystems function as carbon sinks under varying climatic conditions and across different stages of stand development.

Some uncertainty also stems from model-based estimates, particularly regarding nighttime respiration, which remains challenging to represent accurately. Although the RF model performed strongly and provided the most reliable framework for gap-filling and integrating below-canopy fluxes, the absence of a below-canopy PAR sensor limits the precision of $GPP_{bel}$ estimates and may have contributed to a slight overestimation of $NEE_{bel}$.

Data gaps in the meteorological records similarly introduce uncertainty. Continuous, high-quality meteorological inputs are essential for robust gap-filling and flux calculations; therefore, more complete long-term datasets would strengthen future estimates of NEE and $CH_4$ fluxes.

Despite these caveats, the results provide a strong foundation for recognising woodland on cutaway peatlands as a meaningful carbon sink. Combining site-based flux measurements with remote-sensing approaches could offer a promising route for scaling these findings to the wider network of sites across Ireland. Advanced remote sensing techniques could aid in mapping peat, soil, and vegetation classifications (Gilet *et al.*, 2024; Habib *et al.*, 2024; O'Leary *et al.*, 2025), helping scale carbon fluxes to broader areas with similar woodland characteristics.

# 8 Conclusions and Recommendations

The primary objective of this study was to quantify the emissions of key GHGs specifically $CO_2$ and $CH_4$, from a cutaway peatland that has naturally established with mixed tree species. Both gases are critical contributors to climate change, with $CO_2$ playing a dominant role in long-term warming and $CH_4$ having a higher short-term warming potential (Günther *et al.*, 2020; Wilson *et al.*, 2022). This research aimed to continuously monitor NEE ($CO_2$) and $CH_4$ exchange from the peatland to assess its GHG dynamics and role in climate mitigation.

An estimation of the overall emission factor for the site was established, incorporating literature values for gases not monitored directly in the study. In addition, the study trialled machine-learning gap-filling methods alongside more traditional approaches, allowing a direct comparison of their performance and reliability in modelling fluxes.

Through detailed quality control and data analysis, this research revealed that the mixed woodland on degraded cutaway peatland functions as a substantial carbon sink. The $NEE_{bel}$ from chamber measurements had negligeable impact on the total NEE, increasing the total by just 1.3 t $CO_2$ ha $^{-1}$ yr$^{-1}$, when values from $NEE_{bel}$ were used to replace low-quality NEE values in the timeseries. However, when the total contribution of $NEE_{bel}$ to NEE was assessed directly, the results were notable, indicating that $NEE_{bel}$ accounted for approximately 61% of total NEE, underscoring its importance in ecosystem carbon dynamics.

Overall, the site was a minor source of atmospheric $CH_4$. While the emissions were lower than those reported for rewetted peatland sites, they were higher than the estimates provided by the IPCC (2013) for forested sites. Incorporating the measured atmospheric $CO_2$ and $CH_4$ from this research with default values for other GHGs (DOC, POC, and $N_2O$), from Evans et al. (2017) (not measured in this study), the estimated GHG emission factor is a strong sink for GHG's (-26.4 t $CO_2$-eq ha$^{-1}$ yr$^{-1}$). This value contrasts with IPCC (2013) emission factors for drained forests and rewetted peatlands, demonstrating the strong carbon-sink capacity of naturally established woodland on cutaway peat.

One of the key strengths of this study was the application of machine learning, particularly the RF algorithm, for gap filling flux timeseries. RF proved to be the most effective method for handling missing data, outperforming traditional gap-filling techniques such as MDS and other ML used in the chamber flux modelling. Its ability to model complex relationships between environmental variables and $CO_2$ fluxes allowed for more accurate estimations of annual $CO_2$ uptake, making it a valuable tool for improving the reliability of flux data in this study. RF also outperformed MDS for estimating $CH_4$ gaps in the dataset. Its performance metrics were lower than those reported in other studies (e.g., Kim et al., 2020). This suggests that while RF was the strongest performer within this study, there remains potential for further optimisation. Additionally, alternative ML algorithms, such as Artificial Neural Networks (ANNs), as explored in previous research (Kim *et al.*, 2020), could offer additional improvements in accuracy and further strengthen the gap-filling process.

Additionally, this study used default values for fluvial carbon losses and did not include carbon that may be leached into the watercourse, which could affect overall carbon estimates. To address this, future research should involve a dedicated study to map and assess the site's old drainage network, as this data is currently lacking. A study focused on measuring fluvial carbon losses could be conducted. This would provide a clearer understanding of the hydrological pathways and the potential GHG losses from the watercourse.

Further research could also incorporate remote sensing techniques to improve site-specific emission estimates by using classification maps to assign emissions based on vegetation communities. The vegetation classification map (Figure 3.6) shows a significant area of birch-willow woodland, with birch-willow scrub also identified as a dominant vegetation type across the site. This indicates the substantial role woodlands could play in influencing the site's overall emission factor. Lullymore is just one example of a revegetated cutaway peatland on Bord na Móna sites, with potential for scaling this approach to larger areas. This approach would offer greater accuracy compared to applying a generic emission factor to sites with a mosaic of vegetation cover, with potentially significant implications for national climate mitigation policies and reporting emissions. Additionally, these findings highlight the importance of preserving such habitats rather than clear-felling woodlands to rewet, particularly where degradation is too severe for successful peatland restoration.

Looking ahead, longer-term monitoring is essential to better understand how these ecosystems perform under changing climatic conditions. As highlighted by both Hargreaves et al. (2003) and Besnard et al. (2018), younger forests are effective carbon sinks, while older forests exhibit reduced sequestration capabilities, eventually reaching a plateau. Such long-term studies would provide a more comprehensive understanding of the role of mixed woodlands on peat soil in mitigating climate change and offer clear guidance on the future trajectory of GHG emissions. As the woodland matures, adjustments to the measurement infrastructure, such as raising the tower height to above canopy, would be necessary to maintain accurate data collection. In addition, replicating elements of the EC instrumentation below-canopy where resources allow would further reduce uncertainty in $NEE_{bel}$ these estimates and should be prioritised in future woodland flux studies.

In closing, this research demonstrates the significant potential of naturally established mixed woodlands on degraded peatlands to act as effective carbon sinks. Despite the low $CH_4$ emissions observed at the site, the strong and sustained uptake of $CO_2$ ensured that the ecosystem operated as a clear net carbon sink, underscoring the climate mitigation value of this habitat. A major contribution of this work is its evidence that low-maintenance mixed woodland on shallow cutaway peatlands can serve as an effective carbon mitigation strategy, distinct from both conventional forestry on organic soils and rewetted peatland categories. These findings challenge current emission factors used in national (EPA, 2024) and international (IPCC 2013) reporting frameworks and strengthen the case for recognising mixed woodlands on shallow cutaway peatlands as a separate land-use class for GHG accounting. Such recognition would support more accurate reporting, more effective conservation, planning, and policies that maximise the climate benefits of peatland restoration. Finally, the study also highlights the value of advanced gap-filling approaches, with random forest proving to be a reliable method for improving EC flux continuity and strengthening carbon budget estimates. Continued research will be essential to refine understanding of the long-term dynamics of these ecosystems and to fully harness their potential in national climate strategies.

## References


Abdalla, M., Hastings, A., Truu, J., Espenberg, M., Mander, Ü. and Smith, P. (2016) 'Emissions of methane from northern peatlands: a review of management impacts and implications for future management options', *Ecology and Evolution*, 6(19), pp. 7080–7102. doi:10.1002/ece3.2469.

Aitova, E., Morley, T., Wilson, D. and Renou-Wilson, F. (2023) 'A review of greenhouse gas emissions and removals from Irish peatlands', *Mires and Peat*, 29, pp. 1–17. doi:10.19189/MaP.2022.SNPG.StA.2414.

Allen, M.R., Shine, K.P., Fuglestvedt, J.S., Millar, R.J. and Cain, M. (2018) 'A solution to the misrepresentations of CO2 -equivalent emissions of short-lived climate pollutants under ambitious mitigation', *Climate and Atmospheric Science*, (February), pp. 1–8. doi:10.1038/s41612-018-0026-8.

Alm, J., Shurpali, N.J., Tuittila, E.-S., Laurila, T., Maljanen, M., Saarnio, S. and Minkkinen, K. (2007) 'Methods for determining emission factors for the use of peat and peatlands—flux measurements and modelling'.

Altman, D., Machin, D., Bryant, T. and Gardner, M. (2013) *Statistics with confidence: confidence intervals and statistical guidelines*. John Wiley & Sons.

Andrews, C.S. (1982) 'Man of no property: Autobiography'. Dublin, Ireland: Mercier Press.

Aubinet, M., Chermanne, B., Vandenhaute, M., Longdoz, B., Yernaux, M. and Laitat, E. (2001) 'Long term carbon dioxide exchange above a mixed forest in the Belgian Ardennes ', *Agricultural and forest meteorology* . Amsterdam;Oxford;New York, NY; : Elsevier B.V , pp. 293–315. doi:10.1016/S0168-1923(01)00244-1.

Aubinet, M., Heinesch, B. and Yernaux, M. (2003) 'Horizontal and Vertical Co2 Advection In A Sloping Forest ', *Boundary-layer meteorology* . Dordrecht : Kluwer Academic Publishers , pp. 397–417. doi:10.1023/A:1024168428135.

Aubinet, M., Vesala, T. and Papale, D. (2012) 'Eddy covariance: a practical guide to measurement and data analysis'. New York;Dordrecht; Springer.

Badorek, T., Tuittila, E.-S., Ojanen, P. and Minkkinen, K. (2011) 'Forest floor photosynthesis and respiration in a drained peatland forest in southern Finland', *Plant Ecology & Diversity*, 4(2–3), pp. 227–241.

Baldocchi, D. *et al.* (2001) 'FLUXNET: A New Tool to Study the Temporal and Spatial Variability of Ecosystem-Scale Carbon Dioxide, Water Vapor, and Energy Flux Densities ', *Bulletin of the American Meteorological Society* . Boston : American Meteorological Society , pp. 2415–2434. doi:10.1175/1520-0477(2001)082<2415:FANTTS>2.3.CO;2.

Baldocchi, D. (2014) 'Measuring fluxes of trace gases and energy between ecosystems and the atmosphere - the state and future of the eddy covariance method', *Global Change Biology*, 20(12), pp. 3600–3609.

Baldocchi, D., Detto, M., Sonnentag, O., Verfaillie, J., Teh, Y.A., Silver, W. and Kelly, N.M. (2012) 'The challenges of measuring methane fluxes and concentrations over a peatland pasture ', *Agricultural and forest meteorology* . Elsevier B.V , pp. 177–187. doi:10.1016/j.agrformet.2011.04.013.

Baldocchi, D.D. (2003) 'Assessing the eddy covariance technique for evaluating carbon dioxide exchange rates of ecosystems: Past, present and future', *Global Change Biology*, 9(4), pp. 479–492. doi:10.1046/j.1365-2486.2003.00629.x.

Baldocchi, D.D., Hincks, B.B. and Meyers, T.P. (1988) 'Measuring Biosphere-Atmosphere Exchanges of Biologically Related Gases with Micrometeorological Methods ', *Ecology (Durham)* . Brooklyn, N.Y., etc : Wiley , pp. 1331–1340. doi:10.2307/1941631.

Baldocchi, D.D. and Vogel, C.A. (1996) 'Energy and CO(2) flux densities above and below a temperate broad-leaved forest and a boreal pine forest ', *Tree physiology U6 - ctx_ver=Z39.88-2004&ctx_enc=info%3Aofi%2Fenc%3AUTF-8&rfr_id=info%3Asid%2Fsummon.serialssolutions.com&rft_val_fmt=info%3Aofi%2Ffmt%3Akev%3Amtx%3Ajournal&rft.genre=article&rft.atitle=Energy+and+CO%282%29+flux+densities+above+and+below*. Canada , pp. 5–16.

Baranov, Y.I., Lafferty, W.J. and Fraser, G.T. (2004) 'Infrared Spectrum of the Continuum and Dimer Absorption in the Vicinity of the O2 Vibrational in Od2/CO^ d2 Mixtures'.

Barr, A.G., Morgenstern, K., Black, T.A., McCaughey, J.H. and Nesic, Z. (2006) 'Surface energy balance closure by the eddy-covariance method above three boreal forest stands and implications for the measurement of the CO2 flux', *Agricultural and Forest Meteorology*, 140(1–4), pp. 322–337. doi:10.1016/j.agrformet.2006.08.007.

Battin, T.J., Luyssaert, S., Kaplan, L.A., Aufdenkampe, A.K., Richter, A. and Tranvik, L.J. (2009) 'The boundless carbon cycle', *Nature geoscience*. London: Springer Science and Business Media LLC, pp. 598–600. doi:10.1038/ngeo618.

Begon, M., Harper, J.L. and Townsend, C.R. (1996) 'Ecology: individuals, populations, and communities '. Oxford, UK;Cambridge, Mass; : Blackwell Science .

Besnard, S. *et al.* (2018) 'Quantifying the effect of forest age in annual net forest carbon balance', *Environmental Research Letters*, 13(12). doi:10.1088/1748-9326/aaeaeb.

Black, K., Bolger, T., Davis, P., Nieuwenhuis, M., Reidy, B., Saiz, G., Tobin, B. and Osborne, B. (2007) 'Inventory and eddy covariance-based estimates of annual carbon sequestration in a Sitka spruce (Picea sitchensis (Bong.) Carr.) forest ecosystem', *European Journal of Forest Research*, 126(2), pp. 167–178. doi:10.1007/s10342-005-0092-4.

Bonn, A., Reed, M.S., Evans, C.D., Joosten, H., Bain, C., Farmer, J., Emmer, I., Couwenberg, J., Moxey, A., Artz, R., Tanneberger, F., von Unger, M., Smyth, M.-A. and Birnie, D. (2014) 'Investing in nature: Developing ecosystem service markets for peatland restoration ', *Ecosystem services* . Elsevier BV , pp. 54–65. doi:10.1016/j.ecoser.2014.06.011.

Bord na móna (2024) 'Delivering Climate Solutions, Sustainabilty Update'.

Bord na Móna (2019) *Bord na Móna and Coillte collaborate to transform 1500 hectares into native woodland*. Available at: https://www.bordnamona.ie/company/news/articles/bord-na-mona-and-coillte-collaborate-transform-native-woodland/ (Accessed: 4 February 2020).

Bord na Móna (2021a) *100 million tonne carbon store secured under major Peatland Restoration Plan*. Available at: https://www.bordnamona.ie/company/news/articles/100-million-tonne-carbon-store-secured-under-major-peatland-restoration-plan/ (Accessed: 26 March 2021).

Bord na Móna (2021b) *Bord na Móna announce formal end to all peat harvesting on its lands*, *Online news report*. Available at: https://www.bordnamona.ie/bord-na-mona-announce-formal-end-to-all-peat-harvesting-on-its-lands/ (Accessed: 15 January 2021).

Breiman, L. (2001) ‘Random forests’, *machine learning*, 45, pp. 5–32.

Bremer, L.L. and Farley, K.A. (2010) ‘Does plantation forestry restore biodiversity or create green deserts? A synthesis of the effects of land-use transitions on plant species richness’, *Biodiversity and conservation*, 19(14), pp. 3893–3915. doi:10.1007/s10531-010-9936-4.

Brockerhoff, E.G., Barbaro, L., Castagneyrol, B., Forrester, D.I., Gardiner, B., González-Olabarria, J.R., Lyver, P.O., Meurisse, N., Oxbrough, A., Taki, H., Thompson, I.D., van der Plas, F. and Jactel, H. (2017) ‘Forest biodiversity, ecosystem functioning and the provision of ecosystem services ’, *Biodiversity and conservation* . Dordrecht : Springer Science and Business Media LLC , pp. 3005–3035. doi:10.1007/s10531-017-1453-2.

Bubier, J.L., Crill, P.M., Moore, T.R., Savage, K. and Varner, R.K. (1998) ‘Seasonal patterns and controls on net ecosystem CO2 exchange in a boreal peatland complex’, *Global Biogeochemical Cycles*, 12(4), pp. 703–714. doi:10.1029/98GB02426.

Burba, G. (2013) ‘Eddy Covariance Method for Scientific, Industrial, Agricultural, and Regulatory Applications A Field Book on Measuring Ecosystem Gas Exchange and Areal Emission Rates’. Lincoln, Nebraska 68504 USA: Li-Cor Biosciences.

Burba, G. (2022) *Eddy Covariance Method for Scientific, Regulatory, and Commercial Applications*. Lincoln, Nebraska 68504 USA: LI-COR Biosciences, Lincoln, Nebraska.

Byrne, K.A. and Farrell, E.P. (2005) ‘The effect of afforestation on soil carbon dioxide emissions in blanket peatland in Ireland’, *Forestry*, 78(3), pp. 217–227. doi:10.1093/forestry/cpi020.

Cai, R.G. and Kim, S.P. (2005) ‘First law of thermodynamics and Friedmann equations of Friedmann-Robertson- Walker universe’, *Journal of High Energy Physics*, (2), pp. 1279–1291. doi:10.1088/1126-6708/2005/02/050.

Cámaro García, W. and Dwyer, N. (2021) *Climate Status Report for Ireland 2020*. MaREI, University College Cork.

Charman, D.J., Barber, K.E., Blaauw, M., Langdon, P.G., Mauquoy, D., Daley, T.J., Hughes, P.D.M. and Karofeld, E. (2009) ‘Climate drivers for peatland palaeoclimate records’, *Quaternary Science Reviews*, 28(19), pp. 1811–1819.

doi:https://doi.org/10.1016/j.quascirev.2009.05.013.

Chen, T. and Guestrin, C. (2016) ‘Xgboost: A scalable tree boosting system’, in *Proceedings of the 22nd acm sigkdd international conference on knowledge discovery and data mining*, pp. 785–794.

Clarke, D. (2010) ‘Brown gold: a history of Bord na Móna and the Irish peat industry’. Dublin: Gill & Macmillan.

Connolly, J. and Holden, N.M. (2009) ‘Mapping peat soils in Ireland: updating the derived Irish peat map’, *Irish Geography*, 42(3), pp. 343–352.

Connolly, J., Holden, N.M. and Ward, S.M. (2007) ‘Mapping Peatlands in Ireland using a Rule-Based Methodology and Digital Data’, *Soil Science Society of America Journal*, 71(2), pp. 492–499. doi:10.2136/sssaj2006.0033.

Crippa, M., Guizzardi, D., Pagani, F., Banja, M., Muntean, M., Schaaf, E., Monforti-Ferrario, F., Becker, W.E., Quadrelli, R., Risquez Martin, A., Taghavi-Moharamli, P., Köykkä, J., Grassi, G., Rossi, S., Melo, J., Oom, D. and Branco, A., San-Miguel, J., Manca, G., Pisoni, E., Vignati, E. and Pekar, F. (2024) *GHG emissions of all world countries*. European C, *Publications Office of the European Union*. European C. doi:10.2760/0115360.

Curley, M., Coonan, B., Ruth, C.. and Ryan, C. (2024) ‘Ireland ’s Climate Averages 1991-2020’, p. Climatological Note No. 22.

Dabberdt, W.F., Lenschow, D.H., Horst, T.W., Zimmerman, P.R., Oncley, S.P. and Delany, A.C. (1993) ‘Atmosphere-Surface Exchange Measurements’, *Science (American Association for the Advancement of Science)*. Washington, DC: American Society for the Advancement of Science, pp. 1472–1481. doi:10.1126/science.260.5113.1472.

DAFM (2015) *Forestry Programme 2014 – 2020: Ireland*, *Forest Service, Department of Agriculture, Food and the Marine*.

DAFM (2017) *Ireland’s National Forest Inventory 2017 Main Findings*. Johnstown Castle Estate Co. Wexford Ireland Y35 PN52.

DAFM (2020) ‘Forest Statistics Ireland 2020’, *Department of Agriculture, Food & the Marine, Ireland*, pp. 1–89.

DAFM, D. of A.F. and the M. (2022) *Ireland ' s National Forest Inventory 2022 – Main Findings Covering the fourth National Forest Inventory , 2020 to 2022*.

David Wilson Catherine Farrell, F.R.-W. and Müller, C.B. and C.N.V.-R.S.N. 15 (2012) *Carbon Restore: The Potential of Restored Irish Peatlands for Carbon Uptake and Storage*, *Climate Change Research Programme (CCRP) 2007-2013*. Environmental Protection Agency.

Denman, K.L., Brasseur, G., Chidthaisong, A., Ciais, P., Cox, P.M., Dickinson, R.E., Hauglustaine, D., Heinze, C., Holland, E., Jacob, D., Lohmann, U., Ramachandran, S., Dias, P.L. da S., Wofsy, S.. and Zhang, X. (2007) 'Couplings Between Changes in the Climate System and Biogeochemistry', *Climate Change 2007: The Physical Science Basis. Contribution of Working Group I to the Fourth Assessment Report of the Intergovernmental Panel on Climate Change* [Preprint].

Dieleman, C.M., Lindo, Z., McLaughlin, J.W., Craig, A.E. and Branfireun, B.A. (2016) 'Climate change effects on peatland decomposition and porewater dissolved organic carbon biogeochemistry', *Biogeochemistry*, 128(3), pp. 385–396. doi:10.1007/s10533-016-0214-8.

Dillon, P.J. and Molot, L.A. (1997) 'Effect of landscape form on export of dissolved organic carbon, iron, and phosphorus from forested stream catchments ', *Water Resources Research* , pp. 2591–2600. doi:10.1029/97WR01921.

Directorate-General for Environment (2024) *Degraded ecosystems to be restored across Europe as Nature Restoration Law enters into force*, *15 August 2024*. Available at: https://environment.ec.europa.eu/news/nature-restoration-law-enters-force-2024-08-15_en.

Duffy, P., Black, K., Hyde, B., Ryan, A.M. and Ponzi., J. (2021) *Ireland's National Inventory Report 2021. 1990-2019*.

Dunn, A.L., Barford, C.C., Wofsy, S.C., Goulden, M.L. and Daube, B.C. (2007) 'A long-term record of carbon exchange in a boreal black spruce forest: means, responses to interannual variability, and decadal trends', *Global change biology*. Oxford, UK: Blackwell Publishing Ltd, pp. 577–590. doi:10.1111/j.1365-2486.2006.01221.x.

Eaton, J.M., McGoff, N.M., Byrne, K.A., Leahy, P. and Kiely, G. (2008) 'Land cover change and soil organic carbon stocks in the Republic of Ireland 1851-2000', *Climatic Change*, 91(3–4), pp. 317–334. doi:10.1007/s10584-008-9412-2.

EPA (2024) *Ireland ' s National Inventory Report 2024*.

Evans, C., Artz, R., Moxley, J., Smyth, M.-A., Taylor, E., Archer, N., Burden, A., Williamson, J., Donnelly, D., Thomson, A., Buys, G., Malcolm, H., Wilson, D., Renou-Wilson, F. and Potts, J. (2017) 'Implementation of an Emissions Inventory for UK Peatlands', *Centre for Ecology and Hydrology*, (1), p. 88.

Falge, E. *et al.* (2001) 'Gap filling strategies for defensible annual sums of net ecosystem exchange', *Agric. For. Meteorol.*, 107, pp. 43–69.

Falge, E., Baldocchi, D., *et al.* (2002) 'Seasonality of ecosystem respiration and gross primary production as derived from FLUXNET measurements', *Agricultural and Forest Meteorology*, 113(1), pp. 53–74. doi:https://doi.org/10.1016/S0168-1923(02)00102-8.

Falge, E., Tenhunen, J., Baldocchi, D., Aubinet, M., Bakwin, P., Berbigier, P., Bernhofer, C., Bonnefond, J.-M., Burba, G. and Clement, R. (2002) 'Phase and amplitude of ecosystem carbon release and uptake potentials as derived from FLUXNET measurements', *Agricultural and Forest Meteorology*, 113(1–4), pp. 75–95.

Farrell, C.A. and Doyle, G.J. (2003) 'Rehabilitation of industrial cutaway Atlantic blanket bog in County Mayo, North-West Ireland', *Wetlands Ecology and Management*, 11(1–2), pp. 21–35. doi:10.1023/A:1022097203946.

Feehan, J. and O'Donovan, G. (1996) 'The bogs of Ireland: an introduction to the natural, cultural and industrial heritage of Irish peatlands'. Dublin: University College, Dublin, Environmental Institute.

Fernandez, F., Connolly, K., Crowley, W., Denyer, J., Duff, K. and Smith, G. (2014) 'Raised bog monitoring and assessment survey 2013. Irish Wildlife Manuals, No. 81', *National Parks and Wildlife Service, Department of Arts, Heritage and Gaeltacht, Dublin, Ireland* [Preprint].

Fiedler, J., Fuß, R., Glatzel, S., Hagemann, U., Huth, V., Jordan, S., Jurasinski, G., Kutzbach, L., Maier, M., Schäfer, K. and Weber, T. (2022) 'Measurement of carbon dioxide , methane and nitrous oxide fluxes between', *Deutsche Bodenkundliche Gesellschaft (German Soil Science Society)*, pp. 1–70.

Finkelstein, P.L. and Sims, P.F. (2001) 'Sampling error in Eddy correlation flux measurements', *Journal of Geophyscical research*, 106, pp. 3503–3509.

Fix, E. and Hodges, J.L. (1951) 'Discriminatory analysis', *Nonparametric discrimination: Small sample performance. Report A*, 193008.

Foken, T., Aubinet, M. and Leuning, R. (2011) 'The Eddy Covariance Method', in *Eddy Covariance*. Dordrecht: Springer Netherlands, pp. 1–19. doi:10.1007/978-94-007-2351-1_1.

Forrester, D.I. and Bauhus, J. (2016) 'A Review of Processes Behind Diversity—Productivity Relationships in Forests ', *Current Forestry Reports* . Cham : Springer Science and Business Media LLC , pp. 45–61. doi:10.1007/s40725-016-0031-2.

Foss, P., O'Connell, C. and Crushell, P.H. (2001) *Bogs and Fens of Ireland. Conservatioin Plan 2005*. Dublin: Irish Peatland Conservation Council.

Fossitt, J.A. (2000) *A guide to habitats in Ireland*. Heritage.

Fowler, D., Hargreaves, K.J., Macdonald, J.A. and Gardiner, B. (1995) 'Methane and CO2 exchange over peatland and the effects of afforestation', *Forestry*, 68(4), pp. 327–334. doi:10.1093/forestry/68.4.327.

Friedman, J.H. (2001) 'Greedy function approximation: a gradient boosting machine', *Annals of statistics*, pp. 1189–1232.

Frolking, S., Talbot, J., Jones, M.C., Treat, C.C., Kauffman, J.B., Tuittila, E.S. and Roulet, N. (2011) 'Peatlands in the Earth's 21st century climate system', *Environmental Reviews*, 19(1), pp. 371–396. doi:10.1139/a11-014.

Frolking, S.E., Bubier, J.L., Moore, T.R., Ball, T., Bellisario, L.M., Bhardwaj, A., Carroll, P., Crill, P.M., Lafleur, P.M., McCaughey, J.H., Roulet, N.T., Suyker, A.E., Verma, S.B., Waddington, J.M. and Whiting, G.J. (1998) 'Relationship between ecosystem productivity and photosynthetically active radiation for northern peatlands ', *Global Biogeochemical Cycles* , pp. 115–126. doi:10.1029/97GB03367.

Gallego-Sala, A. V., Charman, D.J., Harrison, S.P., Li, G. and Prentice, I.C. (2016) 'Climate-driven expansion of blanket bogs in Britain during the Holocene', *Climate of the Past*, 12(1), pp. 129–136. doi:10.5194/cp-12-129-2016.

Gilet, L., Morley, T.R., Flynn, R. and Connolly, J. (2024) 'An adaptive mapping framework for the management of peat soils: A new Irish peat soils map', *Geoderma*, 447(November 2023), p. 116933. doi:10.1016/j.geoderma.2024.116933.

Gilmanov, T.G., Verma, S.B., Sims, P.L., Meyers, T.P., Bradford, J.A., Burba, G.G. and Suyker, A.E. (2003) 'Gross primary production and light response parameters of four Southern Plains ecosystems estimated using long-term CO_2-flux tower measurements', *Global Biogeochemical Cycles*, 17(2).

Girkin, N.T., Burgess, P.J., Cole, L., Cooper, H. V, Honorio Coronado, E., Davidson, S.J., Hannam, J., Harris, J., Holman, I. and McCloskey, C.S. (2023) 'The three-peat challenge: business as usual, responsible agriculture, and conservation and restoration as management trajectories in global peatlands', *Carbon management*, 14(1), p. 2275578.

Gockede, M. *et al.* (2008) 'Quality control of CarboEurope flux data - Part 1: Coupling footprint analyses with flux data quality assessment to evaluate sites in forest ecosystems ', *Biogeosciences* . European Geosciences Union , pp. 433–450. doi:10.5194/bg-5-433-2008.

Goffin, S., Wylock, C., Haut, B., Maier, M., Longdoz, B. and Aubinet, M. (2015) 'Modeling soil CO2 production and transport to investigate the intra-day variability of surface efflux and soil CO2 concentration measurements in a Scots Pine Forest (Pinus Sylvestris, L.)', *Plant and Soil*, 390(1–2), pp. 195–211. doi:10.1007/s11104-015-2381-0.

Government of Ireland (2020) *Cabinet approves €108 million funding for groundbreaking Bord na Móna bog rehabilitation plan*, *Press release*. Available at: https://www.gov.ie/en/press-release/2aae1-cabinet-approves-108m-funding-for-groundbreaking-bord-na-mona-bog-rehabilitation-plan-minister-ryan-also-announces-that-47-more-projects-in-the-midlands-totalling-278m-are-approved-under-the-just-transition-fund/# (Accessed: 17 December 2020).

Graham, C.T., Graham, C.T., Wilson, M.W., Wilson, M.W., Gittings, T., Gittings, T., Kelly, T.C., Kelly, T.C., Irwin, S., Irwin, S., Quinn, J.L., Quinn, J.L., O'Halloran, J. and O'Halloran, J. (2017) 'Implications of afforestation for bird communities: the importance of preceding land-use type ', *Biodiversity and Conservation* . Dordrecht : Springer Netherlands , pp. 3051–3071. doi:10.1007/s10531-015-0987-4.

Green, S.M. and Page, S. (2017) 'Tropical peatlands: current plight and the need for responsible management', *Geology Today*, 33(5), pp. 174–179. doi:10.1111/gto.12197.

Greifswald Mire Centre (2022) *Global Peatland Map 2.0. Underlying dataset of the Global Peatlands Assessment - The State of the World's Peatlands*, *Global Peatlands Initiative, United Nations Environment Programme, Nairobi*. Available at: file:///C:/Users/Admin/Downloads/GloPeMap.png.

Griffis, T.J., Rouse, W.R. and Waddington, J.M. (2000) 'Scaling net ecosystem CO2 exchange from the community to landscape-level at a subarctic fen ', *Global change biology* . Oxford, UK : Blackwell Science Ltd , pp. 459–473. doi:10.1046/j.1365-2486.2000.00330.x.

Günther, A., Barthelmes, A., Huth, V., Joosten, H., Jurasinski, G., Koebsch, F. and Couwenberg, J. (2020) 'Prompt rewetting of drained peatlands reduces climate warming despite methane emissions ', *Nature communications* . England : Nature Publishing Group , p. 1644. doi:10.1038/s41467-020-15499-z.

Günther, A., Huth, V., Jurasinski, G. and Glatzel, S. (2015) 'The effect of biomass harvesting on greenhouse gas emissions from a rewetted temperate fen', *GCB Bioenergy*, 7(5), pp. 1092–1106. doi:10.1111/gcbb.12214.

HAAHR, T. (2024) *Nature restoration: Parliament adopts law to restore 20% of EU's land and sea*, *European Parliament*. Available at: https://www.europarl.europa.eu/news/en/press-room/20240223IPR18078/nature-restoration-parliament-adopts-law-to-restore-20-of-eu-s-land-and-sea (Accessed: 18 February 2025).

Habib, W., Ingle, R., Saunders, M. and Connolly, J. (2024) 'Quantifying peatland land use and CO2 emissions in Irish raised bogs: mapping insights using Sentinel-2 data and Google Earth Engine', *Scientific Reports*, 14(1), p. 1171. doi:10.1038/s41598-024-51660-0.

Halder, R.K., Uddin, M.N., Uddin, M.A., Aryal, S. and Khraisat, A. (2024) 'Enhancing K-nearest neighbor algorithm: a comprehensive review and performance analysis of modifications', *Journal of Big Data*, 11(1). doi:10.1186/s40537-024-00973-y.

Hambley, G., Andersen, R., Levy, P., Saunders, M., Cowie, N.R., Teh, Y.A. and Hill, T.C. (2019) 'Net ecosystem exchange from two formerly afforested peatlands undergoing restoration in the Flow Country of northern Scotland', *Mires and Peat*, 23(5), pp. 1–14.

doi:10.19189/MaP.2018.DW.346.

Hammond, R.F. (1981) *The Peatlands of Ireland*, *Soil Survey Bulletin No. 35*. 19 Sandymount Avenue, Dublin 4: An Foras Taluntais.

Hamrani, A., Akbarzadeh, A. and Madramootoo, C.A. (2020) 'Machine learning for predicting greenhouse gas emissions from agricultural soils', *Science of The Total Environment*, 741, p. 140338. doi:https://doi.org/10.1016/j.scitotenv.2020.140338.

Hanson, P.J., Edwards, N.T., Garten, C.T. and Andrews, J.A. (2000) 'Separating root and soil microbial contributions to soil respiration: A review of methods and observations', *Biogeochemistry*, 48(1), pp. 115–146. doi:10.1023/A:1006244819642.

Hargreaves, K.J., Milne, R. and Cannell, M.G.R. (2003) 'Carbon balance of afforested peatland in Scotland', *Forestry*, 76(3), pp. 299–317. doi:10.1093/forestry/76.3.299.

Hastie, T. and Tibshirani, R.J. (1986) 'Generalized Additive Models', *Statistical Science*, 1(3), pp. 297–318. doi:10.2307/2246134.

Hastie, T.J. (2017) 'Generalized additive models', in *Statistical models in S*. Routledge, pp. 249–307.

He, H., Jansson, P.-E., Svensson, M., Björklund, J., Tarvainen, L., Klemedtsson, L. and Kasimir, Ã. (2016) 'Forests on drained agricultural peatland are potentially large sources of greenhouse gases – insights from a full rotation period simulation ', *Biogeosciences* . Katlenburg-Lindau : Copernicus GmbH , pp. 2305–2318. doi:10.5194/bg-13-2305-2016.

Heinemeyer, A., Di Bene, C., Lloyd, A.R., Tortorella, D., Baxter, R., Huntley, B., Gelsomino, A. and Ineson, P. (2011) 'Soil respiration: implications of the plant-soil continuum and respiration chamber collar-insertion depth on measurement and modelling of soil CO2 efflux rates in three ecosystems', *European journal of soil science*, 62(1), pp. 82–94. doi:10.1111/j.1365-2389.2010.01331.x.

Heinemeyer, A. and McNamara, N.P. (2011) 'Comparing the closed static versus the closed dynamic chamber flux methodology: Implications for soil respiration studies ', *Plant and soil* . Dordrecht : Springer , pp. 145–151. doi:10.1007/s11104-011-0804-0.

Holden, J. (2005) 'Peatland hydrology and carbon release: Why small-scale process matters', *Philosophical Transactions of the Royal Society A: Mathematical, Physical and Engineering Sciences*, 363(1837), pp. 2891–2913. doi:10.1098/rsta.2005.1671.

Holden, J., Chapman, P.J. and Labadz, J.C. (2004) 'Artificial drainage of peatlands: hydrological and hydrochemical process and wetland restoration', *Progress in physical geography*. Thousand Oaks, CA: SAGE Publications, pp. 95–123. doi:10.1191/0309133304pp403ra.

Holden, J., Shotbolt, L., Bonn, A., Burt, T.P., Chapman, P.J., Dougill, A.J., Fraser, E.D.G., Hubacek, K., Irvine, B., Kirkby, M.J., Reed, M.S., Prell, C., Stagl, S., Stringer, L.C., Turner, A. and Worrall, F. (2007) 'Environmental change in moorland landscapes ', *Earth-science reviews* . Elsevier BV , pp. 75–100. doi:10.1016/j.earscirev.2007.01.003.

Holden, J., Wallage, Z.E., Lane, S.N. and McDonald, A.T. (2011) 'Water table dynamics in undisturbed, drained and restored blanket peat', *Journal of Hydrology*, 402(1–2), pp. 103–114. doi:10.1016/j.jhydrol.2011.03.010.

Holden, N.M. and Connolly, J. (2011) 'Estimating the carbon stock of a blanket peat region using a peat depth inference model', *Catena*, 86(2), pp. 75–85. doi:10.1016/j.catena.2011.02.002.

Holl, D., Pfeiffer, E.-M. and Kutzbach, L. (2020) 'Comparison of eddy covariance CO2 and CH4 fluxes from mined and recently rewetted sections in a northwestern German cutover bog ', *Biogeosciences* . Katlenburg-Lindau : Copernicus GmbH , pp. 2853–2874. doi:10.5194/bg-17-2853-2020.

Hollinger, D.Y., Kelliher, F.M., Schulze, E.-D., Bauer, G., Arneth, A., Byers, J.N., Hunt, J.E., McSeveny, T.M., Kobak, K.I. and Milukova, I. (1998) 'Forest–atmosphere carbon dioxide exchange in eastern Siberia', *Agricultural and Forest Meteorology*, 90(4), pp. 291–306.

Hommeltenberg, J., Schmid, H.P., Drösler, M. and Werle, P. (2014) 'Can a bog drained for forestry be a stronger carbon sink than a natural bog forest? ', *Biogeosciences* . Katlenburg-Lindau : Copernicus GmbH , pp. 3477–3493. doi:10.5194/bg-11-3477-2014.

Horst, T.W. and Weil, J.C. (1992) 'Footprint estimation for scalar flux measurements in the atmospheric surface layer', *Boundary-layer meteorology*. Dordrecht: Springer, pp. 279–296. doi:10.1007/BF00119817.

Hutchinson, G.L., Livingston, G.P., Healy, R.W. and Striegl, R.G. (2000) 'Chamber measurement of surface-atmosphere trace gas exchange: Numerical evaluation of dependence on soil, interfacial layer, and source/sink properties ', *Journal of Geophysical Research: Atmospheres* , pp. 8865–8875. doi:10.1029/1999JD901204.

Ingle, R., Bhatnagar, S., Ghosh, B., Gill, L., Regan, S., Connolly, J. and Saunders, M. (2023) 'Development of Hybrid Models to Estimate Gross Primary Productivity at a Near-Natural Peatland Using Sentinel 2 Data and a Light Use Efficiency Model', *Remote Sensing*, 15(6). doi:10.3390/rs15061673.

Ingle, R., Habib, W., Connolly, J., McCorry, M., Barry, S. and Saunders, M. (2023) 'Upscaling methane fluxes from peatlands across a drainage gradient in Ireland using PlanetScope imagery and machine learning tools', *Scientific Reports*, 13(1), p. 11997. doi:10.1038/s41598-023-38470-6.

IPCC (2013) *Methodological Guidance on Lands with Wet and Drained Soils, and Constructed Wetlands for Wastewater Treatment*, *2013 Supplement to the 2006 IPCC Guidelines for National Greenhouse Gas Inventories: Wetlands*.

IPCC (2018) *Global Warming of 1.5°C.An IPCC Special Report on the impacts of global warming of 1.5°C above pre-industrial levels and related global greenhouse gas emission pathways, in the context of strengthening the global response to the threat of climate change,* . Edited by V. Masson-Delmotte  P. Zhai, H.-O. Pörtner, D. Roberts, J. Skea, P.R. Shukla, A. Pirani, W. Moufouma-Okia, C. Péan, R. Pidcock, S. Connors, J.B.R. Matthews, Y. Chen, X. Zhou, M.I. Gomis, E. Lonnoy, T. Maycock, M. Tignor, and T. Waterfield.

IPCC (2021) 'Climate Change, Mitigation of Climate Change', *Cambridge University Press*, (Mitigation of Climate Change-Working Group III Contribution to the Sixth Assessment of the Intergovernmental Panel on Climate Change), p. 1454.

IPCC (2022) *Climate Change 2022 - Mitigation of Climate Change - Summary for Policymakers (SPM)*, *Cambridge University Press*.

IPCC (2024) 'IPCC Global Warming Potential Values', (2), pp. 1–10.

IPCC, I.P. on C.C. (2001) 'Climate Change 2001. The Scientific Basis. Contribution of Working Group 1  to the Third Assessment Report of the Inter-Governmental Panel on Climate

Change.’ The Pitt Building, Trumpington Street, Cambridge, United Kingdom: THE PRESS SYNDICATE OF THE UNIVERSITY OF CAMBRIDGE The Pitt Building, Trumpington Street, Cambridge, United Kingdom.

IPCC, I.P. on C.C. (2023) ‘Summary for Policymakers of the Intergovernmental Panel on Climate Change’.

IUPAC, I.U. of and Chemistry, P. and A. (2022) ‘IUPAC Periodic Table of the Elements’, (103), p. 2022.

Jain, N., Bhatia, A., Pathak, D.S., Gupta, N., Sharma, D. and Kaushik, R. (2015) ‘Greenhouse Gas emissions and Global warming’, in, pp. 379–411.

Janssens, I.A., Kowalski, A.S. and Ceulemans, R. (2001) ‘Forest floor CO2 fluxes estimated by eddy covariance and chamber-based model’, *Agricultural and Forest Meteorology*, 106(1), pp. 61–69. doi:10.1016/S0168-1923(00)00177-5.

Janssens, I.A., Kowalski, A.S., Longdoz, B. and Ceulemans, R. (2000) ‘Assessing forest soil CO2 efflux: an in situ comparison of four techniques ’, *Tree physiology* , pp. 23–32. doi:10.1093/treephys/20.1.23.

Jovani-Sancho, A.J., Cummins, T. and Byrne, K.A. (2017) ‘Collar insertion depth effects on soil respiration in afforested peatlands’, *Biology and Fertility of Soils*, 53(6), pp. 677–689. doi:10.1007/s00374-017-1210-4.

Jovani-Sancho, A.J., Cummins, T. and Byrne, K.A. (2018) ‘Soil respiration partitioning in afforested temperate peatlands’, *Biogeochemistry*, 141(1), pp. 1–21. doi:10.1007/s10533-018-0496-0.

Jovani-Sancho, A.J., Cummins, T. and Byrne, K.A. (2021) ‘Soil carbon balance of afforested peatlands in the maritime temperate climatic zone ’, *Global change biology* . England : Wiley Subscription Services, Inc , pp. 3681–3698. doi:10.1111/gcb.15654.

Jovani Sancho, A.J., Brosnan, S. and Byrne, K.A. (2017) ‘Partitioning of soil respiration in a first rotation beech plantation’, *Biology and environment : proceedings of the Royal Irish Academy*. Royal Irish Academy, pp. 91–105. doi:10.3318/bioe.2017.09.

Kaimal, J.C. and Finnigan, J.J. (1994) ‘Atmospheric Boundary Layer Flows: Their Structure and Measurement ’. Cary : Oxford University Press, Incorporated .

Kiely, G., Leahy, P., Sottocornola, M., Laine, A., Mishurov, M., Albertson, J. and Carton, O. (2009) ‘CELTICFLUX: Measurement and Modelling of Greenhouse Gas Fluxes from Grasslands and a Peatland in Ireland STRIVE’, *STRIVE report series*, No.24.

Kim, Y., Johnson, M.S., Knox, S.H., Black, T.A., Dalmagro, H.J., Kang, M., Kim, J. and Baldocchi, D. (2020) ‘Gap-filling approaches for eddy covariance methane fluxes: A comparison of three machine learning algorithms and a traditional method with principal component analysis’, *Global Change Biology*, 26(3), pp. 1499–1518. doi:10.1111/gcb.14845.

Kirk-Davidoff, D. (2018) ‘The greenhouse effect, aerosols, and climate change’, in *Green chemistry*. Elsevier, pp. 211–234. doi:10.1016/B978-0-12-809270-5.00009-1.

Kirschbaum, M.U.F., Eamus, D., Gifford, R.M., Roxburgh, S.H. and Sands, P.J. (2001) ‘Definitions Of Some Ecological Terms Commonly Used In Carbon Accounting’, in *Net Ecosystem Exchange*, pp. 1–144.

Kljun, N., Calanca, P., Rotach, M.W. and Schmid, H.P. (2004) ‘A Simple Parameterisation for Flux Footprint Predictions ’, *Boundary-layer meteorology* . Dordrecht : Kluwer Academic Publishers , pp. 503–523. doi:10.1023/B:BOUN.0000030653.71031.96.

Kljun, N., Calanca, P., Rotach, M.W. and Schmid, H.P. (2015) ‘A simple two-dimensional parameterisation for Flux Footprint Prediction (FFP)’, *Geoscientific Model Development*, 8(11), pp. 3695–3713. doi:10.5194/gmd-8-3695-2015.

Kljun, N., Rotach, M.W. and Schmid, H.P. (2002) ‘A Three-Dimensional Backward Lagrangian Footprint Model For A Wide Range Of Boundary-Layer Stratifications ’, *Boundary-layer meteorology* . Dordrecht : Kluwer Academic Publishers , pp. 205–226. doi:10.1023/A:1014556300021.

Klumpp, K., Tallec, T., Guix, N. and Soussana, J. (2011) ‘Long-term impacts of agricultural practices and climatic variability on carbon storage in a permanent pasture’, *Global Change Biology*, 17(12), pp. 3534–3545.

Kováč, D., Ač, A., Šigut, L., Peñuelas, J., Grace, J. and Urban, O. (2022) ‘Combining NDVI, PRI and the quantum yield of solar-induced fluorescence improves estimations of carbon fluxes in deciduous and evergreen forests', *Science of the Total Environment*, 829. doi:10.1016/j.scitotenv.2022.154681.

Kuzyakov, Y. (2010) 'Soil Biology & Biochemistry Priming effects : Interactions between living and dead organic matter', *Soil Biology and Biochemistry*, 42(9), pp. 1363–1371. doi:10.1016/j.soilbio.2010.04.003.

Lafleur, P.M., Roulet, N.T., Bubier, J.L., Frolking, S. and Moore, T.R. (2003) 'Interannual variability in the peatland-atmosphere carbon dioxide exchange at an ombrotrophic bog', *Global Biogeochemical Cycles*, 17(2), pp. 1–14. doi:10.1029/2002gb001983.

Laiho, R. (2006) 'Decomposition in peatlands: Reconciling seemingly contrasting results on the impacts of lowered water levels', *Soil Biology and Biochemistry*, 38(8), pp. 2011–2024. doi:https://doi.org/10.1016/j.soilbio.2006.02.017.

Laine, A.M. (2006) *Carbon gas fluxes in an Irish Lowland blanket bog*, *Department of Civil and Environmental Engineering*. NUI.

Laino, E. and Iglesias, G. (2025) 'ScienceDirect Extreme weather events and environmental contamination under climate change : A comparative review of ten European coastal cities', *Current Opinion in Environmental Science & Health*, 45, p. 100606. doi:10.1016/j.coesh.2025.100606.

Law, B.E., Falge, E., Gu, L., Baldocchi, D.D., Bakwin, P., Berbigier, P., Davis, K., Dolman, A.J., Falk, M. and Fuentes, J.D. (2002) 'Environmental controls over carbon dioxide and water vapor exchange of terrestrial vegetation', *Agricultural and Forest Meteorology*, 113(1–4), pp. 97–120.

Leuning, R., Zegelin, S.J., Jones, K., Keith, H. and Hughes, D. (2008) 'Measurement of horizontal and vertical advection of CO2 within a forest canopy', *Agricultural and forest meteorology*. Amsterdam: Elsevier, pp. 1777–1797. doi:10.1016/j.agrformet.2008.06.006.

Levy, P.E. and Gray, A. (2015) 'Greenhouse gas balance of a semi-natural peatbog in northern Scotland', *Environmental Research Letters*, 10(9). doi:10.1088/1748-9326/10/9/094019.

Lewis, C., Albertson, J., Zi, T., Xu, X. and Kiely, G. (2013) 'How does afforestation affect the hydrology of a blanket peatland? A modelling study', *Hydrological Processes*, 27(25), pp. 3577–3588. doi:10.1002/hyp.9486.

Liang, J. *et al.* (2016) 'Positive biodiversity-productivity relationship predominant in global forests', *Science (American Association for the Advancement of Science)*. United States: American Association for the Advancement of Science (AAAS), pp. aaf8957–aaf8957. doi:10.1126/science.aaf8957.

Liaw, A. and Wiener, M. (2002) 'Classification and regression by randomForest', *R news* [Preprint].

Livingston, G.. and Hutchinson, G.. (1995) 'Enclosure-based measurement of trace gas exchange: applications and sources of error', in *Biogenic trace gases: measuring emissions from soil and water*. John Wiley & Sons, Incorporated, pp. 14–49.

Lloyd, J. and Taylor, J.A. (1994) 'On the Temperature Dependence of Soil Respiration', *Functional ecology*, 8(3), pp. 315–323.

Lohila, A., Minkkinen, K., Aurela, M., Tuovinen, J.-P., Penttilä, T., Ojanen, P. and Laurila, T. (2011) 'Greenhouse gas flux measurements in a forestry-drained peatland indicate a large carbon sink ', *Biogeosciences* . Katlenburg-Lindau : Copernicus GmbH , pp. 3203–3218. doi:10.5194/bg-8-3203-2011.

Luo, Y. and Zhuo, X. (2007) 'Soil Respiration and the Environment. By Y. Luo and X. Zhuo. Burlington, MA, and San Diego, CA, USA: Academic Press (2006), pp. 320, £39.99. ISBN-10: 0-12-088782-7', *Experimental Agriculture*, 43(3), pp. 402–403. doi:10.1017/S0014479707005078.

Malone, S. and O'Connell, C. (2009) *Ireland's Peatland Conservation Action Plan 2020 halting the loss of peatland biodiversity*. Irish Peatland Conservation Council, Kildare.

Mann, J. and Lenschow, D.H. (1994) 'Errors in airborne flux measurements', *JGR Atmospheres*, 99(D7), pp. 14519–14526.

Matson, P.A., Harriss, R.C. and (Firm), P. (1995) 'Trace gas exchange in an ecosystem context: multiple approaches to measurement and analysis', in *Biogenic Trace Gases : Measuring Emissions from Soil and Water*. Oxford [England];Cambridge, MA, USA; Blackwell

Science.

Mauder, M. and Foken, T. (2004) ‘Documentation and instruction manual of the eddy covariance software package TK2, Arbeitsergebn’, *Univ. Bayreuth, Abt. Mikrometeorol., ISSN*, pp. 1614–89166.

McNicholas, D. and Ellison, P. (2023) ‘Lullymore Cutover Bog Woodland Assessment-Bord na Móna Ecology’, *Unpublished Bord na Móna Ecology Report* [Preprint].

Mealy, H. (2022) ‘Meteorological data from the Ballaghurt Eddy Covariance tower, Offaly Ireland (unpublished data)’.

Le Mer, J. and Roger, P. (2001) ‘Production, oxidation, emission and consumption of methane by soils: A review’, *European Journal of Soil Biology*, 37(1), pp. 25–50. doi:https://doi.org/10.1016/S1164-5563(01)01067-6.

Met Éireann (2020) *Climate of Ireland*, *The Irish meteoroogical service*. Available at: https://www.met.ie/climate/climate-of-ireland (Accessed: 30 May 2022).

Met Éireann (2022) *Lullymore nature Centre Climate data*, *data.gov.ie*. Available at: https://data.gov.ie/dataset/lullymore-nature-centre-climate-data (Accessed: 30 May 2022).

Met Éireann (no date) *Met Éireann Historical data*, *Met Éireann*. Available at: https://www.met.ie/climate/available-data/historical-data (Accessed: 21 December 2021).

Mitchell, F. and Ryan, M. (1997) *Reading the Irish landscape*. Rev. Dublin: Town House.

Murphy, C. *et al.* (2018) ‘A 305-year continuous monthly rainfall series for the island of Ireland (1711-2016)’, *CLIMATE OF THE PAST*, 14(3), pp. 413–440.

Natekin, A. and Knoll, A. (2013) ‘Gradient boosting machines, a tutorial’, *Frontiers in Neurorobotics*, 7(DEC). doi:10.3389/fnbot.2013.00021.

National Parks and Wildlife Service (2015) *National Peatlands Strategy*. 7 Ely Place, Dublin 2, D02 TW98, Ireland.

Nolan, P. (2024) *Updated High-resolution Climate Projections for Ireland*.

Noone, C., McClean, D., Gallagher, D., McElwain, J. and Thorne, P. (2023) ‘Ireland’s Climate Change Assessment Volume 1. Climate Science – Ireland in a Changing World. Summary for

Policy Makers', *Environmental Protection Agency*, 1.

NPWS (2019) 'The Status of EU Protected Habitats and Species in Ireland', *Unpublished NPWS Report*, 1: Summary, pp. 1–100.

O'Callaghan, C.J., O'Callaghan, C.J., Irwin, S., Irwin, S., Byrne, K.A., Byrne, K.A., O'Halloran, J. and O'Halloran, J. (2017) 'The role of planted forests in the provision of habitat: an Irish perspective ', *Biodiversity and Conservation* . Dordrecht : Springer Netherlands , pp. 3103–3124. doi:10.1007/s10531-016-1125-7.

O'Connell, C.A., Madigan, N., Whyte, T. and Farrell, P. (2021) *Peatlands and Climate Change Action Plan 2030*. Irish Peatland Conservation Council, Co. Kildare.

O'Leary, D., Brown, C., Hodgson, J., Connolly, J., Gilet, L., Tuohy, P., Fenton, O. and Daly, E. (2025) 'Airborne radiometric data for digital soil mapping of peat at broad and local scales', *Geoderma*, 453(August 2024). doi:10.1016/j.geoderma.2024.117129.

Oh, Y., Zhuang, Q., Welp, L.R., Liu, L., Lan, X., Basu, S., Dlugokencky, E.J., Bruhwiler, L., Miller, J.B., Michel, S.E., Schwietzke, S., Tans, P., Ciais, P. and Chanton, J.P. (2022) 'Improved global wetland carbon isotopic signatures support post-2006 microbial methane emission increase', *Communications Earth and Environment*, 3(1). doi:10.1038/s43247-022-00488-5.

Ojanen, P., Minkkinen, K., Lohila, A., Badorek, T. and Penttilä, T. (2012) 'Chamber measured soil respiration: A useful tool for estimating the carbon balance of peatland forest soils?', *Forest Ecology and Management*, 277, pp. 132–140. doi:https://doi.org/10.1016/j.foreco.2012.04.027.

Page, S.E. and Baird, A.J. (2016) 'Peatlands and Global Change: Response and Resilience', *Annual Review of Environment and Resources*, 41(1), pp. 35–57. doi:10.1146/annurev-environ-110615-085520.

Palmer, S.M., Hope, D., Billett, M.F. and Bryant, C.L. (2001) 'Sources of Organic and Inorganic Carbon in a Headwater Stream: Evidence from Carbon Isotope Studies ', *Biogeochemistry* . Dordrecht : Kluwer Academic Publishers , pp. 321–338. doi:10.1023/A:1006447706565.

Papale, D. and Valentini, R. (2003) 'A new assessment of European forests carbon exchanges by eddy fluxes and artificial neural network spatialization', *Global Change Biology*, 9(4), pp. 525–535.

Pastorello, G. *et al.* (2020) 'The FLUXNET2015 dataset and the ONEFlux processing pipeline for eddy covariance data', *Scientific Data*, 7(1), p. 225. doi:10.1038/s41597-020-0534-3.

Paul-Limoges, E., Wolf, S., Eugster, W., Hörtnagl, L. and Buchmann, N. (2017) 'Below-canopy contributions to ecosystem CO2 fluxes in a temperate mixed forest in Switzerland ', *Agricultural and forest meteorology* . Elsevier B.V , pp. 582–596. doi:10.1016/j.agrformet.2017.08.011.

Pavelka, M. *et al.* (2018) 'Standardisation of chamber technique for CO 2 , N 2 O and CH 4 fluxes measurements from terrestrial ecosystems', *International Agrophysics*, 32(4), pp. 569–587. doi:10.1515/intag-2017-0045.

Peichl, M., Öquist, M., Ottosson Löfvenius, M., Ilstedt, U., Sagerfors, J., Grelle, A., Lindroth, A. and Nilsson, M.B. (2014) 'A 12-year record reveals pre-growing season temperature and water table level threshold effects on the net carbon dioxide exchange in a boreal fen', *Environmental Research Letters*, 9(5), p. 55006. doi:10.1088/1748-9326/9/5/055006.

Perrin, P.M. (2015) 'Irish Vegetation Classification ERICA – Engine for Relevés to Irish Communities Assignment User ' s Manual Prepared by 2 Preparing your data', (December), pp. 0–10.

Phelps, J., Webb, E.L. and Adams, W.M. (2012) 'Biodiversity co-benefits of policies to reduce forest-carbon emissions ', *Nature climate change* . London : Springer Science and Business Media LLC , pp. 497–503. doi:10.1038/nclimate1462.

Polonik, P., Chan, W.S., Billesbach, D.P., Burba, G., Li, J., Nottrott, A., Bogoev, I., Conrad, B., Biraud, S.C. and Lawrence Berkeley National Lab. (LBNL) CA (United States), B. (2019) 'Comparison of gas analyzers for eddy covariance: Effects of analyzer type and spectral corrections on fluxes', *Agricultural and forest meteorology*, 272–273(C), pp. 128–142. doi:10.1016/j.agrformet.2019.02.010.

Pörtner, H.-O., Roberts, D.C., Adams, H., Adler, C., Aldunce, P., Ali, E., Begum, R.A. and Richard, B. (2022) *Climate Change 2022 - Impacts, Adaptation and Vulnerability - Summary for Policymakers*, *Ipcc*.

Poyda, A., Reinsch, T., Skinner, R.H., Kluß, C., Loges, R. and Taube, F. (2017) 'Comparing chamber and eddy covariance based net ecosystem CO2 exchange of fen soils ', *Journal of plant nutrition and soil science* . Wiley Subscription Services, Inc , pp. 252–266. doi:10.1002/jpln.201600447.

PP Systems (2013) 'EGM-4 Environmental Gas Monitor For CO2 Operator's Manual', *Main*, pp. 1–54.

Price, J.S. and Ketcheson, S.J. (2009) 'Water relations in cutover peatlands', *Carbon Cycling in Northern Peatlands*, 184, pp. 277–287.

Rambal, S., Ourcival, J., Joffre, R., Mouillot, F., Nouvellon, Y., Reichstein, M. and Rocheteau, A. (2003) 'Drought controls over conductance and assimilation of a Mediterranean evergreen ecosystem: scaling from leaf to canopy', *Global Change Biology*, 9(12), pp. 1813–1824.

Reichstein, M. *et al.* (2005) 'On the separation of net ecosystem exchange into assimilation and ecosystem respiration: Review and improved algorithm', *Global Change Biology*, 11(9), pp. 1424–1439. doi:10.1111/j.1365-2486.2005.001002.x.

Reichstein, M. *et al.* (2007) 'Reduction of ecosystem productivity and respiration during the European summer 2003 climate anomaly: a joint flux tower, remote sensing and modelling analysis', *Global Change Biology*, 13(3), pp. 634–651.

Reichstein, M., Tenhunen, J.D., Roupsard, O., Ourcival, J-M, Rambal, S., Dore, S. and Valentini, R. (2002) 'Ecosystem respiration in two Mediterranean evergreen Holm Oak forests: drought effects and decomposition dynamics', *Functional Ecology*, 16(1), pp. 27–39.

Reichstein, M., Tenhunen, J.D., Roupsard, O., Ourcival, Jean-marc, Rambal, S., Miglietta, F., Peressotti, A., Pecchiari, M., Tirone, G. and Valentini, R. (2002) 'Severe drought effects on ecosystem CO2 and H2O fluxes at three Mediterranean evergreen sites: revision of current hypotheses?', *Global Change Biology*, 8(10), pp. 999–1017.

Renou-Wilson, F., Bolger, T., Bullock, C., Convery, F., Curry, J., Ward, S., Wilson, D. and Müller, C. (2011) 'BOGLAND: Sustainable management of Peatlands in Ireland', *STRIVE report series*, 181.

Renou-Wilson, F. and Byrne, K.A. (2015) ‘Irish peatland forests: Lessons from the past and pathways to a sustainable future’, *Restoration of Boreal and Temperate Forests, Second Edition*, 13, pp. 321–335. doi:10.1201/b18809.

Renou-Wilson, F., Byrne, K.A., Flynn, R., Riondato, E., Saunders, M., Walz, K. and Wilson, D. (2022) *Peatland Properties Influencing Greenhouse Gas Emissions and Removal*.

Renou-Wilson, F., Keane, M., Mcnally, G., Sullivan, J.O. and Farrell, E.P. (2008) *Developing a forest resource on industrial cutaway peatland The BOGFOR programme*, *Agriculture*. Dublin: COFORD National Council for Forest Research and Development.

Renou-Wilson, F., Moser, G., Fallon, D., Farrell, C.A., Müller, C. and Wilson, D. (2019) ‘Rewetting degraded peatlands for climate and biodiversity benefits: Results from two raised bogs’, *Ecological Engineering*, 127, pp. 547–560. doi:10.1016/j.ecoleng.2018.02.014.

Renou, F., Scallan, Ú., Keane, M. and Farrell, E.P. (2007) ‘Early performance of native birch (Betula spp.) planted on cutaway peatlands: Influence of species, stock types and seedlings size’, *European Journal of Forest Research*, 126(4), pp. 545–554. doi:10.1007/s10342-007-0175-5.

Rigney, C., Wilson, D., Renou-Wilson, F., Müller, C., Moser, G. and Byrne, K.A. (2018) ‘Greenhouse gas emissions from two rewetted peatlands previously managed for forestry ’, *Mires and peat U6 - ctx_ver=Z39.88-2004&ctx_enc=info%3Aofi%2Fenc%3AUTF-8&rfr_id=info%3Asid%2Fsummon.serialssolutions.com&rft_val_fmt=info%3Aofi%2Ffmt%3Akev%3Amtx%3Ajournal&rft.genre=article&rft.atitle=Greenhouse+gas+emissions+from+two+rewetted+peatlands*. International Mire Conservation Group and International Peat Society , pp. 1–23. doi:10.19189/MaP.2017.OMB.314.

Roland, T.P., Daley, T.J., Caseldine, C.J., Charman, D.J., Turney, C.S.M., Amesbury, M.J., Thompson, G.J. and Woodley, E.J. (2015) ‘The 5.2 ka climate event: Evidence from stable isotope and multi-proxy palaeoecological peatland records in Ireland’, *Quaternary Science Reviews*, 124, pp. 209–223. doi:https://doi.org/10.1016/j.quascirev.2015.07.026.

Roulet, N., Moore, T., Bubier, J. and Lafleur, P. (1992) ‘Northern fens: methane flux and climatic change’, *Tellus B*, 44(2), pp. 100–105. doi:10.1034/j.1600-0889.1992.t01-1-00002.x.

Ryan, M.G. (1991) ‘Effects of climate change on plant respiration’, *Ecological Applications*, 1(2), pp. 157–167. doi:10.2307/1941808.

Sauer, T.J. and Horton, R. (2015) 'Soil heat flux', *Micrometeorology in Agricultural Systems*, pp. 131–154. doi:10.2134/agronmonogr47.c7.

Saunders, M., Tobin, B., Black, K., Gioria, M., Nieuwenhuis, M. and Osborne, B.A. (2012) 'Thinning effects on the net ecosystem carbon exchange of a Sitka spruce forest are temperature-dependent', *Agricultural and Forest Meteorology*, 157(October 2017), pp. 1–10. doi:10.1016/j.agrformet.2012.01.008.

Schindler, D.W., Stainton, M.P., Parker, B.R. and Curtis, P.J. (1996) 'Consequences of climate warming and lake acidification for UV-B penetration in North American boreal lakes', *Nature*. London: Nature Publishing Group, pp. 705–708. doi:10.1038/379705a0.

Schmid, H.P. (1994) 'Source areas for scalars and scalar fluxes ', *Boundary-layer meteorology* . Springer Science and Business Media LLC , pp. 293–318. doi:10.1007/bf00713146.

Schmid, H.P. and Lloyd, C.R. (1999) 'Spatial representativeness and the location bias of flux footprints over inhomogeneous areas ', *Agricultural and forest meteorology* . Elsevier B.V , pp. 195–209. doi:10.1016/S0168-1923(98)00119-1.

Schouten, M.G.C. (2002) *Conservation and restoration of raised bogs: geological, hydrological and ecological studies*. The Government Stationary Office.

Schuepp, P.H., Leclerc, M.Y., MacPherson, J.I. and Desjardins, R.L. (1990) 'Footprint prediction of scalar fluxes from analytical solutions of the diffusion equation ', *Boundary-layer meteorology* . Springer Science and Business Media LLC , pp. 355–373. doi:10.1007/bf00120530.

Solomon, S., Daniel, J.S., Sanford, T.J., Murphy, D.M. and Plattner, G. (2010) 'Persistence of climate changes due to a range of greenhouse gases'. doi:10.1073/pnas.1006282107/-/DCSupplemental.www.pnas.org/cgi/doi/10.1073/pnas.1006282107.

Sottocornola, M. (2007) *Four years of observations of carbon dioxide fluxes, water and energy budgets, and vegetation patterns in an Irish Atlantic blanket bog*, *Department of Civil and Environmental Engineering*. NUI.

Sottocornola, M. and Kiely, G. (2005) 'An Atlantic Blanket Bog is a modest $CO_2$ sink', *Geophysical Research Letters* [Preprint], (L23804).

Sottocornola, M. and Kiely, G. (2010) ‘Energy fluxes and evaporation mechanisms in an Atlantic blanket bog in southwestern Ireland ’, *Water Resources Research* . Washington : Blackwell Publishing Ltd , p. n/a-n/a. doi:10.1029/2010WR009078.

Strack, M., Waddington, J.M., Rochefort, L. and Tuittila, E.-S. (2006) ‘Response of vegetation and net ecosystem carbon dioxide exchange at different peatland microforms following water table drawdown ’, *Journal of Geophysical Research: Biogeosciences* . American Geophysical Union , pp. G02006-n/a. doi:10.1029/2005JG000145.

Stull, R.B. (1988) *An introduction to boundary layer meteorology*. Springer Science & Business Media.

Swenson, M., Regan, S., Bremmers, D., Lawless, J., Saunders, M. and Gill, L. (2018) ‘Carbon balance of a restored and cutover raised bog: Comparison to global trends’, *Biogeosciences Discussions*, pp. 1–48.

Swindles, G.T. *et al.* (2019) ‘Widespread drying of European peatlands in recent centuries’, *Nature Geoscience*, 12(11), pp. 922–928. doi:10.1038/s41561-019-0462-z.

The Climate Change Advisory Council (2019) *Climate Change Advisory Council Annual Review 2019*. McCumiskey House Richview, Clonskeagh Road, Dublin 14, D14 YR62.

The European Commission (2025) *The European Green Deal; striving to be the first climate-neutral continent*, *European Commission*. Available at: https://commission.europa.eu/strategy-and-policy/priorities-2019-2024/european-green-deal_en.

Tikkasalo, O.-P., Peltola, O., Alekseychik, P., Heikkinen, J., Launiainen, S., Lehtonen, A., Li, Q., Martinez-García, E., Peltoniemi, M., Salovaara, P., Tuominen, V. and Mäkipää, R. (2024) ‘Eddy covariance fluxes of CO2, CH4 and N2O on a drained peatland forest after clearcutting’, *EGUsphere*, 2024, pp. 1–36. doi:10.5194/egusphere-2024-1994.

Tomlinson, R.W. (2005) ‘Soil carbon stocks and changes in the Republic of Ireland’, *Journal of Environmental Management*, 76(1), pp. 77–93. doi:10.1016/j.jenvman.2005.02.001.

Tranmer, M., Murphy, J., Elliot, M. and Pampaka, M. (2020) ‘Multiple Linear Regression (2nd

Edition)', *The Cathie Marsh Centre for Census and Survey Research (CCSR)*, 5(5), pp. 1–5.

Tsubo, M. and Walker, S. (2005) 'Relationships between photosynthetically active radiation and clearness index at Bloemfontein, South Africa', *Theoretical and Applied Climatology*, 80(1), pp. 17–25. doi:10.1007/s00704-004-0080-5.

Tuittila, E.-S., Komulainen, V.-M., Vasander, H. and Laine, J. (1999) 'Restored cut-away peatland as a sink for atmospheric CO 2', *Oecologia*, 120, pp. 563–574.

Tuittila, E., Vasander, H. and Laine, J. (2004) 'Sensitivity of C Sequestration in Reintroduced Sphagnum to Water-Level Variation in a Cutaway Peatland', *Restoration Ecology*, 12(4), pp. 483–493. doi:10.1111/j.1061-2971.2004.00280.x.

Turetsky, M.R. *et al.* (2014) 'A synthesis of methane emissions from 71 northern, temperate, and subtropical wetlands', *Global Change Biology*, 20(7), pp. 2183–2197. doi:10.1111/gcb.12580.

UNFCCC and Change, U.N.F.C. on C. (2017) *UN ClimateChange Annual Report 2017*. Bonn, Germany.

Waddington, J.M., Strack, M. and Greenwood, M.J. (2010) ' Toward restoring the net carbon sink function of degraded peatlands: Short-term response in CO 2 exchange to ecosystem-scale restoration ', *Journal of Geophysical Research*, 115(G1), p. n/a-n/a. doi:10.1029/2009jg001090.

Walsh, S. (2012) 'Climatological Note No.14: A Summary of Climate Averages for Ireland 1981-2010', *Met Éireann*, 582(417), p. 16.

Wang, M., Guan, D.-X., Han, S.-J. and Wu, J.-L. (2010) 'Comparison of eddy covariance and chamber-based methods for measuring CO2 flux in a temperate mixed forest ', *Tree physiology* . Canada : Oxford University Press , pp. 149–163. doi:10.1093/treephys/tpp098.

Wang, X., Wang, C., Bond-Lamberty, B. and Pacific Northwest National Lab. (PNNL) WA (United States), R. (2017) 'Quantifying and reducing the differences in forest CO2-fluxes estimated by eddy covariance, biometric and chamber methods: A global synthesis ', *Agricultural and forest meteorology* . United States : Elsevier B.V , pp. 93–103. doi:10.1016/j.agrformet.2017.07.023.

Waring, R.H. and Running, S.W. (2007) 'Forest Ecosystems: Analysis at Multiple Scales'. US: Academic Press.

Webb, E.K., Pearman, G.I. and Leuning, R. (1980) 'Correction of flux measurements for density effects due to heat and water vapour transfer', *The Royal Meteorological Society*, 106(447), pp. 85–100. doi:https://doi.org/10.1002/qj.49710644707.

Wehr, R., Munger, J.W., McManus, J.B., Nelson, D.D., Zahniser, M.S., Davidson, E.A., Wofsy, S.C. and Saleska, S.R. (2016) 'Seasonality of temperate forest photosynthesis and daytime respiration ', *Nature* . England : Nature Publishing Group , pp. 680–683. doi:10.1038/nature17966.

Wellock, M.L., Reidy, B., Laperle, C.M., Bolger, T. and Kiely, G. (2011) 'Soil organic carbon stocks of afforested peatlands in Ireland', *Forestry*, 84(4), pp. 441–451. doi:10.1093/forestry/cpr046.

Whalen, S.C. (2005) 'Biogeochemistry of methane exchange between natural wetlands and the atmosphere', *Environmental Engineering Science*, 22(1), pp. 73–94.

Wilczak, J.M., Oncley, S.P. and Stage, S.A. (2001) 'Sonic anemometer tilt correction algorithms', *Boundary-layer Meteorology*, 99(1), pp. 127–150.

Wilson, D., Blain, D., Couwenberg, J., Evans, C.D., Murdiyarso, D., Page, S.E., Renou-Wilson, F., Rieley, J.O., Sirin, A. and Strack, M. (2016) 'Greenhouse gas emission factors associated with rewetting of organic soils', *Mires and Peat*, 17.

Wilson, D., Dixon, S.D., Artz, R.R.E., Smith, T.E.L., Evans, C.D., Owen, H.J.F. and Archer, E. (2015) 'Derivation of greenhouse gas emission factors for peatlands managed for extraction in the Republic of Ireland and the United Kingdom', pp. 5291–5308. doi:10.5194/bg-12-5291-2015.

Wilson, D., Farrell, C., Fallon, D., Moser, G., Müller, C. and Renou-Wilson, F. (2016) 'Multiyear greenhouse gas balances at a rewetted temperate peatland', *Global Change Biology*, 22(12), pp. 4080–4095. doi:10.1111/gcb.13325.

Wilson, D., Farrell, C., Mueller, C., Hepp, S. and Renou-Wilson, F. (2013) 'Rewetted industrial cutaway peatlands in western Ireland: a prime location for climate change mitigation?', *Mires and Peat*, 11, p. 1.

Wilson, D., Mackin, F., Tuovinen, J.P., Moser, G., Farrell, C. and Renou-Wilson, F. (2022) ‘Carbon and climate implications of rewetting a raised bog in Ireland’, *Global Change Biology*, 28(21), pp. 6349–6365. doi:10.1111/gcb.16359.

Wilson, D., Tuittila, E.-S., Alm, J., Laine, J., Farrell, E.P. and Byrne, K.A. (2007) ‘Carbon dioxide dynamics of a restored maritime peatland’, *Ecoscience*, 14(1), pp. 71–80. doi:10.2980/1195-6860(2007)14[71:cddoar]2.0.co;2.

Wilson, K. *et al.* (2002) ‘Energy balance closure at FLUXNET sites’, *Agricultural and Forest Meteorology*, 113(1–4), pp. 223–243.

Winck, B.R., Bloor, J.M.G. and Klumpp, K. (2023) ‘Eighteen years of upland grassland carbon flux data: reference datasets, processing, and gap-filling procedure’, *Scientific Data*, 10(1), pp. 1–17. doi:10.1038/s41597-023-02221-z.

WMO (2022) *State of the Global Climate 2021*.

WMO (2024) ‘State of the Climate 2024 Update for COP29’.

Wutzler, T., Lucas-Moffat, A., Migliavacca, M., Knauer, J., Sickel, K., Šigut, L., Menzer, O. and Reichstein, M. (2018) ‘Basic and extensible post-processing of eddy covariance flux data with REddyProc’, *Biogeosciences*, 15(16), pp. 5015–5030.

Xu, J., Morris, P.J., Liu, J. and Holden, J. (2018) ‘PEATMAP: Refining estimates of global peatland distribution based on a meta-analysis’, *Catena*, 160, pp. 134–140. doi:10.1016/j.catena.2017.09.010.

Xu, Y. and Goodacre, R. (2018) ‘On Splitting Training and Validation Set: A Comparative Study of Cross-Validation, Bootstrap and Systematic Sampling for Estimating the Generalization Performance of Supervised Learning’, *Journal of Analysis and Testing*, 2(3), pp. 249–262. doi:10.1007/s41664-018-0068-2.

Yamashita, M. and Yoshimura, M. (2019) ‘Estimation of Global and Diffuse Photosynthetic Photon Flux Density under Various Sky Conditions Using Ground-Based Whole-Sky Images ’, *Remote Sensing* . Basel : MDPI AG , p. 932. doi:10.3390/rs11080932.

Yamulki, S., Anderson, R., Peace, A. and Morison, J.I.L. (2013) ‘Soil CO2 CH4 and N2O fluxes from an afforested lowland raised peatbog in Scotland: Implications for drainage and restoration', *Biogeosciences*, 10(2), pp. 1051–1065. doi:10.5194/bg-10-1051-2013.

Yu, Z., Beilman, D.W., Frolking, S., MacDonald, G.M., Roulet, N.T., Camill, P. and Charman, D.J. (2011) 'Peatlands and their role in the global carbon cycle', *Eos, Transactions American Geophysical Union*, 92(12), pp. 97–98.

Zhou, Y., Sühring, M. and Li, X. (2023) 'Evaluation of energy balance closure adjustment and imbalance prediction methods in the convective boundary layer – A large eddy simulation study', *Agricultural and Forest Meteorology*, 333(March), p. 109382. doi:10.1016/j.agrformet.2023.109382.

Zhu, S., Clement, R., McCalmont, J., Davies, C.A. and Hill, T. (2022) 'Stable gap-filling for longer eddy covariance data gaps: A globally validated machine-learning approach for carbon dioxide, water, and energy fluxes', *Agricultural and Forest Meteorology*, 314, p. 108777.

Zhu, S., McCalmont, J., Cardenas, L.M., Cunliffe, A.M., Olde, L., Signori-Müller, C., Litvak, M.E. and Hill, T. (2023) 'Gap-filling carbon dioxide, water, energy, and methane fluxes in challenging ecosystems: Comparing between methods, drivers, and gap-lengths', *Agricultural and Forest Meteorology*, 332(February), p. 109365. doi:10.1016/j.agrformet.2023.109365.

# Appendices

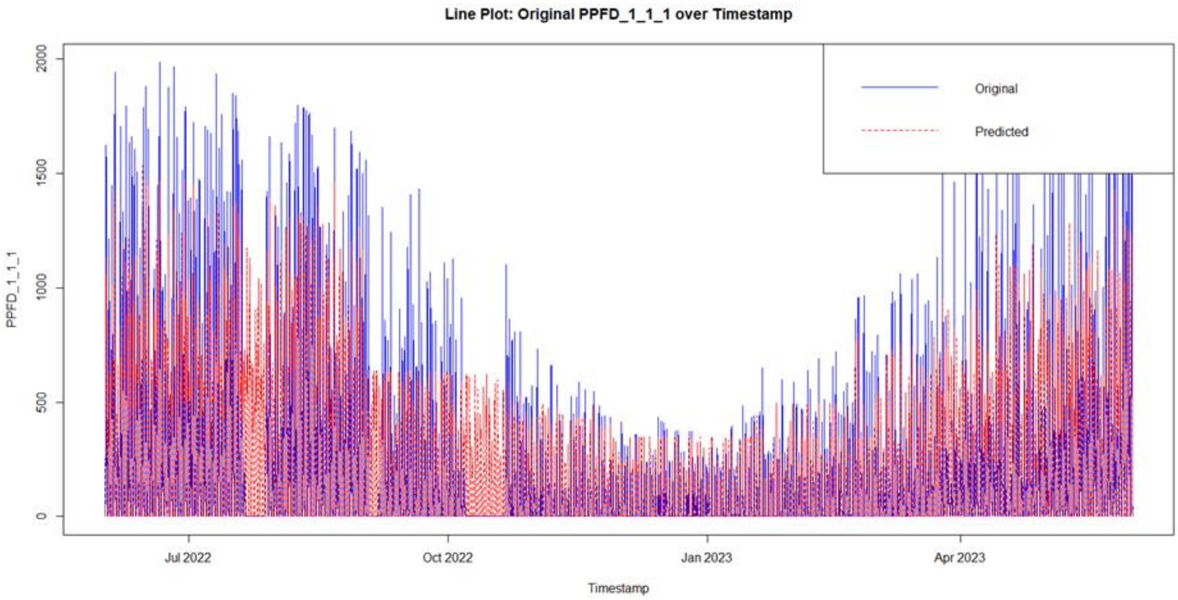


*Time Series of PPFD observed versus predicted data using GAMs model, original values in blue and red dotted line shows the gap filled data.*

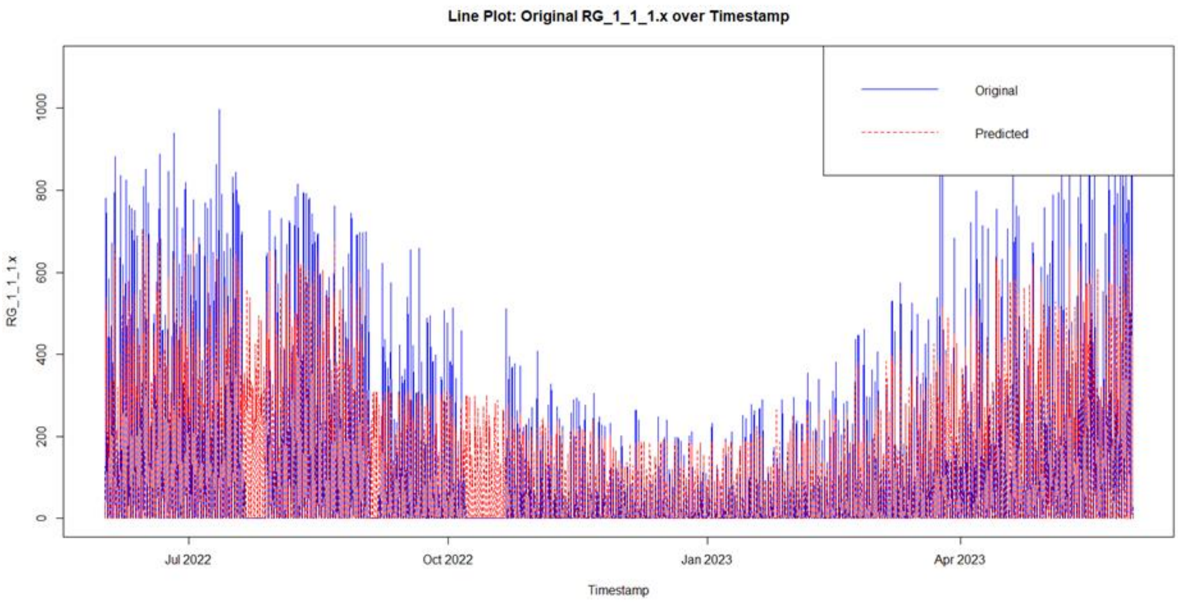


*Timeseries of observed and predicted global radiation using GAMs model, original values in blue and red dotted line shows the gap filled data.*

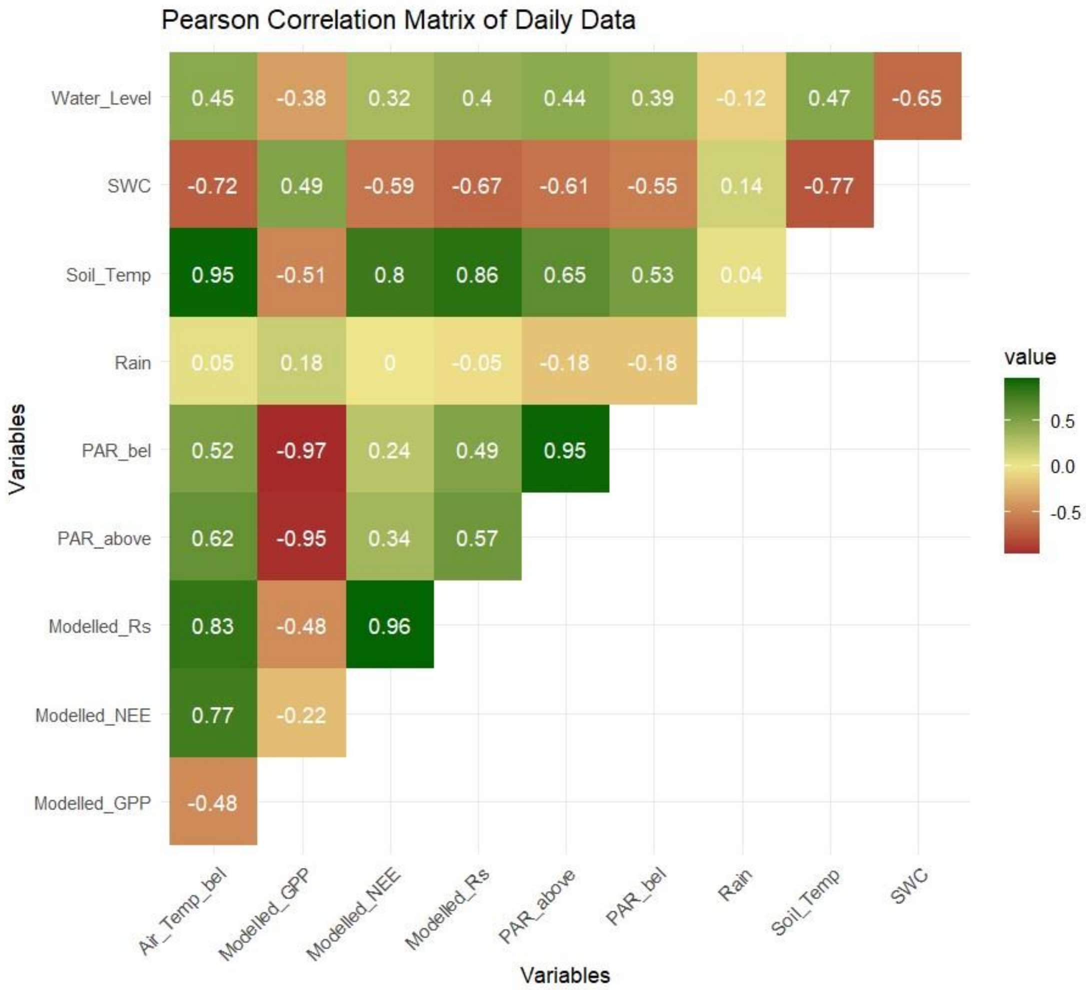


*Pearson Correlation Matrix Below canopy fluxes and meteorological variables*

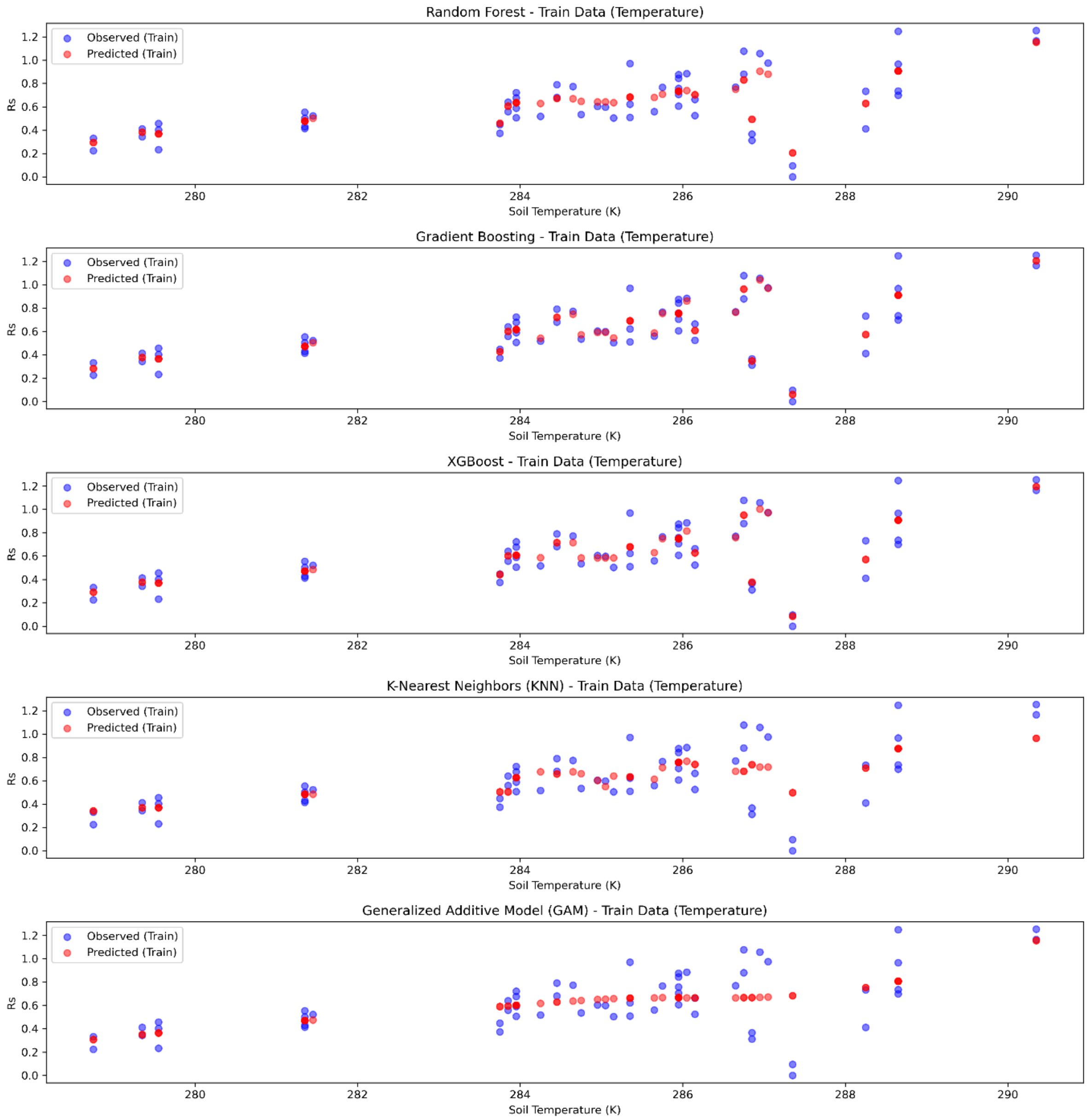


*Model performance on training data plotted with observed data for Respiration below canopy*

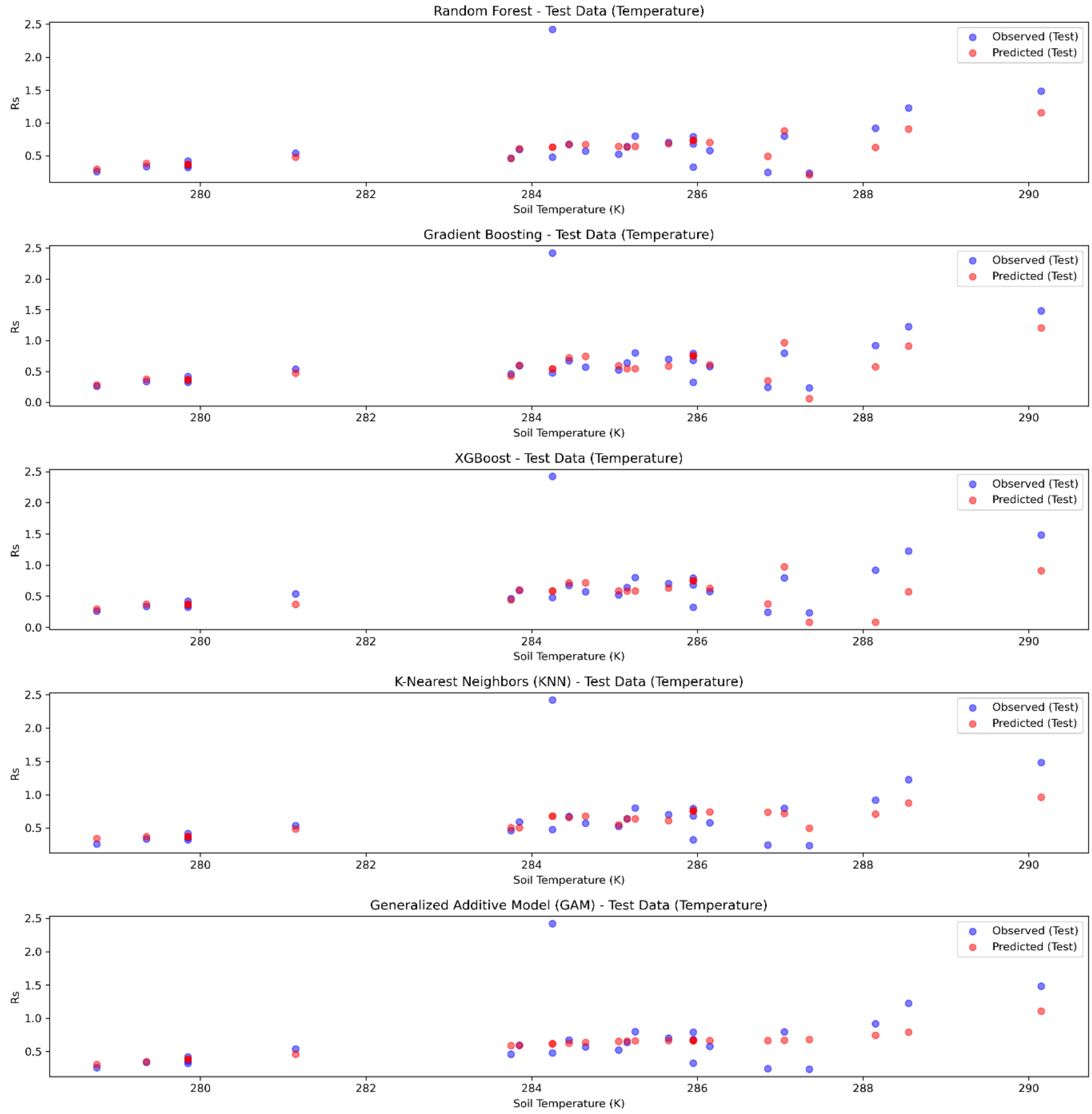


*Model performance test data plotted with observed data for Respiration below canopy*

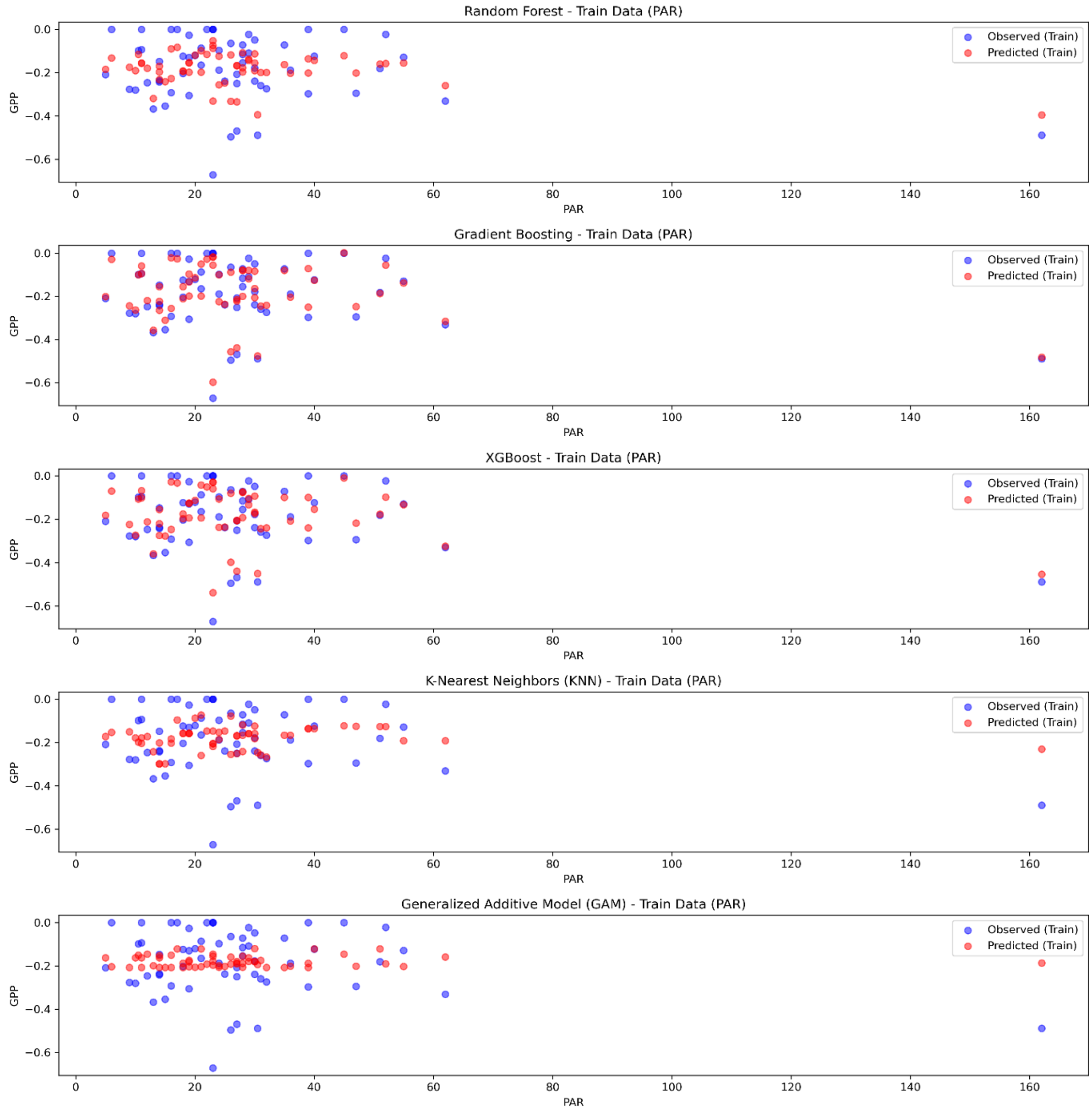


*Model performance training data plotted with observed data for GPP below canopy*

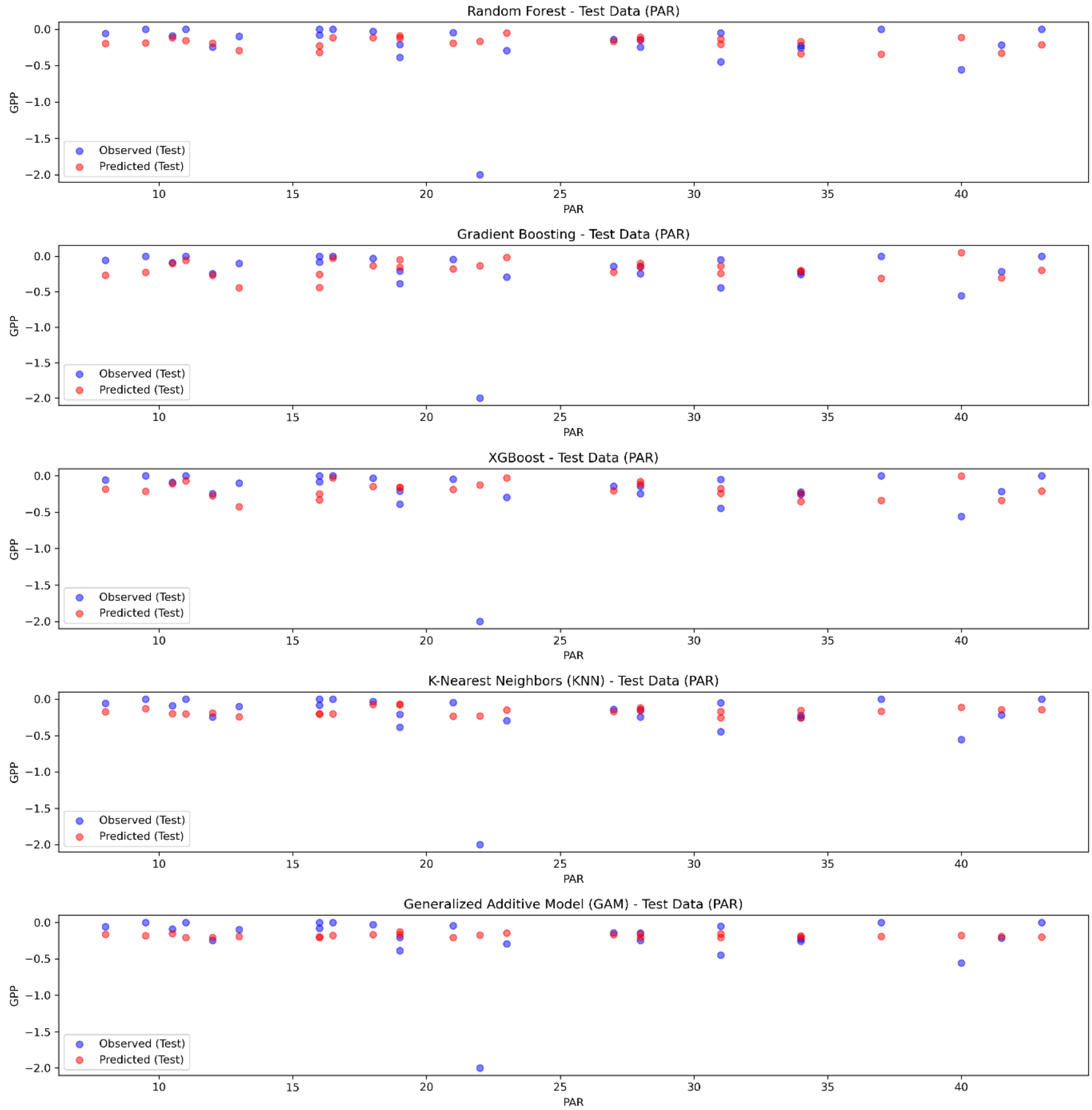


*Model performance test data plotted with observed data for GPP below canopy*

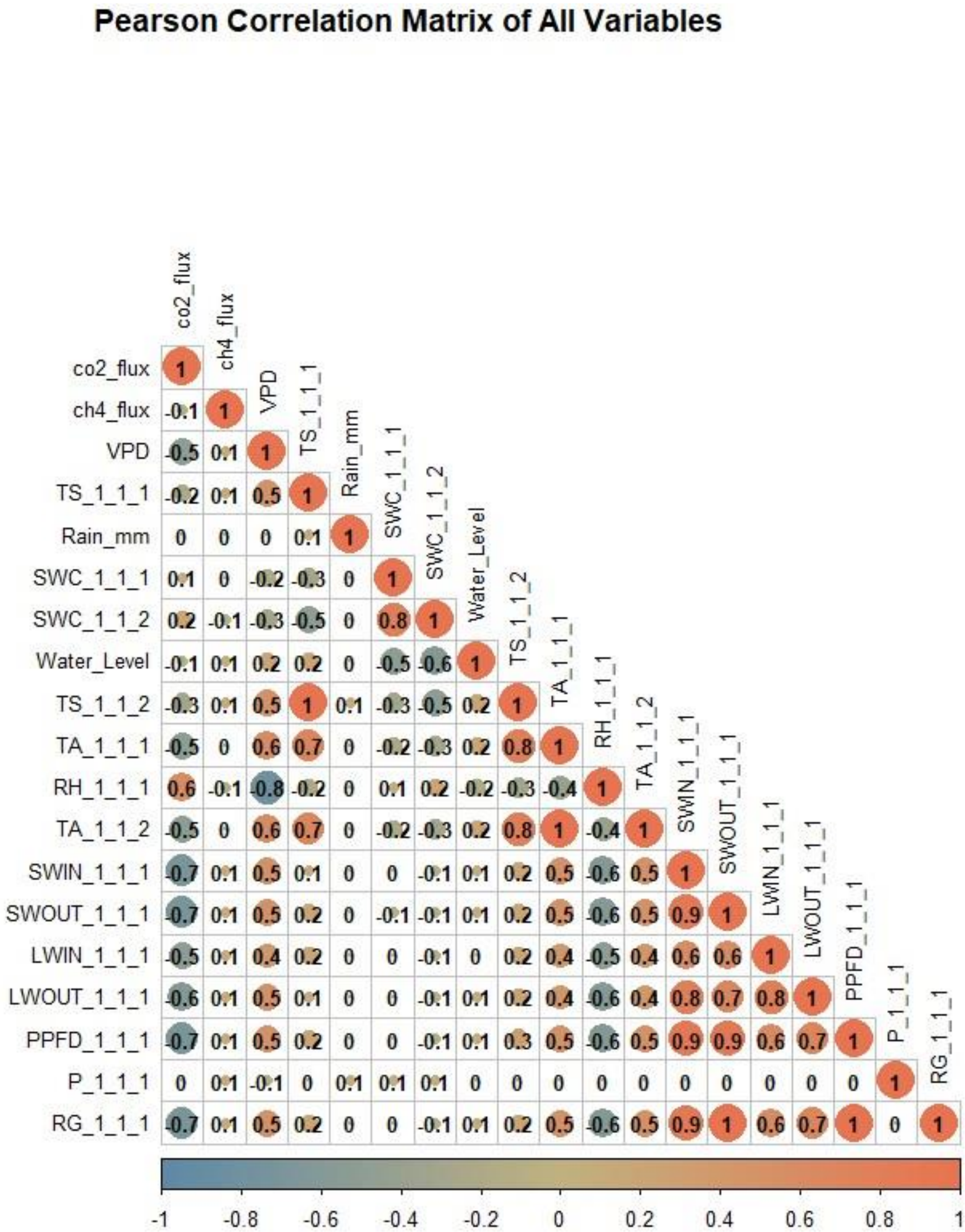


*Pearson correlation matrix for above canopy $CO_2$ and $CH_4$ fluxes and all meteorological data available*

CR200 data logger Cambel Scientific, USA, programme to run soil sensors from Lullymore site:

```
'CR200/CR200X Series

'Created by Short Cut (4.4)


'Declare Variables and Units

Public BattV

Public T109_C

Public Rain_mm

Public VW

Public PA_us


Units BattV=Volts

Units T109_C=Deg C

Units Rain_mm=mm

Units PA_us=us


'Define Data Tables

DataTable(Lullymore_Soil,True,-1)

	DataInterval(0,30,Min)

	Average(1,BattV,False)

	Average(1,T109_C,False)

	Totalize(1,Rain_mm,False)

	Average(1,VW,False)
```

```
EndTable

DataTable(Table2,True,-1)
	DataInterval(0,1440,Min)
	Minimum(1,BattV,False,False)
EndTable

'Main Program
BeginProg
	'Main Scan
	Scan(60,Sec)
		'Default CR200 Series Datalogger Battery Voltage measurement 'BattV'
		Battery(BattV)
		'109 Temperature Probe (CSL) measurement 'T109_C'
		Therm109(T109_C,1,1,1,1,0)
		'Generic Tipping Bucket Rain Gauge measurement 'Rain_mm'
		PulseCount(Rain_mm,P_SW,2,0,0.2,0)
		'CS625 Water Content Reflectometer measurement 'VW'
		If IfTime(0,1,Hr) Then
				PeriodAvg(PA_us,2,0,100,10,2,1,0)
				VW=-0.0663-0.0063*PA_us+0.0007*PA_us^2
		EndIf
		'Call Data Tables and Store Data
```

```
        CallTable Lullymore_Soil

        CallTable Table2

    NextScan

EndProg
```

CR3000 Data Logger Programme for Biomet Sensor Measurements at Lullymore Site (Campbell Scientific, USA)

```
'CR3000 Series Datalogger

'EddyPro compliant biomet example

'Modified , added 107 and Hygroclip TA and RH

'Updated 30.08.2021 with net radiometer

'Updated 27.01.2022 with CS320 pyranometer and SW,LW net radiometer CNR100

'update 10.06.2022 change from 1m to 30 m


'Declare Variables and Units

'=================

' Temperature/RH data from top of tower (vertical loc 1)

' from HC2S3 combined Temp/RH sensor - use array TRHsensorvalues to contain both

Public TRHsensorvalues(2)

Alias TRHsensorvalues(1) = TA_2_1_1_1_1

Alias TRHsensorvalues(2) = RH_19_3_1_1_1

' CS107 temperature data from top of tower, vertical loc 1, replicate 2

Public TA_2_1_1_1_2


'CNR100 radiometer shortwave in & out, longwave in & out, and temperature
```

```
Public SWIN_6_10_1_1_1

Public SWOUT_6_11_1_1_1

Public LWIN_6_14_1_1_1

Public LWOUT_6_15_1_1_1

Public CNR1TC            ' CNR100 radiometer body temperature

Public Batt_Volt   'declared but not used

Public CM3Up

Public CM3Dn

Public CG3Up

Public CG3Dn

Public CNR1TK

Public NetRs

Public NetRl

Public Albedo

Public UpTot

Public DnTot

Public NetTot

Public CG3UpCo

Public CG3DnCo

'PAR sensors skye 215

Public PPFD_6_21_1_1_1

'Range Gauge

Public P_8_18_1_1_1
```

```
'CS320 Global Pyranometer

Public CS320(6)

Public SlrMJ

Public DewPtC

Public HtrCtrl As Boolean


Alias CS320(1)=RG_6_4_1_1_1

Alias CS320(2)=Raw_mV

Alias CS320(3)=CS320_Temp

Alias CS320(4)=CS320_X

Alias CS320(5)=CS320_Y

Alias CS320(6)=CS320_Z


Units SlrMJ=MJ/m^2

Units DewPtC=Deg C

Units RG_6_4_1_1_1=W/m^2

Units Raw_mV=mV

Units CS320_Temp=Deg C

Units CS320_X=degrees

Units CS320_Y=degrees

Units CS320_Z=degrees
```